ACTIVITY OF PEPTIDE-BASED AND SMALL MOLECULE LIGANDS OF THE KININ RECEPTOR FROM MOSQUITO *AEDES AEGYPTI* AND TICK *RHIPICEPHALUS MICROPLUS* THROUGH FUNCTIONAL ASSAYS

A Dissertation

by

CAIXING XIONG

Submitted to the Office of Graduate and Professional Studies of
Texas A&M University
in partial fulfillment of the requirements for the degree of

DOCTOR OF PHILOSOPHY

Chair of Committee,	Patricia V. Pietrantonio
Committee Members,	Gabriel Hamer
	Nancy Ing
	Cecilia Tamborindeguy
Head of Department,	Phillip Kaufman

December 2020

Major Subject: Entomology

ABSTRACT

Due to the worldwide prevalence of pesticide resistance in disease vectors, novel targets and corresponding reagents for alternative pest control are needed. Invertebrate neuropeptide G protein-coupled receptors (GPCRs) are involved in regulating many important physiological processes and are promising insecticide targets. In this study, we used the invertebrate-specific kinin receptor as a proof-of-principle for novel ligand discovery of arthropod neuropeptide GPCRs. Kinins are pleiotropic neuropeptides that are known to modulate insect diuresis, hindgut contraction, pre-ecdysis, digestion and chemosensory perception.

We utilized both forward and reverse pharmacological approaches to identify peptidomimetic and small molecule ligands of the kinin receptors from the yellow fever mosquito, *Aedes aegypti*, and the cattle fever tick, *Rhipicephalus microplus*. In forward approaches, novel peptidomimetics with enhanced biostability and bioavailability designed based on insect kinins were tested on the recombinant receptors using a calcium bioluminescence assay and analyzed for their EC_{50} and efficacy. These experiments yielded potent agonists for both receptors. I cloned the cDNA of the kinin neuropeptide precursor from *R. microplus*, predicted the sequences of 17 tick kinins, and functionally characterized fourteen of them on the cognate receptor. In this process, I found the tick kinins have a slightly different sequence motif compared to insect kinins, with proline being conserved in the variable position two of the C-terminal pentapeptide core.

For the reverse approach, I developed a high-throughput screening (HTS) calcium fluorescence assay using the recombinant tick kinin receptor, reporting the first HTS on a neuropeptide GPCR of any tick species. Through experimental screens and virtual screens, 36 antagonists were identified. Three of them were validated as antagonists on the mosquito

receptor. These molecules also inhibited the mosquito hindgut contractions in the isolated hindgut contraction inhibition assay. By analyzing the structure-activity relationships of peptidomimetic agonists and small molecule antagonists respectively, we improved the understanding of ligand structures which will facilitate the design of potent ligands.

In summary, this study identified potent peptidomimetic agonists, and for the first time, identified antagonists of mosquito and tick kinin receptors. These ligands are important reagents and tools for studying the role of kinin in arthropod physiology in arthropods and potential leads of novel pesticides. This study improved our understanding of the arthropod kinin signaling system.

ACKNOWLEDGEMENTS

First, my heartful thanks go to my committee chair, Dr. Patricia V. Pietrantonio, nothing will be possible without her endless support and patience throughout the course of my Ph.D. program. I become a better scientist thanks to her who always holds up a high standard for research quality and is persistent in searching for truth in science. I am also deeply thankful for the time she spends with me to improve my professional skills and share her valuable experiences with me about research, work and life, from which I gained a lot. Thanks to my committee members, Dr. Cecilia Tamborindeguy, Dr. Gabriel Hamer, and Dr. Nancy Ing, for their guidance and support. I would also like to thank our collaborators Dr. Ronald J. Nachman and Dr. Dwight Baker for their collaborations and inputs in this project.

My thanks also go to A.W.E.S.O.M.E. faculty group in the College of Agriculture and Life Sciences at Texas A&M University and Aggie Women in Entomology graduate student writing club of Department of Entomology for their assistances with reviewing and editing of this dissertation.

Many thanks also go to my friends and colleagues and the department faculty and staff for making my time at Texas A&M University a great experience. Finally, thanks to my parents for their encouragement and to my husband for his patience and love.

CONTRIBUTORS AND FUNDING SOURCES

Contributors

This work was supervised by a dissertation committee consisting of Professors Patricia V. Pietrantonio, Dr. Cecilia Tamborindeguy and Dr. Gabriel Hamer of the Department of Entomology and Professors Nancy Ing of the Department of Animal Science.

The peptides analogs tested in Chapter 2 were designed and synthesized by Dr. Ronald J. Nachman (USDA). Tick kinin analogs tested in Chapter 4 were also designed and synthesized by Dr. Nachman. Dr. Nachman also assisted in analyzing the structure-activity relationships (SAR) of kinin analogs in Chapters 2 and 4. Dr. Dwight provided suggestions on HTS assay optimization and hit selection for Chapter 5. The chemical library used for HTS in Chapter 5 was provided by Professor James C. Sacchettini of Department of Biochemistry and Biophysics. The cytotoxicity assay in Chapter 5 was performed by Dr. Wen Dong in Dr. Sacchettini laboratory. The SAR analysis for small molecule analogs in Chapter 5 was done by Dr. Nian Zhou in Dr. Sacchettini lab.

All other work conducted for this dissertation was completed by the student independently.

Funding Sources

This work was supported part by Texas A&M AgriLife Research Insect Vector Diseases Grant Program (FY'17-18 and FY'19-21) to P. V. Pietrantonio and NIFA-AFRI Animal Health and Well-being Award under Grant Number [2016-67015-24918] to P. V. Pietrantonio and K. Temeyer. Its contents are solely the responsibility of the authors and do not necessarily represent the official views of the NIFA or Texas A&M AgriLife Research.

NOMENCLATURE

ACE	Angiotensin Converting Enzyme
Aib	α-Aminoisobutyric Acid
AIT	Adult Immersion Test
ANOVA	Analysis of Variance
ATP	Adenosine Triphosphate
BRET	Bioluminescence Resonance Energy Transfer
Ca^{2+}	Calcium ion
CAFÉ	No-Choice Capillary Feeding
cAMP	3', 5'-Cyclic Adenosine Monophosphate
Cl^-	Chloride ion
CFT	Cattle Fever Tick
CFTEP	Cattle Fever Tick Eradication Program
CHIKV	Chikungunya Virus
CHO	Chinese Hamster Ovary
CNS	Central Nervous System
DPBS	Dulbecco's Phosphate-Buffered Saline
DEET	N, N-Diethyl-meta-tolumide
DENV	Dengue Virus
DMEM	Dulbecco's Modified Eagle Medium
DMF	Dimethyl Formamide
DMSO	Dimethyl Sulfoxide
DNA	Deoxyribonucleic Acid

ERK	Extracellular Signal-regulated Kinases
FBS	Fetal Bovine Serum
FRET	Förster resonance energy transfer
GPCR	G Protein-Coupled Receptors
GRK	GPCR Kinase
HBSS	Hank’s Buffer Saline Solution
HEK	Human Embryonic Kidney
HDF	Human Dermal Fibroblasts
HHBS	Hank’s Buffer Saline with HEPES
HTS	High-Throughput Screening
IK	Insect Kinin
KR	Kinin Receptor
LK	Leucokinin
LKR	Leucokinin Receptor
LIT	Larval Immersion Test
MAFFT	Multiple Alignment using Fast Fourier Transform
MAPK	Mitogen-Activated Protein Kinases
MIP	Myoinhibitory Peptide
mRNA	Messenger Ribonucleic Acid
MT	Malpighian Tubule
NC	Negative Control
NCBI	National Center for Biotechnology Information
NEP	Neprilysin

NPA	Normalized Percent Activation
NPY	Neuropeptide Y
PBS	Phosphate-Buffered Saline
PC	Positive Control
PCR	Polymerase Chain Reaction
PEG	Polyethylene Glycol
PLC	Phospholipase C
RACE	Rapid Amplification of Complementary Dixoyribonucleic Acid Ends
RT	Room Temperature
IP_3	Inosititol-1,4,5-Triphosphate
RFU	Relative Fluorescence Unit
RhoGEF	Rho Guanine Nucleotide Exchange Factor for Rho/Rac/Cdc42-like GTPases
SIT	Sterile Insect Technique
TAHC	Texas Animal Health Commission
TKSM	Tachykinin Small Molecule
USDA	United States Department of Agriculture
USDA-APHIS-VS	U.S. Department of Agriculture-Animal Plant Health Inspection Service-Veterinary Service
V/O	Vector-Only cells
ZIKV	Zika Virus

TABLE OF CONTENTS

Page

LIST OF FIGURES

Page

LIST OF TABLES

Page

1. INTRODUCTION

1.1 General background of human and animal disease-vectors

Blood-feeding arthropods threaten human and animal health by transmitting the etiological agents of various vector-borne diseases. Among blood-feeding arthropods, mosquitoes and ticks are the primary vectors affecting humans and livestock, respectively (Mansfield et al., 2017). Vector-borne diseases constitute 17% of infectious diseases worldwide and lead to more than 700,000 human deaths annually (Faulde, 2018). The yellow fever mosquito, *Aedes aegypti,* is the most important vector of arboviruses to humans, including dengue virus (DENV), chikungunya virus (CHIKV), Zika virus (ZIKV) and yellow fever virus. The southern cattle tick, *Rhipicephalus microplus* (Canestrini), is the world's most economically important tick as it transmits the pathogens that cause tick cattle fever and anaplasmosis. The most effective and fastest approaches to prevent vector-borne diseases rely on vector management (Benelli, 2019).

1.1.1. The yellow fever mosquito, *Aedes aegypti*

Ae. aegypti (Diptera: Culicidae) originated in Africa and is now widely distributed in tropical and subtropical regions of the world (Kraemer et al., 2015). A long history of adaptation to domestic environments makes this mosquito species the most important vector of human virus diseases (Powell et al., 2018). This mosquito's threat to public health as an important disease vector is increasing, as its suitable habitats are expanding globally with urbanization (Brady and Hay, 2020). About half of the world's population (3.9 billion in 128 countries) is at risk of DENV infection (Brady et al., 2012), and 390 million new cases are recorded every year (Bhatt et al., 2013). There is currently no specific treatment for dengue fever (WHO, 2018). Aside of DENV, the recent outbreaks of CHIKV and ZIKV occurred in Americas have caused infection

of more than 2 million people since 2015 (Carvalho and Machado, 2020). Yet, there is no commercially available vaccine for the three above mentioned viruses (Carvalho and Machado, 2020), making vector control the most effective method for disease control. Repellents are recommended, but even the repellent "standard" DEET (N, N-Diethyl-meta-tolumide) is not 100% effective and requires repeated application every few hours (Cilek et al., 2004).

There are two well-known subspecies of *Ae. aegypti*, *Ae. aegypti formosus* and *Ae. aegypti aegypti*. The more ancient 'forest' subspecies, *Ae. aegypti formosus*, originates from sub-Saharan Africa. Females preferentially feed on wild animals and lay eggs in tree holes (Christophers, 1960; McBride et al., 2014; Powell et al., 2018). Whereas the globally invasive subspecies, also known as the 'domestic form', *Ae. aegypti aegypti*, has evolved the preference for human blood about 500 years ago (Powell et al., 2018). Ecologically, the shift to human-biting behavior of *Ae. aegypti* is shown to be associated with increased human population (urbanization) and originated from areas with long, hot dry seasons (Rose et al., 2020). These data suggest that human-biting is associated with the vital needs of accessible water resources for mosquito breeding in these dry areas. Physiologically, the domestic mosquitoes have evolved to express a higher level of *AeagOr*4, an odorant receptor is responsible for detecting a key compound in human odor (McBride et al., 2014).

Mosquitoes have four life stages: egg, larval, pupal, and adult. It takes 8-10 days for *Ae. aegypti* to develop from egg to adult (Christophers, 1960). Mosquitoes spend their larval (1-4 instars) and pupal stages in water. Female and male adults both feed on plant nectar, but females need to take at least one blood meal to lay eggs. The female *Ae. aegypti* typically seeks hosts and feeds in daylight hours (Yasuno and Tonn, 1970). During the female adult life span, which can

range from two weeks to a month, the female can go through up to five gonotrophic cycles and lay 100-200 eggs in each cycle (Clemons et al., 2010).

1.1.2. The southern cattle tick, *Rhipicephalus microplus*

The southern cattle tick, *Rhipicephalus (Boophilus) microplus* (Canestrini) (Acari: Ixodidae), is a one-host hard tick. These ticks live, feed, and reproduce on a single host. Although *R. microplus* has evolved with domestic bovine hosts (Hoogstraal and Aeschlimann, 1982), it can be found on other domestic animals, such as horses, goats, sheep and buffaloes (da Silva et al., 2018; Ghosh et al., 2006; Obregón et al., 2020; Stiller and Coan, 1995; Thomas et al., 2020). It can also use wild animals as alternative hosts, including red deer, white-tail deer, and nilgai antelope (Busch et al., 2014; Pérez de León et al., 2012; Rodríguez-Vivas et al., 2013). Their whole parasitic life cycle (larva, nymph, adult), from unfed larva to engorged female, can be complete in 3-4 weeks, feeding only once per life stage (Sonenshine and Roe, 2013). Adults mate on the host and engorged females then drop off, lay eggs, and die. An engorged female can lay up to 3,000 eggs, with a hatching success of 80-90% if conditions are optimal (Davey et al., 2006; Leal et al., 2020). The newly hatched larvae will crawl up on grass to find a new host and if hosts are scarce, the larvae can enter diapause for 8-9 months without feeding (Leal et al., 2020). *R. microplus* is highly invasive in tropical and subtropical areas due to its adaptability and high reproduction rate; it originated from South-East Asia and has quickly spread to Australia, East and Southern Africa, and South and Central America (Bram et al., 2002; Jongejan and Uilenberg, 2004). As a result of global climate change, the habitats for *R. microplus* are expanding: a model predicted an 1-134% increase of *R. microplus* infestation in different areas around the world, particularly in the Nearctic Region (Marques et al., 2020).

1.1.2.1. Health impact of *R. microplus* on animal hosts

Rhipicephalus microplus, along with its closely related sister species, *R. annulatus,* are the primary vectors of the disease agent for the tick cattle fever, *Babesia spp.*. These two tick species combined are known as the cattle fever ticks (CFTs). *R. microplus* is particularly important as a highly adaptable ectoparasite. The majority of the recent CFT outbreaks in the U.S. were caused by *R. microplus* and some ticks from these outbreaks tested positive for *B. bigemina* (Guerrero et al., 2007; Lohmeyer et al., 2011). Cattle fever was known as 'red water fever', which name is associated with the production of dark red or brown-colored urine due to the presence of hemoglobin from lysed red blood cells (Bock, 2008). Bovine babesiosis is characterized by sudden onset of anemia, jaundice, irritability, and aggression in infected cattle (Bock, 2008). The lifecycle and transmission of the Apicomplexa protozoan species *Babesia* depends on the life stages of cattle fever ticks. During blood feeding, the pathogens are transferred to the host from the tick salivary glands. Both *B. bovis* and *B. bigemina* have shown the potential for transovarial and transstadial transmission in ticks (Angus, 1996). Only larval *R. microplus* ticks can transmit *B. bovis* as infective sporozoites are not present in nymphs or adult ticks, while *B. bigemina* can be transmitted by larvae, nymphs and adults (Pérez de León et al., 2014). Bovine babesiosis can cause over 90% mortality in the naïve cattle population across the southern United States (Smith and Kilborne, 1893) and is a major arthropod-borne disease of domestic cattle. In addition, *R. microplus* is the vector of bovine anaplasmosis (*Anaplasma marginale*) (Kocan et al., 2004) and equine piroplasmosis (Jongejan and Uilenberg, 2004; Uilenberg, 2006).

1.1.2.2. Economic impact of *R. microplus*

It is estimated that 1.2 billion cattle are exposed to babesiosis worldwide (Bock, 2008). *R. microplus* causes significant losses to the cattle industry around the world. In US dollars, tick infestation causes $3.24 billion losses in beef cattle and dairy in Brazil (Grisi et al., 2014). In Mexico, annual losses inflicted by *R. microplus* were estimated at $573 million (Rodríguez-Vivas et al., 2017). In the U.S. FY20, $100 million dollars were directed for Cattle Health according to the United States Department of Agriculture (USDA), and includes $13.5 million for CFT containment and eradication. CFTs cost approximately $130 million in the U.S. every year in the 19th century (Graham and Hourrigan, 1977), which is equivalent to $3 billion today (Busch et al., 2014). The Cattle Fever Tick Eradication Program (CFTEP) declared *R. microplus* was eradicated in the U.S. by 1943 (Graham and Hourrigan, 1977), except in the permanent tick eradication quarantine area (TEQA) along the Texas-Mexico border. *R. microplus* is endemic in Mexico, and stray animals and wildlife that cross the US border pose a constant threat to the Texas cattle industry (Miller et al., 2007; Thomas et al., 2020). Outbreaks both inside and outside of TEQA were detected every year; from 2014-2017, 44 % of tick outbreaks happened in premises outside of the TEQA (Thomas et al., 2020). It is estimated that 55 % of beef cows, valued $96 billion in 2020 by USDA[1], will be in danger if the CFT returned to the regions of its historical range (Anderson et al., 2010).

[1] https://data.ers.usda.gov/reports.aspx?ID=17832

1.1.3. Pest management strategies

1.1.3.1. Control of *Aedes aegypti* mosquito

The prevention of vector-borne diseases mainly relies on vector control because of the absence of vaccines to fully protect humans and livestock (Benelli, 2019). For mosquitos, there are only two classes of adulticides approved for public health use in the United States[2]. These adulticides are pyrethroids and organophosphates, both targeting the nervous system at the voltage-gated sodium channel and acetylcholine esterase, respectively. The widespread use of pyrethroids and organophosphates has led to increasing resistance in the global mosquito *Ae. aegypti* population at various level (Moyes et al., 2017; Smith et al., 2016). A study in Iquitos, Peru, used deltamethrin (a pyrethroid) treated curtains in response to outbreaks of dengue which had resulted in an increased disease infections rate in the local community and development of pyrethroid resistance in the mosquito population within as short as six months (Lenhart et al., 2020). In Brazil, a study showed that resistance to pyrethroids in an *Ae. aegypti* population remains at high level despite ten years of suspended use of this type of insecticides in the public mosquito control program (Macoris et al., 2018). These situations emphasize the urgent need for novel pesticide targets and for insecticides that are safe for mammals.

Other alternative approaches for control are available such as eco-friendly botanical insecticides (Chellappandian et al., 2019), and attractive toxic sugar baits for controlling adult mosquitoes (Sissoko et al., 2019). Some strategies target mosquito larvae, including biocontrol using *Bti* (*Bacillus thuringiensis israelensis*) toxin (Boyce et al., 2013) and mosquito-eating fish. However, none of above strategies is fully effective by itself (Benelli, 2019). For long-term management strategies, genetic modification using sterile insect technique (SIT) is considered as

[2] https://www.epa.gov/mosquitocontrol/controlling-adult-mosquitoes

a future trend in global mosquito control (Bouyer et al., 2020). A *Wolbachia*-based SIT technique shows desired efficiency in reducing *Ae. aegypti* population under laboratory conditions (Joubert et al., 2016). However, a standardized risk control protocol of SIT for mosquito control is currently lacking (Bouyer et al., 2020). The World Health Organization emphasizes the urgent need for novel mosquito control strategies (WHO, 2017).

1.1.3.2. CFT control in the United States

The commercial vaccines such as Bm86-based (a glycoprotein antigen on the midgut of *R. microplus*) TickGard® and Gavac™ are used for CFT control in Cuba and New Zealand. In the U.S., only recently, the development of a new formulation of the Bm-86 vaccine allows integrating a vaccine as part of the operations of the CFTEP in the permanent quarantine zone in the U.S. (Pérez de León et al., 2018). Anti-tick vaccine development is slow and does not provide 100% tick killing efficiency (de la Fuente and Contreras, 2015).

Environmental control is an important part of the integrated pest management strategy implemented in the quarantine zone. It integrates surveillance and quarantine (Pérez de León et al., 2012). The cattle herds are under surveillance by the U.S. Department of Agriculture-Animal Plant Health Inspection Service-Veterinary Service division (USDA-APHIS-VS) as part of the CFTEP. The responsibility of the patrol is to quickly eliminate cattle fever tick incursions from Mexico, either on imported cattle or wildlife crossing the border. The CFTEP also enforces inspection and precautionary acaricides treatment on livestock in the permanent quarantine zone. Current surveillance outside of the quarantine zone continues to be based on ranch owners and veterinarians reporting the presence of the tick to the Texas Animal Health Commission (TAHC) and the USDA. If a property is suspected to be infested with cattle fever ticks, then a temporary quarantine is set up. In this situation, cattle from this property are not to be sold or moved to

another property until the animals are treated and shown to not have the ticks for 14 days. Once the cattle are deemed to be tick-free and sold, no new animals are allowed on the land for 6-9 months (Pérez de León et al., 2012). In recent years, due to the spread of cattle fever ticks in Texas, the Texas Animal Health Commission had to expand surveillance and control efforts throughout the state.

The current response to tick infestations still heavily relies on the application of acaricides of a few classes including pyrethroids, organophosphates, amidine (amitraz), phenylpyrazole (fipronil), and macrocyclic lactones (ivermectin, moxidectin) (Rodriguez-Vivas et al., 2018). In addition, intensive application of pesticides results in excessive pesticide residues in meat and milk products and increased tick resistance. Acaricide resistance to commonly applied acaricides is detected in tick population worldwide including the U.S., in some cases, resistance is due to multiple molecular mechanisms (Li et al., 2003, 2004; Rodriguez-Vivas et al., 2018). The *R. microplus* tick resistance to pyrethroids was first detected in 2007 in the U.S. (Miller et al., 2007), in ten years, the resistance has increased by 7.5-fold in the Texas tick populations (Thomas et al., 2020). Thus, research on validating new molecular targets that could serve for developing new selective insecticides and acaricides is needed. Invertebrate-specific G protein- coupled receptors are promising targets for novel target-specific vector control. The success of commercial acaricide amitraz (a formamidine) which acts by binding to the tick octopamine receptor represents the proof-of-principle for invertebrate-specific GPCRs as successful targets for vector control (Sparks and Nauen, 2015).

1.2. G protein-coupled receptors

G protein-coupled receptors (GPCRs) are the largest family of cell surface receptors in many organisms (Hanlon and Andrew, 2015). The neuropeptide hormones GPCRs are particularly important in regulating key physiological processes such as development, reproduction, and behavior (Hauser et al., 2006). GPCRs share the common structural feature of seven transmembrane (7TM) regions, an extracellular N-terminus and an intracellular C-terminus. These proteins are categorized into six major classes (or families): A (Rhodopsin), B1 (Secretin), B2 (Adhesion), C (Glutamate), F (Frizzled) and Taste 2 (Pándy-Szekeres et al., 2018). GPCRs interact with different types of ligands, including photons, ions, biogenic amines, peptide and non-peptide neurotransmitters, and hormones (Zhang and Xie, 2012). Human GPCRs are the targets of about 34% of marketed therapeutic drugs (Hauser et al., 2018). Further, 50% of the marketed drugs targeting peptidergic GPCRs are small molecules (Wu et al., 2017). Arthropod GPCRs are of great interest as novel targets for pesticide development (Audsley and Down, 2015; Duvall, 2019; Ohta and Ozoe, 2014; Pietrantonio, P.V. et al., 2018; Sharan and Hill, 2017).

1.2.1. Receptor classification and signaling pathway

GPCRs couple to heterotrimer G proteins (Gα, Gβ, and Gγ) to transmit downstream signals. Upon agonist binding, receptors catalyze the exchange of guanidine diphosphate (GDP) for guanidine triphosphate (GTP) on the Gα subunit, leading to the disassociation of the Gα subunits from the dimeric Gβγ subunits. Both Gα and Gβγ subunits can modulate activities of downstream effectors. Four different Gα proteins induce different secondary messengers (Fig. 1.1). GPCRs coupled to $G\alpha_s$ and $G\alpha_{i/o}$ proteins activate or decrease, respectively, the intracellular 3', 5'-cyclic adenosine monophosphate (cAMP) level through adenylate cyclase

(AC), which converts adenosine triphosphate (ATP) to cAMP; GPCRs coupled to $G\alpha_{q/11}$ induce calcium release from the endoplasmic reticulum calcium stores through the phospholipase C (PLC)-inosititol-1,4,5-triphosphate (IP_3) pathway; GPCRs coupled to $G\alpha_{12/13}$ activate RhoGTPase nucleotide exchange factors (Hilger et al., 2018). G protein activation is terminated upon hydrolysis of the GTP to inactive GDP, followed by reassociation of $G\alpha$ to $G\beta\gamma$ dimer (Hilger et al., 2018).

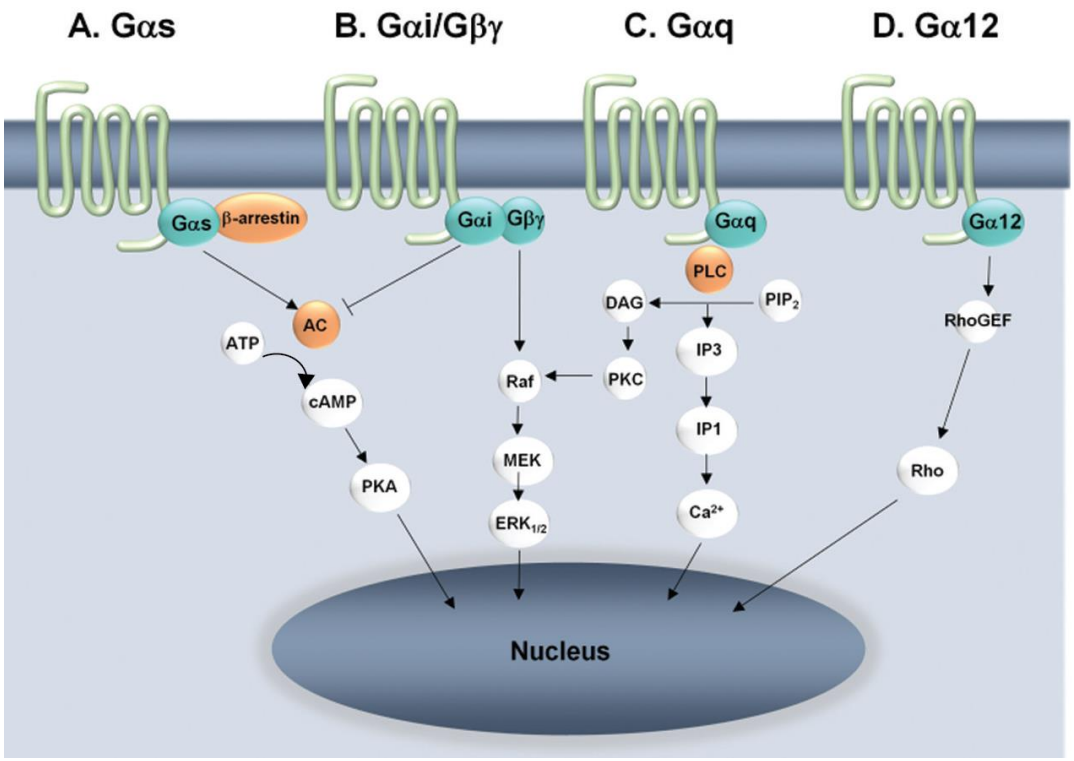

Figure 1.1 Schematic diagram showing four G protein-coupling mechanisms Sharan and Hill (2017),[3] reprinted with permission.
(A: $G\alpha_S$, B, Gαi: C: $G\alpha_{q/11}$ and D, $G\alpha_{12/13}$) recognized in mammals and corresponding cAMP, MAP/ERK, PLC/IP_3 and Rho-dependent signaling pathways. Molecular components comprising these pathways are shown: G protein-coupled receptors (green), G proteins (aqua), effector molecules (orange) and enzymes (white). AC, adenylyl cyclase, ATP, adenosine triphosphate; cAMP, cyclic adenosine monophosphate; DAG, diacylglycerol; ERK, extracellular signal-regulated kinase; IP1, inositol phosphate; IP_3, inositol trisphosphate; MEK (MAPKK), mitogen activated protein kinase kinase; PKA, protein kinase A; PKC, protein kinase C; PIP_2, phosphatidylinositol 4,5-bisphosphate; PLC, phospholipase C; Raf, RAF kinase; Rho, Rho GTPase, RhoGEF, Rho guanine nucleotide exchange factor for Rho/Rac/Cdc42-like GTPases.

[3] Adapted with permission from (Sharan, Shruti, and Catherine A. Hill. "Potential of GPCR-targeting insecticides for control of arthropod vectors." *Advances in Agrochemicals: Ion Channels and G Protein-Coupled Receptors (GPCRs) as Targets for Pest Control: Volume 2: GPCRs and Ion Channels*. American Chemical Society, 2017. 55-84. Copyright (2017) American Chemical Society.

A different mechanism exists to attenuate GPCR signaling. Activation of the GPCRs triggers a G protein-independent signaling pathway which terminates the activation. GPCRs are phosphorylated by specific GPCR kinases (GRKs) and then couple to β-arrestins. This eventually leads to receptor desensitization and internalization (Hanlon and Andrew, 2015; Hilger et al., 2018).

1.2.2. Ligand identification

The deorphanization of a GPCR is the process of receptor-ligand pair identification. The most common approach for ligand identification is through the use of heterologous expression systems such as *Xenopus* oocytes, or Chinese hamster ovary (CHO-K1), or human embryonic kidney (HEK293) mammalian cells (Hauser et al., 2006). These systems allow identification of the ligand-receptor pair by screening potential ligands on specific recombinantly expressed GPCRs. The downstream messengers (Ca^{2+} or cAMP) are measured to represent the activation of the receptor. The process of GPCR functional validation can be achieved by both forward and reverse pharmacological approaches (Frooninckx et al., 2012; Pietrantonio, P.V. et al., 2018). The forward approach involves validation of known ligands either purified from tissue or synthesized molecules for specific GPCRs based on prior knowledge, while the reverse approach employs the screening of random chemical libraries on the receptor. These approaches will be discussed in section 1.4.

1.3. Invertebrate-specific kinin signaling system

Kinin is an ancient signaling neuropeptide which is present in the Mollusca, Crustacea, Insecta, and Acari (Cox et al., 1997; Dircksen, 2013; Pietrantonio, P.V. et al., 2018). Kinins were first isolated from the Madeira cockroach *Leucophaea maderae* and named for both, the insect genus and their hindgut myotropic activity, as leucokinin neuropeptides (Holman et al., 1986).

The ‘leucokinin’ and ‘kinin’ names are interchangeable, and in this chapter, I will use ‘kinin’ to be consistent except when ‘leucokinin’ was used in the cited publication. Years after their initial discovery kinins are recognized as multifunctional peptides acting at the central and peripheral levels. They regulate diuresis, feeding and meal size, sensory sugar perception and ecdysis; these functions will be reviewed in section 1.3 below. Kinins are widely distributed in insects, and at least 299 kinin isoforms have been identified in various insect species in different orders according to the nEUROSTRESSPEP database (Yeoh et al., 2017).

Despite the wide distribution of the kinin signaling system in invertebrate, it is lost in coleopterans (Derst et al., 2016). In addition, the sequence of the kinin gene is more variable compared to other neuropeptides within Hymenoptera. The kinin gene has not been found in any ant species so far. It is also absent in the parasitic wasp, *Nasonia vitripennis*, and is weakly expressed in the workers of the honey bee, *Apis mellifera* (Calkins et al., 2018; Veenstra et al., 2012). There are no homologous kinins or kinin receptors in vertebrates. The closest mammalian GPCRs with ~30% sequence similarity with tick and mosquito kinin receptor are neurokinin receptors, which are the homologous to invertebrate tachykinin receptors (Poels et al., 2009).

The arthropod specificity, the small size of the endogenous ligand that makes them amenable to small molecule interference, and the pleiotropic functions in insects make the kinin receptor a promising target for pest control (Pietrantonio, P.V. et al., 2018).

Three endogenous mosquito kinins (aedeskinin 1-3) were isolated and validated on the *Ae. aegypti* mosquito for canonical biological activities: diuretic activity on Malpighian tubules (MTs) and contractile activity on the hindgut (Veenstra, 1994; Veenstra et al., 1997b). Due to the lack of a genome of any insect species in the late 1990’s, the canonical kinin receptor was cloned using degenerate primers (GenBank: AAT95982) and functionally validated almost a decade

later by Pietrantonio, P.V. et al. (2005). In the most updated genome of *Ae. aegypti* (Matthews et al., 2018), only one kinin receptor gene is predicted and two transcript variants of the gene are identical in the protein coding regions, therefore, there is only one kinin receptor protein expressed in *Ae. aegypti* (Matthews et al., 2016). The homologous kinin receptor in our target tick species *R. microplus* (GenBank: AF228521) was also cloned (Holmes, S.P. et al., 2000) and was functionally validated with insect kinin analogs (core pentapeptide and hexapeptide) and muscakinin because the sequence of endogenous kinins from *R. microplus* were unknown (Holmes, S.P. et al., 2003; Taneja- Bageshwar et al., 2006). While the *R. microplus* genome is less well-annotated (Barrero et al., 2017), there is also only one functional kinin receptor identified so far (Holmes, S.P. et al., 2000).

1.3.1. Kinin neuropeptide biosynthesis and structure

Neuropeptides are generated from larger peptide precursors. Cell-specific gene transcription leads to the expression of neuropeptide in a time-, and space-specific manner (Nässel, 2002). The kinin precursors encode variable numbers of kinin paracopies, from one copy in *Drosophila melanogaster* to 15 paracopies in the kissing bug, *Rhodnius prolixus* (Bhatt et al., 2014). After removal of the signal peptide, the active peptides are obtained by processing the propeptide at dibasic cleavage sites. The predominant enzyme cutting sites on the insect neuropeptide precursors are Lys-Lys, Arg-Lys, or Arg-Arg pairs (Veenstra, 2000). After cleavage, the peptides can undergo posttranslational modification, such as amidation on the carboxyl terminus (Nässel, 2002). The kinin peptide features an evolutionarily conserved C-terminal pentapeptide Phe-X^1-X^2-Trp-Gly-NH_2, where X^1 = His, Asn, Ser, or Tyr and X^2 = Ser, Pro, or Ala

(Holman et al., 1990; Torfs et al., 1999a). This C-terminal pentapeptide kinin core is the minimum sequence required for full activities in tissue assays, myotropic activity (hindgut contraction) in cockroach *L. maderae* and diuresis in the cricket *Acheta domesticus* (Nachman et al., 1995; Nachman and Holman, 1991a). Using the alanine scan, previous studies revealed that the Phe^1, Trp^4 and the C-terminal amide of the insect kinins are key positions for activating the kinin receptor, while the variable position 2 (X^2 in the above sequence) tolerates a wide range of chemical characteristics. These changes could be from acidic to basic residues, and from hydrophilic to hydrophobic, although the most potent peptides had aromatic residues at this position (Nachman et al., 1995; Taneja- Bageshwar et al., 2006).

1.3.2. Kinin receptor signaling pathway

The kinin receptor is a neuropeptide GPCR which signals through a Ca^{2+}-dependent pathway and has no effect on cAMP or cGMP production (Holmes, S.P. et al., 2003; Radford et al., 2002). Activation of the kinin receptor leads to an increase in the production IP_3, which activate the IP_3-gated calcium channel on the membranes of intracellular calcium stores, causing intracellular calcium release (Lu et al., 2011d). The kinin receptor expressed in stellate cells of MTs induces Ca^{2+} release upon activation, which stimulates Cl^- channels and increases the transport of Cl^- and water from the hemolymph into the MT lumen space (Cabrero et al., 2020; Lu et al., 2011a).

1.3.3. Distribution and function of kinin signaling system

1.3.3.1. In the model organism *Drosophila melanogaster* (Insecta)

The distribution and function of the kinin signaling system were extensively investigated in the model organism *D. melanogaster* and were recently reviewed by Nässel and Zandawala (2019). As the model organism, the availability of various mutant *Drosophila* strains and gene-driven systems facilitates the characterization of kinin functions in a tissue- and time-specific manner. Using immunolabeling and GAL-4 gene driven lines, the expression of the leucokinin gene was mapped in detail on the central and periphery nervous system (de Haro et al., 2010; Nässel, 2002). Leucokinin is expressed in the CNS of both adult and larva *Drosophila*; leucokinins neurons are distributed in the brain lateral horn, suboesophageal ganglion (gustatory center), and abdominal ganglion (de Haro et al., 2010). It is assumed that leucokinins are released primarily from abdominal ganglion neurons into the hemolymph as hormones and reach target sites such as hindgut and renal organs of adult *Drosophila*. In addition, leucokinin is expressed in peripheral organs including sensory cells in the sensilla on wings, femurs, and tarsi, as well as corpora cardiaca, and probable endocrine cells in the midgut of adult and taste organs from pharyngeal and labella regions of the mouthpart (de Haro et al., 2010; Nässel and Zandawala, 2019).

According to FlyAtlas, the leucokinin receptor (LKR) is expressed in the hindgut, MTs, and CNS of both larva and adult (Chintapalli et al., 2007; Nässel and Zandawala, 2019). LKRs expressed in the neurons and neurosecretory cells of CNS and they are responsible for regulating pre-ecdysis (Kim et al., 2006), stress responses (Zandawala et al., 2018), feeding (Al-Anzi et al., 2010), metabolism through insulin producing cells (Yurgel et al., 2019), and sleep activity patterns (Nässel and Zandawala, 2019; Yurgel et al., 2019), as well as larval locomotion

(Okusawa et al., 2014). LKRs expression in peripheral tissues such as MTs, hindgut, and chemosensory cells suggests their function, respectively, in water balance, gut function, and chemosensory modulation (Cabrero et al., 2020; Charroux et al., 2020; López-Arias et al., 2011; Zandawala et al., 2018). LKRs expressed in larval tracheal epithelial cells are involved in tracheal clearance and air-filling during the larval molting process (Kim, D.-H. et al., 2018b). In addition, LKR is also expressed in the neurons along the wing margins, they are found to modulate the defensive behavior post mating (Liu et al., 2020). LKRs are also detected in the spermatheca of female *Drosophila* (Chintapalli et al., 2007; Nässel and Zandawala, 2019).

1.3.3.2. In mosquitoes (Insecta)

In *Ae. aegypti* mosquitoes, kinin receptors (KRs) were immunolocalized in the stellate cells of the MTs, midgut endocrine cells, rectal papillae cells, in the gustatory neurons in prothoracic tarsi and in accessory cells of long sensilla in the distal labellum (Kersch and Pietrantonio, 2011; Kwon et al., 2016; Lu et al., 2011a). Mosquitoes take up large volume of blood during blood feeding, therefore, fluid secretion and digestion post blood-feeding regulated by hormones are fundamental adaptations for their survival (Adams, 1999; Wheelock et al., 1988). RNAi knock-down of the KR expression decreases the post-blood feeding fluid excretion in intact females of *Ae. aegypti* (Kersch and Pietrantonio, 2011), highlighting the role of kinins in the success of blood feeding adaptation. The KRs expressed in the midgut endocrine cells are likely to be involved in gut functions such as digestive enzyme release, as found in the larvae of *Opisina arenosella* (Lepidoptera), in which leucokinins are involved in regulating the release of digestive enzymes (Harshini et al., 2002). In addition to blood-feeding, kinins also modulate mosquito sugar-feeding by modulating the chemosensory neuron housed in the tarsi and mouthparts. A kinin analog (known as Aib-K-1; ID 1728, (Taneja-Bageshwar, Suparna et al.,

2009)) activates the kinin receptor expressed on chemosensory neurons in labella and elicites aversive behavior to sugar feeding in female mosquitoes (Kwon et al., 2016). This study found that this kinin analog regulates sugar feeding behavior by inhibiting the electrical neuron responses to the sucrose solution containing the analog. Starved female mosquitoes would fly- or walk-away from the sugar water containing the kinin analog upon contact, while this avoidance behavior is eliminated in KR-silenced mosquitoes (Kwon et al., 2016). A similar kinin-mediated aversive feeding behavior is observed in *Drosophila.* This aversive behavior is mediated by kinin through regulation of gustatory receptors. However, *Drosophila* can overcome the kinin mediated anti-feeding behavior when it is starved (Charroux et al., 2020). All the findings described above suggest kinins play key roles in the key physiological functions of mosquitoes, therefore, this signaling system is a promising target to interfere with mosquito physiology and feeding behavior.

1.3.3.3. In ticks (Acari)

The transcript expression level of kinin and kinin receptor seems to be low in ticks, as their transcripts are not detected in the salivary gland transcriptomes of *R. microplus*, *Ixodes scapularis* (Ixodidae) and *Ornithodoros turicata* (Argasidae) (Egekwu et al., 2016; Egekwu et al., 2014; Gulia-Nuss et al., 2016). Nevertheless, 16 paracopies of kinins were predicted from the genome of the blacklegged tick, *Ix. scapularis* (Šimo et al., 2014). In the tick *Ix. ricinus*, leucokinin (LK)-immunoreactivity is detected in four neurons on each side of the bilateral cheliceral ganglion (Neupert et al., 2005), in the same study, the authors also identified similar LK-immunoreactivity patterns in homologous cells of the cheliceral ganglion in *R. microplus*. Later, a similar distribution of LK-immunoactivity was found in *R. appendiculatus* (Šimo et al., 2009). Using RT-PCR (reverse transcription polymerase chain reaction), LKR was found

expressed in all life stages of *R. microplus* including egg, larva, and nymph (Holmes, 2004). In the adult, LKR mRNA is detected the ovary, synganglia, salivary gland and MTs (Holmes, 2004). The immunochemistry with LKR-antibody confirms the expression of LKR in the midgut basal thin muscle layer (Brock et al., 2019a), which points to a potential myotropic activity. When the expression of LKR is knocked-down by RNAi, the female *R. microplus* shows a significant decrease in reproductive fitness, manifested as a reduction in the weight of the egg mass and in the hatching rate. In addition, a phenotype with discolored midgut is found (Brock et al., 2019a). Yet the mechanism causing this phenotype, and the function of kinins in ticks are largely unknown.

1.3.4. Bioassays to validate ligand activity

In non-model organisms, the functional validation of neuropeptides and GPCRs primarily utilize two approaches, as summarized in Pietrantonio, P.V. et al. (2018) (Fig. 1.2): 1) a chemical approach by testing the candidate ligands in tissue or *in vivo* bioassay; 2) a reverse genetic approach by silencing target receptor or neuropeptides to determine the phenotypes. In our target pests, the function of kinin receptors were revealed primarily through the reverse approach as discussed in the last section. Nevertheless, functional validation of endogenous or synthetic ligands in bioassays is necessary. Here I will discuss some bioassays that can potentially be used or be modified to help validate the novel ligands of kinin receptors for their physiological activities in mosquitoes and ticks.

In addition to bioassays that help validate the ligand biological activity, novel ligands should be evaluated for their direct impacts on the longevity and/or mobility of target pests. This is an essential step for the downstream development and optimization of ‘lead’ molecules for

pest control (Hill et al., 2013; Pietrantonio, P.V. et al., 2018; Sharan and Hill, 2017). Some classical mortality bioassays and stress tolerance assays are reviewed below.

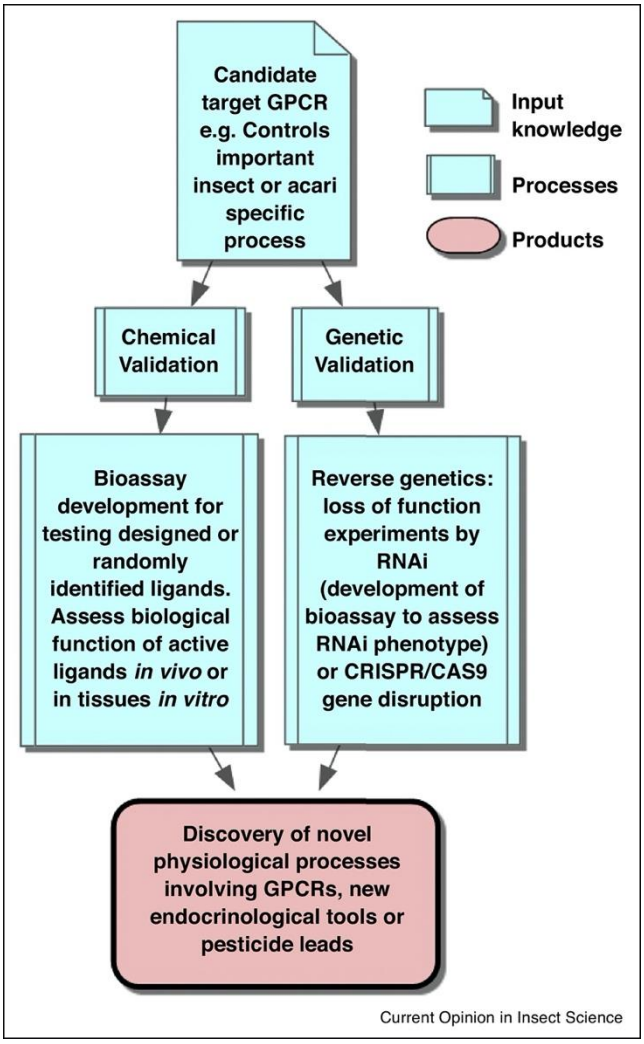

Figure 1.2 Key elements of GPCR target validation.
For chemical validation of a GPCR as a candidate target, the designed or identified ligand that is active on the recombinant receptor is applied in vivo and in tissues in vitro. Bioactivity must be determined, either as mortality or by another adverse biological effect derived from its action as antagonist (i.e. paralysis) or as superagonist (i.e. increased diuresis, dessication). For genetic validation, `loss of function' experiments most typically (i.e. RNAi), or 'gain of function' experiments (gene overexpression or ectopic expression) (Prelich, 2012), must confirm the disruption of receptor function has a measurable effect. Through these processes, we validated stable potent peptidomimetics for, and discovered novel functions of the kinin receptor. Figure credits and source: Pietrantonio, P.V. et al. (2018).

1.3.4.1. Mosquito bioassays

The pleiotropic functions of kinins in mosquito were elucidated as discussed above. A variety of mosquito bioassays, including tissue and live mosquito bioassays, are already available for validating the biological effects of novel ligands of the kinin receptor. Some examples are: 1) Myotropic activity by the mosquito hindgut tissue contraction assay (Kwon and Pietrantonio, 2013; Odland and Jones, 1975); 2) Diuretic activity by a Ramsay assay to measure the fluid secretion of the isolated Malpighian tubule upon stimulation by diuretic peptides or small molecule surrogates of these peptides (Kwon et al., 2012); 3) Diuretic activity by an *in vivo* humid chamber fluid excretion assay to measure diuresis of the live mosquito post blood meal in real time (Kersch and Pietrantonio, 2011); 4) Feeding modulation activity by a no-choice capillary feeding (CAFÉ) assay and non-choice or choice feeding assays in Petri dishes to observe behavioral responses and/or diuresis by using Evans blue in the sucrose feeding solution and counting blue droplets (Kwon et al., 2016).

1.3.4.2. Tick bioassays

Given the likely immunolocalization of LKR in the *R. microplus* midgut muscular layers and the discolored midgut phenotype obtained in LKR-RNAi females (Brock et al., 2019a), it is plausible that kinins may preserve the canonical myotropic activity in ticks as in insects, and may also may be involved in gut digestion function. The tick hindgut is innervated by peptidergic synganglion neurons: both mass-spectrometry signal and immunoactivity of myoinhibitory peptide (MIP), SIFamide, orcokinin, FGLa/AST (alatostatin) peptides were detected in the hindgut of unfed *Ix. scapularis* females (Šimo and Park, 2014). However, the kinin peptide signal was not detected in the mass spectrometry analysis of the hindgut tissue. The temporal analysis of neuropeptides in tick tissues will be useful for better understanding the function of

tick neuropeptides. Nevertheless, the tick hindgut contraction assay developed by Šimo and Park could be used for validating the kinin myotropic activity on the *R. microplus* hindgut potentially acting as neurohormones (Šimo and Park, 2014). The authors confirmed the myotropic activity of SIFamide and myoinhibitory activity of MIP in *Ix. scapularis* using this hindgut contraction assay (Šimo and Park, 2014).

Similar to what was found in *R. microplus,* the leucokinin receptor transcripts are the most abundant in the gut and salivary glands in the brown dog tick, *R. sanguineus* (Holmes, 2004; Lees et al., 2010). Tick salivary glands are the primary organs for maintaining osmotic balance and secrete excessive water and ions during blood feeding (Šimo et al., 2014). In unfed *Ix. scapularis* females, the pair of salivary glands is innervated with neurons that produce a variety of neuropeptides including MIP, SIFamide, elevenin, neuropeptide pigment dispersing factor (PDF), and orcokinin (Kim, D.-H. et al., 2018b; Vancová et al., 2019). Kinins are diuretic peptides in various species of insects and are involved in mosquito diuresis post blood feeding (Halberg et al., 2015; Kersch and Pietrantonio, 2011; Veenstra, 1994), it is possible that the kinin receptors on tick salivary glands could be activated during blood feeding. Therefore, the modified Ramsay assay developed by Kim et al. (2014) with isolated salivary glands to measure the fluid secretion of salivary gland can measure the potential fluid secretion evoked by kinin or kinin analogs. Furthermore, Rhopr-kinin is found to stimulate contractions of salivary gland of the blood-feeding kissing bug, *R. prolixus*, at 5×10^{-8} M using a impedance converter (Orchard and Brugge, 2002). Similar tissue contraction assays can be used to test whether kinins have similar activity in salivary glands of ticks.

1.3.4.3. Bioassays for evaluating pesticidal activities

After identification of potent ligands of the target receptor, the pesticidal activity of the compound can be evaluated. A mosquito larval bioassay using 3rd instar larvae in 24-well plates was utilized to test the toxicity of small molecule ligands of the mosquito dopamine receptor. The mortality was observed from 1-72 h at every few hours after addition of the tested compounds (Hill et al., 2013). For ticks, acaricidal activity is evaluated by larval immersion test (LIT) and/or adult immersion test (AIT), the former assay has been used as a sensitive assay for acaricide efficacy (Adenubi et al., 2018; Klafke et al., 2006). Other alternative bioassays are available including membrane blood feeding bioassays, repellency, and behavior bioassays, the advantages and disadvantages of these bioassays were reviewed by Adenubi et al. (2018).

The kinin signaling system in *D. melanogaster* is known to modulate physiologically stressful conditions such as desiccation and starvation. LKR-mutant strains showed higher survival rate than the wild strain either under starvation or desiccation (Zandawala et al., 2018). Consistent with these results, in an independent study which tested the effects of kinin analogs on stress responses of *Drosophila*, microinjection of a kinin analog (2139-AC) reduced the survival rate of *D. suzukii* under desiccation stress (Alford et al., 2019a). However, this analog significantly increased the survival rate of starved female *D. suzukii* (Alford et al., 2019a). Aphids (*Myzus persicae* and *Macrosiphum rosae*) treated with kinin analogs also show decreased survival rate under condition of desiccation, starvation and cold stress (Alford et al., 2019b). These findings suggest that kinins are involved in regulating stress tolerance. Similar stress tolerance bioassays can be used to evaluate the insecticide activity of kinin analogs and/or novel small molecule ligands.

1.4. Novel ligand discovery through high-throughput screening

Current drug discovery approaches for the identification of new compounds that activate or inhibit GPCRs integrate molecular informatics, structural biology, combinatorial library design, and high-throughput screening (HTS) (Phatak et al., 2009). The lack of crystal structures for insect or tick GPCRs is a major obstacle for conducting in silico screens and for the rational design of active ligands targeting these receptors. This is why despite well-characterized physiological roles of invertebrate neuropeptide GPCRs, progress in exploring them as targets for vector control has been slow.

HTS involves assay development, miniaturization, and automation. The details of each step were reviewed by Hansen and Bräuner-Osborne (2009). The goal of HTS is to identify hit molecules that can modulate receptor functions. Hit molecules can primarily be identified as agonist, antagonist, partial agonist, or partial antagonists through a commonly used two-addition HTS assay (Ma et al., 2017). The selection of GPCR to initiate a HTS should meet the criteria of having a small molecule ligand. For example, the kinin core is only 5 amino-acid residues long. The "Lipinski rule of five" which defines small molecules for therapeutic purposes (oral drugs <500 Da) (Lipinski, 2016) is an important criterion because small peptides may have lesser interactions with the receptor and thus, it should be easier to design or randomly screen libraries to find a small synthetic molecule as ligand that may have commercial potential as lead compounds.

1.4.1. Cellular functional assays for HTS

In the early days of GPCR discovery, the most commonly used assay to characterize ligand-receptor interactions was the receptor binding assay which provided important information on the ligand affinity for invertebrate GPCRs (Meeusen et al., 2003). The advantage

of this assay is its accuracy and low interference from the downstream signaling events, but it cannot demonstrate the functional activation of the receptor, therefore, a secondary functional assay is required. For human GPCRs, most functional assays that detect the GPCR activation measure certain molecular events primarily in two major signaling pathways: G protein-dependent and G protein-independent pathways. G protein-dependent assays measure GTPgS (a non-hydrolyzable or slowly hydrolyzable G protein-activating analog of guanosine triphosphate), Ca^{2+}, inositol triphosphate (IP_3), or cAMP concentrations, while G protein-independent assays detect primarily the receptor trafficking, or b-arrestins recruitment (Hansen and Bräuner-Osborne, 2009). Different assays utilize different technologies for readouts, such as Ca^{2+}-sensitive dyes (fluorescence assays), photoproteins such as aequorin (Ca^{2+} bioluminescence assays), tagged fluorescence proteins, Förster resonance energy transfer (FRET)-based assay, bioluminescence resonance energy transfer (BRET)-based assay, or label-free optical biosensors-based cellular assays, etc. These assays and corresponding available readout technologies were reviewed in detail by Zhang and Xie (2012). Some assays are applicable to any GPCR and some are specific to certain GPCRs (*eg*, Ca^{2+} assay for $G\alpha_q$-coupled receptors, cAMP for $G\alpha_{i/o}$- or $G\alpha_s$- coupled receptors). However, by promiscuously co-expressing certain G proteins with the receptor in the recombinant cells the signaling pathway can be altered. For example, $G\alpha_{q15/16}$ proteins can be co-expressed with non-Gq-coupled receptors for PLC-IP_3-Ca^{2+} signaling detection (Hansen and Bräuner-Osborne, 2009; Offermanns and Simon, 1995). In contrast to the assay which measures a single molecular event, there are high content analysis assays which collect massive biological data to improve the ligand specificity. This type of assay is also more complex and expensive to perform (Hansen and Bräuner-Osborne, 2009).

In invertebrate research, the most widely functional assays detect GPCR activation by analyzing the concentration fluctuation of the second messengers, such as Ca^{2+} and cAMP. Due to the distant differences in the signaling pathways between mammals and invertebrates, most of the other above-mentioned techniques have not been adopted for invertebrate GPCR studies. However, Gα-proteins are relatively conserved across the animal kingdom. Recently, Lismont et al. (2020) demonstrated that some human BRET-based Gα-protein biosensors can also be adapted to detect the activation of an insect GPCR when co-expressed in the receptor recombinant cells. By co-expressing each of different Gα protein-based biosensor ($G\alpha_s$, $G\alpha_{i/o}$, $G\alpha_{q/11}$, or $G\alpha_{12/13}$) with specific GPCR, the G protein-coupling mechanism can be elucidated. In this study, the authors found Schgr-CRF-DH could dose-dependently activate $G\alpha_{i/o}$ and $G\alpha_{q/11}$ biosensors and did not activate $G\alpha_s$ and $G\alpha_{12/13}$ biosensors. This finding provides new technologies for characterizing the G proteins coupling mechanisms of insect GPCRs.

1.4.2. Novel small molecules ligands discovery for pest control

There are only two published studies of HTS performed in academic settings for novel ligand discovery on arthropod vector GPCR targets. A novel small molecule agonist of the mosquito neuropeptide Y (NPY) receptor was identified through HTS and the hit molecule was able to suppress mosquito biting behavior in a cage feeding assay (Duvall et al., 2019). Another study targeted the invertebrate dopamine receptor, a biogenic amine GPCR, that was subjected to HTS with target-specific libraries, and antagonists exhibiting considerable toxicity to mosquito larvae were discovered (Ejendal et al., 2012; Hill et al., 2016).

The kinin receptor is a promising target for interfering with pest physiology as discussed in the above sections. However, there is a gap between the current knowledge in kinin functions and available tools to be integrated in real pest management strategies. The goal of this study

was to fill this gap by identifying novel ligands of the kinin receptor, which would feature improved ligand activity and/or enhanced biostability and bioavailability. Furthermore, this study also aimed to improve the understanding of neuropeptide kinin signaling system in insects and ticks through the process of validating the functional activity and pesticidal activity of these novel ligands.

The dissertation includes multidisciplinary research that was published in peer-reviewed journal articles with multiple collaborators as co-authors (Chapters 2-5). I mention in each chapter the work I performed and the contributions of other collaborators. Chapter 2 deals with the characterization of activity of insect kinins and insect kinin analogs on the tick and mosquito recombinant kinin receptors using a calcium bioluminescence assay in the 96-well plate. Of note is the new regression analyses of potency (EC_{50}) and efficacy (percent maximal bioluminescence at 1 uM) that allowed to rank more active compounds and make some deductions about structure-activity relationships. This is included the characterization of analogs designed based on the mosquito endogenous kinins and analogs that incorporated α-aminoisobutyric acid (Aib) and acetyl- or pyroglutamate-group at the N-terminus for enhancing resistance to peptidase degradation and other analogs that incorporated polyethylene glycol (PEG) polymers to improve cuticle penetration.

In Chapter 3, I investigated the kinin system in ticks in comparison to the insect kinin system. An endpoint calcium fluorescence assay which allows high-throughput screening (HTS) in 384-well plates was developed that complemented the already developed calcium bioluminescence assay in the 96-well plate used in the Pietrantonio laboratory. Using this HTS fluorescence assay and a newly adopted dual-addition protocol (Fig. 1.3).

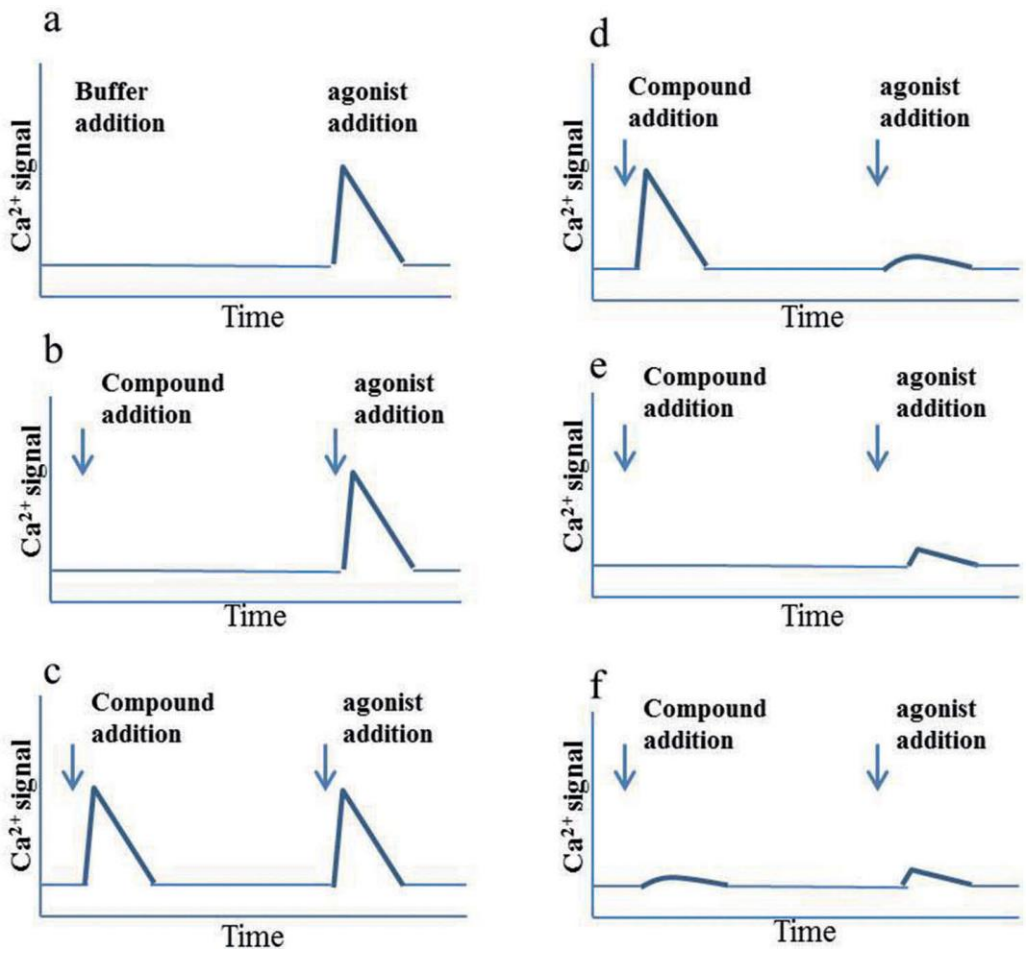

Figure 1.3 Schematic diagram for the 2-addition assay, Ma et al. (2017)[4], reprinted with permission.

In this assay, two sequential additions are performed in a single assay. In the 1st addition, either buffer (a) or screening compounds (b, c, d, e, f) are added. In the 2nd addition, agonist specific to the target GPCR is added (a, b, c, d, e, f). b indicates that compound neither activates the cells nor inhibits the target. c shows that compound activates the cells but the activation is not target-specific. d indicates that the compound specifically stimulates the target receptor. e demonstrates that the compound specifically inhibits the target. f suggests that the compound is a partial agonist for the target.

[4] Reprinted with permission from (Qiang Ma, Lingyan Ye, Hongxia Liu, Ying Shi & Naiming Zhou (2017) An overview of Ca2+ mobilization assays in GPCR drug discovery, Expert Opinion on Drug Discovery, 12:5, 511-523, DOI: 10.1080/17460441.2017.1303473). Copyright (2017) Taylor & Francis

We screened (using serial dilutions) a commercial chemical library composed of fourteen antagonists of the human neurokinin receptors (NK1-3), which is the GPCR with the highest sequence similarity to the kinin receptor. This screen lead to the identification of the first antagonists of the kinin receptor, although of low potency (IC_{50} = 45 μM). In addition, in Chapter 3, I cloned the cDNA of the tick kinin neuropeptide precursor and predicted the sequence of 17 endogenous tick kinins from *R. microplus*. The complete cDNA of this tick kinin precursor allowed us to predict not only the amino acid sequence of the cattle fever tick kinins but also the kinins of other seven tick species. A consensus sequence for tick kinins revealed the conservation of proline (Pro) in the second variable position (X^2) of the C-terminal pentapeptide kinin core.

We then, in Chapter 4, experimentally tested on the recombinant receptor eleven kinin Aib-analogs (Designed by Dr. Ron Nachman) and fourteen of the predicted seventeen endogenous tick kinins. I verified that all were potent agonists on the recombinant *R. microplus* tick receptor using the HTS calcium fluorescence assay developed in the 384-well plate. This was followed by ranking the native tick kinins and Aib-analogs by their potency (EC_{50}). We identified one Aib-analog that has both high activity and enhanced water solubility, expanding the toolbox for tick kinin studies.

Finally, in Chapter 5, I presented the HTS of a library of small molecules on the tick recombinant receptor that allowed us to discover novel kinin receptor antagonists. Here we further optimized the HTS calcium fluorescence assay to allow screening with a single-concentration. Some of the most potent antagonists identified on the tick receptor were validated on the mosquito receptor as antagonists. In the hindgut contraction inhibition bioassay, these molecules inhibited the contractile activity of mosquito hindgut.

1.5 References

Adams, T., 1999. Hematophagy and hormone release. Ann. Entomol. Soc. Am. 92(1), 1-13.

Adenubi, O.T., McGaw, L.J., Eloff, J.N., Naidoo, V., 2018. In vitro bioassays used in evaluating plant extracts for tick repellent and acaricidal properties: a critical review. Veterinary parasitology 254, 160-171.

Al-Anzi, B., Armand, E., Nagamei, P., Olszewski, M., Sapin, V., Waters, C., Zinn, K., Wyman, R.J., Benzer, S., 2010. The leucokinin pathway and its neurons regulate meal size in *Drosophila*. Curr. Biol. 20(11), 969-978.

Alford, L., Marley, R., Dornan, A., Dow, J.A., Nachman, R.J., Davies, S.A., 2019a. Desiccation, thermal stress and associated mortality in *Drosophila* fruit flies induced by neuropeptide analogue treatment. Journal of Pest Science 92(3), 1123-1137.

Alford, L., Marley, R., Dornan, A., Pierre, J.S., Dow, J.A., Nachman, R.J., Davies, S.A., 2019b. Assessment of neuropeptide binding sites and the impact of biostable kinin and CAP2b analogue treatment on aphid (*Myzus persicae* and *Macrosiphum rosae*) stress tolerance. Pest Manag. Sci.

Anderson, D., Hagerman, A., Teel, P., Wagner, G., Outlaw, J., Herbst, B., 2010. Economic impact of expanded fever tick range. Agricultural & Food Policy Center, Texas A&M University, College Station, TX.

Audsley, N., Down, R.E., 2015. G protein coupled receptors as targets for next generation pesticides. Insect Biochem. Molec. 67(Supplement C), 27-37.

Barrero, R.A., Guerrero, F.D., Black, M., McCooke, J., Chapman, B., Schilkey, F., de Leon, A.A.P., Miller, R.J., Bruns, S., Dobry, J., 2017. Gene-enriched draft genome of the cattle tick *Rhipicephalus microplus*: assembly by the hybrid Pacific Biosciences/Illumina

approach enabled analysis of the highly repetitive genome. Int. J. Parasitol. 47(9), 569-583.

Benelli, G., 2019. Managing mosquitoes and ticks in a rapidly changing world–Facts and trends. Saudi journal of biological sciences 26(5), 921-929.

Bhatt, G., da Silva, R., Nachman, R.J., Orchard, I., 2014. The molecular characterization of the kinin transcript and the physiological effects of kinins in the blood-gorging insect, *Rhodnius prolixus*. Peptides 53, 148-158.

Bhatt, S., Gething, P.W., Brady, O.J., Messina, J.P., Farlow, A.W., Moyes, C.L., Drake, J.M., Brownstein, J.S., Hoen, A.G., Sankoh, O., 2013. The global distribution and burden of dengue. Nature 496(7446), 504-507.

Bock, R.E., Jackson, L.A., de Vos, A.J., and Jorgensen, W.K., 2008. Babesiosis of cattle. Cambridge University Press.

Bouyer, J., Yamada, H., Pereira, R., Bourtzis, K., Vreysen, M.J., 2020. Phased conditional approach for mosquito management using sterile insect technique. Trends Parasitol. 36(4), 325-336.

Boyce, R., Lenhart, A., Kroeger, A., Velayudhan, R., Roberts, B., Horstick, O., 2013. *Bacillus thuringiensis israelensis* (Bti) for the control of dengue vectors: systematic literature review. Tropical Medicine & International Health 18(5), 564-577.

Brady, O.J., Gething, P.W., Bhatt, S., Messina, J.P., Brownstein, J.S., Hoen, A.G., Moyes, C.L., Farlow, A.W., Scott, T.W., Hay, S.I., 2012. Refining the global spatial limits of dengue virus transmission by evidence-based consensus. PLoS Negl Trop Dis 6(8), e1760.

Brady, O.J., Hay, S.I., 2020. The global expansion of dengue: How *Aedes aegypti* mosquitoes enabled the first pandemic arbovirus. Annu. Rev. Entomol. 65, 191-208.

Bram, R.A., George, J.E., Reichard, R.E., Tabachnick, W.J., 2002. Threat of foreign arthropod-borne pathogens to livestock in the United States. J. Med. Entomol. 39(3), 405-416.

Brock, C.M., Temeyer, K.B., Tidwell, J., Yang, Y., Blandon, M.A., Carreón-Camacho, D., Longnecker, M.T., Almazán, C., de León, A.A.P., Pietrantonio, P.V., 2019. The leucokinin-like peptide receptor from the cattle fever tick, *Rhipicephalus microplus*, is localized in the midgut periphery and receptor silencing with validated double-stranded RNAs causes a reproductive fitness cost. Int. J. Parasitol. 49(3-4), 287-299.

Busch, J.D., Stone, N.E., Nottingham, R., Araya-Anchetta, A., Lewis, J., Hochhalter, C., Giles, J.R., Gruendike, J., Freeman, J., Buckmeier, G., 2014. Widespread movement of invasive cattle fever ticks (*Rhipicephalus microplus*) in southern Texas leads to shared local infestations on cattle and deer. Parasite. Vector. 7(1), 188.

Cabrero, P., Terhzaz, S., Dornan, A.J., Ghimire, S., Holmes, H.L., Turin, D.R., Romero, M.F., Davies, S.A., Dow, J.A., 2020. Specialized stellate cells offer a privileged route for rapid water flux in *Drosophila* renal tubule. Proc. Natl. Acad. Sci.

Calkins, T.L., Tamborindeguy, C., Pietrantonio, P.V., 2018. GPCR annotation, G proteins, and transcriptomics of fire ant (*Solenopsis invicta*) queen and worker brain: An improved view of signaling in an invasive superorganism. Gen. Comp. Endocrinol.

Carvalho, A.M.d.S.A., Machado, C.M., 2020. Emerging Tropical Viral Infections: Dengue, Chikungunya, and Zika. Emerging Transplant Infections: Clinical Challenges and Implications, 1-24.

Charroux, B., Daian, F., Royet, J., 2020. *Drosophila* aversive behavior towards *Erwinia carotovora* carotovora is mediated by bitter neurons and leukokinin. Iscience, 101152.

Chellappandian, M., Senthil-Nathan, S., Vasantha-Srinivasan, P., Karthi, S., Thanigaivel, A., Kalaivani, K., Sivanesh, H., Stanley-Raja, V., Chanthini, K.M.-P., Shyam-Sundar, N., 2019. Target and non-target botanical pesticides effect of Trichodesma indicum (Linn) R. Br. and their chemical derivatives against the dengue vector, *Aedes aegypti L*. Environmental science and pollution research 26(16), 16303-16315.

Chintapalli, V.R., Wang, J., Dow, J.A., 2007. Using FlyAtlas to identify better *Drosophila melanogaster* models of human disease. Nature genetics 39(6), 715-720.

Christophers, S.R., 1960. *Aedes aegypti*: the yellow fever mosquito. CUP Archive.

Cilek, J., Petersen, J., Hallmon, C., 2004. Comparative efficacy of IR3535 and DEET as repellents against adult *Aedes aegypti* and *Culex quinquefasciatus*. Journal of the American Mosquito Control Association 20(3), 299-304.

Clemons, A., Haugen, M., Flannery, E., Tomchaney, M., Kast, K., Jacowski, C., Le, C., Mori, A., Holland, W.S., Sarro, J., 2010. *Aedes aegypti*: an emerging model for vector mosquito development. Cold Spring Harbor Protocols 2010(10), pdb. emo141.

Cox, K.J., Tensen, C.P., Van der Schors, R.C., Li, K.W., van Heerikhuizen, H., Vreugdenhil, E., Geraerts, W.P., Burke, J.F., 1997. Cloning, characterization, and expression of a G-protein-coupled receptor from *Lymnaea stagnalis* and identification of a leucokinin-like peptide, PSFHSWSamide, as its endogenous ligand. J. Neurosci. 17(4), 1197-1205.

da Silva, N.B., Taus, N.S., Johnson, W.C., Mira, A., Schnittger, L., Valente, J.D., Vidotto, O., Masterson, H.E., Vieira, T.S., Ueti, M.W., 2018. First report of *Anaplasma marginale* infection in goats, Brazil. PloS one 13(8), e0202140.

Davey, R.B., George, J.E., Miller, R.J., 2006. Comparison of the reproductive biology between acaricide-resistant and acaricide-susceptible *Rhipicephalus (Boophilus) microplus* (Acari: Ixodidae). Veterinary parasitology 139(1-3), 211-220.

de Haro, M., Al-Ramahi, I., Benito-Sipos, J., López-Arias, B., Dorado, B., Veenstra, J.A., Herrero, P., 2010. Detailed analysis of leucokinin-expressing neurons and their candidate functions in the *Drosophila* nervous system. Cell. Tissue. Res. 339(2), 321-336.

de la Fuente, J., Contreras, M., 2015. Tick vaccines: current status and future directions. Expert review of vaccines 14(10), 1367-1376.

Derst, C., Dircksen, H., Meusemann, K., Zhou, X., Liu, S., Predel, R., 2016. Evolution of neuropeptides in non-pterygote hexapods. BMC Evol. Biol. 16(1), 51.

Dircksen, H., 2013. Chapter 32 - Crustacean Bioactive Peptides, in: Kastin, A.J. (Ed.) Handbook of Biologically Active Peptides (Second Edition). Academic Press, Boston, pp. 209-221.

Duvall, L.B., 2019. Mosquito Host-Seeking Regulation: Targets for Behavioral Control. Trends Parasitol.

Duvall, L.B., Ramos-Espiritu, L., Barsoum, K.E., Glickman, J.F., Vosshall, L.B., 2019. Small-molecule agonists of *Ae. aegypti* neuropeptide Y receptor block mosquito biting. Cell 176(4), 687-701. e685.

Egekwu, N., Sonenshine, D., Garman, H., Barshis, D., Cox, N., Bissinger, B., Zhu, J., M. Roe, R., 2016. Comparison of synganglion neuropeptides, neuropeptide receptors and neurotransmitter receptors and their gene expression in response to feeding in *Ixodes scapularis* (Ixodidae) vs. *O rnithodoros turicata* (Argasidae). Insect Mol. Biol. 25(1), 72-92.

Egekwu, N., Sonenshine, D.E., Bissinger, B.W., Roe, R.M., 2014. Transcriptome of the female synganglion of the black-legged tick *Ixodes scapularis* (Acari: Ixodidae) with comparison between Illumina and 454 systems. PLoS One 9(7), e102667.

Ejendal, K.F.K., Meyer, J.M., Brust, T.F., Avramova, L.V., Hill, C.A., Watts, V.J., 2012. Discovery of antagonists of tick dopamine receptors via chemical library screening and comparative pharmacological analyses. Insect Biochem. Molec. 42(11), 846-853.

Faulde, M.K., 2018. Long-Lasting Insecticide-Treated Textiles Preventing from Mosquito Bite and Mosquito-Borne Diseases, Mosquito-borne Diseases. Springer, pp. 281-303.

Frooninckx, L., Van Rompay, L., Temmerman, L., Van Sinay, E., Beets, I., Janssen, T., Husson, S.J., Schoofs, L., 2012. Neuropeptide GPCRs in *C. elegans*. Front. Endocrinol. 3, 167.

Ghosh, S., Azhahianambi, P., de la Fuente, J., 2006. Control of ticks of ruminants, with special emphasis on livestock farming systems in India: present and future possibilities for integrated control—a review. Experimental & applied acarology 40(1), 49-66.

Graham, O., Hourrigan, J., 1977. Eradication programs for the arthropod parasites of livestock. J. Med. Entomol. 13(6), 629-658.

Grisi, L., Leite, R.C., Martins, J.R.d.S., Barros, A.T.M.d., Andreotti, R., Cançado, P.H.D., León, A.A.P.d., Pereira, J.B., Villela, H.S., 2014. Reassessment of the potential economic impact of cattle parasites in Brazil. Rev. Bras. Parasitol. V. 23(2), 150-156.

Guerrero, F.D., Bendele, K.G., Davey, R.B., George, J.E., 2007. Detection of Babesia bigemina infection in strains of *Rhipicephalus (Boophilus) microplus* collected from outbreaks in South Texas. Veterinary Parasitology 145(1), 156-163.

Gulia-Nuss, M., Nuss, A.B., Meyer, J.M., Sonenshine, D.E., Roe, R.M., Waterhouse, R.M., Sattelle, D.B., de la Fuente, J., Ribeiro, J.M., Megy, K., Thimmapuram, J., Miller, J.R.,

Walenz, B.P., Koren, S., Hostetler, J.B., Thiagarajan, M., Joardar, V.S., Hannick, L.I., Bidwell, S., Hammond, M.P., Young, S., Zeng, Q., Abrudan, J.L., Almeida, F.C., Ayllón, N., Bhide, K., Bissinger, B.W., Bonzon-Kulichenko, E., Buckingham, S.D., Caffrey, D.R., Caimano, M.J., Croset, V., Driscoll, T., Gilbert, D., Gillespie, J.J., Giraldo-Calderón, G.I., Grabowski, J.M., Jiang, D., Khalil, S.M.S., Kim, D., Kocan, K.M., Koči, J., Kuhn, R.J., Kurtti, T.J., Lees, K., Lang, E.G., Kennedy, R.C., Kwon, H., Perera, R., Qi, Y., Radolf, J.D., Sakamoto, J.M., Sánchez-Gracia, A., Severo, M.S., Silverman, N., Šimo, L., Tojo, M., Tornador, C., Van Zee, J.P., Vázquez, J., Vieira, F.G., Villar, M., Wespiser, A.R., Yang, Y., Zhu, J., Arensburger, P., Pietrantonio, P.V., Barker, S.C., Shao, R., Zdobnov, E.M., Hauser, F., Grimmelikhuijzen, C.J.P., Park, Y., Rozas, J., Benton, R., Pedra, J.H.F., Nelson, D.R., Unger, M.F., Tubio, J.M.C., Tu, Z., Robertson, H.M., Shumway, M., Sutton, G., Wortman, J.R., Lawson, D., Wikel, S.K., Nene, V.M., Fraser, C.M., Collins, F.H., Birren, B., Nelson, K.E., Caler, E., Hill, C.A., 2016. Genomic insights into the *Ixodes scapularis* tick vector of Lyme disease. Nat. Commun. 7, 10507.

Halberg, K.A., Terhzaz, S., Cabrero, P., Davies, S.A., Dow, J.A., 2015. Tracing the evolutionary origins of insect renal function. Nat. Commun. 6, 6800.

Hanlon, C.D., Andrew, D.J., 2015. Outside-in signaling – a brief review of GPCR signaling with a focus on the *Drosophila* GPCR family. J. Cell Sci. 128(19), 3533-3542.

Hansen, K.B., Bräuner-Osborne, H., 2009. FLIPR® Assays of Intracellular Calcium in GPCR Drug Discovery, G Protein-Coupled Receptors in Drug Discovery. Springer, pp. 269-278.

Harshini, S., Nachman, R., Sreekumar, S., 2002. Inhibition of digestive enzyme release by neuropeptides in larvae of *Opisina arenosella* (Lepidoptera: Cryptophasidae).

Comparative Biochemistry and Physiology Part B: Biochemistry and Molecular Biology 132(2), 353-358.

Hauser, A.S., Chavali, S., Masuho, I., Jahn, L.J., Martemyanov, K.A., Gloriam, D.E., Babu, M.M., 2018. Pharmacogenomics of GPCR Drug Targets. Cell 172(1), 41-54.e19.

Hauser, F., Cazzamali, G., Williamson, M., Blenau, W., Grimmelikhuijzen, C.J., 2006. A review of neurohormone GPCRs present in the fruitfly Drosophila melanogaster and the honey bee Apis mellifera. Prog. Neurobiol. 80(1), 1-19.

Hilger, D., Masureel, M., Kobilka, B.K., 2018. Structure and dynamics of GPCR signaling complexes. Nat. Struct. Mol. Biol. 25(1), 4-12.

Hill, C.A., Doyle, T., Nuss, A.B., Ejendal, K.F., Meyer, J.M., Watts, V.J., 2016. Comparative pharmacological characterization of D 1-like dopamine receptors from *Anopheles gambiae, Aedes aegypti* and *Culex quinquefasciatus* suggests pleiotropic signaling in mosquito vector lineages. Parasite. Vector. 9(1), 192.

Hill, C.A., Meyer, J.M., Ejendal, K.F., Echeverry, D.F., Lang, E.G., Avramova, L.V., Conley, J.M., Watts, V.J., 2013. Re-invigorating the insecticide discovery pipeline for vector control: GPCRs as targets for the identification of next gen insecticides. Pestic. Biochem. Phys. 106(3), 141-148.

Holman, G., Cook, B., Nachman, R., 1986. Isolation, primary structure and synthesis of two neuropeptides from *Leucophaea maderae*: members of a new family of cephalomyotropins. Comp. Biochem. Phys. C. 84(2), 205-211.

Holman, G.M., Nachman, R., Wright, M., 1990. Insect neuropeptides. Annu. Rev. Entomol. 35(1), 201-217.

Holmes, S.P., 2004. The characterization, functional expression, and localization of the first arthropod myokinin receptor from the southern cattle tick, *Boophilus microplus* (Acari: ixodidae). Texas A&M University.

Holmes, S.P., Barhoumi, R., Nachman, R.J., Pietrantonio, P.V., 2003. Functional analysis of a G protein- coupled receptor from the Southern cattle tick *Boophilus microplus* (Acari: Ixodidae) identifies it as the first arthropod myokinin receptor. Insect Mol. Biol. 12(1), 27-38.

Holmes, S.P., He, H., Chen, A.C., Ivie, G.W., Pietrantonio, P.V., 2000. Cloning and transcriptional expression of a leucokinin- like peptide receptor from the Southern cattle tick, *Boophilus microplus* (Acari: Ixodidae). Insect Mol. Biol. 9(5), 457-465.

Hoogstraal, H., Aeschlimann, A., 1982. Tick-host specificity. Bulletin de la société entomologique suisse 55, 5-32.

Jongejan, F., Uilenberg, G., 2004. The global importance of ticks. Parasitology 129(S1), S3-S14.

Joubert, D.A., Walker, T., Carrington, L.B., De Bruyne, J.T., Kien, D.H.T., Hoang, N.L.T., Chau, N.V.V., Iturbe-Ormaetxe, I., Simmons, C.P., O'Neill, S.L., 2016. Establishment of a Wolbachia superinfection in *Aedes aegypti* mosquitoes as a potential approach for future resistance management. PLoS pathogens 12(2), e1005434.

Kersch, C.N., Pietrantonio, P.V., 2011. Mosquito *Aedes aegypti* (L.) leucokinin receptor is critical for in vivo fluid excretion post blood feeding. FEBS Lett. 585(22), 3507-3512.

Kim, D., Šimo, L., Park, Y., 2014. Orchestration of salivary secretion mediated by two different dopamine receptors in the blacklegged tick *Ixodes scapularis*. J. Exp. Biol. 217(20), 3656-3663.

Kim, D.-H., Kim, Y.-J., Adams, M.E., 2018. Endocrine regulation of airway clearance in *Drosophila*. Proc. Natl. Acad. Sci., 201717257.

Kim, Y.-J., Žitňan, D., Cho, K.-H., Schooley, D.A., Mizoguchi, A., Adams, M.E., 2006. Central peptidergic ensembles associated with organization of an innate behavior. Proc. Natl. Acad. Sci. 103(38), 14211-14216.

Klafke, G.M., Sabatini, G.A., Thais, A., Martins, J.R., Kemp, D.H., Miller, R.J., Schumaker, T.T., 2006. Larval immersion tests with ivermectin in populations of the cattle tick *Rhipicephalus (Boophilus) microplus* (Acari: Ixodidae) from State of Sao Paulo, Brazil. Veterinary parasitology 142(3-4), 386-390.

Kocan, K., De La Fuente, J., Blouin, E., Garcia-Garcia, J., 2004. Anaplasma marginale (Rickettsiales: Anaplasmataceae): recent advances in defining host-pathogen adaptations of a tick-borne rickettsia. Parasitology 129(S1), S285.

Kraemer, M.U., Sinka, M.E., Duda, K.A., Mylne, A.Q., Shearer, F.M., Barker, C.M., Moore, C.G., Carvalho, R.G., Coelho, G.E., Van Bortel, W., 2015. The global distribution of the arbovirus vectors *Aedes aegypti* and *Ae. albopictus*. elife 4, e08347.

Kwon, H., Agha, M.A., Smith, R.C., Nachman, R.J., Marion-Poll, F., Pietrantonio, P.V., 2016. Leucokinin mimetic elicits aversive behavior in mosquito *Aedes aegypti* (L.) and inhibits the sugar taste neuron. Proc. Natl. Acad. Sci. 113(25), 6880-6885.

Kwon, H., Lu, H.-L., Longnecker, M.T., Pietrantonio, P.V., 2012. Role in diuresis of a calcitonin receptor (GPRCAL1) expressed in a distal-proximal gradient in renal organs of the mosquito *Aedes aegypti* (L.). PLoS One 7(11), e50374.

Kwon, H., Pietrantonio, P.V., 2013. Calcitonin receptor 1 (AedaeGPCRCAL1) hindgut expression and direct role in myotropic action in females of the mosquito *Aedes aegypti* (L.). Insect Biochem. Molec. 43(7), 588-593.

Leal, B., Zamora, E., Fuentes, A., Thomas, D.B., Dearth, R.K., 2020. Questing by Tick Larvae (Acari: Ixodidae): A Review of the Influences That Affect Off-Host Survival. Ann. Entomol. Soc. Am.

Lees, K., Woods, D., Bowman, A.S., 2010. Transcriptome analysis of the synganglion from the brown dog tick, *Rhipicephalus sanguineus*. Insect Mol. Biol. 19(3), 273-282.

Lenhart, A., Morrison, A.C., Paz-Soldan, V.A., Forshey, B.M., Cordova-Lopez, J.J., Astete, H., Elder, J.P., Sihuincha, M., Gotlieb, E.E., Halsey, E.S., 2020. The impact of insecticide treated curtains on dengue virus transmission: A cluster randomized trial in Iquitos, Peru. PLoS Neglect. Trop. D. 14(4), e0008097.

Li, A.Y., Davey, R.B., Miller, R.J., George, J.E., 2003. Resistance to coumaphos and diazinon in *Boophilus microplus* (Acari: Ixodidae) and evidence for the involvement of an oxidative detoxification mechanism. J. Med. Entomol. 40(4), 482-490.

Li, A.Y., Davey, R.B., Miller, R.J., George, J.E., 2004. Detection and characterization of amitraz resistance in the southern cattle tick, *Boophilus microplus* (Acari: Ixodidae). J. Med. Entomol. 41(2), 193-200.

Lipinski, C.A., 2016. Rule of five in 2015 and beyond: Target and ligand structural limitations, ligand chemistry structure and drug discovery project decisions. Adv. Drug. Deliver. Rev 101, 34-41.

Lismont, E., Verbakel, L., Vogel, E., Corbisier, J., Degroot, G.-N., Verdonck, R., Verlinden, H., Marchal, E., Springael, J.-Y., Broeck, J.V., 2020. Can BRET-based biosensors be used to

characterize G-protein mediated signaling pathways of an insect GPCR, the *Schistocerca gregaria* CRF-related diuretic hormone receptor? Insect Biochem. Molec., 103392.

Liu, C., Zhang, B., Zhang, L., Yang, T., Zhang, Z., Gao, Z., Zhang, W., 2020. A neural circuit encoding mating states tunes defensive behavior in *Drosophila*. Nat. Commun. 11(1), 1-14.

Lohmeyer, K., Pound, J., May, M., Kammlah, D., Davey, R., 2011. Distribution of *Rhipicephalus (Boophilus) microplus* and *Rhipicephalus (Boophilus) annulatus* (Acari: Ixodidae) infestations detected in the United States along the Texas/Mexico border. J. Med. Entomol. 48(4), 770-774.

López-Arias, B., Dorado, B., Herrero, P., 2011. Blockade of the release of the neuropeptide leucokinin to determine its possible functions in fly behavior: chemoreception assays. Peptides 32(3), 545-552.

Lu, H.L., Kersch, C., Pietrantonio, P.V., 2011a. The kinin receptor is expressed in the Malpighian tubule stellate cells in the mosquito *Aedes aegypti* (L.): A new model needed to explain ion transport? Insect Biochem. Molec. 41(2), 135-140.

Lu, H.L., Kersch, C.N., Taneja-Bageshwar, S., Pietrantonio, P.V., 2011b. A calcium bioluminescence assay for functional analysis of mosquito (*Aedes aegypti*) and tick (*Rhipicephalus microplus*) G protein-coupled receptors. Jove-J Vis Exp(50).

Ma, Q., Ye, L., Liu, H., Shi, Y., Zhou, N., 2017. An overview of Ca2+ mobilization assays in GPCR drug discovery. Expert Opin. Drug Dis. 12(5), 511-523.

Macoris, M.d.L., Martins, A.J., Andrighetti, M.T.M., Lima, J.B.P., Valle, D., 2018. Pyrethroid resistance persists after ten years without usage against *Aedes aegypti* in governmental

campaigns: Lessons from São Paulo State, Brazil. PLoS Neglect. Trop. D. 12(3), e0006390.

Mansfield, K.L., Jizhou, L., Phipps, L.P., Johnson, N., 2017. Emerging Tick-Borne Viruses in the Twenty-First Century. Frontiers in Cellular and Infection Microbiology 7(298).

Marques, R., Krüger, R.F., Peterson, A.T., de Melo, L.F., Vicenzi, N., Jiménez-García, D., 2020. Climate change implications for the distribution of the babesiosis and anaplasmosis tick vector, *Rhipicephalus (Boophilus) microplus*. Veterinary research 51(1), 1-10.

Matthews, B.J., Dudchenko, O., Kingan, S.B., Koren, S., Antoshechkin, I., Crawford, J.E., Glassford, W.J., Herre, M., Redmond, S.N., Rose, N.H., 2018. Improved reference genome of *Aedes aegypti* informs arbovirus vector control. Nature 563(7732), 501-507.

Matthews, B.J., McBride, C.S., DeGennaro, M., Despo, O., Vosshall, L.B., 2016. The neurotranscriptome of the *Aedes aegypti* mosquito. BMC genomics 17(1), 1-20.

McBride, C.S., Baier, F., Omondi, A.B., Spitzer, S.A., Lutomiah, J., Sang, R., Ignell, R., Vosshall, L.B., 2014. Evolution of mosquito preference for humans linked to an odorant receptor. Nature 515(7526), 222-227.

Meeusen, T., Mertens, I., De Loof, A., Schoofs, L., 2003. G protein-coupled receptors in invertebrates: a state of the art. International review of cytology 230, 189-263.

Miller, R.J., Davey, R.B., George, J.E., 2007. First report of permethrin-resistant *Boophilus microplus* (Acari: Ixodidae) collected within the United States. J. Med. Entomol. 44(2), 308-315.

Moyes, C.L., Vontas, J., Martins, A.J., Ng, L.C., Koou, S.Y., Dusfour, I., Raghavendra, K., Pinto, J., Corbel, V., David, J.-P., 2017. Contemporary status of insecticide resistance in

the major *Aedes* vectors of arboviruses infecting humans. PLoS Neglect. Trop. D. 11(7), e0005625.

Nachman, R.J., Coast, G.M., Holman, G.M., Beier, R.C., 1995. Diuretic activity of C-terminal group analogues of the insect kinins in *Acheta domesticus*. Peptides 16(5), 809-813.

Nachman, R.J., Holman, G.M., 1991. Myotropic Insect Neuropeptide Families from the Cockroach *Leucophaea maderae*: Structure-Activity Relationships, in: Menn, J.J., Masler, Edward P. (Ed.) Insect neuropeptides: chemistry, biology, and action. American Chemical Society, Washington, D.C., pp. 194-214.

Nässel, D.R., 2002. Neuropeptides in the nervous system of *Drosophila* and other insects: multiple roles as neuromodulators and neurohormones. Prog. Neurobiol. 68(1), 1-84.

Nässel, D.R., Zandawala, M., 2019. Recent advances in neuropeptide signaling in *Drosophila*, from genes to physiology and behavior. Prog. Neurobiol.

Neupert, S., Predel, R., Russell, W.K., Davies, R., Pietrantonio, P.V., Nachman, R.J., 2005. Identification of tick periviscerokinin, the first neurohormone of Ixodidae: single cell analysis by means of MALDI-TOF/TOF mass spectrometry. BIiochem. Bioph. Res. Co. 338(4), 1860-1864.

Obregón, D., Corona-González, B., Díaz-Sánchez, A.A., Armas, Y., Roque, E., de Sena Oliveira, M.C., Cabezas-Cruz, A., 2020. Efficient Transovarial Transmission of *Babesia Spp.* in *Rhipicephalus microplus* Ticks Fed on Water Buffalo (*Bubalus bubalis*). Pathogens 9(4), 280.

Odland, G.C., Jones, J.C., 1975. Contractions of the hindgut of adult *Aedes aegypti* with special reference to the development of a physiological saline. Ann. Entomol. Soc. Am. 68(4), 613-616.

Offermanns, S., Simon, M.I., 1995. Gα15 and Gα16 couple a wide variety of receptors to phospholipase C. J. Biol. Chem. 270(25), 15175-15180.

Ohta, H., Ozoe, Y., 2014. Chapter Two - Molecular Signalling, Pharmacology, and Physiology of Octopamine and Tyramine Receptors as Potential Insect Pest Control Targets, in: Cohen, E. (Ed.) Adv. Insect Physiol. Academic Press, pp. 73-166.

Okusawa, S., Kohsaka, H., Nose, A., 2014. Serotonin and downstream leucokinin neurons modulate larval turning behavior in *Drosophila*. J. Neurosci. 34(7), 2544-2558.

Orchard, I., Brugge, V.T., 2002. Contractions associated with the salivary glands of the blood-feeding bug, *Rhodnius prolixus*: evidence for both a neural and neurohormonal coordination. Peptides 23(4), 693-700.

Pándy-Szekeres, G., Munk, C., Tsonkov, T.M., Mordalski, S., Harpsøe, K., Hauser, A.S., Bojarski, A.J., Gloriam, D.E., 2018. GPCRdb in 2018: adding GPCR structure models and ligands. Nucleic Acids Res. 46(D1), D440-D446.

Pérez de León, A.A., Mahan, S., Messenger, M., Ellis, D., Varner, K., Schwartz, A., Baca, D., Andreotti, R., Valle, M.R., Cruz, R.R., 2018. Public-private partnership enabled use of anti-tick vaccine for integrated cattle fever tick eradication in the USA, Pests and vector-borne diseases in the livestock industry. Wageningen Academic Publishers, pp. 783-784.

Pérez de León, A.A., Teel, P.D., Auclair, A.N., Messenger, M.T., Guerrero, F.D., Schuster, G., Miller, R.J., 2012. Integrated strategy for sustainable cattle fever tick eradication in USA is required to mitigate the impact of global change. Front. Physiol. 3, 195.

Pérez de León, A.A., Vannier, E., Almazán, C., Krause, P.J., 2014. Tick-borne protozoa, Biology of ticks. Oxford University Press New York, pp. 147-179.

Phatak, S.S., Stephan, C.C., Cavasotto, C.N., 2009. High-throughput and in silico screenings in drug discovery. Expert Opin. Drug Dis. 4(9), 947-959.

Pietrantonio, P.V., Jagge, C., Taneja-Bageshwar, S., Nachman, R.J., Barhoumi, R., 2005. The mosquito *Aedes aegypti* (L.) leucokinin receptor is a multiligand receptor for the three Aedes kinins. Insect Mol. Biol. 14(1), 55-67.

Pietrantonio, P.V., Xiong, C., Nachman, R.J., Shen, Y., 2018. G protein-coupled receptors in arthropod vectors: Omics and pharmacological approaches to elucidate ligand-receptor interactions and novel organismal functions. Curr. Opin. Insect Sci. 29, 12-20.

Poels, J., Birse, R.T., Nachman, R.J., Fichna, J., Janecka, A., Broeck, J.V., Nässel, D.R., 2009. Characterization and distribution of NKD, a receptor for *Drosophila* tachykinin-related peptide 6. Peptides 30(3), 545-556.

Powell, J.R., Gloria-Soria, A., Kotsakiozi, P., 2018. Recent history of *Aedes aegypti:* Vector genomics and epidemiology records. Bioscience 68(11), 854-860.

Prelich, G., 2012. Gene overexpression: uses, mechanisms, and interpretation. Genetics 190(3), 841-854.

Radford, J.C., Davies, S.A., Dow, J.A., 2002. Systematic G-protein-coupled Receptor Analysis in *Drosophila melanogaster* Identifies a Leucokinin Receptor with Novel Roles. J. Biol. Chem. 277(41), 38810-38817.

Rodríguez-Vivas, R., Ojeda-Chi, M., Rosado-Aguilar, J., Trinidad-Martínez, I., Torres-Acosta, J., Ticante-Perez, V., Castro-Marín, J., Tapia-Moo, C., Vázquez-Gómez, G., 2013. Red deer (*Cervus elaphus*) as a host for the cattle tick *Rhipicephalus microplus* (Acari: Ixodidae) in Yucatan, Mexico. Exp. Appl. Acarol. 60(4), 543-552.

Rodríguez-Vivas, R.I., Grisi, L., de León, A.A.P., Villela, H.S., de Jesús Torres-Acosta, J.F., Sánchez, H.F., Salas, D.R., Cruz, R.R., Saldierna, F., Carrasco, D.G., 2017. Potential economic impact assessment for cattle parasites in Mexico. Revista Mexicana de Ciencias Pecuarias 8(1), 61-74.

Rodriguez-Vivas, R.I., Jonsson, N.N., Bhushan, C., 2018. Strategies for the control of *Rhipicephalus microplus* ticks in a world of conventional acaricide and macrocyclic lactone resistance. Parasitol. Res. 117(1), 3-29.

Rose, N.H., Sylla, M., Badolo, A., Lutomiah, J., Ayala, D., Aribodor, O.B., Ibe, N., Akorli, J., Otoo, S., Mutebi, J.-P., Kriete, A.L., Ewing, E.G., Sang, R., Gloria-Soria, A., Powell, J.R., Baker, R.E., White, B.J., Crawford, J.E., McBride, C.S., 2020. Climate and Urbanization Drive Mosquito Preference for Humans. Curr. Biol.

Sharan, S., Hill, C.A., 2017. Potential of GPCR-Targeting Insecticides for Control of Arthropod Vectors, Advances in Agrochemicals: Ion Channels and G Protein-Coupled Receptors (GPCRs) as Targets for Pest Control. American Chemical Society, pp. 55-84.

Šimo, L., Park, Y., 2014. Neuropeptidergic control of the hindgut in the black-legged tick *Ixodes scapularis*. Int. J. Parasitol. 44(11), 819-826.

Šimo, L., Slovák, M., Park, Y., Žitňan, D., 2009. Identification of a complex peptidergic neuroendocrine network in the hard tick, *Rhipicephalus appendiculatus*. Cell. Tissue. Res. 335(3), 639-655.

Šimo, L., Sonenshine, D., Park, Y., Žitňan, D., 2014. Nervous and sensory systems: structure, function, genomics, and proteomics. Sonenshine, DE, Roe, RM, Eds, Biology of Ticks, vol. 1. 2nd ed., Oxford University Press, Oxford; 309-367.

Sissoko, F., Junnila, A., Traore, M.M., Traore, S.F., Doumbia, S., Dembele, S.M., Schlein, Y., Traore, A.S., Gergely, P., Xue, R.-D., 2019. Frequent sugar feeding behavior by *Aedes aegypti* in Bamako, Mali makes them ideal candidates for control with attractive toxic sugar baits (ATSB). PloS one 14(6), e0214170.

Smith, L.B., Kasai, S., Scott, J.G., 2016. Pyrethroid resistance in *Aedes aegypti* and *Aedes albopictus*: Important mosquito vectors of human diseases. Pestic. Biochem. Phys. 133, 1-12.

Smith, T., Kilborne, F.L., 1893. Investigations into the nature, causation, and prevention of Texas or southern cattle fever. US Department of Agriculture, Bureau of Animal Industry.

Sonenshine, D.E., Roe, R.M., 2013. Biology of ticks. Oxford University Press.

Sparks, T.C., Nauen, R., 2015. IRAC: Mode of action classification and insecticide resistance management. Pestic. Biochem. Phys. 121, 122-128.

Stiller, D., Coan, M., 1995. Recent developments in elucidating tick vector relationships for anaplasmosis and equine piroplasmosis. Veterinary Parasitology 57(1-3), 97-108.

Taneja-Bageshwar, S., Strey, A., Isaac, R.E., Coast, G.M., Zubrzak, P., Pietrantonio, P.V., Nachman, R.J., 2009. Biostable agonists that match or exceed activity of native insect kinins on recombinant arthropod GPCRs. Gen. Comp. Endocrinol. 162(1), 122-128.

Taneja- Bageshwar, S., Strey, A., Zubrzak, P., Pietrantonio, P.V., Nachman, R.J., 2006. Comparative structure- activity analysis of insect kinin core analogs on recombinant kinin receptors from Southern cattle tick *Boophilus microplus* (Acari: Ixodidae) and mosquito *Aedes aegypti* (Diptera: Culicidae). Arch. Insect Biochem. 62(3), 128-140.

Thomas, D.B., Klafke, G., Busch, J.D., Olafson, P.U., Miller, R.A., Mosqueda, J., Stone, N.E., Scoles, G., Wagner, D.M., Perez-De-Leon, A., 2020. Tracking the increase of acaricide resistance in an invasive population of Cattle Fever Ticks (Acari: Ixodidae) and implementation of real-time PCR assays to rapidly genotype resistance mutations. Ann. Entomol. Soc. Am.

Torfs, P., Nieto, J., Veelaert, D., Boon, D., Van De Water, G., Waelkens, E., Derua, R., CalderÓn, J., De Loof, A., Schoofs, L., 1999. The kinin peptide family in invertebrates. Ann. NY. Acad. Sci. 897(1), 361-373.

Uilenberg, G., 2006. *Babesia*—a historical overview. Veterinary parasitology 138(1-2), 3-10.

Vancová, M., Bílý, T., Nebesářová, J., Grubhoffer, L., Bonnet, S., Park, Y., Šimo, L., 2019. Ultrastructural mapping of salivary gland innervation in the tick *Ixodes ricinus*. Sci. Rep-Uk 9(1), 6860.

Veenstra, J.A., 1994. Isolation and identification of 3 leucokinins from the mosquito *Aedes aegypti*. BIiochem. Bioph. Res. Co. 202(2), 715-719.

Veenstra, J.A., 2000. Mono- and dibasic proteolytic cleavage sites in insect neuroendocrine peptide precursors. Arch. Insect Biochem. 43(2), 49-63.

Veenstra, J.A., Pattillo, J.M., Petzel, D.H., 1997. A single cDNA encodes all three aedesleucokinins, which stimulate both fluid secretion by the malpighian tubules and hindgut contractions. J. Biol. Chem. 272(16), 10402-10407.

Veenstra, J.A., Rodriguez, L., Weaver, R.J., 2012. Allatotropin, leucokinin and AKH in honey bees and other Hymenoptera. Peptides 35(1), 122-130.

Wheelock, G., Petzel, D., Gillett, J., Beyenbach, K., Hagedorn, H., 1988. Evidence for hormonal control of diuresis after a blood meal in the mosquito *Aedes aegypti*. Arch. Insect Biochem. 7(2), 75-89.

WHO, 2017. Global vector control response 2017-2030.

WHO, 2018. Weekly epidemiological record: Dengue vaccine: WHO position paper–September 2018. Wkly Epidemiol Rec. 93(36), 457-476.

Wu, F., Song, G., de Graaf, C., Stevens, R.C., 2017. Structure and Function of Peptide-Binding G Protein-Coupled Receptors. J. Mol. Biol. 429(17), 2726-2745.

Yasuno, M., Tonn, R.J., 1970. A study of biting habits of *Aedes aegypti* in Bangkok, Thailand. Bull World Health Organ 43(2), 319-325.

Yeoh, J.G.C., Pandit, A.A., Zandawala, M., Nässel, D.R., Davies, S.-A., Dow, J.A.T., 2017. DINeR: Database for Insect Neuropeptide Research. Insect Biochem. Molec. 86, 9-19.

Yurgel, M.E., Kakad, P., Zandawala, M., Nässel, D.R., Godenschwege, T.A., Keene, A.C., 2019. A single pair of leucokinin neurons are modulated by feeding state and regulate sleep–metabolism interactions. PLoS Biol. 17(2), e2006409.

Zandawala, M., Yurgel, M.E., Texada, M.J., Liao, S., Rewitz, K.F., Keene, A.C., Nässel, D.R., 2018. Modulation of *Drosophila* post-feeding physiology and behavior by the neuropeptide leucokinin. PLoS Genet. 14(11), e1007767.

Zhang, R., Xie, X., 2012. Tools for GPCR drug discovery. Acta Pharmacol. Sin. 33, 372.

2. EVALUATION OF AIB AND PEG-POLYMER INSECT KININ ANALOGS ON MOSQUITO AND TICK GPCRS IDENTIFIES POTENT NEW PEST MANAGEMENT TOOLS WITH POTENTIALLY ENHANCED BIOSTABILITY AND BIOAVAILABILITY[*]

2.1. Overview

Insect kinins modulate aspects of diuresis, digestion, development, and sugar taste perception in tarsi and labellar sensilla in mosquitoes. They are, however, subject to rapid biological degradation by endogenous invertebrate peptidases. A series of α-aminoisobutyric (Aib) acid-containing insect kinin analogs incorporating sequences native to the *Aedes aegypti* mosquito aedeskinins were evaluated on two recombinant kinin invertebrate receptors stably expressed in cell lines, discovering a number of highly potent and biostable insect kinin mimics. On the *Ae. aegypti* mosquito kinin receptor, three highly potent, biostable Aib analogs matched the activity of the Aib-containing biostable insect kinin analog 1728, which previously showed disruptive and/or aversive activity in aphid, mosquito and kissing bug. These three analogs are IK-Aib-19 ([Aib]FY[Aib]WGa, EC_{50} = 18 nM), IK-Aib-12 (pQKFY[Aib]WGa, EC_{50} = 23 nM) and IK-Aib-20 ([Aib]FH[Aib]WGa, EC_{50} = 28 nM). On the *Rhipicephalus (Boophilus) microplus* tick receptor, IK-Aib-20 ([Aib]FH[Aib]WGa, EC_{50} = 2 nM) is more potent than 1728 by a factor of 3. Seven other potentially biostable analogs exhibited an EC_{50} range of 5-10 nM, all of which match the potency of 1728. Among the multi-Aib hexapeptide kinin analogs tested the tick receptor has a preference for the positively-charged, aromatic H over the aromatic

[*] Reprinted with permission from "Evaluation of Aib and PEG-polymer Insect Kinin Analogs on Mosquito and Tick GPCRs Identifies Potent New Pest Management Tools with Potentially Enhanced Biostability and Bioavailability" by Xiong, C., Kaczmarek, K., Zabrocki, J., Pietrantonio, P. V., Nachman, R. J., 2019. General and Comparative Endocrinology, 278: 58-67, Copyright [2019] by Elsevier Inc.

residues Y and F in the X^1 variable position ([Aib]FX^1[Aib]WGa), whereas the mosquito receptor does not distinguish between them. In contrast, in a mono-Aib pentapeptide analog framework (FX^1[Aib]WGa), both receptors exhibit a preference for Y over H in the variable position. Among analogs incorporating polyethylene glycol (PEG) polymer attachments at the N-terminus that can confer enhanced bioavailability and biostability, three matched or surpassed the potency of a positive control peptide. On the tick receptor IK-PEG-9 (P_8-R[Aib]FF[Aib]WGa) was the most potent. Two others, IK-PEG-8 (P_8-RFFPWGa) and IK-PEG-6 (P_4-RFFPWGa), were most potent on the mosquito receptor, with the first surpassing the activity of the positive control peptide. These analogs and others in the IK-Aib series expand the toolbox of potent analogs accessible to invertebrate endocrinologists studying the structural requirements for bioactivity and the as yet unknown role of the insect kinins in ticks. They may contribute to the development of selective, environmentally friendly pest arthropod control agents.

2.2. Introduction

Insect neuropeptides of the insect kinin (**IK**) class regulate important biological functions in invertebrates (Coast, 2007; Coast et al., 2002; De Loof, 2008; Gäde, 2004a; Nässel, 2002). In diverse species insect kinins stimulate hindgut contractions, diuresis, digestive enzyme release, probably inhibit lepidopteran larval weight gain, participate in tracheal clearance and air filling prior to ecdysis in *Drosophila*, and modulate sugar taste perception in contact chemosensory neurons in *Ae. aegypti* mosquitoes (Coast et al., 1990; Harshini et al., 2003; Holman et al., 1990; Kersch and Pietrantonio, 2011; Kim, D.-H. et al., 2018a; Kwon et al., 2016; Lu et al., 2011a; Nachman et al., 2002a; Pietrantonio, P. et al., 2005; Seinsche et al., 2000).

Neuropeptides have been studied as potential leads for the development of new, environmentally friendly pest control agents due to their specificity and high activity at very low doses. However, the natural peptides cannot be directly used, as they are susceptible to degradation by endogenous peptidases (Cornell et al., 1995; Gäde and Goldsworthy, 2003; Lamango et al., 1996; Nachman et al., 2002a). In addition, they are not suitably designed to penetrate the exoskeleton of invertebrate pests. Knowledge of both chemical and conformational requirements responsible for neuropeptide biological activity can aid in the design of analogs containing unnatural moieties that can overcome these limitations (Nachman et al., 1994).

The endogenous arthropod insect kinins are 6-14 amino acid long neuropeptides characterized by the evolutionarily conserved C-terminal pentapeptide Phe-X^1-X^2-Trp-Gly-NH_2, where X^1 = His, Asn, Ser, or Tyr and X^2 = Ser, Pro, or Ala (Holman et al., 1999; Torfs et al., 1999b). This C-terminal pentapeptide kinin core is the minimum sequence required for full cockroach myotropic and cricket diuretic activity in tissue assays *in vitro* (Nachman et al., 2003; Nachman and Holman, 1991b). Recombinant kinin receptors from the southern cattle tick, *Rhipicephalus* (*Boophilus) microplus* (Holmes, S. et al., 2003; Holmes, S. et al., 2000a) and the dengue vector, the mosquito *Aedes aegypti* (Pietrantonio, P. et al., 2005) were previously stably expressed in CHO-K1 cells for comparative structure-activity relationship studies of kinin analogs. This assay system confirmed the activity of the kinin pentapeptide core in both receptors (Holmes, S. et al., 2003; Pietrantonio, P. et al., 2005; Taneja- Bageshwar et al., 2006). Both the tissue assays and the receptor expressing system revealed that the C-terminal amide of the insect kinins is important for their activity(Nachman et al., 1995; Taneja- Bageshwar et al., 2006). Activity was also lost when either Phe^1 or Trp^4 was replaced with Ala, confirming the importance of these two key positions (Taneja- Bageshwar et al., 2006). However, the variable

position 2 tolerates a wide range of chemical characteristics, from acidic to basic residues, and from hydrophilic to hydrophobic, although highest potencies were observed with aromatic residues at this position (Nachman and Holman, 1991b; Roberts et al., 1997; Taneja-Bageshwar et al., 2006). Based on these observations the plausible receptor interaction model positions the side chains of Phe^{1} and Trp^{4} towards the same region via a β-turn involving the Pro^{3} where they interact with the receptor, and away from the side chain of position 2.

Insect kinins are subject to rapid degradation by peptidases present in the haemolymph and bound to tissues of invertebrate pests. The primary hydrolysis-susceptible site lies within the insect kinin C-terminal pentapeptide core region between the Ser^{3} (or Pro^{3}) and conserved Trp^{4} residues. A secondary site is found just outside of the core region at the peptide bond N-terminal to Phe^{1}. Experimentally, the fly angiotensin converting enzyme (ACE) can cleave the insect kinin primary hydrolysis site, and neprilysin (NEP) can cleave both the primary and secondary hydrolysis sites (Cornell et al., 1995; Lamango et al., 1996; Nachman et al., 1997a; Nachman et al., 1997c; Nachman et al., 1990; Nachman et al., 2002a; Roberts et al., 1997). Replacement of Ser^{3} (or Pro^{3}) with an unnatural, sterically bulky residue Aib leads to analogs that not only mimic a critical β-turn conformation but also blocks tissue-bound peptidase, ANCE, and NEP hydrolysis, with FF[Aib]WGa maintaining potency in mosquito and tick recombinant receptors (Nachman et al., 1997a; Nachman et al., 1997c; Nässel, 2002; Taneja-Bageshwar, S. et al., 2009; Taneja- Bageshwar et al., 2006). Incorporation of a second Aib residue adjacent to the secondary peptidase hydrolysis site further enhances biostability *(Nachman et al., 2002a).* The disubstituted Aib kinin analog [Aib]FS[Aib]WGa was resistant to enzymatic degradation up to 4 h (Nachman et al., 2002a). Analog 1728, [Aib]FF[Aib]WGa (also referred to as K-Aib-1), and related to the aforementioned multi-Aib analog, does not contain residues specific to the native aedeskinins

apart from the C-terminal pentapeptide FX^1X^2WGa that is conserved in invertebrate kinins. It was several fold (from 300 to 20) less susceptible to hydrolysis by a number of these enzymes as compared with the insect kinin FFFSWGa (Taneja-Bageshwar, S. et al., 2009). The resistance to aminopeptidase hydrolysis is likely due to the steric hindrance of the α,α-disubstituted nature of the amino acid Aib located at the N-terminus. In both tick and mosquito kinin receptor expressing cell lines, analog 1728 was more potent than the positive control (FFFSWGa) and aedeskinin 2 (Taneja-Bageshwar, S. et al., 2009). The N-terminus of FF[Aib]WGa is still vulnerable to hydrolysis by aminopeptidases. This analog is less potent than the aedeskinins (up to 14 residues in length), as the mosquito receptor prefers sequences extended beyond the C-terminal pentapeptide core (Taneja-Bageshwar, S. et al., 2009; Taneja-Bageshwar et al., 2008; Taneja- Bageshwar et al., 2006). Extended insect kinin analogs would also require additional protection from peptidases that attack at the secondary site.

We now continued the design of pseudopeptides with enhanced resistance to peptidases that retain biological activity on 'insect kinin' receptors of arthropod vectors in search of analogs with higher potency, biostability and bioavailability. In this paper, we develop a new series of kinin analog pest management tools by further exploring the use of the sterically-hindered Aib moiety in biostable analogs that also specifically incorporate residues from insect kinins native to the mosquito *Aedes aegypti*, aedeskinin-1, -2 and -3 (Predel et al., 1997; Veenstra et al., 1997a). In a few of these analogs the N-terminus is further protected from aminopeptidases with either acetyl (Ac-) or pyroglutamate (pQ-) groups (Nachman et al., 2002a).

Another approach to the stabilization of peptides and/or proteins to enzymatic degradation in the digestive system as well as the enhancement of penetration across cell membranes of the gut or cuticle into the hemolymph (blood) of insects is the conjugation of

polyethylene glycol (PEG) polymers (Fig. 2.1) to the N-terminus (Boccù et al., 1982; Jeffers and Roe, 2008; Shen et al., 2009). Although not previously applied to neuropeptides of the insect kinin class, conjugation of PEG polymers to the insect peptide trypsin modulating oostatic factor (TMOF) enhanced the resistance to degradation by the digestive enzyme leucine aminopeptidase, leading to accumulation of the peptide in hemolymph of insects and ticks (Boccù et al., 1982; Jeffers and Roe, 2008; Shen et al., 2009). Five insect kinin analogs incorporating PEG_4 (P_4) and PEG_8 (P_8) polymers (Fig. 2.1) at the N-terminus, three of which also incorporate the sterically-hindered Aib residue were evaluated in this study on the two recombinant invertebrate 'insect kinin' receptors. We have determined their potency (EC_{50}), their efficacy in comparison to a kinin analog serving as positive control (FFFSWGa) and correlated these two variables to rank these analogs.

2.3. Materials and Methods

2.3.1. Analog synthesis and purification*

Analogs were synthesized on an ABI 433A peptide synthesizer with a modified FastMoc 0.25 procedure using an Fmoc-strategy starting from Rink amide resin (Novabiochem, San Diego, CA, 0.5 mM/g). The Fmoc protecting group was removed by 20% 4-methyl piperidine in DMF (Dimethyl formamide). A fourfold excess of the respective Fmoc-amino acids was activated *in situ* using HBTU (2-(1h-benzotriazol-1-yl)-1,1,3,3-tetramethyluronium hexafluorophosphate) (1 eq.) /HOBt (1-hydroxybenzotriazole) (1 eq.) in NMP (N-methylpyrrolidone) or HATU (2-(7-Aza-1H-Benzotiazole-1-yl)-1,1,3,3-tetramethyluronium hexafluorophosphate) (1 eq.)/HOAt (1-hydroxy-7-azabenzotriazole) (1 eq.) in NMP for Aib and the amino acid immediately following it in the sequence. The coupling reactions were base

* Design, synthesis, and purification of peptide analogs was performed by co-author Dr. Ron J. Nachman of USDA.

catalyzed with DIPEA (N,N-diisopropylethylamine) (4 eq.) The amino acid side chain protecting groups were PMC for Arginine and Boc for Tryptophan. Acetylation was accomplished as previously described (Taneja-Bageshwar et al., 2009).

The PEG polymer conjugations were accomplished as follows: after transferring peptidyl resin with the completed peptide sequence into an 8 ml polypropylene syringe, a 1.2 molar equivalent of MS(PEG_4) or MS(PEG_8) reagent was added as a 10% solution in NMP (100 mg of viscous reagent was reconstituted with 900 mg NMP). Both reagents are commercially available (Thermo Scientific, Waltham, MA) and they are N-hydroxysuccinimide esters of O-methyl-tetra- and octa-ethyleneglycolcarboxylic acid, respectively. The syringes were shaken over night at RT and, following a positive Kaiser

test, EDC was added (0.5 eq.) and shaken for one additional day. After washing with DCM (3×) and methanol (3×) and drying the PEGylated peptide analogs, cleavage from the resin was accomplished with a cocktail composed of TFA/DMB/TIS (92.5:5:2.5), and precipitated with ether.

The analogs were cleaved from the resin with side-chain deprotection by treatment with TFA (Trifluoroacetic acid):H_2O:TIS (Triisopropylsilane) (95.5:2.5:2.5 v/v/v) for 1.5 h. The solvents were evaporated by vacuum centrifugation and the analogs were desalted on a Waters C_{18} Sep Pak cartridge (Milford, MA) in preparation for purification by HPLC.

The analogs were purified on a Waters Delta-Pak C_{18} reverse-phase column (8 x 100 mm, 15 µm particle size, 100 Å pore size) with a Waters 510 HPLC system with detection at 214 nm at ambient temperature. Solvent A = 0.1% aqueous trifluoroacetic acid (TFA); Solvent B = 80% aqueous acetonitrile containing 0.1% TFA. Initial conditions were 10% B followed by a linear increase to 90 % B over 40 min.; flow rate, 2 ml/min. Delta-Pak C_{18} retention times: **IK-Aib-5**,

Ac-FF[Aib]WGa, 4.5 min.; **IK-PEG-6**, MS[PEG_4]-RFFPWGa, 10.5 min.; **IK-Aib-7**, MS[PEG_4]-R[Aib]FF[Aib]WGa, 12.0 min.; **IK-PEG-8**, MS[PEG_8]-RFFPWGa, 9.0 min.; **IK-PEG-9**, MS[PEG_8]-R[Aib]FH[Aib]WGa, 12.0 min.; **IK-PEG-10**, MS[PEG_8]-[Aib]FH[Aib]WGa, 12.5 min.; **IK-Aib-11**, NSKYVSKQKFY[Aib]WGa, 2.5 min.; **IK-Aib-12**, pQKFY[Aib]WGa, 2.3 min.; **IK-Aib-13**, NPFH[Aib]WGa, 2.4 min.; **IK-Aib-14**, Ac-FH[Aib]WGa, 2.4 min**; IK-Aib-15**, FH[Aib]WGa, 2.3 min.; **IK-Aib-16**, FY[Aib]WGa, 2.3 min.; **IK-Aib-17**, VFY[Aib]WGa, 2.5 min.; **IK-Aib-18**, pQVFY[Aib]WGa, 6.6 min.; **IK-Aib-19**, [Aib]FY[Aib]WGa, 2.3 min.; **IK-Aib-20**, [Aib]FH[Aib]WGa, 2.5 min. The analogs were further purified on a Waters Protein Pak I 125 column (7.8 x 300 mm). Conditions: isocratic using 80% acetonitrile containing 0.1% TFA; flow rate, 2 ml/min. Waters Protein Pak retention times: **IK-Aib-5**, 5.9 min.; **IK-PEG-6**, 6.0 min.; **IK-PEG-7**, 6.0 min.; **IK-PEG-8**, 6.25 min.; **IK-PEG-9**, 5.9 min.; **IK-PEG-10**, 4.75 min.; **IK-Aib-11**, 9.25 min.; **IK-Aib-12**, 6.25 min. ; **IK-Aib-13**, 7.0 min.; **IK-Aib-14**, 6.25 min.; **IK-Aib-15**, 6.25 min.; **IK-Aib-16**, 6.0 min.; **IK-Aib-17**, 6.0 min.; **IK-Aib-18**, 6.0 min.; **IK-Aib-19**, 6.0 min.; **IK-Aib-20**, 6.25 min. Amino acid analysis was carried out under previously reported conditions (Nachman et al., 2004) to quantify the analogs and to confirm identity: **IK-Aib-5**: F[2.0], G[0.9]; **IK-PEG-6**: F[2.0], G[0.9]; P[1.0]; R[1.1]; **IK-PEG-7**: F[2.0], G[0.9], R[1.0]; **IK-PEG-8**: F[2.0], G[0.9], R[1.0]; **IK-PEG-9**: F[2.0], G[0.9], R[0.8]; **IK-PEG-10**: F[2.0], G[0.9]; **IK-Aib-11**: E[1.0]; F[1.0], G[0.9], K[2.7]; N[0.9]; S[0.9]; V[0.9]; Y[2.0]; **IK-Aib-12**: E[1.1]; F[1.1], G[1.0]; K[1.1]; P[1.0]; R[1.1], Y[1.2]; **IK-Aib-13**: D[1.0]; F[1.0], G[1.0]; H[1.0]; **IK-Aib-14**: F[1.0], G[1.1]; H[1.0]; **IK-Aib-15**: F[1.0], G[1.1]; H[1.0]; **IK-Aib-16**: F[1.0], G[1.0]; Y[1.2]; **IK-Aib-17**: F[1.0], G[1.1]; V[0.9]; Y[1.2]; **IK-Aib-18**: E[1.1]; F[1.0], G[1.0]; V[1.0]; Y[1.1]; **IK-Aib-19**: F[1.0], G[1.0]; Y[1.1]; **IK-Aib-20**: F[1.0], G[1.1]; H[0.9]. The identity of the analogs was also confirmed by MALDI-MS on a

Kratos Kompact Probe MALDI-MS instrument (Shimadzu, Columbia, Maryland). The following molecular ions (MH^+) were observed: **IK-Aib-5**, 704.7 (calc.704.5 [MNa^+]); **IK-PEG-6**, 1027.3 (1027.5 calc.); **IK-PEG-7**, 1100.2 (1100.2 calc.); **IK-PEG-8**, 1203.7 (1203.4 calc.); **IK-PEG-9**, 1276.9 (1276.4 calc.); **IK-PEG-10**, 1120.0 (1120.3 calc.); **IK-Aib-11**, 1719.2 (1719.0 calc.); **IK-Aib-12**, 895.4 (895.0 calc.); **IK-Aib-13**, 841.7 (841.0 calc.); **IK-Aib-14**, 673.3 (673.0 calc.); **IK-Aib-15**, 630.4 (630.0 calc.); **IK-Aib-16**, 656.3 (656.0 calc.); **IK-Aib-17**, 755.3 (755.0 calc.); **IK-Aib-18**, 866.0 (866.0 calc.); **IK-Aib-19**, 741.1 (740.0 calc.); **IK-Aib-20**, 715.4 (715.0 calc.).

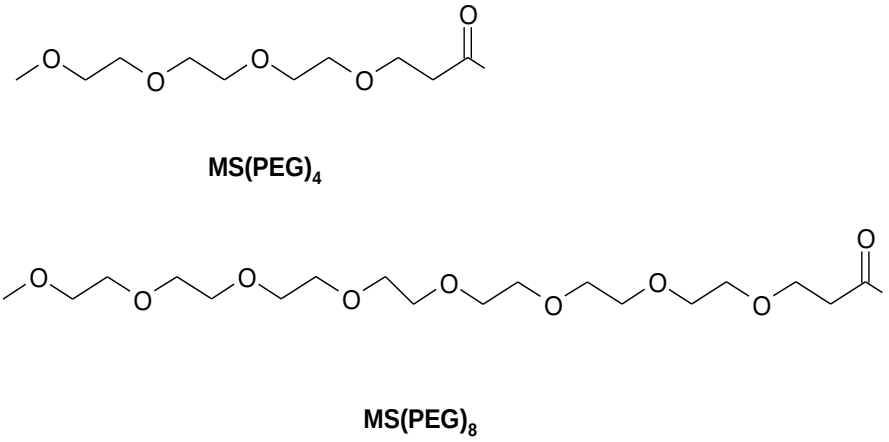

Figure 2.1 Structures of P4 and P8 attached to the N-terminus of the IK-PEG analogs.

2.3.2. Cell lines

BMLK3 and IGKN F10 are CHO-K1 cell lines stably expressing the cattle fever tick (*Rhipicephalus microplus* (Canestrini)) and yellow fever mosquito (*Aedes aegypti* L.) kinin receptors, respectively. Receptor cloning, transfection and selection of single clonal cell lines expressing these kinin receptors were reported previously (Holmes, S. et al., 2003; Pietrantonio, P. et al., 2005). A cell line similarly transfected with empty vector plasmid pcDNA3.1 (Invitrogen) was designated "vector-only" (V/O) and used as negative control in all experiments.

Cells were maintained in T-25 flasks (CELLSTAR®, Greiner Bio-one) with maintenance medium consisting of F-12K medium (Corning™ cellgro™, Mediatech, Inc. VA, US), fetal bovine serum (FBS) (10%) (Equitech-Bio, Kerrville, TX) and 400µg/ml G418 Sulfate (Gibco™, New York, US). Cells were maintained in a humidified incubator at 37°C, 5% CO_2. Unless specified otherwise, cells were incubated under these conditions.

2.3.3. Analysis of activity of kinin analogs by a calcium-mobilization bioluminescence assay

Kinin receptors of both *R. microplus* and *A. aegypti* couple to G_q protein, and its signaling cascade triggers calcium release from intracellular calcium stores (Holmes, S. et al., 2003; Pietrantonio, P. et al., 2005). The functional analyses of kinin analogs with stably transformed CHO-K1 cells expressing the tick and mosquito receptor was performed by an intracellular calcium mobilization bioluminescence assay. This assay was described in detail elsewhere (Lu et al., 2011b) and uses the calcium reporter aequorin. In brief, receptor-expressing cell lines and V/O cell line maintained in T-25 flasks were cultured to about 90% confluency, and were then trypsinized. The cells were suspended in maintenance medium, counted and diluted to 1×10^5 cells/ml; 2 ml of this cell suspension were placed into each well of 6-well-plates (CELLSTAR®, Greiner Bio-one). After overnight incubation, when the cells reached a confluency of 40-60%, old medium was replaced with 1 ml of serum-reduced Opti-MEM™ medium (Gibco™, New York, US) in each well. Following the instructions of the transfection reagent manufacturer, cells in each well of 6-well plate were transiently transfected with 1 µg mtAequorin/pcDNA1 plasmid mixed in 4 µl of FuGENE6 (Promega, Madison, WI) and 96 µl of Opti-MEM™ medium. After 6h of incubation, the old medium was then replaced with 2 mL of F-12K medium with FBS (10%) (antibiotic-free medium). Following 24h incubation, cells were trypsinized and seeded into white-wall clear-bottom 96-well-plates (CELLSTAR® 655098,

Greiner Bio-one) at 20,000 cell/well in 100 µl of antibiotic-free medium, and incubated overnight until cells reached confluency of 80%. To reconstitute the aequorin-complex, cells were incubated with 90 µl per well of calcium-free DMEM (1x) (Gibco®, Invitrogen) containing coelenterazine (5 µM) (Regis® Technology, Inc., Morton Grove, IL). After 3h of incubation in the dark, cells were ready for the assay. The assays were performed with a Clariostar™ (BMG Labtechnology, Chicago, IL) plate reader set at 29°C for bioluminescence and well-mode at 469nm emission wavelength.

2.3.4. Determination of agonist activity of peptidomimetics

To determine whether kinin analogs behave as agonists on the kinin receptors and to avoid wasting the valuable custom-synthesized peptides, all 16 analogs were initially screened at 1 µM; only analogs that showed agonist activity (determined by *t*-test comparison with cells injected with blank medium, preliminary data not shown) were chosen to continue testing in concentration-response analyses (IK-AIB-10 did not show activity on mosquito receptor; not shown).

Dose-dependent tests were performed on the 16 new kinin analogs as well as other two insect kinin receptor agonists, FFFSWGa and 1728 ([Aib]FF[Aib]WGa), (Taneja-Bageshwar, S. et al., 2009) for comparison purposes. Dry peptides were solubilized, and serially diluted in calcium-free DMEM medium containing 1% Dimethyl sulfoxide (DMSO) and prepared as 10x stock. Each analog was tested with both receptor cell lines, at each of 9 concentrations from 0.1 nM to 10 µM. For this, cells in wells in 90 µl of DMEM medium were challenged with 10 µl of 10x concentration of potential agonist injected into the wells at a speed of 430 µl/s, for a final volume of 100 µl in the wells. Immediately after the injection, calcium mobilization-dependent bioluminescence was recorded for 30s at 2s interval, as the signal usually diminished within 30s.

In each assay, each concentration was tested in duplicate wells for each receptor cell line and at least two wells of each of the following controls were included: 1) V/O cell line as negative control; 2) DMSO (1%) in DMEM (blank medium) injected to cells as background injection controls for each cell line, and 3) FFFSWGa at 1 µM was injected as positive control (PC). Three independent replicates were performed for all analogs except for analog 1728 (n=2).

2.3.5. Data analysis

In each well, the response of cells to a stimulus was calculated by averaging bioluminescence units elicited during 30s, that is, as readout, the area under the bioluminescence vs. time response curve was chosen. The response for each replicate was represented as the average of responses from the two pseudo-replicate wells for each concentration, and for each control. For analyses, the background cellular response to blank medium injection was subtracted from the cellular responses to analogs.

All statistical analyses and graphs were done with GraphPad Prism 6.0 (GraphPad Software, La Jolla, CA). For calculations of EC_{50s} these values were then normalized to the maximal response (100%) observed among all concentrations tested for each analog. EC_{50} was defined as the concentration that elicited 50% of the highest number of bioluminescence units for that analog (100%). Dose-response curves (Suppl. Fig. 2.1), estimated EC_{50} values, and their respective 95% confidence intervals (Table 2.2) were calculated with "non-linear regression log[agonist] vs. normalized (bioluminescence) response" with "variable slope function". One-way ANOVA was performed to compare potency ($log.EC_{50}$) of active analogs, followed by Tukey multiple comparison test (Suppl. Tables 1.1 and 2.1).

The bioluminescence response of the PC at 1 µM (100%) in each assay plate was used to normalize the bioluminescence dose-response curves of all analogs. These curves (Fig. 2.2) were

generated by “non-linear regression log[agonist] vs. response” with variable slope (four parameters). The efficacy was calculated as percentage of the bioluminescence response of each analog at 1 µM with reference to the bioluminescence response of the PC at 1 µM (100%). The 1 µM concentration was chosen to calculate efficacy because most analog responses plateaued at this concentration and analogs that required higher concentrations were not considered as an improvement over PC, and for this reason were of lesser interest. One-way ANOVA was performed on efficacy of each of the active analog at 1 µM followed by Tukey multiple comparison test (Suppl. Tables 1.2 and 2.2).

Correlation analyses between the Log.EC_{50} of each analog (Table 2.1) and the efficacy (Table 2.2) were performed. The Pearson correlation (two-tailed) analysis was done independently for the tick and mosquito receptor data sets. The linear regression lines and the 95% confidence intervals (dashed lines) were calculated with “Best-fit value” setting using GraphPad Prism 6.0 (GraphPad Software, La Jolla, CA). The analyses aided the discrimination and visualization of groups of analogs with high potency and high efficacy (Fig. 2.3). For both receptors, analogs with efficacy above that of the PC was desirable. For activity on the mosquito receptor, an $EC_{50} < 100$ nM was desirable, and for tick receptor, an $EC_{50} < 10$ nM.

Table 2.1 Novel biostable kinin analogs incorporating aedeskinin sequences, Aib or PEG.

Aib analogs incorporating the aedeskinin 1 sequence NSKYVSKQKFYSWGa:	
IK-Aib-11	NSKYVSKQKFY[Aib]WGa
IK-Aib-12	pQKFY[Aib]WGa
Aib analogs incorporating the aedeskinin 3 sequence NNPNVFYPWGa:	
IK-Aib-18	pQVFY[Aib]WGa
IK-Aib-17	VFY[Aib]WGa
Aib analogs incorporating aedeskinin 1 and 3 sequences (both end in FYXWGa; X=P or S):	
IK-Aib-16	FY[Aib]WGa
IK-Aib-19	[Aib]FY[Aib]WGa
IK-Aib-5	Ac-FF[Aib]WGa
Aib analogs incorporating the aedeskinin 2 sequence NPFHAWGa:	
IK-Aib-13	NPFH[Aib]WGa
IK-Aib-14	Ac-FH[Aib]WGa
IK-Aib-15	FH[Aib]WGa
IK-Aib-20	[Aib]FH[Aib]WGa
Analogs incorporating either PEG4 [MS(PEG4)] or PEG8 [MS(PEG8)] polymer attachments (Fig. 2.1):	
IK-PEG-6	P4-RFFPWGa
IK-PEG-8	P8-RFFPWGa
IK-PEG-7	MS(PEG4)-R[Aib]FF[Aib]WGa
IK-PEG-9	MS(PEG8)-R[Aib]FF[Aib]WGa
IK-PEG-10	MS(PEG8)-[Aib]FF[Aib]WGa

IK stands for Insect Kinin analog, Aib represents α-aminoisobutyric acid and PEG is an abbreviation for polyethylene glycol polymer.

2.4. Results and Discussion

A total of sixteen novel insect kinin (IK) analogs (Table 2.1) were evaluated in both tick and mosquito receptors in an aequorin-based intracellular calcium functional assay. The goal was to extend the number of biostable and highly potent IK analog tools available to endocrinologists studying the role of the IKs and their potential application in pest management strategies. All analogs were compared to a positive control (PC) peptide FFFSWGa without modifications, and to a potent Aib analog, 1728 previously characterized (Suppl. Fig. 2.1, Fig. 2.2). The efficacy was calculated as the ratio of bioluminescence responses of analogs to that of the PC, when all

peptides were applied at 1 µM (Table 2.2). This concentration was chosen because most analogs elicited their maximal response (plateau) at 1 µM (Fig. 2.2), dosages beyond 1 µM would not be considered an improvement over already developed analogs. The normalization of responses to 1 µM (100%) was necessary for comparative purposes of analog responses within tick or mosquito receptor tests (Fig. 2.2).

Statistical analyses run independently for EC_{50} (Suppl. Tables 1.1 and 2.1) and efficacy (Suppl. Tables 1.2 and 2.2) did not always allow a clear ranking of analogs. Therefore, the two variables EC_{50} and the efficacy were subjected to correlation analyses, and based on these results analogs were classified into groups (Fig. 2.3). For both receptors there was a strong positive correlation between efficacy and potency, each with $P < 0.0001$ and $R^2 > 0.7$. In sum, a more potent analog (lower EC_{50}) tended to show a higher efficacy (responded with a higher number of bioluminescence units) (Fig. 2.3). For both receptors, (EC_{50}) (Table 2.2) of the analogs could be separated into three groups with significantly higher EC_{50} than the PC (Suppl. Table 2.1.1 and 2.1). For the mosquito receptor: group *a* had increased potency by at least a factor of 14, group *b* had increased potency by a factor of 5-8, and group *c*, which exhibited increased potency by a factor of 3-4. For the tick receptor: group *a*, had increased potency by a factor of 8, group *b* had increased potency by a factor of 4-6, and group *c* (IK-Aib-15) by a factor of 3.

Figure 2.2 Dose-dependent bioluminescence responses of IK analogs relative to the bioluminescence response elicited by 1 µM of the positive control peptide FFFSWGa. Mosquito (**A-D**) and tick (**E-H**) recombinant kinin receptors expressed in CHO-K1 cells were tested against 17- and 18- insect kinin analogs, respectively, each at 9 concentrations from 10^{-10}-10^{-5} M (Log on X-axis) using a calcium bioluminescence assay (the IK-PEG-10 analog was not active on mosquito receptor). The Y-axis (Mean ± SEM) represents the percentage of bioluminescence response (average bioluminescence units elicited during 30s) of each analog concentration in reference to the bioluminescence response elicited by 1µM of positive control analog, FFFSWGa (100%). This peptide was included in each plate for each analog test for normalization. Three replicates were performed for all analogs except for analog 1728 (n=2). Dose-response curves were generated with non-linear regression log(agonist) vs. response – variable slope (four parameters) function with GraphPad Prism 6.0 (GraphPad Software, La Jolla, CA). Each figure showed receptor responses to a group of analogs of similar design; their complete sequence is shown in Table 1. The panel figure legend highlights analogs' features. **A)** and **E)**: endogenous sequence of either aedeskinin-1 or -3. **B)** and **F)**: endogenous sequence of both aedeskinin-1 and -3. **C)** and **G)**: endogenous sequence of aedeskinin-2. **D)** and **H)**: polyethylene glycol (PEG) modified. The dose-response curves for FFFSWGa (positive control) and 1728 ([Aib]FF[Aib]WGa, a potent [Aib] agonist) were included in each figure for comparison.

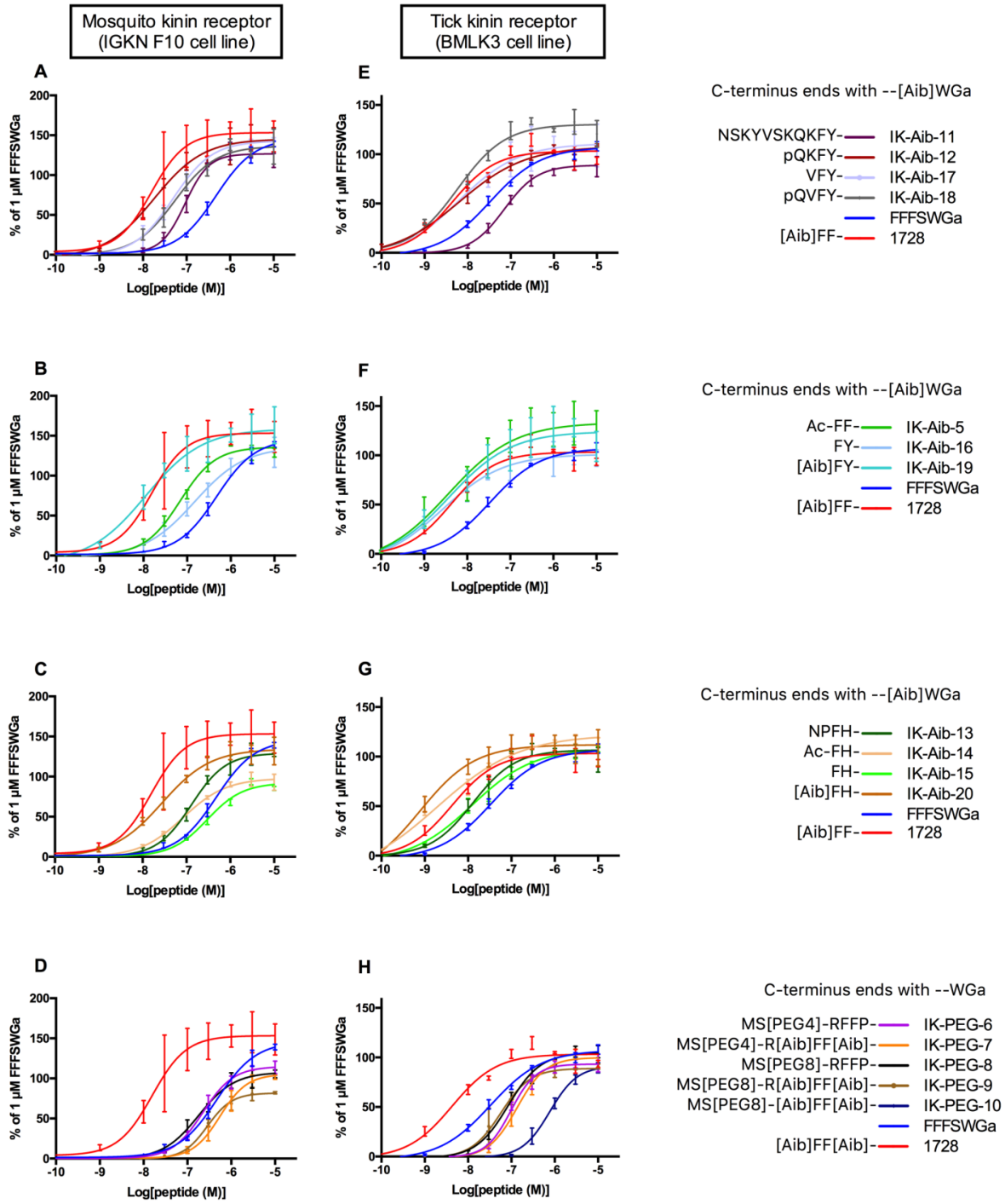
Mosquito kinin receptor (IGKN F10 cell line)
Tick kinin receptor (BMLK3 cell line)
A
E
B
F
C
G
D
H
% of 1 µM FFFSWGa
Log[peptide (M)]
C-terminus ends with --[Aib]WGa
NSKYVSKQKFY-
pQKFY-
VFY-
pQVFY-
[Aib]FF-
IK-Aib-11
IK-Aib-12
IK-Aib-17
IK-Aib-18
FFFSWGa
1728
C-terminus ends with --[Aib]WGa
Ac-FF-
FY-
[Aib]FY-
[Aib]FF-
IK-Aib-5
IK-Aib-16
IK-Aib-19
FFFSWGa
1728
C-terminus ends with --[Aib]WGa
NPFH-
Ac-FH-
FH-
[Aib]FH-
[Aib]FF-
IK-Aib-13
IK-Aib-14
IK-Aib-15
IK-Aib-20
FFFSWGa
1728
C-terminus ends with --WGa
MS[PEG4]-RFFP-
MS[PEG4]-R[Aib]FF[Aib]-
MS[PEG8]-RFFP-
MS[PEG8]-R[Aib]FF[Aib]-
MS[PEG8]-[Aib]FF[Aib]-
[Aib]FF[Aib]-
IK-PEG-6
IK-PEG-7
IK-PEG-8
IK-PEG-9
IK-PEG-10
FFFSWGa
1728

Table 2.2 Estimated potency potencies (EC_{50}) of insect kinin (IK) analogs on recombinant mosquito (IGKNF 10) and tick (BMLK3) receptors.

Rank of EC_{50}[1]	IK Sequence	Name	EC_{50} (nM)	95% Confidence Interval (nM)	Efficacy (%)[2]	SEM of efficacy (%; n=3)
Mosquito receptor (IGKNF10 cell line)						
1[a]	[Aib]FF[Aib]WGa	1728	17.16	11.85-26.17	152.98	9.89
2[a]	[Aib]FY[Aib]WGa	IK-Aib-19	18.17	13.14-24.64	150.70	2.86
3[a]	pQKFY[Aib]WGa	IK-Aib-12	23.23	17.68-30.52	136.12	18.86
4[a]	[Aib]FH[Aib]WGa	IK-Aib-20	28.32	21.58-37.18	132.25	8.71
5[b]	VFY[Aib]WGa	IK-Aib-17	52.63	43.51-63.66	133.07	2.65
6[b]	pQVFY[Aib]WGa	IK-Aib-18	77.12	55.03-108.1	138.07	2.69
7[b]	Ac-FF[Aib]WGa	IK-Aiib-5	78.37	55.19-114.3	144.35	5.92
8[d]	Ac-FH[Aib]WGa	IK-Aib-14	83.88	69.33-101.5	90.17	2.85
9[c]	NSKYVSKQKFY[Aib]WGa	IK-Aib-11	109.6	84.44-142.1	130.16	9.04
10[c]	FY[Aib]WGa	IK-Aib-16	132.3	112.5-155.6	110.84	5.79
11[c]	NPFH[Aib]WGa	IK-Aib-13	151.1	128.1-178.4	114.10	2.51
12[e]	MS[PEG8]-RFFPWGa	IK-PEG-8	181.8	154.8-213.5	97.29	4.55
13[e]	MS[PEG4]-RFFPWGa	IK-PEG-6	240.4	210.4-274.6	94.92	6.52
14[e]	MS[PEG8]-R[Aib]FF[Aib]WGa	IK-PEG-9	308.1	271.7-349.3	68.78	4.01
15[e]	FH[Aib]WGa	IK-Aib-15	310.8	254.4-382.6	67.85	2.79
16[e]	FFFSWGa	PC	398.1	345.6-458.5	100.00	0.00
17[e]	MS[PEG4]-R[Aib]FF[Aib]WGa	IK-PEG-7	505.7	457.4-558.9	72.05	10.53
18[*]	MS[PEG8]-[Aib]FF[Aib]WGa	IK-PEG-10	-	-	1.08	-
Tick receptor (BMLK3 cell line)						
1[a]	[Aib]FH[Aib]WGa	IK-Aib-20	2.091	1.350-3.239	111.74	4.24
2[a]	Ac-FH[Aib]WGa	IK-Aib-14	5.024	3.623-6.967	113.95	1.02
3[a]	FY[Aib]WGa	IK-Aib-16	5.176	3.358-7.978	112.23	10.12
4[b]	[Aib]FF[Aib]WGa	1728	6.612	3.275-13.35	104.80	0.85
5[b]	Ac-FF[Aib]WGa	IK-Aib-5	6.192	4.540-10.52	137.09	5.48
6[b]	pQVFY[Aib]WGa	IK-Aib-18	8.240	5.014-13.54	124.41	1.78
7[b]	pQKFY[Aib]WGa	IK-Aib-12	8.630	6.092-12.23	104.88	0.77
8[b]	[Aib]FY[Aib]WGa	IK-Aib-19	9.561	5.478-16.70	128.91	3.75
9[b]	VFY[Aib]WGa	IK-Aib-17	9.925	7.027-14.02	108.07	1.84
10[c]	FH[Aib]WGa	IK-Aib-15	15.17	11.05-20.28	101.49	0.89
11[c]	NPFH[Aib]WGa	IK-Aib-13	18.08	10.71-27.24	111.19	2.73
12[d]	FFFSWGa	PC	41.01	33.63-50.01	100.00	0.00
13[d]	MS[PEG8]-R[Aib]FF[Aib]WGa	IK-PEG-9	61.90	51.19-74.85	85.30	2.58
14[d]	MS[PEG8]-RFFPWGa	IK-PEG-8	93.41	82.14-106.2	95.35	1.26
15[d]	NSKYVSKQKFY[Aib]WGa	IK-Aib-11	106.6	72.57-156.6	81.92	2.79
16[d]	MS[PEG4]-RFFPWGa	IK-PEG-6	108.0	92.17-126.7	90.27	4.90
17[d]	MS[PEG4]-R[Aib]FF[Aib]WGa	IK-PEG-7	160.2	127.5-201.2	90.36	5.17
18[e]	MS[PEG8]-[Aib]FF[Aib]WGa	IK-PEG-10	758.5	666.1-863.8	53.71	4.43

[1]EC_{50} values: concentration that elicited 50% of the highest number of bioluminescence units for that analog (100%); n= 3 (except for 1728, n=2). Analogs are ranked by EC_{50} from more potent to less potent.[2]Efficacy was calculated as percentage of the bioluminescence response of each analog tested at 1µM concentration, with reference to the bioluminescence response elicited by 1µM of analog FFFSWGa (PC).[*]IK-PEG-10: no activity on mosquito receptor at 1µM; it was not further tested. [a-e] Different groups of analogs were categorized based on their agonist activities from high (a) to low (e) on each receptor, and by potency (EC_{50}) and efficacy. See correlation of potency and efficacy (Fig. 2.3).

Figure 2.3 The correlation between efficacy (efficacy; Y axis) and potency (X axis) of insect kinin (IK) analogs on mosquito (A) and tick (B) kinin receptors.

In both figures the X-axis represents Log[EC_{50}(M)] of each analog (Table 2), and the Y axis represents the efficacy (Table 2). The Pearson correlation (two-tailed) analysis was performed independently for the tick and mosquito receptor data sets. The linear regression lines and the 95% confidence intervals (dashed blue lines) were calculated with the "Best-fit value" setting using GraphPad Prism 6.0 (GraphPad Software, La Jolla, CA). The equations for linear regression lines are shown below each graph. Values outside the 95% confidence intervals were considered outliers and are labeled in magenta color. The 18 analogs were separated into different groups based on their physical location on the plot (sector) for each receptor. The plot was divided in sectors as follows: for both mosquito and tick plots, an horizontal line at the efficacy of PC (100%) and the analogs with efficacy > 100% were subsequently divided into three groups (a-c) by EC_{50}. Group (a) was divided by a vertical line for EC_{50} of 30 nM (mosquito receptor) and 5 nM (for tick receptor). Group a represented the most potent analogs that exhibited the same (on mosquito) or higher (on tick) potency as analog 1728 (a highly potent analog). Analogs in group (b) showed the second-highest potency with EC_{50} lower than 100 nM (on mosquito, and are less potent than group a), and with EC_{50} lower than 10 nM (on tick with similar level of potency as 1728). Group (c) represented analogs with intermediate potency in mosquito, with EC_{50s} above the 100nM line (arbitrarily defined). For tick receptor group (c) included analogs of intermediate potency with EC_{50} between 10 nM and that of the PC = 41nM (line intercept).

The analogs that fell into the lower sector of the plot, relative efficacy < 100% were subdivided as follows: A. For mosquito, there were 2 groups: group (d) on mosquito receptor represented an 'outlier' analog with low efficacy (IK-AIB-14) and (e) which includes all the polyethylene glycol (PEG) modified-analogs. B. For tick, group (d) includes the majority of the PEG analogs and IK-Aib-11, and (e) represented the least potent analogs.

A

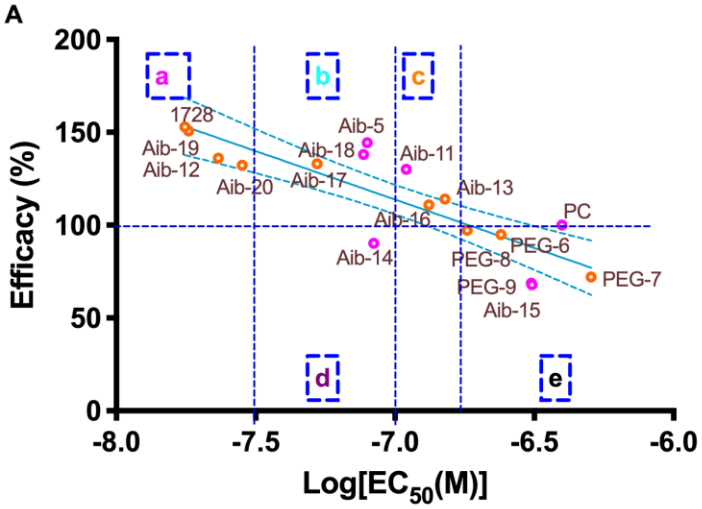

Y = -52.20*X - 251.6
R^2 =0. 73

B

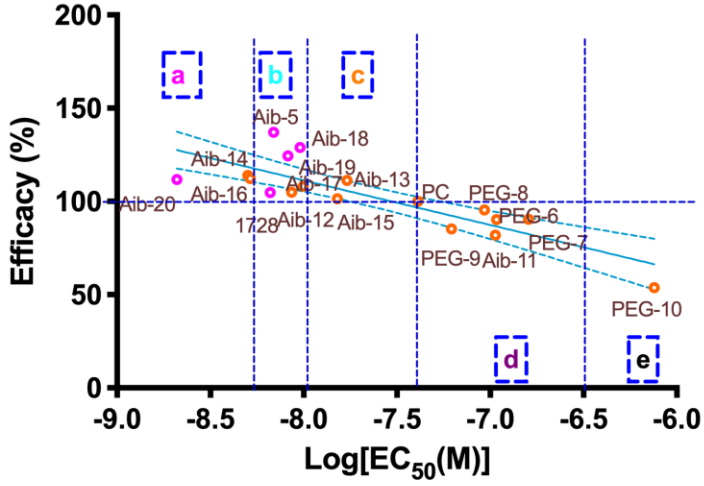

Y = -23.91*X - 80.00
R^2 =0. 71

Table 2.3 Comparative structure-activity relationships of Aib-analogs based on sequences of aedeskinins on mosquito and tick receptors.

	Recombinant mosquito receptor										
Designed based on aedeskinin1 and/or 3[a]		[Aib]F**F** 1728	[Aib]FY IK-Aib-19	p**QK**FY IK-Aib-12	**V**FY IK-Aib-17	p**QV**FY IK-Aib-18	Ac-FF IK-Aib-5	NSKYVSK**Q** **K**FY IK-Aib-11	EC50 (nM)	efficacy %	Activity[b]
[Aib]F**F**	1728	-							**17**	152.98	group a
[Aib]FY	IK-Aib-19	ns	-						**18**	150.70	group a
p**QK**FY	IK-Aib-12	ns	ns	-					**23**	136.12	group a
VFY	IK-Aib-17	*	*	*	-				52	133.07	group b
p**QV**FY	IK-Aib-18	*	*	*	ns	-			77	138.07	group b; OL high efficacy
Ac-F**F**	IK-Aib-5	*	*	*	ns	ns	-		78	144.35	group b; OL high efficacy
NSKYVSK**Q** **K**FY	IK-Aib-11	*	*	*	*	ns	ns	-	110	130.16	group c; OL high efficacy
FY	IK-Aib-16	*	*	*	*	ns	ns	ns	132	110.84	group c
Designed based on aedeskinin2		[Aib]FH IK-Aib-20	Ac-FH IK-Aib-14	NPFH IK-Aib-13	FH IK-Aib-15				EC50 (nM)	efficacy %	
[Aib]FH	IK-Aib-20	-							**28**	132.25	group a
Ac-F**H**	IK-Aib-14	*	-						84	**90.17**	group d; OL low efficacy
NPFH	IK-Aib-13	*	*	-					182	114.10	group c
FH	IK-Aib-15	*	*	*	-				311	**67.85**	group d; OL low efficacy

Table 2.3 Continued

		Recombinant tick receptor									
Designed based on aedeskinin1 and/or 3[a]		FY IK-Aib-16	[Aib]F**F** 1728	Ac-F**F** IK-Aib-5	p**QV**FY IK-Aib-18	p**QK**FY IK-Aib-12	[Aib]FY IK-Aib-19	**V**FY IK-Aib-17	EC50 (nM)	efficacy %	
FY	IK-Aib-16	-							**5.2**	112.23	group a
[Aib]F**F**	1728	ns	-						**6.6**	104.80	group b; OL low efficacy
Ac-F**F**	IK-Aib-5	ns	ns	-					**6.2**	137.09	group b; OL high efficacy; above 1728
p**QV**FY	IK-Aib-18	ns	ns	ns	-				**8.2**	124.41	group b; OL high efficacy; above 1728
p**QK**FY	IK-Aib-12	ns	ns	ns	ns	-			**8.6**	104.88	group b
[Aib]FY	IK-Aib-19	ns	ns	ns	ns	ns	-		**9.6**	128.91	group b; OL high efficacy; above 1728
VFY	IK-Aib-17	ns	ns	ns	ns	ns	ns	-	**9.9**	108.07	group b
NSKYVSK**Q** **K**FY	IK-Aib-11	*	*	*	*	*	*	*	107	**81.92**	group d

Designed based on aedeskinin2		[Aib]FH IK-Aib-20	Ac-FH IK-Aib-14	FH IK-Aib-15	NPFH IK-Aib-13	EC50 (nM)	efficacy %	
[Aib]FH	IK-Aib-20	-				**2.1**	111.74	group a; OL low efficacy; above 1728
Ac-FH	IK-Aib-14	ns	-			**5.0**	113.95	group a; above 1728
FH	IK-Aib-15	*	*	-		15	101.49	group c
NPFH	IK-Aib-13	*	*	ns	-	18	111.19	group c

[a] Only N terminal sequences are shown for clarity; all analogs have the same C-terminus as -[Aib]WGa; for complete sequences see Table 2.2.[b] OL stands for outlier in the correlation analyses (Fig. 3), and 'above 1728' means the analog bioluminescence dose-response curve was higher than that of 1728 (Fig. 2. E-H).For pair comparisons * = significant differences of potency (EC_{50}; * means $P < 0.05$ by Tukey multiple comparison test) and ns = not significant differences. These are the results of the detailed statistical analyses in Supplementary Tables 2.1.1 and 2.2.1.

2.4.1. Novel insect kinin Aib analog design

A new series of eleven biostable, Aib-containing IK analogs incorporated the sequence of the three native aedeskinins neuropeptides of the mosquito *Ae. aegypti* (Table 2.1). One group of six IK analogs featured incorporation of the sequences of aedeskinin 1, aedeskinin 3 or both, and share the same Y residue in the variable 2nd position of the C-terminal pentapeptide FYXWGa (Table 2.1). In aedeskinin 1, the variable position X is occupied by an S, whereas in aedeskinin 3 it is occupied by a P; though the distinction is inconsequential because in this analog series the position is occupied by Aib. Analog IK-Aib-11 (NSKYVSKQFY[Aib]WGa) features an Aib residue imbedded into the turn region of the entire sequence of aedeskinin 1 (Table 2.1). Analogs IK-Aib-19, IK-Aib-5 and IK-Aib-16 are not only analogs of aedeskinin 1, but also of aedeskinin 3. The aedeskinin 2 series shares a histidine (H) in the variable position. Analog IK-Aib-13 features an Aib imbedded in the entire sequence of aedeskinin 2; whereas IK-Aib-15, IK-Aib-14 and IK-Aib-20 are fragment analogs.

The influence of analog length, number of Aib molecules, aromaticity or charge of residues in variable positions, and type of N-terminal protecting groups is discussed as to their influence on potency and efficacy. All eleven Aib IK analogs were active as agonists on both tick and mosquito recombinant receptors, with various potencies (EC_{50}) and binding efficacies on each receptor (Table 2.2).

2.4.2. Insect kinin PEG analogs

Five insect kinin analogs incorporating PEG_4 (MS-PEG_4) and PEG_8 (MS-PEG_8) polymers at the N-terminus were designed, three of which also incorporate the sterically-hindered Aib residue at hydrolysis sites (Table 2.1 and Fig. 2.1).

2.4.3. Activity of Aib analogs on the mosquito kinin receptor

Analogs will be discussed by order of overall activity (Fig. 2.3A). For the mosquito receptor the first four analogs in Table 2.2, 1728 (EC_{50}=17 nM), K-Aib-19 (EC_{50}=18 nM), IK-Aib-12 (EC_{50}=23 nM) and IK-Aib-20 (EC_{50}=28 nM) were significantly more potent than the rest of the analogs (Suppl. Table 2.1.1, Suppl. Fig. 2.1, A-C), but there were no significant differences among the four, either in potency or efficacy (Table 2.2; Suppl. Tables 1.1 and 1.2). All four were designed with a blocked N-terminus, Aib or (pyroglutamic acid (pQ)), to impair activity of degrading aminopeptidases, and three of them featured two molecules of Aib (at primary and secondary hydrolysis sites). The sequences only differ in one amino acid at the X^1 position (F, Y and H). Among all 17 analogs tested, IK-AIB-19 was the only analog that had statistically higher efficacy than the PC (Table 2.2, Suppl. Table 2.1.2). In the correlation analyses there were no outliers among these four analogs (sector a in Fig. 2.3A), and although they do not differ in efficacy with respect to the following group of Aib analogs (Fig. 2.3A, sector b), they have higher potency. For these reasons these are the most desirable IK analogs and candidates to be tested *in vivo*.

After analogs in group *a*, analogs IK-Aib-5, IK-Aib-17, IK-Aib-18 were the most potent group of analogs, with similar EC_{50} values of less than 100 nM, significantly more potent than the PC (Table 2.2, Suppl. Fig. 2.1, A-B, Suppl. Table 2.1.1). Moreover, their relative activity (bioluminescence) curves completely overlapped (Fig. 2.2, A-B). Although the efficacy was not different from that of the PC at 1 µM (Suppl. Table 2.1.2), the analogs' curves in Fig. 2.2 (A and B) are shifted to the left, reflecting the significantly higher potency of these analogs with respect to the PC (Suppl. Fig. 2.1. A-B). Besides, the N-terminus of IK-Aib-5 and -18 were further protected from aminopeptidases with an acetyl group and a pyroglutamate, respectively, making

them potentially more stable than IK-Aib-17 (Table 2.2). Importantly, when comparing IK-Aib-17 to IK-Aib-18, the addition of the protective pQ at the N-terminus did not diminish its potency (Table 2.2, Suppl. Tables 1. 1). Correlation analyses grouped them in sector *b* (Fig. 2.3A), with IK-Aib-5 and IK-Aib-18 being outliers because they had higher efficacy than expected by the regression line.

Notably, IK-Aib-12 (pQ**K**FY[Aib]WGa) in group *a* and IK-Aib-18 (pQ**V**FY[Aib]WGa) in group *b* featured pQ on the N-terminus, and differed only in one residue before the kinin core (Table 2.3). The EC_{50} value of IK-Aib-12 (23 nM) was significantly lower (3.3-fold) than IK-Aib-18 (77 nM), suggesting a positively charged lysine plays a role in enhancing the analog activity in the presence of pQ on the N-terminus.

Among analogs designed as mono Aib pentapeptides, it appears that there is a higher activity for analogs featuring F or Y over H. Analog IK-Aib-5 (Ac-F**F**[Aib]WG) was significantly more efficacious (higher efficacy) on the receptor than IK-Aib-14 (Ac-F**H**[Aib]WGa), of similar structure (Fig. 2.2, B-C; Suppl. Table 2.1.2). This resulted in IK-Aib-14 being an outlier in the correlation analyses (Fig. 2.3A, sector d), despite similar EC_{50}s. Similarly to the above, in unprotected pentapeptides, analog IK-Aib-16 featuring Y (F**Y**[Aib]WGa; EC_{50} =132 nM) was over 2-fold more potent than analog IK-Aib-15 (F**H**[Aib]WGa; EC_{50} =311 nM) (Table 2.2).

Group *c* consisted of analogs of intermediate potency (Fig. 2.3A). They showed significant differences with analog(s) in group *b*, while exhibiting significantly greater potency and similar binding efficacies in comparison with the PC (Suppl. Tables 1.1 and 1.2). Their dose-dependent responses were highly similar (Fig. 2.2, A-C) and no statistical difference was detected in either their EC_{50s} (IK-Aib-11,110 nM; IK-Aib-13, 151 nM, and IK-Aib-16,132 nM)

or binding efficacies (Table 2.2; Suppl.Tables 1.1 and 1.2). This group of analogs featured an Aib molecule embedded in full or as a fragment of sequences of aedeskinin 1-3 without any modification on the 2nd hydrolysis site (Table 2.1), and they are thus expected to be less resistant to hydrolysis by aminopeptidases. Despite its similar potency within group *c*, analog IK-Aib-11 was an outlier above the upper 95% confidence interval for efficacy (Fig. 2.3A).

It is noteworthy that the pentapeptide IK-Aib-16, FY[Aib]WGa had similar activity to IK-Aib-11 (featuring all 14 residues of aedeskinin 1), as the mosquito kinin receptor preferred hexapeptide kinin analogs over their pentapeptide counterparts in a previous study (Taneja-Bageshwar et al., 2006). Thus, the full sequence of aedeskinin 1 as appears in analog IK-Aib-11 would have been expected to have a greater potency than the corresponding C-terminal pentapeptide analogs. Furthermore, despite its greater length, IK-Aib-11 is less potent than a smaller, similar fragment analog IK-Aib-12 (Table 2.3).

IK-Aib-19 and IK-Aib-17, hexapeptides with sequences common to aedeskinin 1 and/or aedeskinin 3, showed higher potency than the respective pentapeptide IK-Aib-16 (FY[Aib]WGa) (Table 2.3, Suppl. Table 2.1.1). Similarly, for aedeskinin 2 based analogs, IK-Aib-20 and IK-Aib-13 also showed significantly greater potency than the pentapeptide IK-Aib-15 (FH[Aib]WGa) (Fig. 2.2C, Table 2.3). IK-Aib-15 had significantly lower potency than all Aib-analogs tested, and in the correlation analyses it was an outlier due to its significantly lower efficacy from groups *a* and *b* (Fig. 2.3A, Suppl. Table 2.1.2).

The presence of a mono-Aib group changed the potency of the endogenous aedeskinins. Their rank order of potency was first analog IK-Aib-11 (similar to aedeskinin 1), followed by analog IK-Aib-13 (similar to aedeskinin 2) (Table 2.2). This is in contrast to the previously

determined potencies of the parent peptides, as aedeskinin 2 was found to be more potent on this recombinant receptor than aedeskinin 1 (Pietrantonio, P. et al., 2005).

2.4.4. Evaluation of Aib analogs on the tick kinin receptor

Evaluation of the Aib IK analog series on the tick recombinant receptor revealed that all retained high potency. The tick receptor is clearly more permissive than the mosquito receptor, as nine of the kinin analogs had potencies at or below 10 nM, two had potencies below 20nM and only one had EC_{50} above 100nM (Table 2.2). All analogs had similar efficacy except for IK-Aib-11, with lower efficacy (Table 2.2; Suppl. Table 2.2.2). In contrast to the mosquito kinin receptor, 1728 was not among the most potent analogs (Table 2.2; Suppl. Fig.1, E-G), and it is an outlier below the 95% intervals of the regression line (Fig. 2.3B). Three of the analogs constituted the most potent with an EC_{50} lower than 5 nM and formed group *a*, with no significant differences among them (Table 2.2; Fig. 2.3B). The high potency of IK-Aib-20 is particularly noteworthy, with an EC_{50} value of 2 nM, being more potent than 1728 by a factor of 3 and exhibiting a dose-response curve higher than that of 1728 (Fig. 2.2G), and it was an outlier in the correlation analysis with lower than expected efficacy (Fig. 2.3). Further, analog IK-Aib-20 was designed based on aedeskinin 2 (features H) (Table 2.3) and its potency was significantly different from the rest of all analogs except for those in group *a* (Suppl. Table 2.2.1). Analogs IK-Aib-20 and IK-Aib-14 feature additional protection from aminopeptidase attack (protection that is lacking in IK-Aib-16), and therefore, they are expected to be more biostable. Analog IK-Aib-14 also showed a dose-response curve above the one of 1728 (Fig. 2.2G).

Analogs with an EC_{50} between 5-10nM were similar in potency (IK-Aib-5, -18, -12, -19, and -17) (Table 2.2), matched the potency of 1728 and were considered as group *b* (Fig. 2.3B). This group of IK analogs was designed based on the sequences of aedeskinins 1 and/or 3 (Table

2.3). Three of them (IK-Aib-5, -18 and -19) showed dose-response curves above that of 1728, and simultaneously were outliers with higher than predicted efficacy in correlation analysis (Figs. 2E-F and 3B). Analogs in group *c*, IK-Aib-15 and IK-Aib-13, were intermediate in potency with a significantly higher EC_{50} that analogs in group *a* (Fig. 2.3B, Suppl. Table 2.2.1). These two analogs were designed based on aedeskinin 2 but are not blocked at the N-terminus (Table 2.3). There is only one analog in group *d* (Fig. 2.3B), IK-Aib-11, that features 14 residues as in aedeskinin 1, and had the lowest potency and efficacy among all Aib analogs (Table 2.2, Fig. 2.2E, Suppl. Table 2.2).

Within the multi-Aib C-terminal hexapeptide framework, differences in the potency of analogs that feature different aromatic residues (F, Y or H) in variable position 2 of the IK C-terminal pentapeptide core, IK-Aib-20, 1728 and IK-Aib-19 (Tables 2), suggest that the tick receptor exhibits a preference for the positively charged, aromatic residue H (IK-Aib-20) (Table 2.2). In the IK core variable position of the mono-Aib C-terminal pentapeptide framework by contrast, as with the mosquito receptor, the tick receptor exhibits a preference for Y over H, as analog IK-Aib-16 is more potent than IK-Aib-15 by a factor of 3, with this difference being statistically significant.

2.4.5. Evaluation of PEG analogs on the mosquito kinin receptor

Five insect kinin analogs incorporating PEG_4 [MS(PEG_4)] and PEG_8 [MS(PEG_8)] polymers, three of which also incorporate the sterically-hindered Aib residue at the core N-terminus, were evaluated on the two recombinant IK receptors. One analog, IK-PEG-10, was not active. As a group, the remaining four PEG analogs had lower potency than the majority of the IK-Aib analogs, with a range of EC_{50}s from 182 nM to 506 nM (Table2, Suppl. Fig. 2.1D). They exhibited similar activity as compared with the PC (Suppl. Table 2.1.2), and in the correlation

analyses fell in group *e* (Fig. 2.3A). The PC was an outlier in the mosquito receptor with a higher efficacy than predicted by the regression line. This may explain that despite having an apparent lower EC_{50}, its dose-response curve closely matches those of IK-PEG-8 and -6. IK-PEG-8, IK-PEG-6 and IK-PEG-9 were similar in potency and the first two are significantly more potent than IK-PEG-7 (Table 2.2; Suppl. Tables 1.1). Further, the overall dose-response curves of IK-PEG-6 and IK-PEG-8 were above the response curves of IK-PEG-7 and IK-PEG-9 (Fig. 2.2D). IK-PEG-6 and IK-PEG-8, with MS(PEG_4) and MS(PEG_8) groups on the N-terminus, respectively, shared the same amino acid sequence (-RFFPWGa), respectively (Table 2.1).

Analog IK-PEG-9 fell within the most potent PEG analogs (not different from IK-PEG-8 and -6), however, it is the only one of this group that is also not different from IK-PEG-7, that featured lower potency. The fact that IK-PEG-9 shows similar potency to the first group but also does not differ from IK-PEG-7 can be explained by the shape of the dose-response curve (Fig. 2.2D): While the efficacy is the same at 1 µM for both analogs, at 10 µM IK-PEG-9 plateaued, behaving as a partial agonist. IK-PEG-7 and IK-PEG-9 have two Aib molecules in the sequence (-R[Aib]FF[Aib]WGa) that can confer additional endopeptidase biostability to the IK sequence, and therefore potentially greater hemolymph residence time when tested *in vivo* than IK-PEG-8 and IK-PEG-10 (-RFFPWGa). Overall, these results revealed that the mosquito kinin receptor did not discriminate PEG analogs with either MS(PEG_4) or MS(PEG_8). The analog IK-PEG-10 (MS(PEG_8)-[Aib]FF[Aib]WGa), which is the only analog that lacks the R residue as in IK-PEG-9 (MS(PEG_8)-R[Aib]FF[Aib]WGa), is not active on the mosquito receptor. The R may confer an advantage by enhancing solubility properties, by providing a spacer between the IK core region and the PEG polymer, and/or a more favorable ligand receptor interaction due to the presence of the positively charged residue.

2.4.6. Evaluation of PEG analogs on the tick kinin receptor

The evaluation of IK analogs incorporating PEG polymer attachments at the N-terminus showed that a few (IK-PEG-8 and IK-PEG-9) retained significant activity that matched the potency of the positive control FFFSWGa (Suppl. Fig. 2.1H, Suppl. Table 2.2.1). The analog IK-PEG-10, that was not active on the mosquito receptor, was the weakest agonist of all analogs tested on the tick receptor (Table 2.2; Suppl. Table 2.2.1). It is the only analog in sector *e* (Fig. 2.3B), with significant lower potency but comparable efficacy to the other PEG analogs, but lower efficacy than the PC (Suppl. Table 2.2, Fig. 2.2H). The remaining four PEG analogs as a group, had lower activity than the majority of the IK-Aib analogs, with an EC_{50} range from 62nM to 160nM (Table 2.2, Suppl. Fig. 2.1D), and are placed in group *d* (Fig. 2.3B).

The Aib-containing analog IK-PEG-9 exhibited the greatest potency among this IK-PEG series on the tick receptor with an EC_{50} of 62 nM. IK-PEG-9 (featuring MS(PEG_8), was significantly more potent than its' P_4 counterpart IK-PEG-7 (MS(PEG_4)-R[Aib]FF[Aib]WGa) with EC_{50} of 160 nM (Table 2.2). These are the only two that exhibited significant differences in potency (Suppl. Table 2.2.1) among the four active PEG analogs featuring overall similar dose-response curves (Fig. 2.2H). Therefore, for PEG analogs containing Aib, the tick receptor reveals a preference for the longer MS(PEG_8) polymer over the MS(PEG_4) polymer. The two Aib residues of these two analogs confer enhanced resistance to endopeptidase hydrolysis, potentially increasing *in vivo* hemolymph residence time.

While IK-PEG-10 retains some activity on the tick receptor, it was inactive on the mosquito receptor, reinforcing the fact that the recombinant tick receptor cell line is more responsive to ligand binding than the mosquito receptor cell line. Of striking significance, however, is the contrast between the most potent PEG analog IK-PEG-9 (MS(PEG_8)-R[Aib]FF[Aib]WGa) and

the least potent, IK-PEG-10 (MS(PEG_8)-[Aib]FF[Aib]WGa). The only difference between these two IK-PEG analogs is the presence of an R residue in the former (Table 2.2). The arginine (R) residue in the more active PEG analogs containing Aib proved to be an important component for activity on both invertebrate receptors. The R (arg) may confer an advantage by enhancing solubility properties, by providing a spacer between the IK core region and the PEG polymer, and/or a more favorable ligand receptor interaction.

2.5. Summary and conclusions

The evaluation of a series of IK-Aib analogs incorporating sequences of endogenous aedeskinins from the *Ae. aegypti* mosquito on two invertebrate receptor cell lines revealed a number of highly potent biostable IK mimics. To prevent hydrolysis by aminopeptidases biostable IK analogs incorporating a second Aib residue N-terminal to Phe^1 of the core were synthesized. On the mosquito *Ae. aegypti* kinin receptor three highly potent, biostable Aib analogs (group *a*) matched the activity of IK analog 1728, that has previously demonstrated insect disruptive and/or aversive activity; therefore it is possible these analogs may have similarly desirable activity. They may also be useful tools in further defining the structural characteristics required to induce aversive and/or deterrent behavior in the mosquito and kissing bug. Evaluation of analogs with PEG polymers attached on the N-terminus revealed certain analogs with similar or higher potency as the positive control peptide, and they are important tools for testing kinin activities *in vivo*.

The most active of the Aib and PEG analogs identified in this study represent new tools for arthropod endocrinologists studying insect kinin regulated processes, particularly in ticks for which a role for the insect kinins has yet to be established. The potent, biostable analogs presented here would demonstrate longer hemolymph residence times, making them particularly

suitable for the study of *in vivo* physiological and behavioral effects of kinin neuropeptides. Furthermore, these analogs, either in isolation or in combination with biostable analogs of other neuropeptide classes that also regulate aspects of diuretic, antidiuretic, digestive, reproductive and/or developmental processes, represent potential leads in the development of selective, environmentally friendly pest arthropod control agents capable of disrupting those critical processes.

2.6. Acknowledgements

RJN received support from the US Department of Agriculture/Department of Defense Deployed War Fighter Protection Initiative 6202-22000-029-00D. We thank Allison Strey (USDA) for able technical assistance in the synthesis, purification and characterization of the peptide analogs. Research in PVP laboratory was supported by USDA-NIFA-AFRI Foundational Grant number 2016-67015-24918 (Animal Health and Well-Being), and by a Vector Biology seed grant from Texas A&M AgriLife Research. C. Xiong is a Ph.D. student in the Entomology graduate program. Drs. Daeweon Lee and Christina Brock are acknowledged for technical assistance for cell assays.

2.7. References

Boccù, E., Velo, G., Veronese, F., 1982. Pharmacokinetic properties of polyethylene glycol derivatized superoxide dismutase. Pharmacological research communications 14, 113-120.

Coast, G., 2007. The endocrine control of salt balance in insects. General and Comparative Endocrinology 152, 332-338.

Coast, G.M., Holman, G.M., Nachman, R.J., 1990. The diuretic activity of a series of cephalomyotropic neuropeptides, the achetakinins, on isolated Malpighian tubules of the house cricket, *Acheta domesticus*. Journal of Insect Physiology 36, 481-488.

Coast, G.M., Orchard, I., Phillips, J.E., Schooley, D.A., 2002. Insect diuretic and antidiuretic hormones. Advances in Insect Physiology 29, 279-409.

Cornell, M.J., Williams, T.A., Lamango, N.S., Coates, D., Corvol, P., Soubrier, F., Hoheisel, J., Lehrach, H., Isaac, R.E., 1995. Cloning and expression of an evolutionary conserved single-domain angiotensin converting enzyme from *Drosophila melanogaster*. Journal of Biological Chemistry 270, 13613-13619.

De Loof, A., 2008. Ecdysteroids, juvenile hormone and insect neuropeptides: recent successes and remaining major challenges. General and Comparative Endocrinology 155, 3-13.

Gäde, G., 2004. Regulation of intermediary metabolism and water balance of insects by neuropeptides. Annual Reviews in Entomology 49, 93-113.

Gäde, G., Goldsworthy, G.J., 2003. Insect peptide hormones: a selective review of their physiology and potential application for pest control. Pest Management Science 59, 1063-1075.

Harshini, S., Manchu, V., Sunitha, V., Sreekumar, S., Nachman, R., 2003. In vitro release of amylase by culekinins in two insects: *Opsinia arenosella* (Lepidoptera) and *Rhynchophorus ferrugineus* (Coleoptera). Trends in Life Sciences 17, 61-64.

Holman, G.M., Nachman, R., Wright, M., 1990. Insect neuropeptides. Annual Review of Entomology 35, 201-217.

Holman, G.M., Nachman, R.J., Coast, G.M., 1999. Isolation, characterization and biological activity of a diuretic myokinin neuropeptide from the housefly, *Musca domestica*. Peptides 20, 1-10.

Holmes, S., Barhoumi, R., Nachman, R., Pietrantonio, P., 2003. Functional analysis of a G protein- coupled receptor from the Southern cattle tick *Boophilus microplus* (Acari: Ixodidae) identifies it as the first arthropod myokinin receptor. Insect Molecular Biology 12, 27-38.

Holmes, S., He, H., Chen, A., Ivie, G., Pietrantonio, P., 2000. Cloning and transcriptional expression of a leucokinin- like peptide receptor from the Southern cattle tick, *Boophilus microplus* (Acari: Ixodidae). Insect Molecular Biology 9, 457-465.

Jeffers, L.A., Roe, R.M., 2008. The movement of proteins across the insect and tick digestive system. Journal of Insect Physiology 54, 319-332.

Kersch, C.N., Pietrantonio, P.V., 2011. Mosquito *Aedes aegypti* (L.) leucokinin receptor is critical for *in vivo* fluid excretion post blood feeding. FEBS letters 585, 3507-3512.

Kim, D.-H., Kim, Y.-J., Adams, M.E., 2018. Endocrine regulation of airway clearance in *Drosophila*. Proceedings of the National Academy of Sciences 115, 1535-1540.

Kwon, H., Agha, M.A., Smith, R.C., Nachman, R.J., Marion-Poll, F., Pietrantonio, P.V., 2016. Leucokinin mimetic elicits aversive behavior in mosquito *Aedes aegypti* (L.) and inhibits the sugar taste neuron. Proceedings of the National Academy of Sciences 113, 6880-6885.

Lamango, N.S., Sajid, M., Isaac, R.E., 1996. The endopeptidase activity and the activation by Cl- of angiotensin-converting enzyme is evolutionarily conserved: purification and properties

of an an angiotensin-converting enzyme from the housefly, *Musca domestica*. Biochemical Journal 314, 639.

Lu, H.L., Kersch, C., Pietrantonio, P.V., 2011a. The kinin receptor is expressed in the Malpighian tubule stellate cells in the mosquito *Aedes aegypti* (L.): A new model needed to explain ion transport? Insect Biochemistry and Molecular Biology 41, 135-140.

Lu, H.L., Kersch, C.N., Taneja-Bageshwar, S., Pietrantonio, P.V., 2011b. A Calcium Bioluminescence Assay for Functional Analysis of Mosquito (*Aedes aegypti*) and Tick (*Rhipicephalus microplus*) G Protein-coupled Receptors. Jove-J Vis Exp 50, e273210.273791/272732.

Nachman, R.J., Coast, G.M., Douat, C., Fehrentz, J.-A., Kaczmarek, K., Zabrocki, J., Pryor, N.W., Martinez, J., 2003. A C-terminal aldehyde insect kinin analog enhances inhibition of weight gain and induces significant mortality in *Helicoverpa zea* larvae. Peptides 24, 1615-1621.

Nachman, R.J., Coast, G.M., Holman, G.M., Beier, R.C., 1995. Diuretic activity of C-terminal group analogues of the insect kinins in *Acheta domesticus*. Peptides 16, 809-813.

Nachman, R.J., Holman, G.M., 1991. Myotropic Insect Neuropeptide Families from the Cockroach *Leucophaea maderae*: Structure—Activity Relationships, in: Menn, J.J., Masler, Edward P. (Ed.), Insect neuropeptides: chemistry, biology, and action. American Chemical Society, Washington, D.C., pp. 194-214.

Nachman, R.J., Isaac, R.E., Coast, G.M., Holman, G.M., 1997a. Aib-Containing Analogues of the Insect Kinin Neuropeptide Family Demonstrate Resistance to an Insect Angiotensin-Converting Enzyme and Potent Diuretic Activity. Peptides 18, 53-57.

Nachman, R.J., Isaac, R.E., Coast, G.M., Roberts, V.A., Lange, A.B., Orchard, I., Holman, G.M., Teal, P.E., 1997b. Active conformation and mimetic analog development for the Pyrokinin—PBAN—Diapause—Pupariation and Myosuppressin insect neuropeptide families, in: Hedin, P.A., Hollingworth, R.M., Masler, E.P., Miyamoto, J., Thompson, D.G. (Eds.), Phytochemicals for Pest Control. American Chemical Society, Washington, DC, pp. 277-291.

Nachman, R.J., Roberts, V.A., Holman, G.M., Trainer, J., 1990. Concensus chemistry and conformation of an insect neuropeptide family analogous to tachykinins. Progress in Clinical and Biological Research 342, 60.

Nachman, R.J., Strey, A., Isaac, E., Pryor, N., Lopez, J.D., Deng, J.-G., Coast, G.M., 2002. Enhanced in vivo activity of peptidase-resistant analogs of the insect kinin neuropeptide family. Peptides 23, 735-745.

Nachman, R.J., Tilley, J.W., Hayes, T.K., Holman, G.M., Beier, R.C., 1994. Pseudopeptide mimetic analogs of insect neuropeptides, in: Hedin, P., Menn, J.J., Hollingworth, R.M. (Eds.), Natural and Engineered Pest Management Agents. American Chemical Society, Washington DC, pp. 210-229.

Nässel, D.R., 2002. Neuropeptides in the nervous system of *Drosophila* and other insects: multiple roles as neuromodulators and neurohormones. Progress in Neurobiology 68, 1-84.

Pietrantonio, P., Jagge, C., Taneja- Bageshwar, S., Nachman, R., Barhoumi, R., 2005. The mosquito *Aedes aegypti* (L.) leucokinin receptor is a multiligand receptor for the three Aedes kinins. Insect molecular biology 14, 55-67.

Predel, R., Kellner, R., Rapus, J., Penzlin, H., Gáde, G., 1997. Isolation and structural elucidation of eight kinins from the retrocerebral complex of the American cockroach, *Periplaneta americana*. Regulatory Peptides 71, 199-205.

Roberts, V.A., Nachman, R.J., Coast, G.M., Hariharan, M., Chung, J.S., Holman, G.M., Williams, H., Tainer, J.A., 1997. Consensus chemistry and R-turn conformation of the active core of the insect kinin neuropeptide family. Chemistry & Biology 4, 105-117.

Seinsche, A., Dyker, H., Lösel, P., Backhaus, D., Scherkenbeck, J., 2000. Effect of helicokinins and ACE inhibitors on water balance and development of *Heliothis virescens* larvae. Journal of Insect Physiology 46, 1423-1431.

Shen, H., Brandt, A., Witting-Bissinger, B.E., Gunnoe, T.B., Roe, R.M., 2009. Novel insecticide polymer chemistry to reduce the enzymatic digestion of a protein pesticide, trypsin modulating oostatic factor (TMOF). Pesticide Biochemistry and Physiology 93, 144-152.

Taneja-Bageshwar, S., Strey, A., Isaac, R.E., Coast, G.M., Zubrzak, P., Pietrantonio, P.V., Nachman, R.J., 2009. Biostable agonists that match or exceed activity of native insect kinins on recombinant arthropod GPCRs. Gen Comp Endocrinol 162, 122-128.

Taneja-Bageshwar, S., Strey, A., Zubrzak, P., Williams, H., Reyes-Rangel, G., Juaristi, E., Pietrantonio, P., Nachman, R.J., 2008. Identification of selective and non-selective, biostable β-amino acid agonists of recombinant insect kinin receptors from the southern cattle tick *Boophilus microplus* and mosquito *Aedes aegypti*. Peptides 29, 302-309.

Taneja- Bageshwar, S., Strey, A., Zubrzak, P., Pietrantonio, P.V., Nachman, R.J., 2006. Comparative structure- activity analysis of insect kinin core analogs on recombinant kinin receptors from Southern cattle tick *Boophilus microplus* (Acari: Ixodidae) and

mosquito *Aedes aegypti* (Diptera: Culicidae). Archives of insect biochemistry and physiology 62, 128-140.

Torfs, P., Nieto, J., Veelaert, D., Boon, D., Water, G., Waelkens, E., Derua, R., Calderon, J., Loof, A., Schoofs, L., 1999. The kinin peptide family in invertebrates. Annals of the New York academy of sciences 897, 361-373.

Veenstra, J.A., Pattillo, J.M., Petzel, D.H., 1997. A single cDNA encodes all three *Aedes* leucokinins, which stimulate both fluid secretion by the Malpighian tubules and hindgut contractions. Journal of Biological Chemistry 272, 10402-10407.

3. THE CATTLE FEVER TICK, *RHIPICEPHALUS MICROPLUS*, AS A MODEL FOR FORWARD PHARMACOLOGY TO ELUCIDATE KININ GPCR FUNCTION IN THE ACARI[*]

3.1. Overview

The success of the acaricide amitraz, a ligand of the tick tyramine/octopamine receptor (a G protein-coupled receptor; GPCR), stimulated interest on arthropod-specific GPCRs as targets to control tick populations. This search advances tick physiology because little is known about the pharmacology of tick GPCRs, their endogenous ligands or their physiological functions. Here we explored the tick kinin receptor, a neuropeptide GPCR, and its ligands. Kinins are pleiotropic insect neuropeptides but their function in ticks is unknown. The endogenous tick kinins are unknown and their cDNAs have not been cloned in any species. In contrast, more than 271 insect kinin sequences are available in the DINeR database. To fill this gap, we cloned the kinin cDNA from the cattle fever tick, *Rhipicephalus microplus,* which encodes 17 predicted kinins, and verified the kinin gene structure. We predicted the kinin precursor sequences from additional seven tick species, including *Ixodes scapularis*. All species showed an expansion of kinin paracopies. The "kinin core" (minimal active sequence) of tick kinins FX_1X_2WGamide is similar to those in insects. Pro was predominant at the X_2 position in tick kinins. Towards accelerating the discovery of kinin function in ticks we searched for novel synthetic receptor ligands. We developed a dual-addition assay for functional screens of small molecules and/or peptidomimetics that uses a fluorescent calcium reporter. A commercial library of fourteen small molecules antagonists of mammalian neurokinin (NK) receptors was screened using this

[*] Reprinted with permission from "The cattle fever tick, *Rhipicephalus microplus*, as a model for forward pharmacology to elucidate kinin GPCR function in the Acari" by Xiong, C., Baker, D., Pietrantonio, P. V., 2019. Frontiers in Physiology, 10: 1008, Copyright [2019] by Frontiers.

endpoint assay. One acted as full antagonist (TKSM02) with inhibitory concentration fifty (IC_{50}) of ~45 µM, and three were partial antagonists. A subsequent calcium bioluminescence assay tested these 4 antagonists through kinetic curves and confirmed TKSM02 as full antagonist and one as partial antagonist (TKSM14). Antagonists of NK receptors displayed selectivity (>10,000-fold) on the tick kinin receptor. Three peptidomimetic ligands of the mammalian NK receptors (hemokinin 1, antagonist G and spantide I) were tested in the bioluminescence assay but none were active. Forward approaches may accelerate discovery of kinin ligands, either as reagents for tick physiological research or as lead molecules for acaricide development, and they demonstrate that selectivity is achievable between mammalian and tick neuropeptide systems.

3.2. Introduction

The cattle fever tick or southern cattle tick, *Rhipicephalus microplus* (Canestrini), and the diseases it transmits cause significant losses to the livestock industry in tropical and subtropical regions of the world (Pérez de León et al., 2012). Considering the lack of effective vaccines against many of these vector-borne pathogens, vector control is still the most efficient approach to block disease transmission. However, worldwide distribution of tick resistance to the most commonly used acaricides, such as amitraz (formamidines), pyrethroids, organophosphates, and ivermectin was detected in tick populations (Guerrero et al., 2012; Pohl et al., 2012). In the near future, the current available pesticides will fail to control populations of these ticks as many exhibit multiple mechanisms of resistance with apparently no fitness cost. Pesticides safe to non-target species with novel modes of actions in vectors are needed. Here we describe a model study using a forward pharmacological approach to investigate a tick neuropeptide G protein-coupled receptor (GPCR) as potential target for tick control (Fig. 3.1). This receptor, known as leucokinin-like peptide receptor (LKR) (accession AF228521), or myokinin receptor (Holmes, S.

et al., 2003; Holmes, S. et al., 2000b) has been suggested as a promising novel target for pest control (Audsley and Down, 2015; Guerrero et al., 2016; Lees et al., 2010; Pietrantonio, P. et al., 2018). A kinin peptidomimetic is antifeedant and lethal to the pea aphid (Smagghe et al., 2010), prevents the blood feeding to repletion in the kissing bug, *Rhodnius prolixus,* decreasing the chance of a successful molt (Lange et al., 2016) and triggers avoidance behavior in the mosquito *Aedes aegypti* when given in a sucrose solution (Kwon et al., 2016).

Kinin receptors are invertebrate-specific neuropeptide GPCRs (Pietrantonio, P. et al., 2018). The kinin system is widely distributed in the Acari and in nearly every order of insects, except Coleoptera (beetles) (Derst et al., 2016; Halberg et al., 2015). Insect kinins are involved in many important physiological processes: they regulate diuresis (Hayes et al., 1989; Kersch and Pietrantonio, 2011), feeding (Al-Anzi et al., 2010; Kwon et al., 2016; Zandawala et al., 2018), pre-ecdysis (Kim et al., 2006) as well as tracheal air clearance post-ecdysis (Adams et al., 2000). In the fruit fly *D. melanogaster*, both leucokinin- and leucokinin receptor (LKR; also known as drosokinin receptor) loss-of-function mutant strains showed significant increases in resistance to desiccation, ionic stress (only tested in LK-mutant fly), and starvation (Cannell et al., 2016; Zandawala et al., 2018). Prior work has deorphanized kinin receptors of two vector species, the yellow fever mosquito *Ae. aegypti* (Pietrantonio, P. et al., 2005) and the cattle fever tick *R. microplus* (Holmes, S. et al., 2003), and found the kinin system is important in regulating diuresis and sugar feeding in *Ae. aegypti* (Kersch and Pietrantonio, 2011; Kwon et al., 2016). The most recent RNAi-mediated silencing of the kinin receptor in the cattle fever tick caused a reproductive fitness cost (Brock et al., 2019b). While our cloning of this receptor represented the first known neuropeptide GPCR in the Acari, there has been no urgent need in establishing the endogenous ligand of the *R. microplus* tick. This was because receptor functional studies were

performed using insect kinin core peptide analogs that activated the tick receptor. The endogenous ligands of the kinin receptor(s) feature a short C-terminal pentapeptide (Phe-X_1-X_2-Trp-Gly-NH_2) as the minimal peptide core required for activity (Nachman et al., 2002b). Insect kinins are among the most well characterized neuropeptides with currently 271 endogenous kinins identified in insects (Yeoh et al., 2017). In the synganglion of the tick *Ixodes ricinus*, we previously identified kinin peptide (leucokinin-like) immunoreactivity, and mass spectral analyses of synganglia of adult *R. microplus* and *Ix. ricinus* detected a strong signal at ~1,008 Da, consistent with the mass of kinin peptides (Neupert et al., 2005). However, the endogenous cDNAs for kinin peptides have not yet been cloned in any tick species and tick sequences are unknown. Herein, we predicted and cloned the putative kinin cDNA which shows an amplification in the number of kinin ligands in *R. microplus*, similar to what was predicted for *Ix. scapularis* (Gulia-Nuss et al., 2016).

Previous functional studies with mosquito- and tick-kinin recombinant receptors tested insect kinin peptides, or kinin peptidomimetics designed for increased stability and/or penetration through the arthropod cuticle (Taneja- Bageshwar et al., 2006; Xiong et al., 2019c). Results showed that the tick kinin receptor was a more permissive receptor; i.e. it was activated by more ligands and with lower EC_{50} than the mosquito receptor. There are no true orthologous mammalian receptors of the tick kinin receptor, which makes it an attractive potential selective target. However, the most similar mammalian receptors are the neurokinin receptors that mediate the biological actions of tachykinins (Pennefather et al., 2004). As also the tick kinin receptor is activated by the tachykinin of the stable fly (Holmes, S. et al., 2003), we hypothesized that ligands of the mammalian neurokinin receptors could be active on the permissive tick kinin receptor.

To test this, a dual-addition assay was developed to determine the activity of peptidomimetics and small molecule ligands of neurokinin receptors on the tick kinin receptor. This assay allows discriminating agonist and antagonist activity in a single assay. Here we report the first small molecule ligands showing antagonistic activities on the tick kinin receptor. Although these small molecules did not exhibit high potency, this exploratory screen provides the methodological foundation for future screens of small molecule libraries in high-throughput mode. The results suggested mammalian NK receptor ligands displayed high selectivity over the arthropod kinin receptor. Additionally, the quantified activities of antagonists provide structure-activity data that helps define ligand-receptor interactions in computational models.

3.3. Materials and Methods

3.3.1. In silico prediction of the kinin precursor cDNA sequence in *R. microplus*

In search of the gene encoding the kinin precursor of the cattle fever tick, *R. microplus*, we first manually curated the protein sequence of the identified orthologous gene from the black legged tick, *Ixodes scapularis*, present in the genomic scaffold (DS680282|583-1410) (Gulia-Nuss et al., 2016). This predicted nucleotide sequence of the kinin gene was translated in the six potential frames. Once the correct open reading frame encoding 19 putative kinin peptides was identified, the putative start codon was located but the stop codon could not be predicted within that scaffold. The curated protein sequence was used as the query for local TBLASTN analyses at the National Center for Biotechnology Information (NCBI) (https://www.ncbi.nlm.nih.gov/) against the *R. microplus* (taxid: 6941) whole genome shotgun contig (WGS) (Rmi2.0; 2017), and its transcriptome shotgun assembly (TSA). The respective identified genomic fragments and transcripts were aligned with MegAlign (Lasergene, Madison, WI) to assist with primer design

for cDNA cloning. All sequence analyses in this study were performed with DNASTAR (Lasergene).

3.3.2. Cloning the kinin precursor cDNA

The synganglia of females fed for 5 days (non-repleted) of the pesticide-susceptible Gonzalez strain of *R. (Boophilus) microplus* were used for cDNA synthesis. Details on tick dissection, mRNA extraction and 3'- and 5'-RACE ready cDNA syntheses were as described previously (Yang et al., 2013). To obtain the cDNA that encodes the putative kinin precursor from *R. microplus,* specific primers (Suppl. Table 3.1) were designed based on the predicted transcript available in NCBI (GEEZ01003316). For 5'- or 3'-RACE (Suppl. Fig. 3.1), reactions were carried out in 50 µl volume, as follows: 2 µl of 5'- or 3'- RACE-ready cDNA of synganglia was added into the mix of 1× Phusion HF buffer, 0.2 mM each dNTPs, 0.5 µM of UPM (5', 3' Race kit, Clontech®, Mountain View, CA), and 0.4 µM of RmkininP1R (for 5' RACE) or RmkininP1F (for 3' RACE), and 0.5 µl Phusion® High-fidelity DNA polymerase (New England Biolabs® Inc., Ipswich, MA). For 5'-RACE, touchdown PCR was as follows: 98 ºC for 30 s; followed by 5 cycles of 98 ºC for 10 s, 72 ºC for 1 min, followed by 5 cycles of 98 ºC for 10 s, 70 ºC for 30, 72 ºC for 1 min, followed by 25 cycles of 98 ºC for 10 s, 68 ºC for 30 s, 72 ºC for 1 min, with a final extension step of 72 ºC for 10 min. For 3' RACE, touchdown PCR was as follows: 5 cycles of 98 ºC for 30 s, 72 ºC for 3 min, followed by 5 cycles of 98 ºC for 30 s, 70 ºC for 30 s, 72 ºC for 3 min, followed by 40 cycles of 98 ºC for 30 s, 68 ºC for 30 s, 72 ºC for 3 min, with a final extension step of 72 ºC for 5 min. The products from 5'- and 3'-RACE were purified with Zymoclean gel DNA recovery kit (Zymo™ Research) and cloned into pCR™2.1 Vector (Invitrogen). Chemical transformation was used to incorporate the plasmids containing PCR products into premade competent *E. coli* cells DH5α (Zymo™ 5α) (Zymo™ Research, Irvine,

CA). Transformants were screened by blue/white colony selection and 100 µg/ml ampicillin (Cayman Chemical, Ann Arbor, MI). Plasmids were isolated using the Zyppy™ plasmid miniprep (Zymo™ Research) and sent to Eton Bioscience Inc. (San Diego, CA) for Sanger sequencing. The full length of cDNA sequence was deduced by aligning the overlapping 5'- and 3'-end DNA fragments (Suppl. Fig. 3.1A). To obtain the coding sequence of the cDNA (ORF) in a single product, gene-specific primers were designed (Rmk-ORF-F/R) outside of the ORF region to amplify the cDNA, using similar reagents as above (Suppl. Table 3.1). Specifically, in a 50 µl volume, 2 µl of 3'-ready cDNA was added into the mixture of 1× Phusion HF buffer, 0.2 mM each dNTPs, 0.4 µM of both Rmk-ORF forward and reverse primers, and 0.5 µl Phusion® High-fidelity DNA polymerase. The reaction was run at the following conditions: 98 ºC for 30 s, followed by 30 cycles of 98 ºC for 10 s, 72 ºC for 90 s, with a final extension step of 72 ºC for 10 min. The PCR product was purified, cloned into pCR™2.1 Vector, and verified by sequencing as described above.

3.3.3. *R. microplus* kinin gene structural characterization

The blastn "hits" obtained on the *R. microplus* genome with the cloned kinin cDNA sequence only overlapped the genome sequence towards the 3' end of the cDNA. Thus, to define the structure of the putative kinin gene, i.e. to determine the precise number and length (bp) of introns and exons, several PCR reactions were performed (Suppl. Fig. 3.1B). The genomic DNA template was extracted from the acaricide-susceptible Deutch strain of *R. microplus* because the Gonzalez strain used for cDNA synthesis is no longer available. Genomic DNA was extracted from one female tick using Zymo™ *Quick*-DNA miniprep kit (Zymo™ Research). To obtain the sequence of the predicted ORF, first, gene-specific primers located towards the 5'- and 3'- ends of the cDNA sequence (Rmk-ORF-F/R) (Suppl. Fig. 3.1B) were used to amplify the genomic

DNA. In a 50 µl volume, 100 ng of genomic DNA was added into the mixture of 1× Phusion HF buffer, 0.2 mM of each dNTPs, 0.4 µM of both Rmk-ORF forward and reverse primers, and 0.5 µl Phusion® High-fidelity DNA polymerase. The reaction was run at 98 ºC for 30 s, followed by 30 cycles of 98 ºC for 10 s, 72 ºC for 120 s, with a final extension step of 72 ºC for 10 min. A 4 kb PCR product was amplified, and it was purified with Select-a-Size DNA clean and concentrator™ kit (Zymo™ research, Irvine, CA). Three forward primers and two reverse primers were designed to "walk" the ~4 kb PCR product obtained for Sanger sequencing (Suppl. Fig. 3.1B). Secondly, a gene-specific forward primer (Bmkinin-g-long-F) and a reverse primer outside the 4 kb product region (Bmkinin-g-long-R) were designed to amplify a 1,375 bp product that includes 40 bp towards the 3' end of the kinin gene. For the reverse primer design, the sequence of the genomic contig (LYUQ01126194.1) was used (Suppl. Fig. 3.1B). Thirdly, gene specific primers were designed based on the cDNA sequence (Suppl. Fig. 3.1B) to amplify a ~3.5 kb product containing additional 20 bp towards the 5' end of the gene.

3.3.4. *R. microplus* kinin peptide precursor characterization

The signal peptide of the translated *R. microplus* kinin peptide precursor sequence was predicted with SignaIP v. 5.0 (http://www.cbs.dtu.dk/services/SignalP/) (Armenteros et al., 2019). The cleavage sites on the precursor were predicted following the principles summarized by Veenstra (2000). The conserved motif logos of the C-terminal pentapeptide of kinins in *R. microplus* and *Ix. scapularis* were created separately by WebLogo (https://weblogo.berkeley.edu/logo.cgi) (Crooks et al., 2004).

3.3.5. Prediction of tick kinin peptide precursors and phylogenetic analysis

The nucleotide sequences encoding the orthologous kinin precursors from other Acari species were predicted through tblastn on NCBI using the cloned kinin precursor of the *R.*

microplus tick as query against the transcriptome data of Acari (taxi: 6933). The protein sequence was manually curated by translating the DNA sequence on ExPASy (https://web.expasy.org/translate). For species with more than one hit in the BLAST results, nucleotide sequences were downloaded and aligned by SeqMan Pro (DNASTAR Lasergene, Madision, WI), before being used for protein curation. For specific genes for which the nucleotide sequences of two hits did not overlap, the encoding polypeptides were curated separately, and later combined from N-terminus to C-terminus retaining a gap between two polypeptides. This procedure applies for the predicted kinin precursor of *Amblyomma sculptum* and *Dermacentor variabilis*. To predict the *Ix. scapularis* kinin precursor, the transcript sequences identified by tblastn were used in combination with the sequence of the genome scaffold (DS680282) which had been previously reported to encode the kinin gene with 19 kinin peptides, with no other details provided (Gulia-Nuss et al., 2016). All the curated kinin precursor protein sequences start with methionine, and their predicted coding sequences end with a stop codon, except for that of *A. sculptum*, in which a stop codon was not present. To help verify the predicted methionine, all deduced tick kinin precursors were aligned using the Clustal W method with MegAlign (Lasergene). The kinin precursor sequence of the common bed bug, *C. lectularius*, was obtained from Predel et al. (2017). Additional insect kinin sequences were obtained from the DINeR database and references therein (http://www.neurostresspep.eu/home) (Yeoh et al., 2017). Those sequences are from one hemipteran, *R. prolixus* [DAA34788.1] (Bhatt et al., 2014), and four dipterans, *Aedes aegypti* [AAC47656.1] (Veenstra et al., 1997b), *Culex quinquefasciatus* [EDS35029.1] (Schooley et al., 2012), *Stomoxys calcitrans* [XP_013117801.1], and *Drosophila melanogaster* [NP_524893.2]. Fourteen protein sequences of putative arthropod kinin precursors were included in the phylogenic analysis. The protein sequences were first

aligned by MAFFT with the iterative refinement algorithm E-INS-i, because of the occurrence of known insertions and deletions during the evolution of neuropeptide genes, (https://mafft.cbrc.jp/alignment/server/) (Katoh and Standley, 2013), with the default online settings. The aligned sequences were processed through Mesquite version 3.6 (build 917) (Maddison, 2005) to convert the terminal gaps into missing data. Phylogeny was constructed using MrBayes version 3.2.6 (Ronquist et al., 2012) executable for Windows 64-bit with four chains and four runs in the mixed amino acid model for 1,000,000 generations. The traces of parameters were visualized in Tracer version 1.7.1 (Rambaut et al., 2018) to confirm that the four runs reached convergence. The consensus tree was generated with 10% burnins and output through FigTree version 1.4.4 (Rambaut, 2012).

3.3.6. Cell lines

BMLK3 is a CHO-K1 cell line stably expressing the southern cattle tick (*R. microplus*) kinin receptor, and served to characterize the functional activity of compounds on the receptor. Receptor cloning, transfection and selection of single clonal cell lines expressing this kinin receptor was reported previously (Holmes, S. et al., 2003; Holmes, S. et al., 2000b). A cell line similarly transfected with empty vector plasmid pcDNA3.1 (Invitrogen, Carlsbad, CA) was designated as a "vector only" cell line and used as the negative control in all experiments. Cells were maintained in T-25 or T-75 flasks (CELLSTAR®, Greiner® Bio-one) with maintenance medium consisting of F-12K medium (Corning™ Cellgro™, Mediatech, Inc. VA, US), fetal bovine serum (FBS) (10%) (Equitech-Bio, Kerrville, TX) and 400 µg/ml G418 Sulfate (Gibco® Invitrogen, New York, US). Cells were maintained in a humidified incubator at 37°C, 5% CO_2. Cells were incubated under the above conditions unless specified otherwise.

Two different calcium reporters (Fluo-8 AM or aequorin/coelenterazine) were utilized in dual-addition assays, which are described in detail in the sections below. Both assays allow the discrimination of agonistic or antagonistic activity of compounds. Briefly, a primary screen of compounds measured the endpoint fluorescence from cells cultured in a 384-well plate format. Compounds that showed potential activity in this screen were further tested at various concentrations with a kinetic assay that measured calcium bioluminescence in a 96-well plate format.

3.3.7. Preparation of small molecule library plates

A commercial library of fourteen small molecule antagonists of mammalian neurokinin receptors (NK1-3) was purchased from Tocris® Bioscience (R&D System, Bristol, UK) (for information on chemicals see Suppl. Table 3.2) to be screened on the BMLK3 cells in 384-well format. Additionally, thapsigargin, which discharges intracellular Ca^{2+} stores by inhibition of the Ca^{2+} ATPase in endoplasmic reticulum (Thastrup et al., 1990), and 2-APB (2-aminoethoxydiphenyl borate), which blocks of store-operated Ca^{2+} entry and may block InsP3-induced Ca^{2+} release (Bootman et al., 2002), were purchased from Tocris® Bioscience and used as positive and negative controls, respectively, for the Ca^{2+} signal assay readout.

All small molecule stock solutions (for library and controls) were prepared in 100% DMSO (Sigma-Aldrich, St. Louis, MO) and aliquoted and stored at -20 °C before use. For the initial screening in the fluorescence assay, compounds were initially prepared in a V-bottom, 384-well plate (Corning®, NY, USA) in Hanks' Saline Buffer containing 20 mM Hepes (HHBS), 2 % DMSO, at a 10× concentration of the final concentration in the assay. The sixteen small molecules were serially diluted in this plate into 22 dosages using a dilution ratio of 1:1.4,

starting at 1 mM (except thapsigargin started at 100 µM, Suppl. Table 3.3) using an automatic-8 channel EPMotion™ liquid handler (Eppendorf Biotech company, Hamburg, Germany).

Ten selected molecules, which were either active in the first screening or could not be dissolved in 2 % DMSO, were further prepared in a V-bottom 384-well plate in HHBS, 10 % DMSO at a 10× concentration of the final concentration in the assay; thapsigargin and 2-APB were also prepared in the same solvent. The twelve small molecules (including thapsigargin and 2-APB) were serially diluted in the plate (dilution ratio 1:1.4) into 10 dosages starting from various concentrations (10 µM to 1 mM) depending on the solubility of each molecule (Suppl. Table 4, Panel A). In this "library subset" plate, each concentration of the small molecules was dispensed into a duplicate well for testing both the kinin-receptor expressing cell line (BMLK3 cells) and the cells transfected with the vector plasmid only, respectively. In both 384-well library plates, 64 wells in four edge columns were filled with blank solvent (first addition) (Suppl. Tables 3 and 4).

3.3.8. Preliminary screen of a small molecule library in an end-point fluorescence assay

The screening of the potential antagonists on BMLK3 cells was performed with an endpoint fluorescence assay in a black/clear 384-well plate (CELLSTAR®, Greiner Bio-one, 781077) coated with Poly-D-Lysine (Sigma-Aldrich). This assay uses Fluo-8 AM (Fluo-8 Calcium Flux Assay Kit - No Wash, Abcam®, Cambridge, UK) as the calcium indicator. Unless specified, the pipetting steps in the 384-well plate fluorescence assay were performed by an automated CyBio® Well Vario System using a 384 pipette-head that allows to simultaneously deliver a volume of up to 60 µl per well. The screening of the first library prepared in 2 % DMSO was performed on BMLK3 cells only (Suppl. Table 3.3). The screening of the 2nd library

plate prepared in 10 % DMSO ("library subset") was tested with half of plate with BMLK3 and another half with vector only cells (Suppl. Table 4).

BMLK3 or vector only cells were cultured in in T-75 flasks. When they reached about 90 % confluency, they were trypsinized and suspended in F-12K medium containing 1 % FBS and 400 µg/ml of G418 Sulfate at 4×10^5 cells/ml to be seeded in 384-well plates. For this, the cell suspension (25 µl; ~10,000 cells/well) was dispensed into all 384 wells of the plate. To distribute cells evenly, mixing was by aspirating and immediately re-dispensing 10 µl of the applied cell suspension three times. Plates were incubated overnight at 37°C under 5% CO_2. On the next day, cells were prepared for the assay following the kit's instructions: the old media in the assay plate was fully removed by inverting the plate and gently blotting it on paper towels, and media was replaced with 45 µl of Fluo-8 AM loading dye (1×). The plate was incubated at 37°C under 5% CO_2 for 30 min, then equilibrated at room temperature in the dark for 30 min. The screening of the small molecule library was achieved by a dual-addition assay. The "first addition" consisted of 5 µl of either the blank solvent or a 10× solution of the potential antagonist transferred from the 384-well library plate, to reach 1× concentration in the wells. After 5 min incubation with cells, a second addition of 5.6 µl of 10 µM kinin receptor-specific agonist peptide (FFFSWGamide) resulted in a final concentration of 1 µM. The calcium fluorescence signal was read by a Varioskan LUX™ (Thermos Scientific, Waltham, MA) plate reader set for fluorescence plate-mode with Ex/Em = 490/525 nm and kept at 29 °C. Endpoint responses were read immediately after the 1st addition and 5 min after the 2nd addition of agonist. The plate was read from both forward and reverse orientations by rotating the plate (180°) on the instrument to compensate the variation in signal kinetics during the lapse in plate reading, because there was a 2 min lag time between the readings of the first and the last well. The

response to each addition was represented as the average value of both forward and reverse plate readings (Suppl. Tables 3 and 4, Panels B-C). The antagonist activity was calculated as the percentage of the response to 1 μM FFFSWGa of cells that had been incubated with the putative antagonist compound in comparison to the response of cells that had been incubated with blank solvent only. A compound was considered to have antagonistic activity, if it minimally inhibited 50 % of the response to the agonist FFFSWGa (1 μM) applied in the second addition. These candidates were selected for further validation in a dose-response kinetic calcium mobilization bioluminescence assay.

3.3.9. Kinetic, dose-response calcium mobilization bioluminescence assay

The calcium bioluminescence assay was used for the kinetic analysis of dose-responses to the compounds identified in the primary screen. Aequorin is the calcium reporter, transiently expressed in the BMLK3 cells (Lu et al., 2011c). This 'dual-addition' kinetic assay was conceived to characterize the diverse activity patterns the putative ligands may display. The "first addition" consists of the compound being tested, either a small molecule or a peptidomimetic; the bioluminescence response elicited is measured for 30 s (if the compound is an agonist there will be bioluminescence response during this first 30 s period). Immediately after, at 32 s, a "second addition" with a single concentration of agonist follows (FFFSWGa, 1 μM), and the response continues to be measured for another 30 s. It is important to emphasize that the response measured after this addition of agonist is influenced by the presence of the unknown compound applied in the first addition. If the compound is an antagonist, the response to the agonist applied in the second addition will be reduced with respect to that of the positive control (buffer + agonist). The pharmacological activity of the unknown molecule can be determined based on the integrated area under the bioluminescence response curve registered during both

these 30 s periods (total bioluminescence expressed as average bioluminescence units per second). That is, it can be inferred if the unknown molecule is a full agonist, full antagonist, partial agonist, partial antagonist, or an allosteric modulator. This approach is widely applied in GPCR drug discovery (Ma et al., 2017).

Selected small molecules were solubilized in 1× DMEM medium (Gibco®, Invitrogen) with 10 % DMSO and prepared from 500 nM to 500 µM as 5× of the final concentration. In addition, three peptidomimetic ligands of neurokinin receptors were purchased from Tocris® Bioscience: one agonist, hemokinin 1 (human), and two antagonists, antagonist G and spantide I. These peptidomimetics were solubilized in 80% acetonitrile: 0.01 % trifluoroacetic acid and then aliquoted (100 nmoles per tube) and freeze-dried; the dry peptidomimetics were stored at -20 °C before use. For the assay, the peptidomimetics were solubilized and diluted in assay buffer (1× DMEM) containing 1% DMSO from 10 nM to 100 µM as 10× of the final concentrations in the assay. All compounds, either small molecules or peptidomimetics were tested in three independent replicates, each with 2-3 wells as pseudo-replicates. Responses from each assay were calculated as the average of individual responses from the pseudo-replicate wells.

The cells preparation was described in detail elsewhere (Lu et al., 2011c). In brief, the BMLK3 and vector-only cells were cultured to ~ 90% confluency in T-25 flasks. The cells were trypsinized and suspended in maintenance medium, counted, and diluted to 1×10^5 cells/ml; 2 ml of this cell suspension was placed into each well of 6-well-plates (CELLSTAR®, Greiner Bio-one). After overnight incubation, when the cells reached a confluency of 40-60%, old medium was replaced with 1 ml of serum-reduced Opti-MEM™ medium (Gibco®, Invitrogen) in each well. Following the instructions of the transfection reagent manufacturer, cells in each well of the 6-well plate were transiently transfected with 1 µg mtAequorin/pcDNA1 plasmid mixed in 4 µl

of FuGENE6 (Promega, Madison, WI) and 96 µl of Opti-MEM™ medium. After 6 h of incubation, the old medium was replaced with 2 ml of F-12K medium with FBS (10%) (antibiotic-free medium). Following 24 h incubation, cells were trypsinized, seeded into white/clear 96-well-plates (CELLSTAR®, Greiner Bio-one) (20,000 cells/well in 100 µl of antibiotic-free medium), and incubated overnight until they reached optimal confluence of 80 %. BMLK3 cells and vector only cells were prepared in the same plate to test different concentrations of each compound. To reconstitute the aequorin-complex, cells were incubated with 90 µl per well of calcium-free DMEM (1×) containing coelenterazine (5 µM) (Regis™ Technology, Inc., Morton Grove, IL). After 3 h of incubation in the dark, cells were ready for the assay. The "dual-addition" assays were performed with a Clariostar™ (BMG Labtechnology, Chicago, IL) plate reader set at 29°C and for bioluminescence and "well" mode at 469 nm emission wavelength. The two additions were performed by the built-in injectors of the Clariostar™ plate reader. The first addition was performed after 2 s of initiating the recording of the bioluminescence response, which continued for 30 s. This addition applied either 22.5 µl (5×) of certain small molecule antagonist at a specific concentration or blank solvent, or 10 µl of peptidomimetic (10×). At 32 s, a second addition of 12.5 µl of agonist peptide FFFSWGa was executed with the second injector into the same well containing the test compound or blank solvent, to reach a final concentration of 1 µM. For peptidomimetics, 11 µl were applied. Recording continued for another 30 s; in sum, the kinetic response of each well was recorded for a total of 65 s at 1 s intervals. The same procedure was performed for each concentration of the ligand tested. The kinetic response to both additions were recorded immediately after addition for 30 s, with 1 s interval, and is expressed as bioluminescence units (BU) per second. The total response of the cells to each addition was represented as the percentage of the averaged BU per

second obtained in each of the two 30 s-ranges, relative to the average BU to the PC (blank solvent + 1 µM FFFSWGa) in the 2nd range (average BU of the PC curve from 35-65 s).

3.3.10. Effect of a prolonged pre-incubation with various concentrations of TKSM14 on the agonist-induced response

Because TKSM14 displayed antagonistic activity in the fluorescence assay but not in the calcium bioluminescence assay, a modified calcium bioluminescence assay was performed in which the incubation time (previously 30 s) was increased to 5 min, as in the fluorescence assay. The 1st addition was performed manually to add 22.5 µl of the blank buffer or different dosages of the TKSM14 (5× solutions), to achieve final concentrations of 1 µM, 10 µM, 30 µM, 50 µM, and 100 µM. The 2nd addition was performed with the built-in injector of the Clariostar™ plate reader (12.5 µl of the 10× agonist FFFSWGa solution for a final concentration of 1 µM), as described in the previous section. The response to the agonist in the second addition was recoded for 30 s, at 1 s intervals. Similarly, as before, three independent assays were performed, with each assay containing 3-4 pseudo-replicates. Responses from each assay were calculated as the average of individual responses from the pseudo-replicate wells. The antagonistic activity was represented as a percentage of the average bioluminescence units obtained during the 30 s after the 2nd addition (wells containing both the small molecule being analyzed and FFFSWGa), divided by the average bioluminescence units obtained from wells containing FFFSWGa only.

3.3.11. Statistical analyses

All statistical analyses were performed with Prism 6.0 (GraphPad Software, La Jolla, CA). In the end-point fluorescence assay, dose-response curves and IC_{50} values were calculated with "log [inhibitor] vs. response – Variable slope (four parameters)" function in Prism 6.0. IC_{50}s of the antagonists were defined as the concentration of antagonist that inhibits agonist response

in the mid-range of the respective fitted dose-response curve (this is not the concentration that inhibits 50 % of the agonist response). In the kinetic calcium bioluminescence assay, to determine the statistical significance of the inhibitory effect from various concentrations of the same compound, the response after the second addition for each concentration within each molecule was compared to the corresponding blank control by one-way ANOVA (n=3) followed by Tukey's multiple comparisons test.

3.4. Results

Our long-term approach for discovering novel ligands for arthropod GPCRs is summarized in Fig. 3.1. In this study, we focused on processes on the left of the figure, by using transcriptomics and genomic data to clone the kinin cDNA, followed by forward pharmacological approaches towards the identification of novel ligands for the kinin receptor of the southern cattle tick, *R. microplus*.

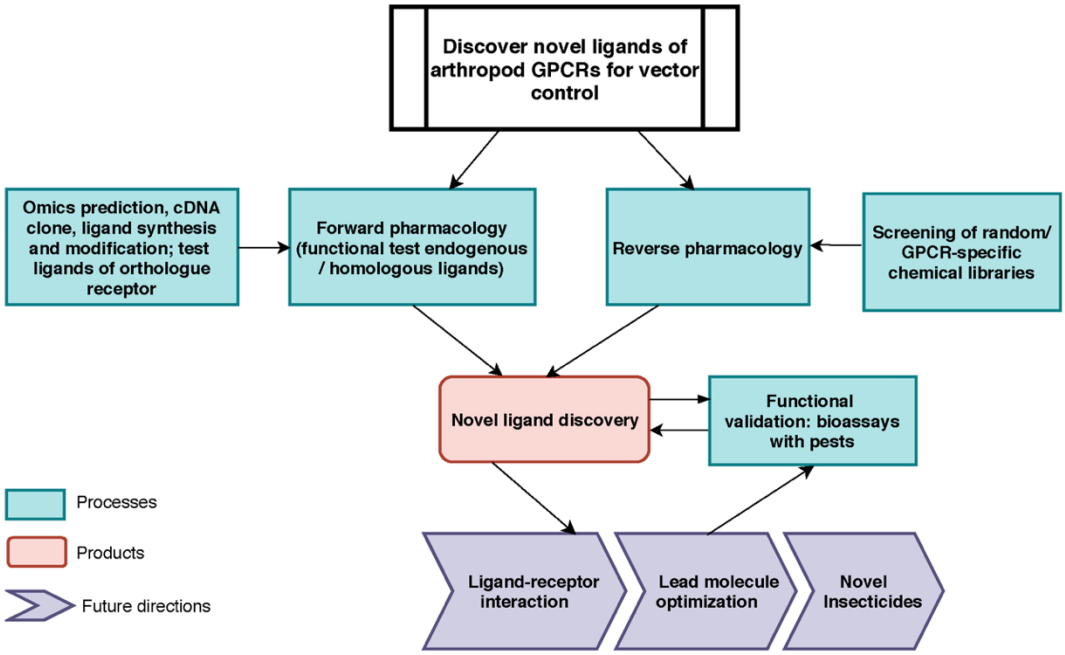

Figure 3.1 Towards vector control: General work-flow for the discovery of novel ligands for arthropod vector GPCRs.

For forward pharmacological characterization of GPCR, endogenous ligands can be identified by *in silico* predictions, cloning, tissue extraction and purification, and subsequently be synthesized (e.g. neuropeptides). Ligands from known orthologues or pseudo-orthologous GPCRs from other animals could be tested (this work). For reverse pharmacology, GPCR-specific or random molecule libraries can be screened on the target GPCR. In both approaches, the active endogenous ligands and screened molecules will be validated through bioassays for their physiological functions *in vivo*. The outputs of this pipeline are: 1) endogenous ligand(s) identification; 2) novel small molecule discovery 3) knowledge of novel biological function of neuropeptide receptor; 4) data for receptor-ligand interactions modeling and for novel chemistry design.

3.4.1. *R. microplus* cDNA sequence and gene structure

We first identified the predicted 332 amino acid residue protein sequence of the putative kinin precursor of *Ix. scapularis* from a genome fragment (DS680282: 583-1410) (Gulia-Nuss et al., 2016). Although it was reported that the gene encoded 19 kinins (Gulia-Nuss et al., 2016), the exact sequences of kinins were not provided. Herein, we listed the sequence of the 19 paracopies of putative bioactive kinins from *Ix. scapularis* (Table 3.1). Using this curated precursor protein as query, the tBLASTn results against WGS assembly and TSA of *R. microplus* (taxid: 6941) identified a genomic DNA fragment of accession number LYUQ01126194.1 and four transcripts with high similarities. Our cloning of the putative kinin precursor cDNA from *R. microplus* verified the full-length cDNA sequence is 1,398 bp long encoding a 1,227 bp open reading frame (ORF). The predicted precursor protein of 409 amino acid residues has a predicted molecular mass of 44.72 kDa (Suppl. Fig. 3.2). The 5'- and 3'-untranslated regions (UTRs) are 85 bp and 86 bp, respectively.

Alignment of the cloned cDNA to the genome sequence revealed that the 5'-end was missing in the genome, as determined by BLAST (Fig. 3.2A). We were able to obtain this missing sequence by genomic PCR amplification using a primer designed based on the sequence of the cDNA 5'-end (Suppl. Fig. 3.1 and Suppl. Table 3.1). By further amplification of the genomic DNA with gene-specific primers we sequenced the putative kinin gene of *R. microplus*, that is encoded in approximately 4.1 kb (Fig. 3.2B), composed of two exons and one intron. The first exon is 140 bp long and the second exon is 1,253 bp long; in between there is an intron of ~ 2,700 bp. Although the genomic DNA and cDNA sequences obtained were from different strains of *R. microplus*, the alignment of their ORF region showed 99 % identity.

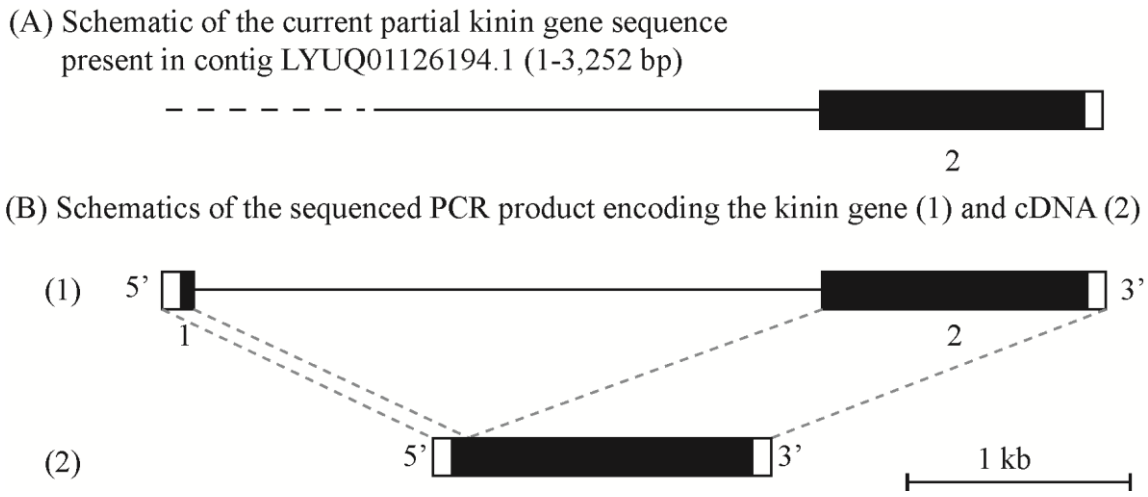

Figure 3.2 Schematic of the kinin gene and cDNA from *Rhipicephalus microplus*.

The black boxes represent the protein-encoding regions and the white boxes are the untranslated regions on the 5' and 3'-end of the kinin gene or cDNA. (A). Depicts a genome contig fragment (the full length of 7,784 bp is not represented here) encoding the 3'-end fragment of the predicted *R. microplus* kinin gene (position 1 to 3,252). The dashed line represents the sequence gap at the 5'-end of the kinin gene in the genome assembly (Rm2.0; NCBI). (B) (1) Depicts the amplified 4.1 kb PCR product sequenced that encodes the kinin gene. The gene is composed of two exons (140 bp and 1,254 bp, respectively, represented by boxes) and one intron (2.7 kb black line). This structure was verified by aligning the gene sequence with the 1398 bp cDNA (2) obtained in this study.

3.4.2. Analysis of the *R. microplus* kinin precursor

The first 38 amino acid residues of the *R. microplus* kinin precursor were predicted with SignalP v 5.0 as belonging to a signal peptide with only 50% probability, denying such conclusive identification. Seventeen paracopies of putative bioactive kinins were encoded by this single cDNA (Table 3.1). Three of them (Rmkinin 10, 13, and 15) have a predicted molecular weight of about 1,009 Da, which was the mass of putative *R. microplus* kinin detected through mass spectrometry in a previous study (Neupert et al., 2005). The *R. microplus* kinins showed the canonical critical residues and necessary characteristics for activity of the insect kinins (FX_1X_2WGa): Phe and Trp at the first and fourth position of the pentapeptide minimally active core, respectively, as well as the amidated Gly at the fifth position. Noticeably, the second variable position (X_2) was dominated by Pro; only two out of 17 kinin paracopies from *R. microplus* have a different amino acid other than Pro on the X_2 position (Table 3.1). This consensus pattern of the kinin C-terminal pentapeptide (FX_1PWGa) was prevalent in other tick species as well (Table 3.1 and Fig. 3.3A).

Table 3.1 Predicted bioactive kinins from *Rhipicephalus microplus* and *Ixodes scapularis.*

Name	***Rhipicephalus microplus***	Predicted Molecular Weight (Daltons)
Rmkinin1	QFSPWGa	720
Rmkinin2	LHPVDIAVRAADLFSPWGa	1963
Rmkinin3	DKDQTFNPWGa	1206
Rmkinin4	AGDHF**G**SWGa	932
Rmkinin5	DTFSAWGa	782
Rmkinin6	QQDSKNAFSPWGa	1363
Rmkinin7	AVRSPTARNDAARAKQEDGEEDEERSF**A**PWGa	3446
Rmkinin8	GTGEDQAFSPWGa	1250
Rmkinin9	GDDGDTSF**T**PWGa	1253
Rmkinin10	DDRFNPWGa	**1005**
Rmkinin11	EGPFSPWGa	875
Rmkinin12	DGSNKEGFFNPWGa	1454
Rmkinin13	GADDPFNPWGa	**1074**
Rmkinin14	QDSFNPWGa	949
Rmkinin15	EDGVF**R**PWGa	**1061**
Rmkinin16	EDNVF**R**PWGa	1118
Rmkinin17	EGNVF**G**PWGa	961
	Ixodes scapularis	
Ixkinin1	QFSPWGa	720
Ixkinin2	GDKQPEDEAFNPWGa	1589
Ixkinin3	ENDKDKELSFNPWGa	1678
Ixkinin4	GSFSSWGa	726
Ixkinin5	DTF**G**SWGa	768
Ixkinin6	DTF**G**PWGa	768
Ixkinin7	DTF**G**PWGa	768
Ixkinin8	DTF**G**PWGa	768
Ixkinin9	DTF**G**PWGa	768
Ixkinin10	DTF**G**PWGa	768
Ixkinin11	QDKESGFNPWGa	1263
Ixkinin12	DPFNPWGa	831
Ixkinin13	EDKNAFSPWGa	1149
Ixkinin14	DQNFNPWGa	976
Ixkinin15	TTKDSTFSPWGa	1225
Ixkinin16	EGPFNPWGa	902
Ixkinin17	GDSDTAF**A**PWGa	1122
Ixkinin18	DNNFNPWGa	962
Ixkinin19	DNGNKDSSFSPWGa	1409

Under name, ordinal numbers reflect the order in which each sequence appears from the 5' to 3' direction either in the cDNA (*R.m.*) or in the predicted gene (*Ix.*). The bolded predicted molecular weights were similar to previously predicted kinin masses (approximately 1,009 Da) (Neupert et al., 2005).

3.4.3. Kinin precursors from other tick species

Using the *R. microplus* kinin precursor as query for TBLASTN against the transcriptomes of all Acari (taxid: 6933) on NCBI, we predicted amino acid sequences of the putative kinin precursors from another seven tick species. Four full amino acid sequences were obtained, those from the relapsing fever tick, *Ornithodoros turicata,* the castor bean tick, *Ix. ricinus,* the brown dog tick, *R. sanguineus,* and the curated kinin precursor of *Ix. scapularis.*

The precursor from *Ix. scapularis* was predicted by aligning the kinin precursors deduced from three transcripts and the genomic scaffold. Missing sequences were identified from each of these: the transcripts provided a sequence of 23 amino acid residues at the N-terminus containing part of the signal peptide, and an additional C-terminal sequence of 23 amino acid residues followed by the stop codon. These sequences are absent in the genomic scaffold. However, the protein deduced from the transcriptome lack 40 amino acid residues, which are present in the genomic scaffold, distributed in two gaps within positions 250-293 in the alignment (see Suppl. Fig. 3.3). These gaps may have arisen from errors in the transcriptome assembly because this genomic region encodes four repeats of the sequence 'DTFGPWGGKR'. Therefore, the hypothetical kinin precursor from *Ix. scapularis,* is predicted as a protein of 378 amino acid residues (Fig. 3.3A).

Three partial kinin precursors were predicted from the American dog tick, *Dermacentor variabilis,* and from *Amblyomma sculptum* and *Hyalomma dromedarii*. The former two were predicted with a gap retained in both amino acid sequences (Fig. 3.3A). Whereas the *H. dromedarii* precursor, while missing approximately 70 amino acid residues at the N-terminus, should contain all the kinin paracopies as inferred from the alignment of tick kinin precursors (Suppl. Fig. 3.3). Similarly, the deduced amino acid sequence of *D. variabilis* kinin precursor

appeared to miss the same 70 residues sequence at the N-terminus (Suppl. Fig. 3.3). Among the seven deduced protein sequences, only the *A. sculptum* kinin precursor lacked the stop codon. Among the eight tick kinin precursors analyzed, SignalP 5.0 predicted the signal peptide from those of *O. turicata*, *Ix. scapularis*, *Ix. ricinus*, and *A. sculptum* (Fig. 3.3A). For *O. turicata*, the signal peptide includes the first 28 amino acid residues, with a cleavage site between residues A and S (Fig. 3.3A). For the latter three species, the signal peptide includes the first 30 amino acid residues, with the cleavage site between C and Q for *Ixodes* spp., and between A and Q for *A. sculptum*.

Putative enzyme cutting sites, characterized by contiguous basic residues (Veenstra, 2000), and those for kinin sequences were predicted in the translated precursor sequences (Fig. 3.3A). The number of kinin paracopies was high, especially in hard ticks. In the curated full-length kinin precursor of four hard tick species, 17 paracopies of kinins were predicted, in average. The transcript of the only soft tick kinin gene analyzed (*O. turicata)* is predicted to encode 10 kinin paracopies.

Within the functional C-terminal pentapeptide (FX$_1$X$_2$WGamide) core of insect kinins, the first (F), fourth (W), and fifth (G) amino acid residues are highly conserved, and similar conservation was observed in tick kinins. However, the 2nd variable position predominantly featured proline in all eight tick species (Fig. 3.3B), and the first variable position showed lower conservation in all analyzed tick species. Asparagine (N) predominately occupied the X_1 position in the soft tick *O. turicata* kinins, while in the *Ixodes* ticks (Prostriata), the X_1 position was equally occupied by either N, G, or S. The amino acid residue in the X_1 position was even less conserved (lower bits value) in ticks of the Metastriata group (Fig. 3.3B, 4-8).

Figure 3.3 Amino acid sequences of kinin precursors from eight tick species.

Amino acid sequences were manually curated after mining the available transcriptomes on NCBI. The number of kinin paracopies in each precursor are denoted in the parentheses. The gaps within the protein are denoted with '**…**'. The signal peptides predicted by SignalP 5.0 were underlined. The predicted cleavage sites are in bold, and potential bioactive kinins containing the kinin C-terminal motif, FX_1X_2WG-amide, are highlighted with gray color. The sequence of kinin precursor from *Ixodes scapularis* was curated based on the putative kinin gene in the genome scaffold (DS680282), while the additional N- and C- terminal sequences were deduced from sequences of three transcripts (Suppl. Fig. 3.3). The number 1 to the left of the *Amblyomma sculptum* sequence points to an unusual cleavage site (K) or a potential sequencing error at this site (K followed by G) (in black square frame). The version numbers are listed on the top of each sequence (accession numbers are identical except do not contain the .1 at the end). **B.** Sequence

Continued Figure 3.3 Amino acid sequences of kinin precursors from eight tick species. logos of the kinins from eight tick species. The logos were created by WebLogo (Crooks et al., 2004) using the amino acid sequences from each tick kinin precursor between predicted cleavage sites (highlighted in panel A). The overall height of each letter stack indicates the sequence conservation at that position (measured in bits), whereas the height of amino acid symbols within the stack reflects the relative frequency of the corresponding residue at that position. On the x axis, the numbers refer to the amino acid position within the alignment, which was anchored to the conserved C-terminal amidated-glycine residue, similarly as shown in the DINeR database (Yeoh et al., 2017). Towards the N-terminus, logos begin at the position within the alignment where bits are above 0 value. Polar amino acids containing an amide group (Q, N) are in purple, other polar amino acids (G, S, T, Y, C) are in green, basic (K, R, H) are in blue, acidic (D, E) in red and hydrophobic (A,V, L, I, P,W ,F, M) amino acids are in black. The dashed-line indicates the bit value of the amino acid residue at the first variable position (X_1) of the kinin C-terminal pentapeptide motif (FX_1X_2WGamide).

3.4.4. Phylogenetic analysis of kinin precursors

To establish how conserved the kinin precursors are between ticks and other insect blood feeders, a phylogenetic Bayesian analysis was performed with the putative kinin precursors from eight tick species and those known from five blood-feeding insect species (Fig. 3.4). Bhatt et al. (2014) validated the *in vivo* activity of the *R. prolixus* kinin sequences used to construct this tree, and the three aedeskinins are active on the cognate receptor (Pietrantonio, P. et al., 2005). The kinins from *C. lectularius* were detected in the CNS by mass spectrometry by Predel et al. (2017).

The number of kinin paracopies in different arthropod species varied dramatically. However, the selection pressure behind these putative insertions or deletions is unclear. The number of kinin copies was high in ticks and some hematophagous insects, but not in all (Fig. 3.4). With the support of the phylogenetic unrooted tree, we found that the kinin precursors from ticks and insects were separated into two different groups. Similarly, within each branch, arthropods that are phylogenetically closer to each other clustered in the same group, indicating substantial conservation of kinin precursors across broad taxonomic groups. The only exception was that a soft tick, *O. turicata*, clustered with *Ixodes* ticks (hard ticks) but with a posterior node probability of 0.76. Insect kinin precursors, even those from species with several paracopies as in the case of ticks (i.e. up to 15 in *R. prolixus*), were more similar among themselves than to tick kinin precursors (Suppl. Information, file 5). Thus, the number of kinin paracopies, does not appear to differentiate sequences of ticks from those of insects.

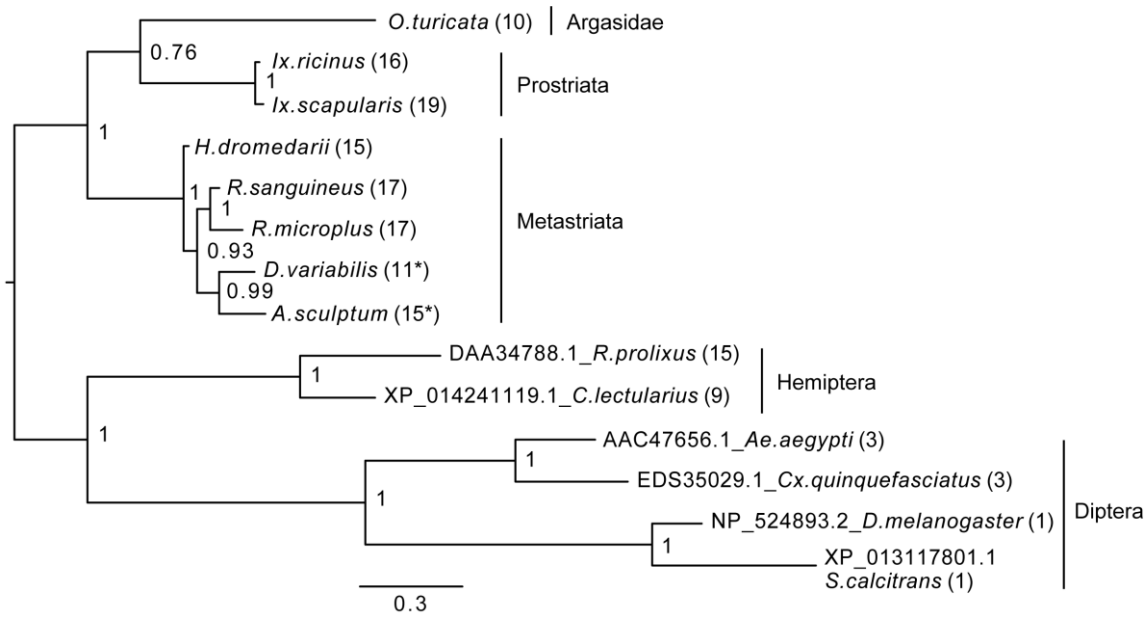

Figure 3.4 Bayesian phylogenetic analysis of kinin precursor.

The phylogenetic tree was constructed in MrBayes with four chains and four runs of the mixed amino acid model for 1,000,000 generations with a 10% burnin. Node values are Bayesian posterior probability rounded to two significant figures. Scale refers to branch length and represents the probability of an amino acid substitution along that interval. The number of kinin paracopies encoded by each precursor is denoted in the parentheses. "*" Indicates there could be more kinin paracopies present in this species as the predicted amino acid sequence likely only encodes a fragment of the kinin precursor due to gaps present in the predicted transcripts in NCBI. The curated protein sequences and version numbers of corresponding transcript sequences are in Fig. 3.3A.

3.4.5. Small molecule screening on recombinant tick kinin receptor

Towards the discovery of novel "small-molecule" ligands (Lipinski, 2016) for the target GPCR, we initiated a small-scale screening with the dual-addition assay we developed. Because kinin receptors are invertebrate-specific GPCRs, there is no available commercial library of ligands from any orthologue mammalian GPCR (Fig. 3.1). To explore the opportunity for discovery of antagonists, we selected a small-molecule library of known antagonists of those mammalian GPCRs that have the highest amino acid sequence identity to the tick kinin receptor. These are the neurokinin receptors (NK1-3 receptors), with approximately 36 % amino acid sequence identity to the tick kinin receptor, as per Blast analyses in NCBI. The preliminary screening of fourteen small molecules was performed with an end-point calcium fluorescence assay. The screening of these small molecules was with 22 concentrations of antagonists prepared in 2% DMSO, performed on the BMLK3 cell line only. Four compounds, TKSM02, TKSM10, TKSM13 and TKSM14 showed some antagonistic activities, as they showed increasing values of fluorescence with decreasing concentrations (Suppl. Table 3.3, panel D, rows C, K, N and O). It was noticed during the plate preparation that compounds TKSM04, TKSM05, TKSM08, TKSM09 and TKSM14 may have precipitated out when prepared in 2% DMSO at 1 mM. Indeed, fluorescence endpoint readings of some of them confirmed this suspicion due to randomness of their values. Therefore, a second small-molecule plate was made in 10% DMSO with ten selected compounds prepared in 10 serial concentrations (Suppl. Table 4, panel A). These small molecules included the four active small molecules from the first screen; those four more hydrophobic molecules that had precipitated; and the small molecules TKSM06 and TKSM07 that had showed erratic activity in the first screen (Suppl. Table 3.3, panel D, rows G and H). When TKSM02 and TKSM14 were tested after being prepared in 10 %

DMSO, they showed dose-dependent antagonistic activities that allowed the estimation of IC_{50}s and confidence intervals (Fig. 3.5, A and D). TKSM02 acted as a full antagonist with IC_{50}= 45 µM (95 % confidence interval of 31-61 µM) (Fig. 3.5A). Three small molecules showed partial antagonism: TKSM14, with IC_{50}= 23 µM (95 % confidence interval of 17-30 µM), only inhibited 60% of the agonist response at the highest concentrations tested of 35 µM and 50 µM (Fig. 3.5D), and TKSM10 and TKSM13 did not have meaningful IC_{50} values because their 95% confidence intervals were too wide (Fig. 3.5B-C). Nevertheless, TKSM10 exhibited antagonist activity at concentrations above 70 µM and inhibited 80 % of agonist response when applied at 100 µM (Fig. 3.5B). Although TKSM13 showed an overall weak antagonistic activity across concentrations, it acted as a potential antagonist (Fig. 3.5C) as it inhibited approximately 50 % of the agonist response at concentrations above 25 µM. The rest of the compounds re-tested (TKSM04-TKSM09) did not show any activity (Suppl. Table 4, panel D).

The small molecule library prepared for the second screening of potentially insoluble molecules (10 % DMSO), was screened on both BMLK3 cells and "vector only" cells to test for the tick receptor specificity of the agonist responses observed after the 1st addition of small molecules, because the endogenous expression of NK receptors in CHO-K1 cells is assumed. Counter screening on vector only cells (Suppl. Table 4). confirmed that none of the agonistic responses observed after the first addition were specific for the tick kinin receptor because the vector only cells showed equivalent agonistic responses to these molecules as BMLK3 cells did (Suppl. Table 4, panel B, compare row F, wells 2-12 to row F, wells 22 to 13). Therefore, only antagonistic activities remain to be demonstrated in tick bioassays.

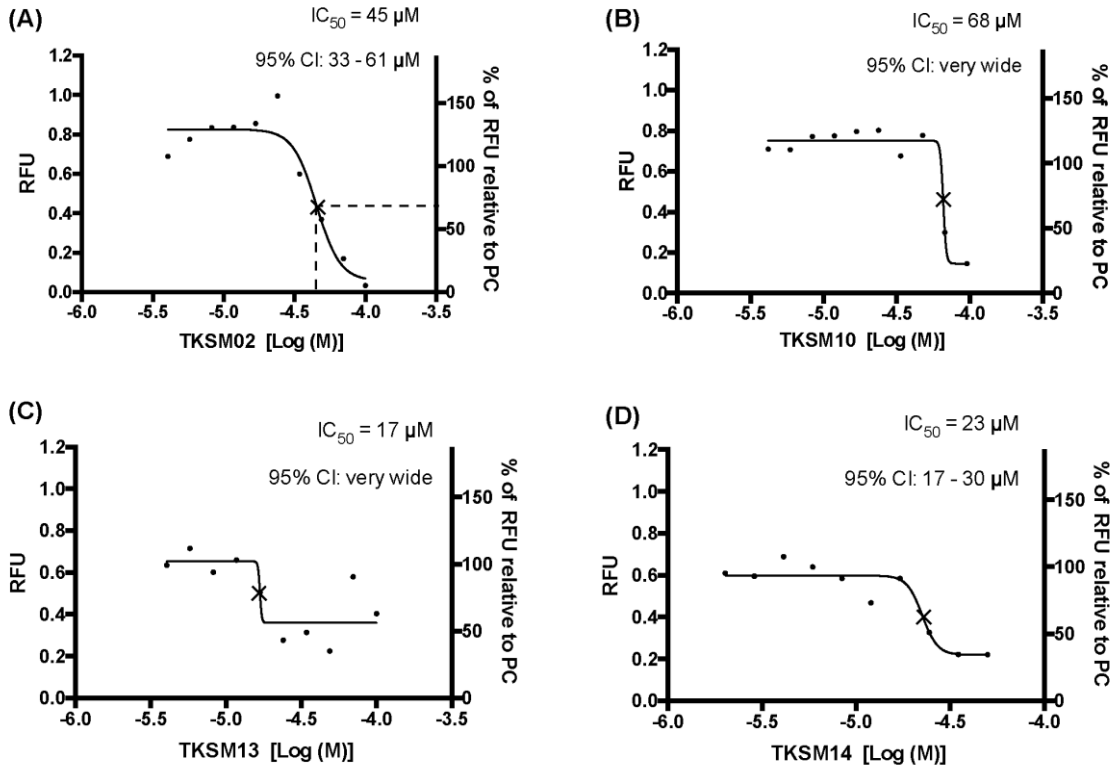

Figure 3.5 Four small molecules antagonized the tick kinin receptor activity.

Only four molecules out of the 10 tested exhibited antagonistic activities. (A-D) Dose-responses of the tick kinin receptor (in the BMLK3 cell line) to small-molecule ligands of mammalian neurokinin receptors were measured in a calcium fluorescence assay. Ten dosages were applied for each compound, starting from 100 µM (except TKSM14, starting from 50 µM) and following a 1:1.4 dilution series. The antagonist activity of 10 selected small molecules was tested by first dispensing the blank buffer or small molecules at various concentration [Log (Molar) on the X-axis] from the library plate into the assay plate. This was followed by incubation with the cells for 5 min, after which the kinin agonist (1 µM FFFSWGa) of the tick kinin receptor was dispensed into all wells and incubated for another 5 min. The end-point relative fluorescence units (RFU) from each well was represented as the average RFU (left Y-axis) of two end-point reads obtained by inverting the orientation of the plate in a Varioskan LUX™ (Thermos Scientific, Waltham, MA) plate reader. Additionally, the right Y-axis represents the percentage of RFU relative to the averaged responses from cells to the PC (blank buffer + agonist). Non-linear dose-response curves IC_{50}s were defined as the concentration of antagonist that inhibits agonist response in the mid-range of its respective fitted dose-response curve and they are marked with a × on the curve. The IC_{50}s and corresponding 95 % confidence intervals of IC_{50S} were calculated with "log(inhibitor) vs. response- Variable slope (four parameters)" in Graphpad 6.0. The IC_{50s} shown here are not the concentrations that inhibit 50 % of the agonist response.

3.4.6. Kinetic responses to selected small molecules and peptidomimetics in a dual-addition calcium bioluminescence assay

The primary screen using fluorescence provided only one end-point reading after 5 min of incubation with cells. A kinetic calcium bioluminescence assay was subsequently performed with molecules identified in the first screen. This was to determine the kinetic responses during the first 30 s after the addition of compound of unknown activity (small molecule or peptidomimetic) and the response after the subsequent addition of known agonist (1 µM FFFSWGa) (Fig. 3.6). In contrast to the results of the fluorescence assay, nearly no agonist responses were detected in the kinetic assay in the first 30 s after the addition of small molecules (Fig 7 A-E, right panel, black bars). The statistical analyses of antagonist activities based on the responses after the agonist addition were calculated by one-way ANOVA followed by Tukey's multiple comparison test among all dosages. Consistent with the preliminary screen, TKSM02 was the most potent antagonist on the tick kinin receptor and inhibited 82.7 ± 1.8% of the FFFSWGa agonist response at 100 µM (Fig. 3.6A; black curve in the left panel and in the histogram, last gray bar). The bioluminescence response of TKSM02 at 100 µM was significantly lower than the responses to the four lower concentrations tested from 100 nM - 30 µM (histogram, four bars to the left), and significantly lower than the response to agonist only (Blank bar), as expected ($p < 0.0001$) (Fig. 3.6A). A dose-dependent trend of antagonistic responses was observed for TKSM10 from 1 µM to 100 µM (Fig. 3.6B, decreasing bar heights in histogram), with the lowest cell response being 84 ± 6% of the response to agonist only (16% inhibition). However, the increasing trend of inhibition with higher concentrations was not detected as statistically significant by ANOVA ($p = 0.08$). The ANOVA for TKSM13 detected significant variation in the response among concentrations ($p = 0.02$) and Tukey's test detected a

significant decrease in the response to the agonist of 72 ± 19% at 100 µM with respect to the 133 ± 17% response to 10 µM concentration ($p < 0.05$) (Fig. 3.6C). Unexpectedly, TKSM14 did not show any antagonistic activity in the calcium bioluminescence assay, which was inconsistent with the result of the primary screen in the fluorescence assay. We then asked whether increasing the preincubation time to 5 min in the bioluminescence assay (previously, 30 s), similar to the fluorescence assay, could reveal TKSM14 antagonistic activity. Indeed, when the preincubation with TKSM14 was 5 min, a dose-dependent antagonistic response was detected after agonist addition (Fig. 3.7A-B). Tukey's test showed significant antagonistic activities of TKSM14 at both 50 µM (63 ± 8 %) and 100 µM (55 ± 4 %) which inhibited ~ 40 % and 45 % of the agonist response (Fig. 3.7A, orange and black curves on the left panel and last two bars on the histogram to the right). This activity matched the result observed in the first screen. This suggested that TKSM14 might have a lower binding affinity, reflected in the longer incubation time with the cells required to block the receptor.

Compound TKSM03 was chosen as a negative control for the bioluminescence assay with small molecules due to its lack of activity in the fluorescence screen. Its lack of activity was confirmed in the bioluminescence assay, as this compound did not decrease the agonist response even at the highest concentration tested of 100 µM (Fig. 3.6E, histogram on right). The corresponding black curve on the left panel (Fig. 3.6E) could be misleading at first sight, giving the impression that TKSM03 could be an antagonist, as the black curve appeared to be lower than other curves. However, it must be emphasized that although the maximal bioluminescence units per second at about 40 s is diminished with respect to the other concentrations, the area under the curve did not change with respect to that of the blank control (Fig. 3.6E, right panel).

This is why it is important to consider the total, integrated bioluminescence response and not only the peak response.

In addition, three peptidomimetic ligands of mammalian neurokinin receptors were tested using this approach. These ligands of NK receptors showed neither agonistic nor antagonistic activities on the tick kinin receptor within the tested concentration range (1 nM-10 µM) (Fig. 3.8, A-C) (ANOVA $p > 0.1$ for all three peptidomimetics). In Fig. 3.8B, a slight agonistic activity of antagonist G at 1-, 3- and 10-µM can be detected, peaking at about 14 s; the same activity is reflected in the histogram to the right. However, this activity was only observed in the first independent replication and could not be seen in the two other independent replications. This agonist response was also not detected in the vector only cells (not shown). We do not know what could have caused this effect.

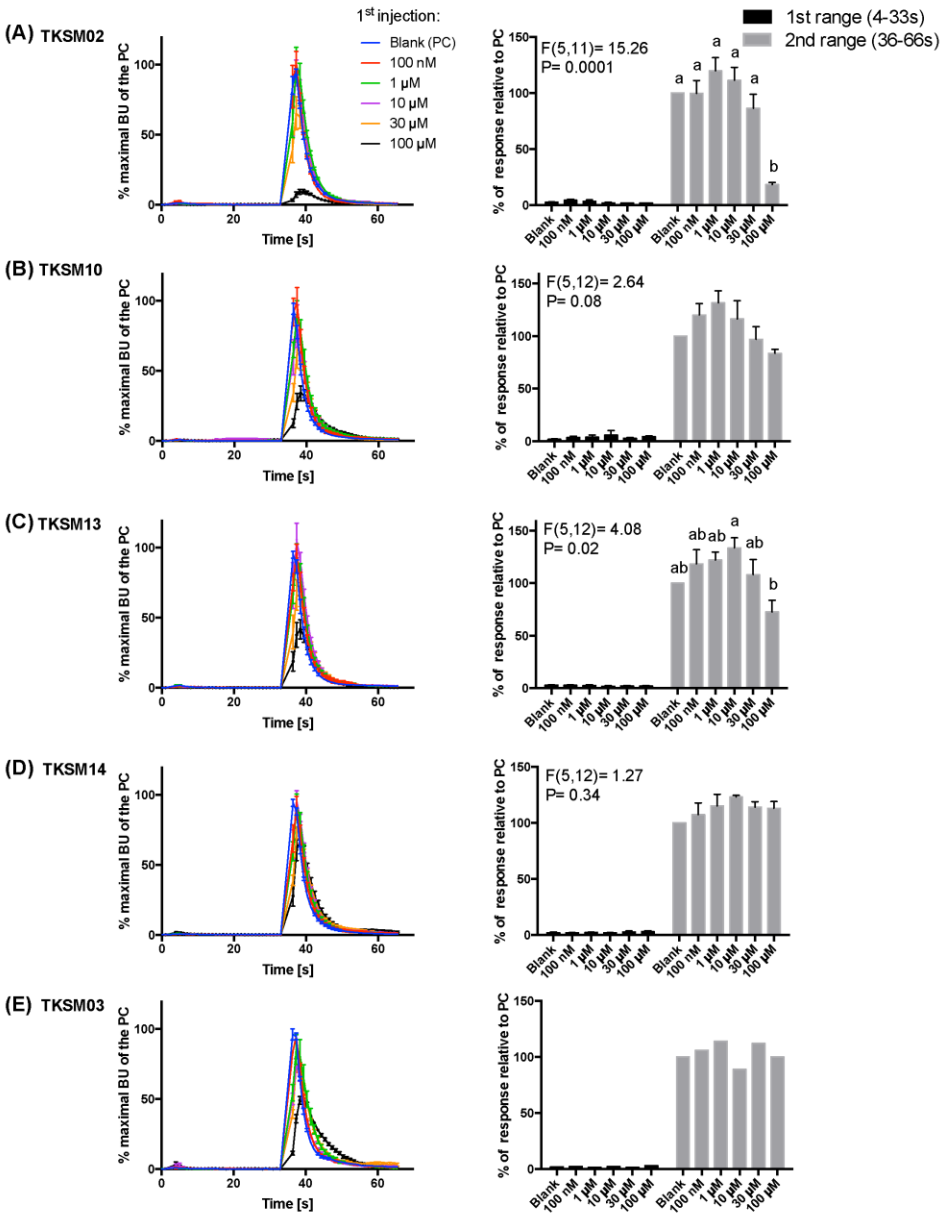

Figure 3.6 Kinetic dose-responses of the BMLK3 cell line to five selective small molecules.

Kinetic bioluminescence responses of tick kinin receptor recombinant cells to (**A-D)** four antagonist candidates (n=3), and (**E)** TKSM03 (negative control (n=1)) in the "dual-addition" calcium bioluminescence assay. All small molecules were tested at five different concentrations from 100 nM to 100 µM. Two additions were performed by the two injectors built-in the Clariostar™ plate reader (BMG Labtechnology) as follows: the 1st addition of various concentrations of small molecules (5×) or corresponding blank buffer, was performed at 2 s after initiation of the recording. The response to the 1st addition was recorded for 30 s with 1 s intervals (1st range). At 32 s, the 2nd addition of the agonist of tick kinin receptor used in this study (1 µM FFFSWGa) was performed in the same well, and the cell response was recorded for another 30 s with 1 s intervals (2nd range). Curves on the left of each panel depict in different colors the kinetic response in bioluminescence units (BU) per second to each concentration (4-9

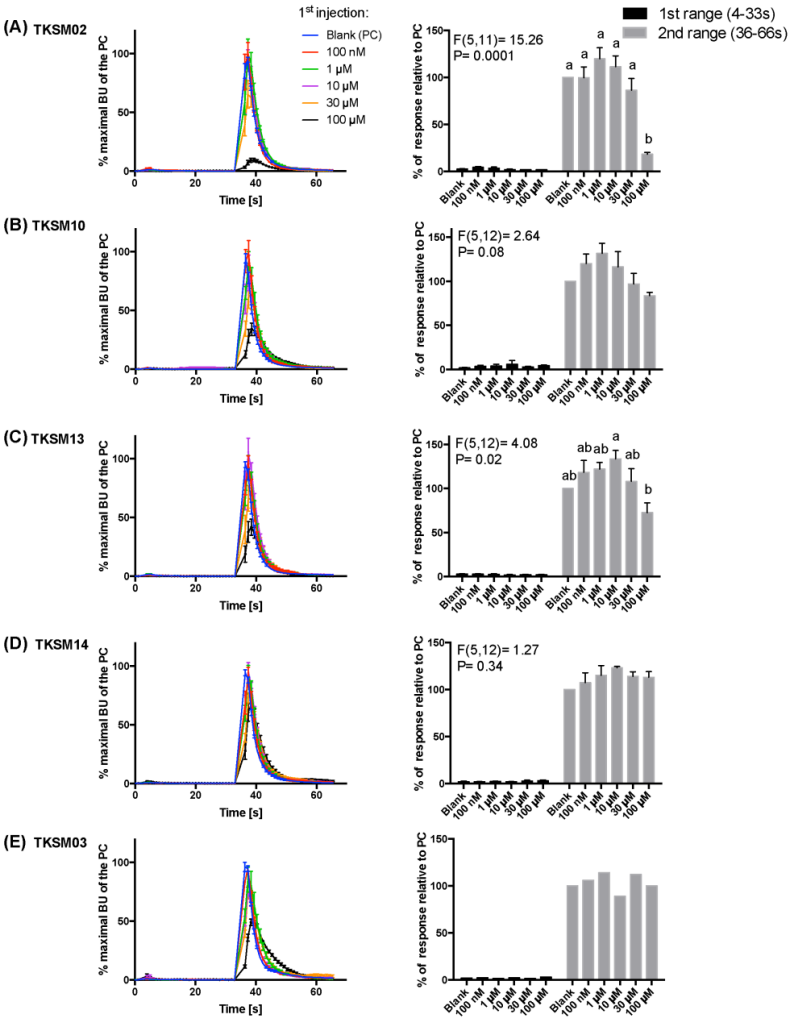

Continued Figure 3.7 Kinetic dose-responses of the BMLK3 cell line to five selective small molecules.

wells) from three independent assays (except TKSM03 n=2 wells from one assay). The Y-axis represents the percentage BU of each concentration normalized to the maximal BU of the positive control (blank buffer + agonist, blue curve) (mean ± SEM). The histogram on the right of each panel shows sequentially the total BU responses of cells to the two additions, the 1st (black) and 2nd (gray) range recordings, respectively. The total response in each range was expressed as the percentages of the average BU (per second) obtained in each of the two 30 s-ranges, relative to the average units to the PC in the 2nd range (average BU of the blue curve at 35-65 s). In each independent assay, the total response to each concentration of each small molecule in the first addition or to the agonist in the second addition was calculated as the average of 2-3 pseudo-replicate wells (Y axis: mean ± SEM; n=3 independent assays). None of the tested compounds showed agonist activity. Statistical differences in inhibitory activities between different concentrations of each compound were analyzed by one-way ANOVA (n=3) followed by Tukey's multiple comparison test ($p \leq 0.05$) with Graphpad 6.0 (GraphPad Software, La Jolla, CA). Bars with different letter superscripts indicate significant differences.

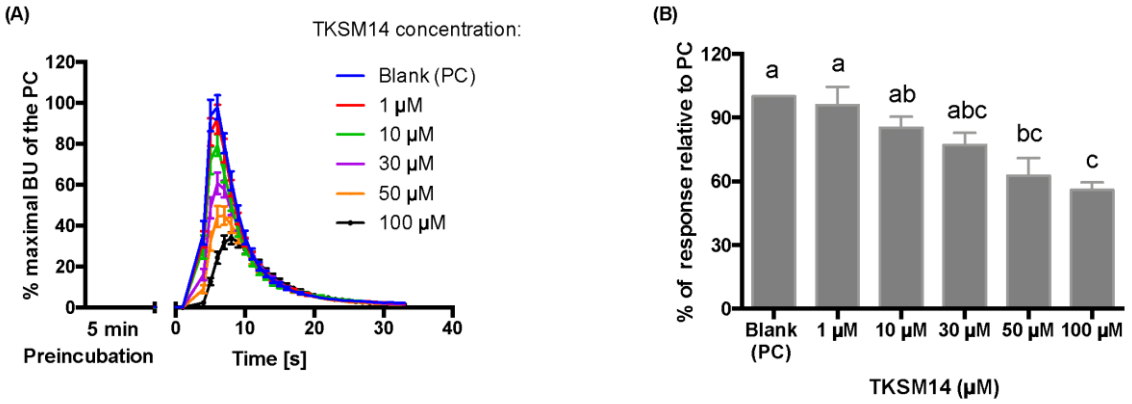

Figure 3.8 BMLK3 preincubation (5 min) with dosages of TKSM14 before agonist addition, enhances its antagonistic activity in the calcium bioluminescence assay.

(A) The kinetic responses of BMLK3 cells to the agonist (1 µM FFFSWGa) after being incubated with various concentrations of TKSM14 (1 -100 µM) or blank solvent for 5 min. The response was recorded for 30 s at 1s intervals by the Clariostar™ plate reader (BMG Labtechnology). The kinetic response is represented as the percentage of the maximal bioluminescence units (BU) of the positive control (PC = blank buffer + agonist, blue curve) in each assay (Mean ± SEM, n= 9-10 wells from three independent assays). **(B)** The total cellular response in each well is expressed as the percentage of the average BU (per second) obtained in the 30 s relative to the average response units to the PC in 30 s. Three independent assays were performed. Responses from each assay were calculated as the average of individual responses from 3-4 pseudo-replicate wells (Y axis: mean ± SEM). Statistical differences in inhibitory activities between different treatment were analyzed by one-way ANOVA (n=3) followed by Tukey's multiple comparison test ($p \leq 0.05$) with Graphpad 6.0 (GraphPad Software, La Jolla, CA). Bars with different letter superscripts indicate significant differences.

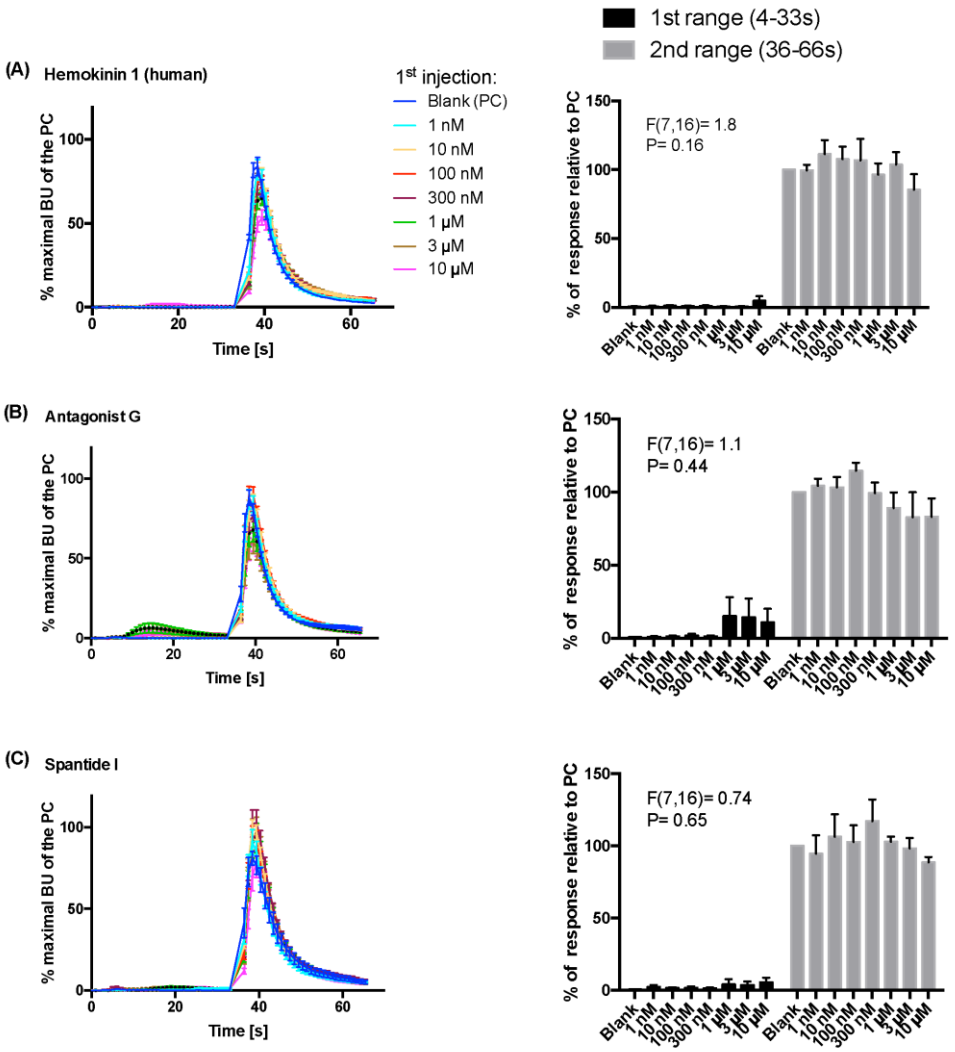

Figure 3.9 Kinetic dose-responses of the BMLK3 cell to three peptidomimetic ligands of mammalian neurokinin receptors in the "dual-addition" calcium bioluminescence assay.

Kinetic bioluminescence responses of tick kinin receptor recombinant cells to (**A-C**) three peptidomimetics (1 nM to 10 µM, n=3). Two additions were performed by the two injectors built-in the Clariostar™ plate reader (BMG Labtechnology) as follows: the 1st addition of various concentrations of peptidomimetics (10×), or corresponding blank buffer, was performed at 2 s after initiation of the recording. The response to the 1st addition was recorded for 30 s with 1 s intervals (1st range). At 32 s, the 2nd addition of the agonist of tick kinin receptor (1 µM FFFSWGa) was performed in the same well, and the cellular response was recorded for another 30 s with 1 s intervals (2nd range). Curves on the left of each panel depict in different colors the kinetic response in bioluminescence units (BU) per second to each concentration (8-9 wells from three independent assays). The Y-axis represents the percentage BU of each concentration normalized to the maximal BU of the positive control (blank buffer + agonist, blue curve) (mean ± SEM). The histogram on the right of each panel shows sequentially the total BU responses of cells to the two additions, the 1st and 2nd range recordings, respectively. The total responses in each range was expressed as the percentages of the average BU (per second) obtained in each of

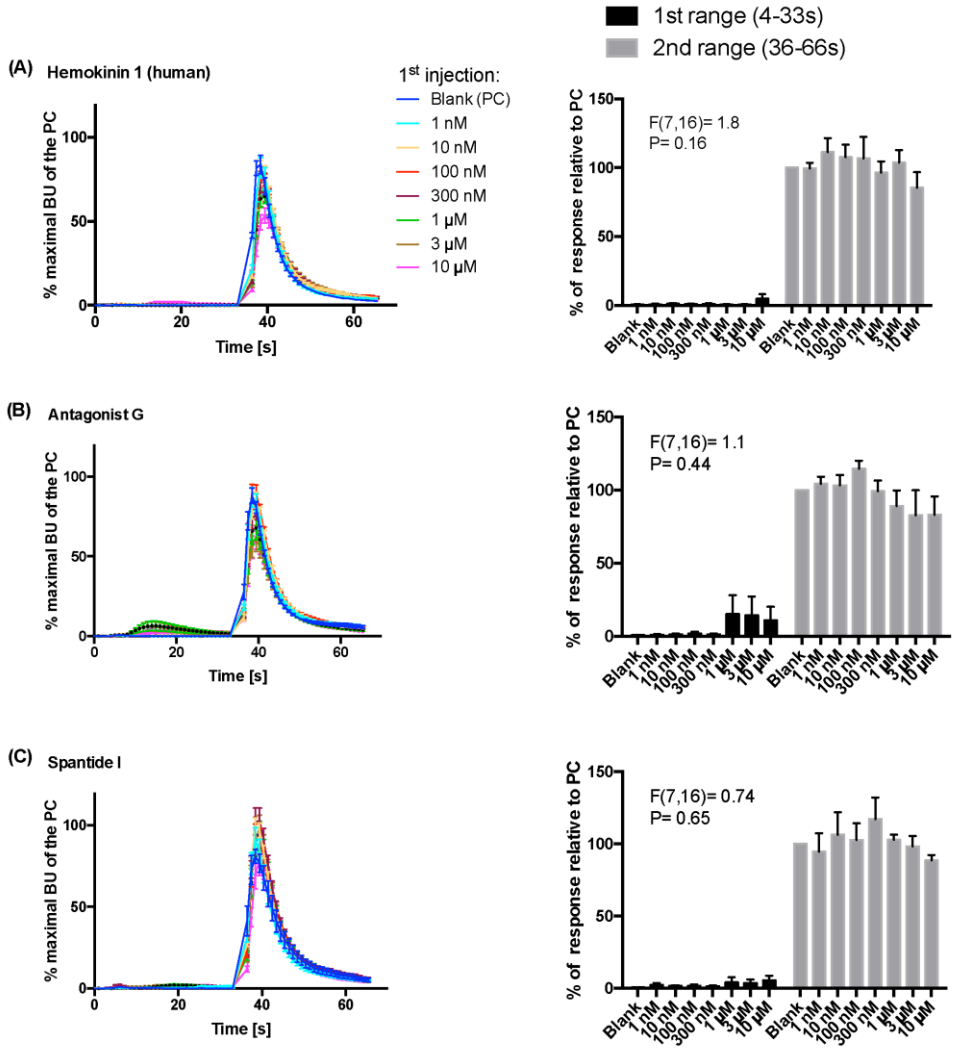

Continued Figure 3.10 Kinetic dose-responses of the BMLK3 cell to three peptidomimetic ligands of mammalian neurokinin receptors in the "dual-addition" calcium bioluminescence assay.

the two 30 s-ranges, relative to the average units to the PC in the 2nd range (average BU of the blue curve at 35-65 s). In each independent assay, the total response to each concentration of each peptidomimetic in the first addition or to the agonist in the second addition was calculated as the average of 2-3 pseudo-replicate wells (Y axis: mean ± SEM, n=3 independent assays). None of the tested compounds showed agonist activity (for B panel, first range, see explanation in text). Statistical differences in inhibitory activities between different concentrations of each compound were analyzed by one-way ANOVA (n=3) but no statistical differences were detected.

3.5. Discussion

The insect kinins were named leucokinins after first being isolated from the roach *Leucophaea maderae* for their myotropic activity (Holman et al., 1986). The kinin neuropeptide signaling system is pleiotropic in insects, regulating physiological functions both at the central and peripheral levels. They regulate myotropic and diuretic activities, orchestrate innate behaviors during pre-ecdysis and influence feeding behavior (Kersch and Pietrantonio, 2011; Kim et al., 2006; Kwon et al., 2016; Pietrantonio, P. et al., 2018; Schooley et al., 2012; Veenstra et al., 1997b). However, the kinin functions in ticks have remained elusive. In the tick *R. microplus* LKR was immunolocalized on the midgut outer surface, and LKR-silenced females displayed variations in gut discoloration, had a reduction in body weight of ~30%, reduced weight of their egg masses, and experienced decreased egg hatching. Thus, LKR silencing in female ticks caused a reproductive fitness cost, perhaps related to defects in heme metabolism because some guts from silenced females were completely white (Brock et al., 2019b). In agreement, the LKR transcript of the tick *R. sanguineous* was apparently expressed at higher levels in the gut and salivary glands than in other tissues, as inferred from RT-PCR analyses (Lees et al., 2010).

Most information on tick GPCRs was obtained from recombinant receptor systems (Gondalia et al., 2016; Gross et al., 2015; Kim, D. et al., 2018; Yang et al., 2013; Yang et al., 2015). Transcripts for tick GPCRs are often expressed *in vivo* at very low levels, which complicates their physiological characterization. For example, results of qRT-PCR after gene silencing is often highly variable in diverse tick tissues due to their normal low expression levels (Brock et al., 2019b). To address this challenge, additional future approaches to elucidate the physiological function of the tick kinin system through loss-of-function experiments include the

knockdown of the endogenous kinin neuropeptide transcript and a pharmacological approach to block receptor function. With these approaches in mind, we cloned the kinin cDNA from *R. microplus*, and developed a dual addition assay to discover antagonists of the receptor to block the response to endogenous ligands and impair the normal physiology of ticks (Fig. 3.1). To expand our current knowledge on the kinin system of the cattle fever tick, *R. microplus*, we used a forward pharmacological approach (Fig. 3.1). Herein, we integrated the cloning of the cDNA encoding the tick endogenous kinins from the synganglion of female *R. microplus* and predicted kinin sequences from other Acari.

Kinins arose before the shared common ancestor of Mollusca, Insecta and Acari, and the lymnokinin receptor (leucokinin-like) was functionally characterized in the pond snail, *Lymnaea stagnailis* (Cox et al., 1997; Grimmelikhuijzen and Hauser, 2012).

In the cattle fever tick, we identified a single cDNA that encodes 17 potential bioactive kinins, all different (Table 3.1). This is the first report for the cloning of a kinin-encoding cDNA from any tick species. Similar to *R. microplus*, the additional tick species analyzed also showed an expansion in the number of predicted kinins (Fig. 3.3), underscoring the potential importance of the kinin system in ticks. Most of the *R. microplus* kinins featured the conserved C-terminal pentapeptide motif found in insects (FX_1X_2WGa). We predict the kinins reported in this study are active because they satisfy the minimal requirement for activity and we have experimental evidence of activity of similar kinin analogs and insect kinins on the *R. microplus* receptor expressed in CHO-K1 cells (Holmes, S. et al., 2003; Taneja-Bageshwar, Suparna et al., 2009; Taneja- Bageshwar et al., 2006; Xiong et al., 2019c). However, the variable position X_1 that in insect kinins is occupied by His, Asn, Ser or Tyr (Torfs et al., 1999a), is different in some of the *R. microplus* kinins, featuring instead Gly, Ala, Thr, or Arg (Bold amino acids in Table 3.1). *R.*

microplus retained the same variable residues as in the insect kinins in position X_2 (Ser/Pro/Ala) (Torfs et al., 1999a), with Pro being more frequent in tick kinins (Table 3.1). These seventeen predicted kinins await to be synthesized and tested in the receptor functional assay to verify their biological activities.

The genome analysis of *Ix. scapularis* identified a putative kinin-encoding gene and four genes encoding kinin receptors (Gulia-Nuss et al., 2016). In contrast, BLAST of *R. microplus* LKR against the updated genome assembly (Rm2.0; NCBI) of this species identified only one receptor and did not reveal kinin receptor paralogs. The same sequence of 1,481 bp was identified in two contigs (sequences ID LYUQ01138740.1 and LYUQ01085891.1), and it matched the 3'-half of the *R. microplus* LKR cDNA with 99.9% identity. Therefore, it appears that in *R. microplus* there is only one kinin receptor gene, or perhaps an identical duplicate. In the genomes of six non-tick chelicerate species (spiders, the house dust mite and a scorpion), five species have one gene for both the kinin peptide and receptor, except that the African social velvet spider (*Stegodyphus mimosarum*) has 3 LKR paralogs (Veenstra, 2016). The transcript expression level of kinin and its receptor(s) seems to be generally low in ticks because transcripts were not reported in transcriptomes from synganglia of females of *R. microplus* from Texas, *Ix. scapularis* and *O. turicata* (Egekwu et al., 2016; Egekwu et al., 2014; Guerrero et al., 2016). As the kinin receptor transcript level is low in ticks (as well as the level of receptor protein (Brock et al., 2019)), it is tempting to speculate that kinin signaling may be regulated by changes in the expression and release of their expanded kinin peptide repertoire. A detailed temporal quantitative analysis of receptor and kinin precursor mRNA transcripts is still lacking. It is also yet unknown whether the high copy number of the tick kinins will result in increased peptide expression (i.e. concentration) or in sustained, constitutive expression. It is worth noting,

however, that kinins are active at nanomolar levels (low concentrations) (Holmes, S. et al., 2003; Xiong et al., 2019c).

Kinins arose before the shared common ancestor of Mollusca, Insecta and Acari, and the lymnokinin receptor (leucokinin-like) was functionally characterized in the pond snail, *Lymnaea stagnailis* (Cox et al., 1997; Grimmelikhuijzen and Hauser, 2012). Among ticks, the Argasidae are considered a basal group to the Ixodidae (Geraci et al., 2007). Arthropod molecular phylogenetic studies have suggested Prostriata are more ancient than Metastriata (Jeyaprakash and Hoy, 2009). Although the pentapeptide core of tick kinins is largely conserved, it is noteworthy that more ancient species show higher conservation on the X_1 position of this core, with asparagine (N), glycine (G) or serine (S) being more frequent. Further, although the Prostriata and Metastriata have a similar number of kinin paracopies (~17), the tick kinins of the Metastriata showed more frequent amino acid substitutions than those of the Prostriata. Specifically, *Ix. scapularis* and *Ix. ricinus* (Prostriata) have multiple iterations of the same kinin sequence (DTFGPWGa) in the kinin precursor, whereas ticks from the Metastriata showed no repetition in the sequence of kinin paracopies (Table 3.1, Fig. 3.3A).

The unrooted phylogenetic tree revealed kinin sequence differences between ticks and insect blood feeders (Fig. 3.4). Although the number of paracopies does not appear to differentiate kinin sequences of ticks from those of insects, we have experimental evidence that kinin receptors from insects and ticks have different ligand structure-activity relationships, as manifested in the differential potency of the same set of kinin analogs (Taneja- Bageshwar et al., 2006; Xiong et al., 2019c). Therefore, differences in the sequences of the mature kinin peptides between ticks and insects further support this differential activation. Additionally, we reiterate that kinins have pleiotropic functions in insects and therefore, it is possible that they are similarly

pleiotropic in ticks. We speculate this pleiotropism could be achieved in ticks either by diversification of receptors or ligands. In *Ixodes* (Prostriata), despite low variation in the kinin sequences, up to four kinin receptors may be present (Gulia-Nuss et al., 2016). In contrast, *Rhipicephalus microplus* appears to have only one receptor but exhibits high variation in the sequences of the kinin ligands (Table 3.1). As a mechanism for pleiotropism, there is evidence that in the mosquito renal organ different kinin analogs promote differential downstream tissue responses, either fluid secretion or changes membrane voltage (Schepel et al., 2010), apparently through the same receptor because only one kinin receptor has been identified in this tissue (Lu et al., 2011a).

To advance the discovery of novel ligands towards application, we tested potential synthetic ligands (small molecules and peptidomimetics) of mammalian neurokinin receptors on the recombinant tick receptor (Fig. 3.1). Our previous success with a kinin mimetic, named 1728, that elicits aversive behavior in the mosquito and inhibits the sugar neuron provided the proof of principle to pursue this approach (Kwon et al., 2016). The NK receptors are considered 'pseudo-orthologs' of the arthropod kinin receptor because while tachykinins exist in both mammals and arthropods, the kinin system is arthropod-specific (Nachman et al., 1999). To accelerate discovery and reduce the cost of screening a commercial GPCR-specific small molecule library and selected peptidomimetics, we developed a dual-addition functional assay using two reporters for calcium, in fluorescence and bioluminescence modes, respectively. A comparable pipeline was developed by Ejendal et al. (2012) for validating the dopamine receptor of *Ix. scapularis* as acaricide target, except their functional assay detects cAMP as the secondary messenger. Using a reverse pharmacological approach, Duvall et al. (2019) recently discovered a novel small

molecule ligand of the mosquito neuropeptide receptor, NPY receptor, which discourages the biting behavior of mosquito (Duvall et al., 2019).

In this study, through the primary screening of a small molecule library of NK receptor antagonists, and their secondary validation by a bioluminescence assay, a small molecule, named TKSM02, was identified as a "full antagonist" of the tick kinin receptor with an IC_{50} of 45 µM (Fig. 3.5A), as it fully blocked receptor activity at 100 µM. Although of weak potency, we believe this is the first antagonist reported for a kinin receptor of any arthropod species. However, it should be noted that we used a generic kinin receptor agonist, FFFSWGa, in the antagonist screen. Therefore, the antagonists identified with this screen may not similarly antagonize endogenous tick kinins on the cognate receptor. Overall, ligands of NK receptors displayed more than a 10,000-fold reduced potency on the tick kinin receptor. The quantitative functional data reported here will provide valuable information to constrain the ligand-receptor interaction surface in computational modeling.

Agonists and antagonist peptidomimetics of NK receptors were tested: hemokinin 1 (human) is an agonist of the NK1 receptor with active concentration at the nanomolar level, antagonist G is a broad antagonist on NK receptors, and spantide I is a selective potent antagonist of the NK1 receptor (Suppl. Table2). Our results provided additional functional evidence that the tick kinin receptor is pharmacologically different from the insect tachykinin receptor as none of the peptidomimetic ligands of NK receptors showed any activity on the tick kinin receptor. However, spantide I antagonizes insect tachykinins in recombinant tachykinin receptors of the stable fly and fruit fly at 1 µM and 50 µM, respectively (Poels et al., 2009; Torfs et al., 2002).

In summary, we report for the first time putative tick kinin sequences. Further, our small molecule screening results confirmed in one direction the target selectivity of the kinin receptor for arthropod vector control, as only one of the small molecule NK antagonists was active. The dual addition assay we developed is amenable and ready for the high throughput screening of random small molecule libraries on the tick kinin receptor or other tick neuropeptide receptors signaling through the calcium cascade. While receptor "hits" of random molecules are expected, the next frontier is to develop suitable tick bioassays to elucidate the physiological functions of kinins that could be impaired by these synthetic ligands.

3.6. Acknowledgements

Funding for this project is from NIFA-AFRI Animal Health and Well-Being Award 2016-67015-24918 to PVP and KT, and from competitive funds from the Texas A&M AgriLife Research Insect Vector Diseases Grant Program (FY19-21) to PVP. NIFA also supports PVP program through Hatch project TX (TEX0-2-9206), accession 1002279 (Y 2018-2023).

We thank Distinguished Professor James C. Sacchettini (Dept. Biochemistry and Biophysics, TAMU) for the support of his staff and for the use of facilities for high throughput screening. Dr. Wen Dong is acknowledged for training C.X. in the use of the Cybio® system. The authors thank the A.W.E.S.O.M.E. faculty group in the College of Agriculture and Life Sciences at Texas A&M University for assistance with editing the manuscript. We acknowledge Professor James Woolley for his advice on the construction of the unrooted phylogenetic tree. We thank both reviewers for their input in improving this manuscript.

3.7. References

Adams, M.D., Celniker, S.E., Holt, R.A., Evans, C.A., Gocayne, J.D., Amanatides, P.G., et al. (2000). The genome sequence of *Drosophila melanogaster*. *Science.* 287(5461)**,** 2185-2195.

Al-Anzi, B., Armand, E., Nagamei, P., Olszewski, M., Sapin, V., Waters, C., et al. (2010). The leucokinin pathway and its neurons regulate meal size in *Drosophila*. *Curr. Biol.* 20(11)**,** 969-978.

Armenteros, J.J.A., Tsirigos, K.D., Sønderby, C.K., Petersen, T.N., Winther, O., Brunak, S., et al. (2019). SignalP 5.0 improves signal peptide predictions using deep neural networks. *Nat. Biotechnol.* 37**,** 420-423.

Audsley, N., and Down, R.E. (2015). G protein coupled receptors as targets for next generation pesticides. *Insect Biochem. Molec.* 67(Supplement C)**,** 27-37.

Bhatt, G., da Silva, R., Nachman, R.J., and Orchard, I. (2014). The molecular characterization of the kinin transcript and the physiological effects of kinins in the blood-gorging insect, *Rhodnius prolixus*. *Peptides.* 53**,** 148-158.

Bootman, M.D., Collins, T.J., MacKenzie, L., Roderick, H.L., Berridge, M.J., and Peppiatt, C.M. (2002). 2-aminoethoxydiphenyl borate (2-APB) is a reliable blocker of store-operated Ca2+ entry but an inconsistent inhibitor of InsP3-induced Ca2+ release. *The FASEB Journal* 16(10)**,** 1145-1150.

Brock, C.M., Temeyer, K.B., Tidwell, J., Yang, Y., Blandon, M.A., Carreón-Camacho, D., et al. (2019). The leucokinin-like peptide receptor from the cattle fever tick, *Rhipicephalus microplus*, is localized in the midgut periphery and receptor silencing with validated double-stranded RNAs causes a reproductive fitness cost. *Int. J. Parasitol.* 49**,** 287-299.

Cannell, E., Dornan, A.J., Halberg, K.A., Terhzaz, S., Dow, J.A., and Davies, S.-A. (2016). The corticotropin-releasing factor-like diuretic hormone 44 (DH44) and kinin neuropeptides modulate desiccation and starvation tolerance in *Drosophila melanogaster*. *Peptides.* 80**,** 96-107.

Cox, K.J., Tensen, C.P., Van der Schors, R.C., Li, K.W., van Heerikhuizen, H., Vreugdenhil, E., et al. (1997). Cloning, characterization, and expression of a G-protein-coupled receptor from *Lymnaea stagnalis* and identification of a leucokinin-like peptide, PSFHSWSamide, as its endogenous ligand. *J. Neurosci* 17(4)**,** 1197-1205.

Crooks, G.E., Hon, G., Chandonia, J.-M., and Brenner, S.E. (2004). WebLogo: a sequence logo generator. *Genome Res.* 14(6)**,** 1188-1190.

Derst, C., Dircksen, H., Meusemann, K., Zhou, X., Liu, S., and Predel, R. (2016). Evolution of neuropeptides in non-pterygote hexapods. *BMC Evol. Biol.* 16(1)**,** 51.

Duvall, L.B., Ramos-Espiritu, L., Barsoum, K.E., Glickman, J.F., and Vosshall, L.B. (2019). Small-molecule agonists of *Ae. aegypti* neuropeptide Y receptor block mosquito biting. *Cell.* 176(4)**,** 687-701. e685.

Egekwu, N., Sonenshine, D., Garman, H., Barshis, D., Cox, N., Bissinger, B., et al. (2016). Comparison of synganglion neuropeptides, neuropeptide receptors and neurotransmitter receptors and their gene expression in response to feeding in *Ixodes scapularis* (Ixodidae) vs. *O rnithodoros turicata* (Argasidae). *Insect Mol. Biol.* 25(1)**,** 72-92.

Egekwu, N., Sonenshine, D.E., Bissinger, B.W., and Roe, R.M. (2014). Transcriptome of the female synganglion of the black-legged tick *Ixodes scapularis* (Acari: Ixodidae) with comparison between Illumina and 454 systems. *PloS one.* 9(7)**,** e102667.

Ejendal, K.F.K., Meyer, J.M., Brust, T.F., Avramova, L.V., Hill, C.A., and Watts, V.J. (2012). Discovery of antagonists of tick dopamine receptors via chemical library screening and comparative pharmacological analyses. *Insect Biochem. Molec.* 42(11)**,** 846-853.

Geraci, N.S., Johnston, J.S., Robinson, J.P., Wikel, S.K., and Hill, C.A. (2007). Variation in genome size of argasid and ixodid ticks. *Insect Biochem. Molec.* 37(5)**,** 399-408.

Gondalia, K., Qudrat, A., Bruno, B., Medina, J.F., and Paluzzi, J.-P.V. (2016). Identification and functional characterization of a pyrokinin neuropeptide receptor in the Lyme disease vector, *Ixodes scapularis*. *Peptides.* 86**,** 42-54.

Grimmelikhuijzen, C.J., and Hauser, F. (2012). Mini-review: the evolution of neuropeptide signaling. *Regulatory peptides* 177**,** S6-S9.

Gross, A.D., Temeyer, K.B., Day, T.A., Pérez de León, A.A., Kimber, M.J., and Coats, J.R. (2015). Pharmacological characterization of a tyramine receptor from the southern cattle tick, *Rhipicephalus (Boophilus) microplus*. *Insect Biochem. Molec.* 63**,** 47-53.

Guerrero, F.D., Kellogg, A., Ogrey, A.N., Heekin, A.M., Barrero, R., Bellgard, M.I., et al. (2016). Prediction of G protein-coupled receptor encoding sequences from the synganglion transcriptome of the cattle tick, *Rhipicephalus microplus*. *Ticks. Tick-Borne. Dis.* 7(5)**,** 670-677.

Guerrero, F.D., Lovis, L., and Martins, J.R. (2012). Acaricide resistance mechanisms in *Rhipicephalus (Boophilus) microplus*. *Rev. Bras. Parasitol. V.* 21(1)**,** 1-6.

Gulia-Nuss, M., Nuss, A.B., Meyer, J.M., Sonenshine, D.E., Roe, R.M., Waterhouse, R.M., et al. (2016). Genomic insights into the *Ixodes scapularis* tick vector of Lyme disease. *Nat. Commun.* 7**,** 10507.

Halberg, K.A., Terhzaz, S., Cabrero, P., Davies, S.A., and Dow, J.A. (2015). Tracing the evolutionary origins of insect renal function. *Nat. Commun.* 6**,** 6800.

Hayes, T., Pannabecker, T.L., Hinckley, D., Holman, G., Nachman, R., Petzel, D., et al. (1989). Leucokinins, a new family of ion transport stimulators and inhibitors in insect Malpighian tubules. *Life Sci.* 44(18)**,** 1259-1266.

Holman, G., Cook, B., and Nachman, R. (1986). Isolation, primary structure and synthesis of two neuropeptides from *Leucophaea maderae*: members of a new family of cephalomyotropins. *Comp. Biochem. Phys. C* 84(2)**,** 205-211.

Holmes, S., Barhoumi, R., Nachman, R., and Pietrantonio, P. (2003). Functional analysis of a G protein- coupled receptor from the Southern cattle tick *Boophilus microplus* (Acari: Ixodidae) identifies it as the first arthropod myokinin receptor. *Insect Mol. Biol.* 12(1)**,** 27-38.

Holmes, S., He, H., Chen, A., Lvie, G., and Pietrantonio, P. (2000). Cloning and transcriptional expression of a leucokinin- like peptide receptor from the Southern cattle tick, *Boophilus microplus* (Acari: Ixodidae). *Insect Mol. Biol.* 9(5)**,** 457-465.

Jeyaprakash, A., and Hoy, M.A. (2009). First divergence time estimate of spiders, scorpions, mites and ticks (subphylum: Chelicerata) inferred from mitochondrial phylogeny. *Exp. Appl. Acarol.* 47(1)**,** 1-18.

Katoh, K., and Standley, D.M. (2013). MAFFT multiple sequence alignment software version 7: improvements in performance and usability. *Mol. Biol. Evol.* 30(4)**,** 772-780.

Kersch, C.N., and Pietrantonio, P.V. (2011). Mosquito *Aedes aegypti* (L.) leucokinin receptor is critical for in vivo fluid excretion post blood feeding. *FEBS Lett.* 585(22)**,** 3507-3512.

Kim, D., Šimo, L., and Park, Y. (2018). Molecular characterization of neuropeptide elevenin and two elevenin receptors, IsElevR1 and IsElevR2, from the blacklegged tick, I*xodes scapularis*. *Insect Biochem. Molec.* 101**,** 66-75.

Kim, Y.-J., Žitňan, D., Cho, K.-H., Schooley, D.A., Mizoguchi, A., and Adams, M.E. (2006). Central peptidergic ensembles associated with organization of an innate behavior. *Proc. Natl. Acad. Sci.* 103(38)**,** 14211-14216.

Kwon, H., Agha, M.A., Smith, R.C., Nachman, R.J., Marion-Poll, F., and Pietrantonio, P.V. (2016). Leucokinin mimetic elicits aversive behavior in mosquito *Aedes aegypti* (L.) and inhibits the sugar taste neuron. *Proc. Natl. Acad. Sci.* 113(25)**,** 6880-6885.

Lange, A.B., Nachman, R.J., Kaczmarek, K., and Zabrocki, J. (2016). Biostable insect kinin analogs reduce blood meal and disrupt ecdysis in the blood-gorging Chagas' disease vector, *Rhodnius prolixus*. *Peptides.* 80**,** 108-113.

Lees, K., Woods, D., and Bowman, A.S. (2010). Transcriptome analysis of the synganglion from the brown dog tick, *Rhipicephalus sanguineus*. *Insect Mol. Biol.* 19(3)**,** 273-282.

Lipinski, C.A. (2016). Rule of five in 2015 and beyond: Target and ligand structural limitations, ligand chemistry structure and drug discovery project decisions. *ADV Drug Deliver. Rev.* 101**,** 34-41.

Lu, H.L., Kersch, C., and Pietrantonio, P.V. (2011a). The kinin receptor is expressed in the Malpighian tubule stellate cells in the mosquito *Aedes aegypti* (L.): A new model needed to explain ion transport? *Insect Biochem. Molec.* 41(2)**,** 135-140. doi: 10.1016/j.ibmb.2010.10.033.

Lu, H.L., Kersch, C.N., Taneja-Bageshwar, S., and Pietrantonio, P.V. (2011b). A Calcium Bioluminescence Assay for Functional Analysis of Mosquito (*Aedes aegypti*) and Tick

(*Rhipicephalus microplus*) G Protein-coupled Receptors. *Jove-J. Vis. Exp.* (50)**,** Immunology and Infection. doi: 10.3791/2732.

Ma, Q., Ye, L., Liu, H., Shi, Y., and Zhou, N. (2017). An overview of Ca2+ mobilization assays in GPCR drug discovery. *Expert Opin. Drug Dis.* 12(5)**,** 511-523.

Maddison, W.P. (2005). Mesquite: a modular system for evolutionary analysis. Version 1.06. *http://mesquiteproject.org*.

Nachman, R.J., Moyna, G., Williams, H.J., Zabrocki, J., Zadina, J.E., Coast, G.M., et al. (1999). Comparison of active conformations of the insectatachykinin/tachykinin and insect kinin/Tyr- W- MIF- 1 neuropeptide family pairs. *Ann. NY. Acad. Sci.* 897(1)**,** 388-400.

Nachman, R.J., Zabrocki, J., Olczak, J., Williams, H.J., Moyna, G., Scott, A.I., et al. (2002). cis-Peptide bond mimetic tetrazole analogs of the insect kinins identify the active conformation. *Peptides.* 23(4)**,** 709-716.

Neupert, S., Predel, R., Russell, W.K., Davies, R., Pietrantonio, P.V., and Nachman, R.J. (2005). Identification of tick periviscerokinin, the first neurohormone of Ixodidae: single cell analysis by means of MALDI-TOF/TOF mass spectrometry. *Biochem. Bioph. Res. Co.* 338(4)**,** 1860-1864.

Pennefather, J.N., Lecci, A., Candenas, M.L., Patak, E., Pinto, F.M., and Maggi, C.A. (2004). Tachykinins and tachykinin receptors: a growing family. *Life Sci.* 74(12)**,** 1445-1463.

Pérez de León, A.A., Teel, P.D., Auclair, A.N., Messenger, M.T., Guerrero, F.D., Schuster, G., et al. (2012). Integrated strategy for sustainable cattle fever tick eradication in USA is required to mitigate the impact of global change. *Front. Physiol.* 3**,** 195.

Pietrantonio, P., Jagge, C., Taneja- Bageshwar, S., Nachman, R., and Barhoumi, R. (2005). The mosquito *Aedes aegypti* (L.) leucokinin receptor is a multiligand receptor for the three Aedes kinins. *Insect Mol. Biol.* 14(1)**,** 55-67.

Pietrantonio, P., Xiong, C., Nachman, R., and Shen, Y. (2018). G protein-coupled receptors in arthropod vectors: Omics and pharmacological approaches to elucidate ligand-receptor interactions and novel organismal functions. *Curr. Opin. Insect Sci.* 29**,** 12-20.

Poels, J., Birse, R.T., Nachman, R.J., Fichna, J., Janecka, A., Broeck, J.V., et al. (2009). Characterization and distribution of NKD, a receptor for *Drosophila* tachykinin-related peptide 6. *Peptides.* 30(3)**,** 545-556.

Pohl, P.C., Klafke, G.M., Júnior, J.R., Martins, J.R., da Silva Vaz, I., and Masuda, A. (2012). ABC transporters as a multidrug detoxification mechanism in *Rhipicephalus (Boophilus) microplus*. *Parasitol. Res.* 111(6)**,** 2345-2351.

Predel, R., Neupert, S., Derst, C., Reinhardt, K., and Wegener, C. (2017). Neuropeptidomics of the bed bug *Cimex lectularius*. *J. Proteome. Res.* 17(1)**,** 440-454.

Rambaut, A. (2012). "FigTree version 1.4.4".).

Rambaut, A., Drummond, A., Xie, D., Baele, G., and Suchard, M. (2018). "Tracer version 1.7.1".).

Ronquist, F., Teslenko, M., Van Der Mark, P., Ayres, D.L., Darling, A., Höhna, S., et al. (2012). MrBayes 3.2: efficient Bayesian phylogenetic inference and model choice across a large model space. *Syst. Biol.* 61(3)**,** 539-542.

Schepel, S.A., Fox, A.J., Miyauchi, J.T., Sou, T., Yang, J.D., Lau, K., et al. (2010). The single kinin receptor signals to separate and independent physiological pathways in Malpighian

tubules of the yellow fever mosquito. *American Journal of Physiology-Regulatory, Integrative and Comparative Physiology* 299(2)**,** R612-R622.

Schooley, D., Horodyski, F., and Coast, G.M. (2012). "Hormones controlling homeostasis in insects," in *Insect Endocrinology*, ed. L.I. Gilbert. (Academic Press), 366-429.

Smagghe, G., Mahdian, K., Zubrzak, P., and Nachman, R.J. (2010). Antifeedant activity and high mortality in the pea aphid *Acyrthosiphon pisum* (Hemiptera: Aphidae) induced by biostable insect kinin analogs. *Peptides.* 31(3)**,** 498-505.

Taneja-Bageshwar, S., Strey, A., Isaac, R.E., Coast, G.M., Zubrzak, P., Pietrantonio, P.V., et al. (2009). Biostable agonists that match or exceed activity of native insect kinins on recombinant arthropod GPCRs. *Gen. Comp. Endocrinol.* 162(1)**,** 122-128.

Taneja- Bageshwar, S., Strey, A., Zubrzak, P., Pietrantonio, P.V., and Nachman, R.J. (2006). Comparative structure- activity analysis of insect kinin core analogs on recombinant kinin receptors from Southern cattle tick *Boophilus microplus* (Acari: Ixodidae) and mosquito *Aedes aegypti* (Diptera: Culicidae). *Arch. Insect Biochem.* 62(3)**,** 128-140.

Thastrup, O., Cullen, P.J., Drøbak, B., Hanley, M.R., and Dawson, A.P. (1990). Thapsigargin, a tumor promoter, discharges intracellular Ca2+ stores by specific inhibition of the endoplasmic reticulum Ca2 (+)-ATPase. *Proc. Natl. Acad. Sci.* 87(7)**,** 2466-2470.

Torfs, H., Poels, J., Detheux, M., Dupriez, V., Van Loy, T., Vercammen, L., et al. (2002). Recombinant aequorin as a reporter for receptor-mediated changes of intracellular Ca 2+-levels in *Drosophila* S2 cells. *Invertebr. Neurosci.* 4(3)**,** 119-124.

Torfs, P., Nieto, J., Veelaert, D., Boon, D., Van De Water, G., Waelkens, E., et al. (1999). The kinin peptide family in invertebrates. *Ann. NY. Acad. Sci.* 897(1)**,** 361-373.

Veenstra, J.A. (2000). Mono- and dibasic proteolytic cleavage sites in insect neuroendocrine peptide precursors. *Arch. Insect Biochem.* 43(2)**,** 49-63.

Veenstra, J.A. (2016). Neuropeptide evolution: Chelicerate neurohormone and neuropeptide genes may reflect one or more whole genome duplications. *Gen. Comp. Endocrinol.* 229**,** 41-55.

Veenstra, J.A., Pattillo, J.M., and Petzel, D.H. (1997). A single cDNA encodes all three aedesleucokinins, which stimulate both fluid secretion by the malpighian tubules and hindgut contractions. *J. Biol. Chem.* 272(16)**,** 10402-10407.

Xiong, C., Kaczmarek, K., Zabrocki, J., Pietrantonio, P.V., and Nachman, R.J. (2019). Evaluation of Aib and PEG-polymer insect kinin analogs on mosquito and tick GPCRs identifies potent new pest management tools with potentially enhanced biostability and bioavailability. *Gen. Comp. Endocrinol.* 278**,** 58-67. doi: 10.1016/j.ygcen.2018.08.002.

Yang, Y., Bajracharya, P., Castillo, P., Nachman, R.J., and Pietrantonio, P.V. (2013). Molecular and functional characterization of the first tick CAP2b (periviscerokinin) receptor from *Rhipicephalus (Boophilus) microplus* (Acari: Ixodidae). *Gen. Comp. Endocrinol.* 194**,** 142-151.

Yang, Y., Nachman, R.J., and Pietrantonio, P.V. (2015). Molecular and pharmacological characterization of the Chelicerata pyrokinin receptor from the southern cattle tick, *Rhipicephalus (Boophilus) microplus*. *Insect Biochem. Molec.* 60**,** 13-23.

Yeoh, J.G.C., Pandit, A.A., Zandawala, M., Nässel, D.R., Davies, S.-A., and Dow, J.A.T. (2017). DINeR: Database for Insect Neuropeptide Research. *Insect Biochem. Molec.* 86**,** 9-19.

Zandawala, M., Yurgel, M.E., Texada, M.J., Liao, S., Rewitz, K.F., Keene, A.C., et al. (2018). Modulation of *Drosophila* post-feeding physiology and behavior by the neuropeptide leucokinin. *PloS Genet.* 14(11)**,** e1007767.

4. ACTIVITY OF NATIVE TICK KININS AND PEPTIDOMIMETICS ON THE COGNATE TARGET G PROTEIN-COUPLED RECEPTOR FROM THE CATTLE FEVER TICK, *RHIPICEPHALUS MICROPLUS* (ACARI: IXODIDAE)[*]

4.1. Overview

BACKGROUND: Kinins are multifunctional neuropeptides that regulate key insect physiological processes such as diuresis, feeding, and ecdysis. However, the physiological roles of kinins in ticks are unclear. Further, ticks have an expanded number of kinin paracopies in the kinin gene. Silencing the kinin receptor in females of *R. microplus* reduces reproductive fitness. Thus, it appears the kinin signaling system is important for tick physiology, and its disruption may have potential for tick control.

RESULTS: We determined the activities of endogenous kinins on the kinin receptor, a G protein-coupled receptor (GPCR), and identified potent peptidomimetics. Fourteen predicted *R. microplus* kinins (Rhimi-K), and eleven kinin analogs containing aminoisobutyric acid (Aib) were tested. The latter either incorporated tick kinin sequences or were modified for enhanced resistance to arthropod peptidases. A high-throughput screen using a calcium fluorescence assay in 384-well-plates was performed. All tested kinins and Aib-analogs were full agonists. The most potent kinin and two kinin analogs were equipotent. Analogs 2414 ([Aib]FS[Aib]WGa) and 2412 ([Aib]FG[Aib]WGa) were the most active with EC_{50} values of 0.9 nM and 1.1 nM, respectively, matching the EC_{50} of the most potent tick kinin, Rhimi-K-14 (QDSFNPWGa) (EC_{50} = 1 nM). The potent analog 2415 ([Aib]FR[Aib]WGa, EC_{50} = 6.8 nM) includes both, Aib

[*] Reprinted with permission from "Activity of native tick kinins and peptidomimetics on the cognate target G protein-coupled receptor from the cattle fever tick, *Rhipicephalus microplus* (Acari: Ixodidae)" by Xiong, C., Kaczmarek, K., Zabrocki, J., Pietrantonio, P. V., Nachman, R. J., 2019. Pest Management Science, 76: 3423-3431 Copyright [2019] by John Wiley and Sons.

molecules for resistance to peptidases, and a positively charged residue, R, for enhanced water solubility and amphiphilic character.

CONCLUSION: These tick kinins and pseudopeptides expand the repertoire of reagents for tick physiology and toxicology towards finding novel targets for tick management.

4.2. Introduction

The cattle fever tick or southern cattle tick, *Rhipicephalus microplus,* is a pest that poses great risk to the global cattle industry (Pérez de León et al., 2012). It transmits the deadly pathogens of cattle, *Babesia* spp. and *Anaplasma* spp. Considering the lack of effective vaccines against these vector-borne pathogens, vector control is still the most efficient approach to block disease transmission. However, resistance to the most commonly used acaricides, such as amitraz (formamidines), pyrethroids, organophosphates, and/or ivermectin is present worldwide in diverse tick populations (Guerrero et al., 2012; Pohl et al., 2012). In searching for novel targets for vector control we have focused on an invertebrate-specific G protein-coupled receptor (GPCR), the kinin receptor. Insect kinins are also known as leucokinins, as they were first discovered and isolated from the roach *Leucophaea maderae* for their myotropic activity (Holman et al., 1986). It was later proven that neuropeptides of the kinin class regulate important biological functions in invertebrates (Coast, 2007; Coast et al., 2002; De Loof, 2008; Gäde, 2004b; Nässel, 2002). In diverse species, insect kinins stimulate hindgut contractions, diuresis, digestive enzyme release, probably inhibit lepidopteran larval weight gain, participate in tracheal clearance and air filling prior to ecdysis in *Drosophila,* and modulate sugar taste perception in contact chemosensory neurons in *Aedes aegypti* mosquitoes (Coast et al., 1990; Harshini et al., 2003; Holman et al., 1990; Kersch and Pietrantonio, 2011; Kim, D.-H. et al., 2018b; Kwon et al., 2016; Lu et al., 2011a; Nachman et al., 2002a; Pietrantonio, P.V. et al., 2005; Seinsche et al.,

2000). The endogenous arthropod kinins are 6-14 amino acid residues long and characterized by the evolutionarily conserved C-terminal pentapeptide Phe-X^1-X^2-Trp-Gly-NH_2, where X^1 = His, Asn, Ser, or Tyr, and X^2 = Ser, Pro, or Ala (Holman et al., 1999; Torfs et al., 1999b). This C-terminal pentapeptide kinin core is the minimum sequence required for full activity in both the cockroach myotropic and the cricket diuretic assays *in vitro* (Nachman et al., 2003; Nachman and Holman, 1991a).

Recombinant kinin receptors from the southern cattle tick, *R. microplus*, and the dengue vector, *Ae. aegypti*, confirmed the activity of the kinin pentapeptide core (Holmes, S.P. et al., 2003; Pietrantonio, P.V. et al., 2005; Taneja- Bageshwar et al., 2006). Both the tissue assays and the receptor expressing system revealed that the Phe at position one, Trp at position four, and the amidated C-terminus of the kinin penta-core are crucial for kinin activity (Nachman et al., 1995; Taneja-Bageshwar, Suparna et al., 2009; Taneja- Bageshwar et al., 2006). In contrast, the first variable position (X^1) tolerates a wide range of chemical characteristics, from acidic to basic residues, and from hydrophilic to hydrophobic (Nachman and Holman, 1991a; Roberts et al., 1997; Taneja- Bageshwar et al., 2006). Based on these observations the plausible receptor interaction model positions the side chains of Phe and Trp towards the same region where they interact with the receptor via a β-turn involving the Pro (or Ser or Ala) at the third position, and away from the side chain of X^1 residue.

Neuropeptides have been studied as potential leads for the development of new, environmentally friendly pest control agents due to their specificity and high activity at very low doses (Pietrantonio, P.V. et al., 2018). The generic kinins as well as modified insect kinins have been used to functionally characterize the tick kinin receptor (Taneja-Bageshwar, Suparna et al., 2009; Taneja- Bageshwar et al., 2006; Xiong et al., 2019d). The tick kinin receptor appears as a

promising target because knocking-down its expression in female ticks results in significant reduction of their reproductive fitness (Brock et al., 2019a). However, the natural peptides cannot be directly used, as they are susceptible to degradation by endogenous peptidases (Cornell et al., 1995; Gäde and Goldsworthy, 2003; Lamango et al., 1996; Nachman et al., 2002a) and may not penetrate the cuticle. Knowledge of both chemical and conformational requirements responsible for endogenous neuropeptide biological activity can aid in the design of analogs containing unnatural moieties that can overcome these limitations (Nachman et al., 1994). The primary hydrolysis-susceptible site lies within the insect kinin C-terminal pentapeptide core region between the second variable (X^2) position (P, S, A) and the conserved Trp, residues present at position 3 and 4, respectively. A secondary site is found just outside of the core region at the peptide bond N-terminal to the important Phe at position 1. Replacement of Ser (or Pro) with an unnatural, sterically bulky residue, aminoisobutyric acid (Aib), leads to analogs that not only mimic a critical β-turn conformation but also block tissue-bound peptidase, angiotensin converting enzyme, and neprilysin hydrolysis (Nachman et al., 1997a; Nachman et al., 1997b; Taneja-Bageshwar, Suparna et al., 2009; Taneja- Bageshwar et al., 2006). Incorporation of a second Aib residue adjacent to the secondary peptidase hydrolysis site further enhances biostability (Taneja-Bageshwar, Suparna et al., 2009).

Knowledge of the endogenous kinin sequences of the target species can aid in developing more potent analogs (Xiong et al., 2019d). To fill this gap in knowledge for the tick kinin receptor, we cloned the cDNA of the kinin neuropeptide precursor from *R. microplus*. Within the translated amino acid sequence, we predicted the sequences of 17 tick kinins, based on both the identification of the canonical conserved residues in the pentapeptide kinin core “FXXWGa” (FXXWGG) and the putative dibasic enzyme cleavage cutting sites (KK/KR/RR) on the

precursor Xiong et al., 2019a), however, their activity on the receptor has not yet been tested. Therefore, the current study determined the activities of the predicted *R. microplus* endogenous kinin ligands and modified analogs on the recombinant tick kinin receptor through a cellular functional assay using calcium fluorescence as a reporter, and in high-throughput mode. Based on the tick kinin sequences, we continued the design of active kinin pseudopeptides with enhanced resistance to peptidases. In this paper, we further explore the use of the sterically-hindered Aib moiety in biostable analogs that also specifically incorporate residues from kinins native to the tick *R. microplus* (Xiong et al., 2019a). We also included an analog of this motif with X^1 = A, found in a predicted *R. microplus* kinin, Rhimi-K-7, which was not tested (see Discussion section) (Xiong et al., 2019a). In a few of these analogs the N-terminus is further protected from aminopeptidases with either acetyl (Ac-) or pyroglutamate (pQ-) groups.(Nachman et al., 2002a) A couple of additional analogs were evaluated on the tick receptor that feature either the strongly basic, positively charged R or dR placed at the N-terminal of the pentapeptide core in order to enhance the aqueous solubility of the generally hydrophobic insect kinin core sequence. One analog featured the replacement of the N-terminal F of the pentapeptide core region with the non-amino acid hydrocinnamic acid (Hca) leading to a smaller pseudo-tetrapeptide fragment. It was evaluated to see if this large structural modification could be tolerated by the tick receptor.

We identified potent ligands of the tick kinin receptor as potential pest management tools with enhanced biostability and bioavailability. Further, the structure-activity relationships between ligands (Rhimi-Ks and pseudopeptides) and the tick kinin receptor were analyzed.

4.3. Materials and Methods

4.3.1. Analog synthesis and purification*

Analogs were synthesized on an ABI 433A peptide synthesizer with a modified FastMoc 0.25 procedure using an Fmoc-strategy starting from Rink amide resin (Novabiochem, San Diego, CA, 0.5 mM/g). The Fmoc protecting group was removed with 20% 4-methyl piperidine in DMF (Dimethyl formamide).(Nachman et al., 1997a) A fourfold excess of the respective Fmoc-amino acids was activated *in situ* using HBTU (2-(1h-benzotriazol-1-yl)-1,1,3,3-tetramethyluronium hexafluorophosphate) (1 eq.) /HOBt (1-hydroxybenzotriazole) (1 eq.) in NMP (N-methylpyrrolidone) or HATU (2-(7-Aza-1H-Benzotiazole-1-yl)-1,1,3,3-tetramethyluronium hexafluorophosphate) (1 eq.)/HOAt (1-hydroxy-7-azabenzotriazole) (1 eq.) in NMP for Aib and the amino acid immediately following it in the sequence. The coupling reactions were base catalyzed with DIPEA (N,N-diisopropylethylamine) (4 eq.). The amino acid side chain protecting groups were PMC for Arginine, tBu for Serine and Threonine, OtBu for Glutamic and Aspartic acids, Trt for Histidine, and Boc for Tryptophan.

The analogs were cleaved from the resin with side-chain deprotection by treatment with TFA (Trifluoroacetic acid):H_2O:TIS (Triisopropylsilane) (95.5:2.5:2.5 v/v/v) for 1.5 h. The solvents were evaporated by vacuum centrifugation and the analogs were desalted on a Waters C_{18} Sep Pak cartridge (Milford, MA) in preparation for purification by HPLC.

The analogs were purified on a Waters Delta-Pak C_{18} reverse-phase column (8 x 100 mm, 15 µm particle size, 100 Å pore size) with a Waters 510 HPLC system with detection at 214 nm at ambient temperature. Solvent A = 0.1% aqueous trifluoroacetic acid (TFA); Solvent B = 80% aqueous acetonitrile containing 0.1% TFA. Initial conditions were 10% B followed by a linear

* Design, synthesis, and purification of peptide analogs was performed by co-author Dr. Ron J. Nachman of USDA.

increase to 90 % B over 40 min.; flow rate, 2 ml/min. Delta-Pak C_{18} retention times: **2379,** QF**S**PWGa, 7.0 min.; **2378,** EGPF**S**PWGa, 7.7 min.; **2373,** GADDPF**N**PWGa, 8.0 min.; **2374,** QDSF**N**PWGa, 7.1 min.; **2375,** EDGVF**R**PWGa, 6.1 min.; **2376,** EDNVF**R**PWGa, 6.7 min.; **2381,** EGNVF**G**PWGa, 7.7 min.; **2383,** AGDHF**G**SWGa, 6.8 min.; **2389,** DTF**S**AWGa, 6.9 min.; **2387,** QQDSKNAF**S**PWGa, 3.2 min.; **2380,** GTGEDQAF**S**PWGa, 7.2 min.; **2384,** GDDGDTSF**T**PWGa, 7.2 min.; **2361**, A[Aib]F**S**[Aib]WGa, 2.6 min.; **2346**, Ac-[dR]F**H**[Aib]WGa, 2.4 min.; **2359**, AKF**S**[Aib]WGa, 2.4 min; **2173-1**, Hca-**F**[Aib]WGa, 2.9 min.; **2345**, pQRF**H**[Aib]WGa, 2.3 min**; 2411**, [Aib]F**N**[Aib]WGa, 2.7 min.; **2412**, [Aib]F**G**[Aib]WGa, 2.7 min; **2413**, [Aib]F**T**[Aib]WGa, 2.6 min.; **2414**, [Aib]F**S**[Aib]WGa, 2.7 min; **2415**, [Aib]F**R**[Aib]WGa, 2.7 min.; **2416**, [Aib]F**A**[Aib]WGa, 3.0 min. The analogs were further purified on a Waters Protein Pak I 125 column (7.8 x 300 mm). Conditions: isocratic using 80% acetonitrile containing 0.1% TFA; flow rate, 2 ml/min. Waters Protein Pak retention times: **2379,** 7.5 min.; **2378,** 6.2 min.; **2373,** 8.2 min.; **2374,** 7.0 min.; **2375,** 7.5 min.; **2376,** 7.5 min.; **2381,** 7.0 min.; **2383,** 7.5 min.; **2389,** 7.5 min.; **2387,** 12.0 min.; **2380,** 8.5 min.; **2384,** 7.5 min.; **2361**, 6.0 min.; **2346**, 9.0 min.; **2359**, 6.0 min; **2173-1**, 6.0 min.; **2345**, 9.2 min**; 2411**, 6.0 min.; **2412**, 6.2 min; **2413**, 6.2 min.; **2414**, 6.0 min; **2415**, 6.0 min.; **2416**, 6.0 min.

Amino acid analysis was carried out under previously reported conditions(Nachman et al., 2004) to quantify the analogs and to confirm identity: **2379,** D[1.0], F[1.0], G[0.9], P[0.8], S[0.9]; **2378,** E[1.0], F[1.0], G[1.9], P[1.8], S[1.0]; **2373,** G[1.0], A[0.9], D[2.7], P[2.0], F[1.0]; **2374,** D[2.2], E[1.2], F[1.0], G[1.2], P[1.0], S[1.0]; **2375,** D[1.0], E[1.0], F[1.0], G[2.0], P[1.0], R[1.0], V[1.0]; **2376,** D[2.2], E[1.0], F[1.0], G[1.1], P[1.1], R[1.1], V[1.0]; **2381,** D[1.0], E[1.2], F[1.0], G[3.0], P[1.0], V[1.0]; **2383,** A[0.9], D[1.0], F[1.0], G[2.7], H[0.9], S[0.9]; **2389,** A[1.2], D[1.3], F[1.0], G[1.2], T[1.0], S[1.3]; **2387,** A[0.9], D[2.0], E[2.0], F[1.0], G[0.7], K[0.9],

P[0.7], S[1.9]; **2380,** A[1.0], D[0.95], E[2.0], F[1.0], G[2.9], P[1.0], S[1.0], T[1.0]; **2384,** D[3.0], F[1.0], G[3.0], P[1.0], S[1.0], T[2.0]; **2361**, A[1.0], F[1.0], G[0.9], S[0.8]; **2346**, F[1.0], G[1.1], H[1.0], R[0.9]; **2359**, A[0.9], F[1.0], G[1.0], K[0.8], S[1.0]; **2173-1**, F[1.0], G[1.0]; **2345**, E[1.0], F[1.0], G[1.1], H[1.0], R[0.9]**; 2411**, D[1.0], F[1.0], G[1.1]; **2412**, F[1.0], G[1.9]; **2413**, F[1.0], G[1.1], T[0.9]; **2414**, F[1.0], G[1.0], S[1.0]; **2415**, F[1.0], G[1.0], R[1.2]; **2416**, A[1.0], F[1.0], G[1.0].

The identity of the analogs was also confirmed by MALDI-MS on a Kratos Kompact Probe MALDI-MS instrument (Shimadzu, Columbia, Maryland). The following molecular ions (MH^+) were observed: **2379,** 720.1 (calc. 720.0); **2378,** 875.3 (calc. 875.0); **2373,** 1074.5 (calc. 1074.0); **2374,** 949.5 (calc. 949.0); **2375,** 1061.7 (calc. 1061.0); **2376,** 1118.8 (calc. 1118.0); **2381,** 962.0 (961.0); **2383,** 932.4 (932.0); **2389,** 782.4 (calc. 782.0); **2387,** 1363.7 (calc. 1363.0); **2380,** 1250.0 (calc. 1250.0); **2384,** 1253.0 (calc. 1253.0); **2361**, 736.2 (calc. 736.0); **2346**, 827.8 (calc. 827.0); **2359**, 779.3 (calc. 779.0); **2173-1**, 647.2 (calc. 647.0 [MNa^+]); **2345**, 896.8 (calc. 896.0)**; 2411**, 692.0 (calc. 692.0); **2412**, 635.7 (calc. 635.0); **2413**, 679.7 (calc. 679.0); **2414**, 665.0 (calc. 665.0); **2415**, 734.2 (calc. 734.0); **2416**, 649.0 (calc. 649.0).

4.3.2. Preparation of kinin peptides and analogs in 384-well plates

Each 384-well flat bottom drug plate (16 rows x 24 columns; Corning® 3680) was prepared to test 14-16 compounds. Dose-response curves were obtained by testing 20 different final concentrations in the assay for each compound, ranging from 10 pM to 10 µM. Two columns adjacent to each plate edge were filled with blank solvent as negative controls. The start concentration solution for each compound dilution series was loaded (80 µl) in the third column. The tested kinin peptides or analogs were freshly solubilized on the day of the assay and serially diluted in the plate from a 5 x starting stock solution of 50 µM (5 nmoles dry peptide in 100 µl of

1 % DMSO in DPBS (Corning®, 21-0310-CV)). The rest of the wells were added 40 µl of blank solvent for serial dilutions that were performed automatically using the EpMotion™ liquid handler (Eppendorf, 5075, Germany). Dilutions of each compound were performed using a ratio of 1:1, and mixing twice before the next dilution. Tips were changed between dilutions because of the high potency of the compounds; any carry-over would skew the results.

4.3.3. Cell lines and cell culture

BMLK3 is a CHO-K1 cell line stably expressing the *R. microplus* kinin receptor, and served to characterize the functional activity of compounds on the receptor. The receptor cloning and production of this single clonal cell line was reported previously.(Holmes, S.P. et al., 2003; Holmes, S.P. et al., 2000) A CHO-K1 cell line transfected with the empty expression vector, plasmid pcDNA3.1 (Invitrogen, Carlsbad, CA), was designated as a "vector only" and used as the negative control. Both cell lines were maintained in T-75 flasks (CELLSTAR®, Greiner® Bio-one) with maintenance medium consisting of F-12K medium (Corning™ Cellgro™, Mediatech, Inc. VA, US), fetal bovine serum (FBS) (10%) (Equitech-Bio, Kerrville, TX) and 400 µg/ml G418 Sulfate (Gibco® Invitrogen, New York, US). Cells were maintained in a humidified incubator at 37°C, 5% CO_2. Cells were incubated under the above conditions unless specified otherwise. Details of cell maintenance were as before (Lu et al., 2011d).

4.3.4. End-point calcium fluorescence assay

BMLK3 or "vector only" cells were cultured in T-75 flasks. When they reached about 90 % confluency (Lu et al., 2011d), they were trypsinized and suspended in F-12K medium containing 1 % FBS and 400 µg/ml of G418 Sulfate at 4×10^5 cells/ml to be seeded in 384-well plates (CELLSTAR®, flat, black wall, clear bottom, Greiner® Bio-one 781091). For this, the cell suspension (25 µl; ~10,000 cells/well) was dispensed into each of the 384 wells of the plate.

Unless specified, the pipetting steps in the 384-well plate fluorescence assay were performed by an automated CyBio® Well Vario System using a 384 pipette-head that allows to simultaneously deliver a volume of up to 60 µl per well (detailed CyBio programs we developed to perform the high-throughput fluorescence assay are listed in Suppl. Appendix 1).

To distribute cells evenly, mixing was by retrieving by aspiration 10 µl of the dispensed cells and immediately returning them to the well; mixing was repeated three times. Plates were incubated overnight at 37°C under 5 % CO_2. On the next day, cells were prepared for the assay: the old media in the assay plate was removed by inverting the plate and gently blotting it on paper towels, and media was replaced with 25 µl of FLUOFORTE® loading dye (1×) (FLUOFORTE® calcium assay kit, Enzo Life Science, Inc. New York, NY), according to the kit's instructions. The plate was incubated at 37°C under 5 % CO_2 for 30 min, then incubated at room temperature in the dark for 30 min. Upon addition of the peptides or analogs, the assay plate was immediately transferred from the CyBio® Well Vario System into the Clariostar® plate reader (BMG Labtech, Germany). The endpoint responses were recorded in fluorescence plate-mode with Ex/Em = 490/525 nm and at 29 °C. The fluorescence cellular response to each concentration was represented as the average of two values that were obtained by both forward and reverse plate readings. For this, the plate was read from both forward and reverse orientations by rotating the plate (180°) on the instrument to compensate for the variation in signal kinetics during the lapse in plate reading, because there was a 1 min lag time between the readings of the first and the last well. Therefore, only one value represents each compound concentration. We had experimentally determined that the intensity of the fluorescence signal is stable for more than 5 min. On BMLK3 cells, three independent replicates of the dose-response of each peptide were performed, except that two replicates were done for peptides Rhimi-K-3

and Rhimi-K-10 due to the lack of availability of these peptides at the time of the first replication. Only the peptides used during the first replication were tested on the "vector-only" cells as negative controls.

The response to each compound concentration in relative fluorescence units (RFU) is provided by the instrument after subtracting the background fluorescence. To normalize the responses, the RFU for each compound and concentration were expressed as the percentage of the maximal RFU obtained among all concentrations tested of each compound.

4.3.5. Statistical analyses

All statistical analyses were performed with Prism 6.0 (GraphPad Software, La Jolla, CA). The normalized dose-response curves, the EC_{50} values and the Hill slope factors of dose-response curves were calculated with the function "log [agonist] vs. response – Variable slope (four parameters)". The EC_{50} of the agonist is the concentration that elicits 50% of the maximal response obtained in the normalized dose-response of each peptide. Two one-way ANOVAs were performed to compare EC_{50} values of: 1) the endogenous tick kinins and control analogs, and 2) the Aib-analogs and control analogs, in both cases followed by Tukey's multiple comparison tests (Suppl. Tables 1 and 2). Similarly, independent ANOVAs for the Hill slopes of dose-response curves of endogenous tick kinins and Aib-containing analogs were performed.

4.3.6. Multiple sequence alignment

To help visualize the sequence conservation of tick kinins across species in relationship to the herein determined potency of the Rhimi kinins, the kinin peptide precursor sequences of seven hard tick species were aligned (Xiong et al., 2019a). Sequences were aligned with MegaPro (DNASTAR, Lasergene v16.0) using the MAFFT(Katoh and Standley, 2013) program with the iterative refinement algorithm E-INS-I, because of the occurrence of known insertions

and deletions during the evolution of neuropeptide genes (Xiong et al., 2019a). The kinin conserved motifs are represented by Logos obtained with the default alignment settings of MegaPro. *R. microplus* kinins nomenclature in this publication follows the one suggested by Coast and Schooley (Coast and Schooley, 2011) using the first three letters of the genus and the first two letters of the species name, followed by arabic numerals to designate the order in which kinin appear in the kinin peptide precursor (Xiong et al., 2019a).

4.4. Results

Fourteen tick endogenous kinins synthesized according to our previous prediction (Xiong et al., 2019a) and six newly designed Aib-analogs based on these endogenous tick kinin sequences, and five others with specific characteristics were functionally characterized using cells expressing the tick kinin receptor. They were simultaneously tested with known potent agonists of kinin receptor, Aib-analogs IK-Aib-20 and 1728 (also known as IK-Aib-1) (Taneja-Bageshwar, Suparna et al., 2009) IK-Aib-20 was the most potent ligand identified on the tick kinin receptor before this study.(Xiong et al., 2019d) All tested tick kinins and their peptidomimetics showed full agonistic activities on the kinin receptor (Fig. 4.1), as no detectable agonistic activity was found on the vector only cells, as expected (data not shown). The maximal relative fluorescence units (RFUs) obtained for each compound among all tested concentrations (value that was used for normalizing the respective dose-response curves for each compound), were similar for all tested compounds (data not shown). Therefore, the comparison of their normalized response expressed as percentage of the maximal RFU obtained is valid as to conclude about their overall activity (Fig. 4.1), because they have similar maximal efficacy (Xiong et al., 2019d). The activities (EC_{50}s) of tick kinins and Aib-analogs, respectively, were analyzed by multiple comparison tests of significance (Table 4.1, Suppl. Table1 and 2).

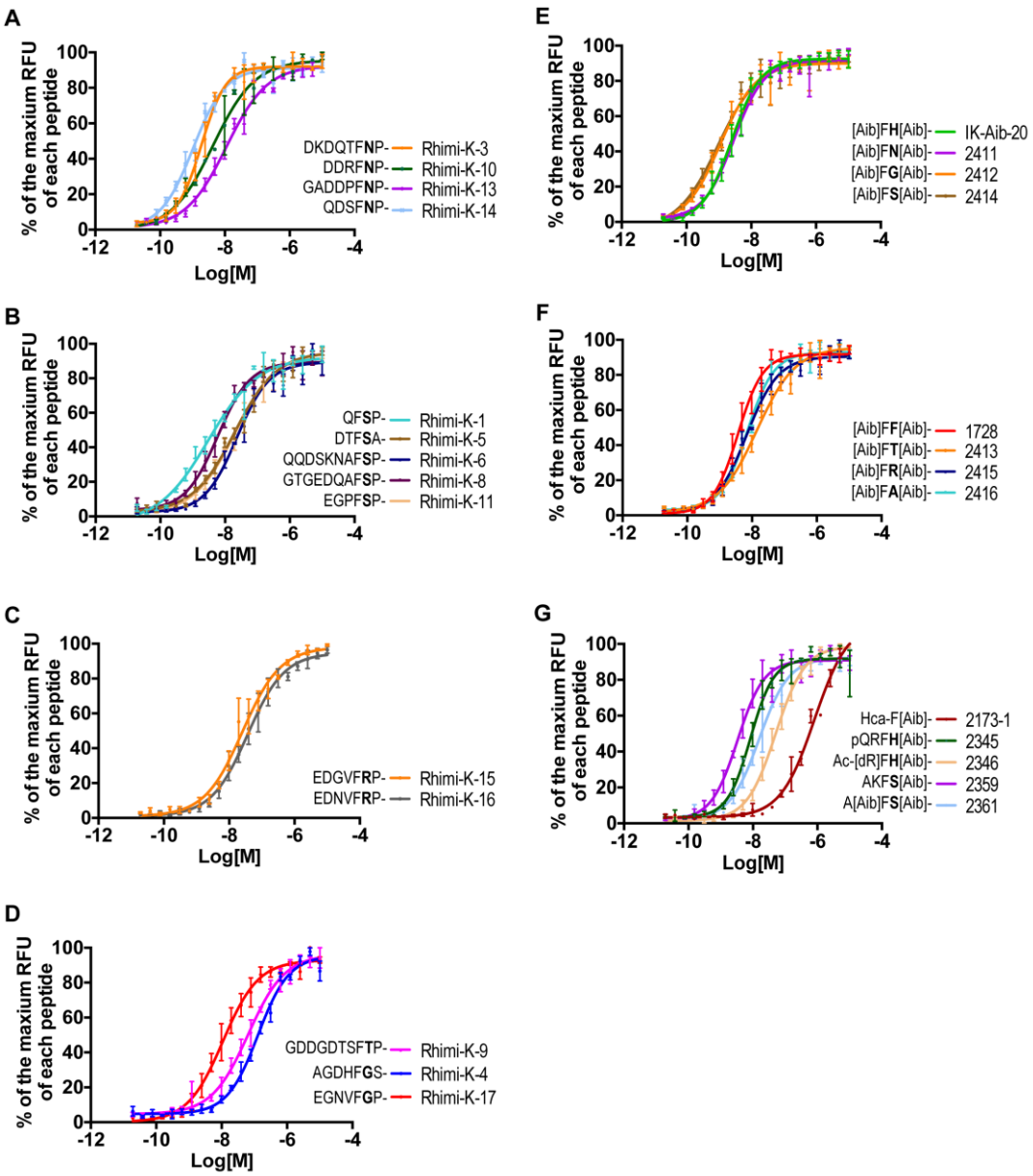

Figure 4.1 Dose-responses of the recombinant tick kinin receptor (BMLK3) to fourteen endogenous kinin ligands (A-D) and thirteen Aib-analogs (E-G).
Curves were obtained using an end-point calcium fluorescence assay. Twenty dosages were applied for each ligand, from 10 pM to 10 µM. The relative fluorescence units (RFU) elicited by each dosage were represented as percentage of the maximal RFU obtained among all concentrations tested for each ligand. Dose-response curves were generated with non-linear regression log(agonist) vs. response - variable slope (four parameters) function with GraphPad Prism 6.0 (GraphPad Software, La Jolla, CA). **A-D**. Each panel shows the group of endogenous kinins that share the same amino acid residue at the X^1 position of the kinin core (shown in bold). **E-F.** Each panel shows a group of "double-Aib-containing" analogs incorporating the native tick sequence at the X^1 position. **G**. The panel shows other Aib-analogs with modifications on the N-terminus. In all panel legends, the dash (-) in the sequences represents the C-terminal sequence "WGa", common to all kinins and analogs tested

Table 4.1 The EC_{50}s of endogenous tick kinins and Aib-analogs.

Names (ID)	Kinin Sequence	EC_{50} (nM)	95% confidence intervals of EC_{50} (nM)	Hill slope	Replicates
Rhimi-K-14	QDSF**N**PWGa	1.0[a]	0.8 to 1.4	0.87[abc]	3
Rhimi-K-3	DKDQTF**N**PWGa	1.9[a]	1.2 to 2.8	1.16[abc]	2
IK-Aib-20	[Aib]FH[Aib]WGa	2.5[a]	2.1 to 2.9	0.95[bc]	6
Rhimi-K-1	QF**S**PWGa	3.0[a]	1.8 to 5.1	0.56[a]	3
1728	[Aib]FF[Aib]WGa	3.7[a]	3.1 to 4.3	1.12[c]	6
Rhimi-K-10	DDRF**N**PWGa	4.3[a]	2.7 to 6.7	0.67[a]	2
Rhimi-K-8	GTGEDQAF**S**PWGa	5.9[a]	4.8 to 7.4	0.86[ab]	3
Rhimi-K-17	EGNVF**G**PWGa	11.0[a]	8.8 to 13.7	0.80[ab]	3
Rhimi-K-13	GADDPF**N**PWGa	11.2[a]	8.0 to 15.5	0.69[a]	3
Rhimi-K-5	DTF**S**AWGa	20.0[ab]	14.2 to 28.2	0.67[a]	3
Rhimi-K-11	EGPF**S**PWGa	20.4[ab]	15.5 to 26.9	0.67[a]	3
Rhimi-K-6	QQDSKNAF**S**PWGa	23.5[ab]	17.3 to 31.8	0.87[abc]	3
Rhimi-K-15	EDGVF**R**PWGa	25.4[ab]	19.0 to 33.9	0.75[ab]	3
Rhimi-K-16	EDNVF**R**PWGa	36.7[ab]	30.4 to 44.3	0.78[ab]	3
Rhimi-K-9	GDDGDTSF**T**PWGa	64.7[b]	52.2 to 80.1	0.78[ab]	3
Rhimi-K-4	AGDHF**G**SWGa	129.3[c]	100.9 to 165.8	0.92[abc]	3
2414	[Aib]F**S**[Aib]WGa	0.9[a]	0.6 to 1.4	0.94[ab]	3
2412	[Aib]F**G**[Aib]WGa	1.1[a]	0.8 to 1.6	0.79[a]	3
IK-Aib-20	[Aib]FH[Aib]WGa	2.5[a]	2.1 to 2.9	0.95[ab]	6
2411	[Aib]F**N**[Aib]WGa	2.9[a]	2.3 to 3.7	0.93[ab]	3
2359	AKFS[Aib]WGa	3.3[a]	2.5 to 4.5	1.06[ab]	3
1728	[Aib]FF[Aib]WGa	3.7[a]	3.1 to 4.3	1.12[b]	6
2415	[Aib]F**R**[Aib]WGa	6.8[a]	5.3 to 8.8	0.88[ab]	3
2416	[Aib]F**A**[Aib]WGa	7.1[a]	5.8 to 8.6	1.05[ab]	3
2345	pQRFH[Aib]WGa	8.8[a]	5.5 to 11.7	1.13[ab]	3
2413	[Aib]F**T**[Aib]WGa	14.2[a]	11.3 to 17.7	0.73[a]	3
2361	A[Aib]FS[Aib]WGa	15.7[a]	13.1 to 18.8	0.94[ab]	3
2346	Ac-[dR]FH[Aib]WGa	51.0[b]	42.7 to 60.7	0.96[ab]	3
2173-1	Hca-F[Aib]WGa	805[c]	525 to 1,173	0.83[ab]	2

Kinins and Aib-analogs are listed separately by their EC_{50s} from low to high. [a-c] Comparisons were done independently for endogenous kinins and analog groups, with both including the control analogs, 1728 and IK-Aib-20: notice six replicates for these two analogs. Different letters indicate statistically significant difference in the EC_{50s} or the Hill slopes ($p < 0.05$) between tick kinin pairs, or between the Aib-analog pairs, as detected in the Tukey's multiple comparison test.

4.4.1. Activity of endogenous kinins from *R. microplus* on the recombinant tick receptor

Twelve out of the fourteen endogenous kinins tested showed high potencies with EC_{50s} ranging from 1 nM to 37 nM (Table 4.1), which statistically did not differ from the potency of the "record-holding" positive control analog, IK-Aib-20 (EC_{50} = 1.7 nM) (Suppl. Table1). Rhimi-K-14 was the most potent (EC_{50} = 1 nM). Rhimi-K-9 (EC_{50} = 65 nM) had lower activity than seven of the twelve above mentioned endogenous kinins that had EC_{50}s between 1-11 nM (see Suppl. Table 4.1, black box). Rhimi-K-9 activity was significantly lower than that of Rhimi-K-14 and IK-Aib-20 (** p <0.01) and also lower than those of Rhimi-K-1, -3, -8, -10, -13, -17 and analog 1728 (* $p < 0.05$). The lowest activity was exhibited by Rhimi-K-4 (AGDHFGSWGa) (EC_{50} = 129 nM), significantly lower (**** $p < 0.0001$) than any other endogenous kinin. The remaining six kinins, Rhimi-K-5, -6, -9, -11, -15 and -16 had EC_{50}s ranging from 20-65 nM (Table 4.1 and Suppl. Table1) that were similar to Rhimi-K-9 but significantly lower than the EC_{50} of Rhimi-K-4.

In Fig. 4.1A-D, each panel shows the dose-response curves of endogenous kinins grouped by the specific amino acid residue present at their first variable position (X^1) of the C-terminal kinin core (either N, S, R or G/T, respectively; shown in bold in the legend). *R. microplus* kinins in panels A-C had similar EC_{50s} and were among the most potent, showing no preference for N, S, or R at the X^1 variable position (Table 4.1). Panel D shows that three kinins with either G or T at the X^1 variable position were significantly different in potency. Rhimi-K-17, one of the most potent kinins features G at this position, while the least potent kinin, Rhimi-K-4, also features a G at that position; however, Rhimi-K-4 has a positive charge represented by histidine towards the N-terminal region of the critical F at position 1 in the pentapeptide core. Rhimi-K-9, the second lowest in potency carries a T at the X^1 position.

The ANOVA for the Hill slope of the endogenous kinins dose-response curves determined that all of these slopes were similar to one another, and ranged in value from 0.56 (Rhimi-K-1) to 1.2 (Rhimi-K-3) (Table 4.1). Positive control analogs 1728 and IK-Aib-20 had higher slopes than most endogenous kinins except for those of Rhimi-K-3, Rhimi-K-4 (0.9), Rhimi-K-6 and Rhimi-K-14.

An alignment of tick kinin peptide precursors sequences from seven tick species together with the sequence and respective potencies of Rhimi-Ks is presented in Suppl. Fig. 4.1. The sequence of Rhimi-K-1, one of the most potent kinins, was conserved among all tick species analyzed. Sequence Logos also showed that the sequence of the most potent Rhimi-K-14 (EC_{50} = 1 nM) was also highly conserved, but only among the five Metastriata species (Suppl. Fig. 4.1).

4.4.2. Activity of tick Aib-analogs on the receptor

In addition to the "double-Aib-containing" analogs used as positive controls (1728 and IK-Aib-20), six "double-Aib-containing" analogs designed based on the endogenous *R. microplus* kinin sequences were tested (IDs 2411 to 2416, Fig. 4.1E, F). Further, of the other five Aib-analogs tested, three had modifications at the N-terminus (IDs 2173-1, 2345, 2346) (Fig. 4.1G). All Aib-analogs (including the two positive controls) acted as full agonists with maximal (raw) RFUs (not shown) similar to those of the endogenous kinins (ANOVA $p = 0.1$).

The multiple comparison test of EC_{50}s differentiated three groups of analogs (Suppl. Table 4.2). Except for analogs 2346 and 2173-1, the rest of the Aib-analogs showed similar potency as the positive control analogs (Table 4.1 and Suppl. Table 4.2). Nine of the eleven analogs were the most potent with EC_{50}s ranging from 1 nM to 16 nM (Table 4.1). These nine analogs were all significantly more potent than 2346 (EC_{50} = 51 nM) (** $p < 0.01$), the analog of intermediate potency. The lowest potency analog was 2173-1 (EC_{50} = 805 nM), significantly

different from the other ten tick kinin analogs and both positive controls (**** $p < 0.0001$). The six "double-Aib-containing" analogs (IDs 2411-2416) that were designed based on the *R. microplus* kinins (with the X^1 position featuring N, G, T, S, R, or A) had similar EC_{50}s to the "double-Aib-containing" control analogs (1728 and IK-Aib-20), ranging from 0.9 nM for 2414 to 14 nM for 2413 (Fig. 4.1E and F, Table1, and Suppl. Table 4.2). The Hill slope of the Aib-analogs varied from 0.73 (analog 2413) to 1.1 (analogs 1728, 2345, 2359, 2416). Among Aib-analogs, the Hill slope of analog 1728 was higher than those of analogs 2412 (G at position X^1) and 2413 (Table 4.1). The "double-Aib-containing" analog 2414 that is equipotent to the most active native peptide Rhimi-K-14 (Table 4.1) is noteworthy in that it contains the S residue of tick kinins at the X^1 variable position, and was experimentally shown to be resistant to peptidase degradation.(Nachman et al., 2002a)

Other modifications on the N-terminus to enhance the resistance to aminopeptidases such as pyroglutamate (pQ-) or acetyl (Ac-) resulted in analogs that retained kinin receptor activity (Fig. 4.1G, Table 4.1). Especially, analog 2345 with pQ-group, retained relatively high potency on the receptor, representing one of the most potent analogs (EC_{50} = 8.8 nM). Whereas analog 2173-1 (Hca-F[Aib]WGa) that featured a replacement of the aromatic, N-terminal F of the kinin pentapeptide with the aromatic, non-amino acid hydrocinnamic acid (Hca), exhibited a large drop in potency of several orders of magnitude.

4.5. Discussion

We focused on the tick kinin receptor (KR) as a model to explore a neuropeptide GPCR as a novel target for tick control (Pietrantonio, P.V. et al., 2018). Our previous reverse functional study demonstrated that female cattle fever ticks in which the KR was silenced exhibited significant reproductive fitness costs (Brock et al., 2019a), such as delay in feeding to

repletion, reduced weight of egg masses and decreased percentage of egg hatching. Therefore, fully inhibiting the function of the tick KR with antagonists could result in similar deleterious phenotypes, and those antagonists could represent "chemical leads" for novel tick control agents (Wu et al., 2017). In addition, the specific, endogenous agonists identified in this study will allow us to perform "unbiased" chemical screens for antagonists of the tick KR. Stable peptide agonists of the tick kinin receptor may also interfere with tick physiology and behavior and may serve as useful tools to discover novel functions of the kinin signaling system in ticks. For example, an Aib-containing kinin analog, "1728" (used as a positive control in this study), is a highly potent agonist of the *Aedes aegypti* KR that allowed us to discover a novel function of the kinin system in mosquitoes. This agonist, when fed in solution with sucrose, inhibited the activity of gustatory neurons in the mosquito peripheral sensory structures in labellum and tarsi and inhibited feeding (Kwon et al., 2016). When mixed with blood, the agonist 1728 is also antifeedant for the Chagas disease vector, *Rhodnius prolixus*, causing incomplete engorgement that results in failure to molt because the insect stretch receptors are not activated when the abdomen fails to fully distend (Lange et al., 2016). Similar kinin agonists showed antifeedant activity on the pea aphid, and CAPA analogs reduced their fitness under environmental stress (Alford et al., 2019b; Smagghe et al., 2010). The tick kinin analogs characterized here may also serve as useful tools to develop tissue-specific *in vitro* assays to help elucidate mechanisms of kinin action. Although direct applications of environmentally friendly peptidomimetics with high potency on animals and/or animal production premises are envisioned as alternative pest management tools to synthetic acaricides, important challenges remain for their utilization. For example, we must demonstrate their activity within a major group of arthropods pests (not single species-specific), decrease the cost of synthesis, and improve their cuticular penetration and

stability. Currently, no peptide GPCR is a target for pesticides. Many peptides are modulatory in the CNS and/or affect organ functions slowly and/or redundantly, and perhaps for this reason biological screens focusing on fast-acting, killing molecules have failed to identify GPCRs as promising targets. Achieving high lethality or quasi-lethality in arthropods (through starvation, paralysis, and desiccation) through such GPCR targets may be feasible but the challenge is achieving these effects at relatively low, cost-effective concentrations of mimetics or antagonists. We have begun addressing these challenges through the identification of the endogenous tick kinins and through the design of tick kinin mimetics with enhanced biostability and bioavailability.

Seventeen kinin peptide paracopies are predicted in the kinin peptide precursor from the cattle fever tick, *R. microplus* (GenBank QDO79406.1) (Xiong et al., 2019a). We had initially speculated that the high number of kinin paracopies (also predicted in seven other tick species analyzed) suggested a variation in their individual potency or physiological function, as shown for the three aedeskinins or kinin analogs on the *Ae. aegypti* kinin receptor, respectively (Pietrantonio, P.V. et al., 2005; Schepel et al., 2010). Alternatively, the high number of kinin copies in a single mRNA may efficiently generate high kinin concentration in the hemolymph and/or at synapses. To begin to explore kinin function in ticks, we synthesized and screened fourteen of the seventeen predicted kinins of the cattle fever tick. The results support the latter hypothesis as there are few differences in the potencies of the majority of the endogenous kinins tested. The three remaining predicted kinins (Xiong et al., 2019a), Rhimi-K-7, Rhimi-K-2 and Rhimi-K-12 were not synthesized or tested because there were predicted as longer than the rest of the fourteen *R. microplus* kinins (Xiong et al., 2019a), having from thirteen to thirty-one residues. Rhimi-K-7, the longest, was also predicted with less confidence than the fourteen

synthesized. Furthermore, long kinins are of limited interest in the development of biostable mimetic analogs, as they feature more peptidase-susceptible sites, which would require chemical stabilization and would lead to higher synthesis costs. Muscakinin (NTVVLG**KK**QRFHSWGa) from the house fly has fifteen residues, and despite featuring an internal KK sequence as a potential peptidase processing site, it is, nevertheless, more active in diuretic assays than the cleaved version (Holman et al., 1999; Holmes, S.P. et al., 2003) tested muscakinin on the *R. microplus* kinin receptor on the same BMLK3 cells we used here, and it exhibited significant activity with EC_{50} of 17 nM in a sensitive calcium fluorescence assay (the core pentamer FFSWGa had an EC_{50}s of 8.4 nM in the same assay). Therefore, the potential for high activity of the longer endogenous *R. microplus* kinins cannot be discounted.

Our results of the receptor functional analyses of the fourteen synthesized tick kinins indicated that there was little difference in their activities on the kinin receptor. All of the kinins acted as full agonists on the *R. microplus* kinin receptor. Among them, twelve out of fourteen kinins showed no difference in their EC_{50}s (Table 4.1). It is worth noting that Rhimi-K-1 being the shortest tick kinin, a pentapeptide, acted as one of the most potent ligands on the tick kinin receptor with EC_{50} = 3 nM. The sequence alignment of tick kinin precursors allows inferences about the potential rank of activity of kinins in other species, i.e. the first predicted kinin sequence in all tick kinin precursors including *R. microplus* (Rhimi-K-1= EC_{50} 3 nM) is the shortest kinin and is absolutely conserved, and similarly may be highly potent in all species. The finding that a pentamer native kinin core is among the most active in a tick, contrasts with activities in dipteran insects, where longer kinins are most active in the mosquito and house fly kinins.(Holman et al., 1999; Pietrantonio, P.V. et al., 2005)

The C-terminal penta-core motif of *R. microplus* tick kinins shows that the first variable position (X^1) could be occupied by residues S, N, A (Rhimi-K-7; not tested), G, T or R.(Xiong et al., 2019a) In tick kinins, N is common at position X^1, being present in the species considered basal, the soft tick *Ornithodorus turicata* (Xiong et al., 2019a) (Suppl. Fig. 4.1). In *R. microplus,* five out of the seventeen kinins (Rhimi-K-3, -10, and -12 to -14) retain N at this position, with *R. microplus* kinins being the most variable in amino acid residues in the X^1 position among the tick species previously analyzed (Xiong et al., 2019a). All tested kinins with N at this position retained high activity. Our functional screen results showed that despite this variation, all Rhimi-Ks have activity at the low nanomolar level except for Rhimi-K-4, AGDHF**GS**WGa (featuring G at position X^1 and S at position X^2). Rhimi-K-4 had the lowest activity among the fourteen kinins tested. It is notable that G is not common in insect kinins at the X^1 position, and it is only present in the Protura,(Derst et al., 2016; Yeoh et al., 2017) which are basal arthropod hexapods. Furthermore, our results on the activity of the designed Aib-analogs confirmed that the X^1 position is indeed very tolerant of variation, from hydrophobic to hydrophilic, and from aromatic to non-aromatic residues (N, G, T, S, A or R present in tick kinins, or F and H present in insect kinins) (Table 4.1). No statistical difference was detected between the EC_{50}s of any of the "double-Aib-containing" analogs ([Aib]FX^1[Aib]WGa) that differed only in the X^1 position. This includes the highly potent analog 2412 (EC_{50}= 1.1 nM) that included G at the X^1 position: [Aib]F**G**[Aib]WGa (Table 4.1). Therefore, the low activity of Rhimi-K-4 cannot be uniquely attributed to the presence of G because the context towards the N-terminus of the pentapeptide core in which residues appear in the native sequences or analogs affect their potency at the receptor. Further, the potent Rhimi-K-17 (EC_{50} = 11 nM) features G at that position but followed by P, which is predominant in the *R. microplus* kinins and in kinins of other tick species.(Xiong

et al., 2019a) It appears that S at position X^2 is less favored than P or A at the same position. We previously showed that the pentamer FFSWGa is significantly less potent than FFAWGa on the same kinin receptor and cell line, with EC_{50}s of 590 nM and 64 nM, respectively. The activity of the native tick kinins also showed that Rhimi-K-5 DTFS**A**WGa (EC_{50}= 20 nM) is more potent than Rhimi-K-4 AGDHFG**S**WGa. However, Rhimi-K-4 (AGD**H**FG**S**WGa) also features a weakly basic, positively charged, and aromatic residue, H (-1 position), towards the N-terminal region of the critical F at position -1 in the pentapeptide core. Another kinin with a strongly basic positively charged residue, R, at the -1 position of the C-terminal penta-core but retaining high potency is Rhimi-K-3 (DD**R**FNPWGa).

Rhimi-K-5 is unusual in that features an alanine residue in the X^2 variable position; this also occurs only in eighteen kinins in few insect orders (lepidopterans, hemipterans, dipterans) out of two hundred and ninety-nine kinin isoforms listed in the DINeR database(Yeoh et al., 2017). Rhimi-K-5 is however equipotent to the most potent kinins.

With respect to the structure of mature Rhimi kinins featuring Gln at the N-terminus, while it is possible that they may cyclize to pGlu, it is clear, based on our structural confirmation through mass spectrometry analyses, that the synthesized peptides retain the uncyclized form of Gln at the N-terminus.

Among analogs containing two-Aib molecules which incorporated the insect kinin residues at the X^1 position H, Y or F, the analog with the aromatic and positively charged H was more active over those with aromatic Y or F (Xiong et al., 2019d). This higher activity explains why the IK-Aib-20 featuring H at the X^1 position was considered the most potent until this study. The endogenous Rhimi-K-15 and -16 have R at the X^1 position, supporting the preference for H observed before. One of the "double-Aib-containing" analogs, ID 2415, is worth highlighting

because it was among the most potent analogs. Analog 2415 contains a Rhimi-K residue (R) at 'X^1 position' and this strongly basic, positively charged, R residue will confer greater aqueous solubility (i.e., 'hemolymph' solubility). The amphiphilic character of this analog enables surfactant properties that can enhance its topical activity. Two analogs containing one Aib molecule with two different modifications at the N-terminus exhibit high and low activity, respectively. Analog ID 2345 (EC_{50} = 8.8 nM), could be of interest due to its potentially greater aqueous solubility because it features the strongly basic R side-chain placed on the N-terminus. Analog 2173-1 (EC_{50} = 805 nM) featured a hydrocinnamic acid (Hca) group, which is equivalent to F lacking the N-terminal amino group. This modification has been shown to lead to activity retention by various degrees in insect kinin analogs demonstrated in the cockroach hindgut myotropic,(Nachman and Holman, 1991a) cricket diuretic(Nachman et al., 2012) and aphid antifeedant insect bioassays.(Zhang et al., 2015) However, lower activity of the analog with this major modification was observed for the tick receptor, as it correlated with a drop in potency of several orders of magnitude.

4.6. Conclusion

The previously identified critical residues for activity of kinins in arthropods are present in the tick kinins C-terminal penta-core **F**X^1X^2**W**G**a** (bold residues). All fourteen tested tick kinins were active, and twelve had similar high activity on the tick kinin receptor. This is despite their diverse sequences, with no two kinins being identical in the kinin peptide precursor. In addition, this study confirmed the high potency of eight "double-Aib-containing" analogs ([Aib]FX^1[Aib]WGa) with enhanced biostability, and demonstrated that the tick kinin receptor can tolerate a variety of amino acid residues on the X^1 position, from hydrophilic to hydrophobic, and from aromatic to non-aromatic. Noteworthy were the biostability-enhanced

analogs 2414 ([Aib]F**S**[Aib]WGa and 2412 ([Aib]F**G**[Aib]WGa), which EC_{50s} matched the EC_{50} (1 nM) of the most potent native tick kinin (Rhimi-K-14). Aib-analog 2415 ([Aib]F**R**[Aib]WGa) also retained strong activity, and it would be expected to demonstrate improved aqueous solubility and amphiphilic character, properties important for tick topical activity. These Aib-analogs expand the tools for tick endocrinology. These potent endogenous tick kinins identified in this study will in the near future facilitate unbiased high-throughput screens in the search for novel synthetic antagonists of the kinin receptor.

4.7. Acknowledgements

Funding for this project is from NIFA-AFRI Animal Health and Well-Being Award 2016-67015-24918 to P.V. Pietrantonio and K. Temeyer, and from competitive funds from the Texas A&M AgriLife Research Insect Vector Diseases Grant Program (FY19-21) to PVP. NIFA also supports PVP program through Hatch project TX (TEX0-2-9206), accession 1002279 (Y 2018-2023). RJN received support from the US Department of Agriculture/Department of Defense Deployed War Fighter Protection Initiative 6202-22000-029-00D. The authors thank the A.W.E.S.O.M.E. faculty group in the College of Agriculture and Life Sciences at Texas A&M University for help editing the manuscript. We thank Professor J. C. Sacchettini (TAMU) for the use of facilities for high-throughput screening. Two anonymous reviewers provided insightful comments that improved the manuscript. C.X. is a Ph.D. candidate in the Entomology graduate program at TAMU.

4.8. References

Alford, L., Marley, R., Dornan, A., Pierre, J.S., Dow, J.A., Nachman, R.J., Davies, S.A., 2019. Assessment of neuropeptide binding sites and the impact of biostable kinin and CAP2b

analogue treatment on aphid (*Myzus persicae* and *Macrosiphum rosae*) stress tolerance. Pest Manag. Sci.

Brock, C.M., Temeyer, K.B., Tidwell, J., Yang, Y., Blandon, M.A., Carreón-Camacho, D., Longnecker, M.T., Almazán, C., de León, A.A.P., Pietrantonio, P.V., 2019. The leucokinin-like peptide receptor from the cattle fever tick, *Rhipicephalus microplus*, is localized in the midgut periphery and receptor silencing with validated double-stranded RNAs causes a reproductive fitness cost. Int. J. Parasitol. 49(3-4), 287-299.

Coast, G., 2007. The endocrine control of salt balance in insects. Gen. Comp. Endocrinol. 152(2-3), 332-338.

Coast, G.M., Holman, G.M., Nachman, R.J., 1990. The diuretic activity of a series of cephalomyotropic neuropeptides, the achetakinins, on isolated Malpighian tubules of the house cricket, *Acheta domesticus*. J. Insect. Physiol. 36(7), 481-488.

Coast, G.M., Orchard, I., Phillips, J.E., Schooley, D.A., 2002. Insect diuretic and antidiuretic hormones. Adv. Insect Physiol. 29(1), 279-409.

Coast, G.M., Schooley, D.A., 2011. Toward a consensus nomenclature for insect neuropeptides and peptide hormones. Peptides 32(3), 620-631.

Cornell, M.J., Williams, T.A., Lamango, N.S., Coates, D., Corvol, P., Soubrier, F., Hoheisel, J., Lehrach, H., Isaac, R.E., 1995. Cloning and expression of an evolutionary conserved single-domain angiotensin converting enzyme from *Drosophila melanogaster*. J. Biol. Chem. 270(23), 13613-13619.

De Loof, A., 2008. Ecdysteroids, juvenile hormone and insect neuropeptides: recent successes and remaining major challenges. Gen. Comp. Endocrinol. 155(1), 3-13.

Derst, C., Dircksen, H., Meusemann, K., Zhou, X., Liu, S., Predel, R., 2016. Evolution of neuropeptides in non-pterygote hexapods. BMC Evol. Biol. 16(1), 51.

Gäde, G., 2004. Regulation of intermediary metabolism and water balance of insects by neuropeptides. Annu. Rev. Entomol. 49(1), 93-113.

Gäde, G., Goldsworthy, G.J., 2003. Insect peptide hormones: a selective review of their physiology and potential application for pest control. Pest Manag. Sci. 59(10), 1063-1075.

Guerrero, F.D., Lovis, L., Martins, J.R., 2012. Acaricide resistance mechanisms in *Rhipicephalus (Boophilus) microplus*. Rev. Bras. Parasitol. V. 21(1), 1-6.

Harshini, S., Manchu, V., Sunitha, V., Sreekumar, S., Nachman, R., 2003. In vitro release of amylase by culekinins in two insects: *Opsinia arenosella* (Lepidoptera) and *Rhynchophorus ferrugineus* (Coleoptera). Trends in Life Sciences 17, 61-64.

Holman, G., Cook, B., Nachman, R., 1986. Isolation, primary structure and synthesis of two neuropeptides from *Leucophaea maderae*: members of a new family of cephalomyotropins. Comp. Biochem. Phys. C. 84(2), 205-211.

Holman, G.M., Nachman, R., Wright, M., 1990. Insect neuropeptides. Annu. Rev. Entomol. 35(1), 201-217.

Holman, G.M., Nachman, R.J., Coast, G.M., 1999. Isolation, characterization and biological activity of a diuretic myokinin neuropeptide from the housefly, *Musca domestica*. Peptides 20(1), 1-10.

Holmes, S.P., Barhoumi, R., Nachman, R.J., Pietrantonio, P.V., 2003. Functional analysis of a G protein- coupled receptor from the Southern cattle tick *Boophilus microplus* (Acari:

Ixodidae) identifies it as the first arthropod myokinin receptor. Insect Mol. Biol. 12(1), 27-38.

Holmes, S.P., He, H., Chen, A.C., Ivie, G.W., Pietrantonio, P.V., 2000. Cloning and transcriptional expression of a leucokinin- like peptide receptor from the Southern cattle tick, *Boophilus microplus* (Acari: Ixodidae). Insect Mol. Biol. 9(5), 457-465.

Katoh, K., Standley, D.M., 2013. MAFFT multiple sequence alignment software version 7: improvements in performance and usability. Mol. Bio. Evol. 30(4), 772-780.

Kersch, C.N., Pietrantonio, P.V., 2011. Mosquito *Aedes aegypti* (L.) leucokinin receptor is critical for in vivo fluid excretion post blood feeding. FEBS Lett. 585(22), 3507-3512.

Kim, D.-H., Kim, Y.-J., Adams, M.E., 2018. Endocrine regulation of airway clearance in *Drosophila*. Proc. Natl. Acad. Sci., 201717257.

Kwon, H., Agha, M.A., Smith, R.C., Nachman, R.J., Marion-Poll, F., Pietrantonio, P.V., 2016. Leucokinin mimetic elicits aversive behavior in mosquito *Aedes aegypti* (L.) and inhibits the sugar taste neuron. Proc. Natl. Acad. Sci. 113(25), 6880-6885.

Lamango, N.S., Sajid, M., Isaac, R.E., 1996. The endopeptidase activity and the activation by Cl- of angiotensin-converting enzyme is evolutionarily conserved: purification and properties of an an angiotensin-converting enzyme from the housefly, *Musca domestica*. Biochem. J. 314(Pt 2), 639.

Lange, A.B., Nachman, R.J., Kaczmarek, K., Zabrocki, J., 2016. Biostable insect kinin analogs reduce blood meal and disrupt ecdysis in the blood-gorging Chagas' disease vector, *Rhodnius prolixus*. Peptides 80, 108-113.

Lu, H.L., Kersch, C., Pietrantonio, P.V., 2011a. The kinin receptor is expressed in the Malpighian tubule stellate cells in the mosquito *Aedes aegypti* (L.): A new model needed to explain ion transport? Insect Biochem. Molec. 41(2), 135-140.

Lu, H.L., Kersch, C.N., Taneja-Bageshwar, S., Pietrantonio, P.V., 2011b. A calcium bioluminescence assay for functional analysis of mosquito (*Aedes aegypti*) and tick (*Rhipicephalus microplus*) G protein-coupled receptors. Jove-J Vis Exp(50).

Nachman, R.J., Coast, G.M., Douat, C., Fehrentz, J.-A., Kaczmarek, K., Zabrocki, J., Pryor, N.W., Martinez, J., 2003. A C-terminal aldehyde insect kinin analog enhances inhibition of weight gain and induces significant mortality in *Helicoverpa zea* larvae. Peptides 24(10), 1615-1621.

Nachman, R.J., Coast, G.M., Holman, G.M., Beier, R.C., 1995. Diuretic activity of C-terminal group analogues of the insect kinins in *Acheta domesticus*. Peptides 16(5), 809-813.

Nachman, R.J., Holman, G.M., 1991. Myotropic Insect Neuropeptide Families from the Cockroach *Leucophaea maderae*: Structure-Activity Relationships, in: Menn, J.J., Masler, Edward P. (Ed.) Insect neuropeptides: chemistry, biology, and action. American Chemical Society, Washington, D.C., pp. 194-214.

Nachman, R.J., Isaac, R.E., Coast, G.M., Holman, G.M., 1997a. Aib-Containing Analogues of the Insect Kinin Neuropeptide Family Demonstrate Resistance to an Insect Angiotensin-Converting Enzyme and Potent Diuretic Activity. Peptides 18(1), 53-57.

Nachman, R.J., Isaac, R.E., Coast, G.M., Roberts, V.A., Lange, A.B., Orchard, I., Holman, G.M., Teal, P.E., 1997b. Active conformation and mimetic analog development for the Pyrokinin-PBAN-Diapause-Pupariation and Myosuppressin insect neuropeptide families, in: Hedin, P.A., Hollingworth, R.M., Masler, E.P., Miyamoto, J., Thompson, D.G. (Eds.),

Phytochemicals for Pest Control. American Chemical Society, Washington, DC, pp. 277-291.

Nachman, R.J., Kaczmarek, K., Williams, H.J., Coast, G.M., Zabrocki, J., 2004. An active insect kinin analog with 4- aminopyroglutamate, a novel cis- peptide bond, type VI β- turn motif. Biopolymers: Original Research on Biomolecules 75(5), 412-419.

Nachman, R.J., Kaczmarek, K., Zabrocki, J., Coast, G.M., 2012. Active diuretic peptidomimetic insect kinin analogs that contain β-turn mimetic motif 4-aminopyroglutamate and lack native peptide bonds. Peptides 34(1), 262-265.

Nachman, R.J., Strey, A., Isaac, E., Pryor, N., Lopez, J.D., Deng, J.-G., Coast, G.M., 2002. Enhanced in vivo activity of peptidase-resistant analogs of the insect kinin neuropeptide family. Peptides 23(4), 735-745.

Nachman, R.J., Tilley, J.W., Hayes, T.K., Holman, G.M., Beier, R.C., 1994. Pseudopeptide mimetic analogs of insect neuropeptides, in: Hedin, P., Menn, J.J., Hollingworth, R.M. (Eds.), Natural and Engineered Pest Management Agents. American Chemical Society, Washington DC, pp. 210-229.

Nässel, D.R., 2002. Neuropeptides in the nervous system of *Drosophila* and other insects: multiple roles as neuromodulators and neurohormones. Prog. Neurobiol. 68(1), 1-84.

Pérez de León, A.A., Teel, P.D., Auclair, A.N., Messenger, M.T., Guerrero, F.D., Schuster, G., Miller, R.J., 2012. Integrated strategy for sustainable cattle fever tick eradication in USA is required to mitigate the impact of global change. Front. Physiol. 3, 195.

Pietrantonio, P.V., Jagge, C., Taneja-Bageshwar, S., Nachman, R.J., Barhoumi, R., 2005. The mosquito *Aedes aegypti* (L.) leucokinin receptor is a multiligand receptor for the three Aedes kinins. Insect Mol. Biol. 14(1), 55-67.

Pietrantonio, P.V., Xiong, C., Nachman, R.J., Shen, Y., 2018. G protein-coupled receptors in arthropod vectors: Omics and pharmacological approaches to elucidate ligand-receptor interactions and novel organismal functions. Curr. Opin. Insect Sci. 29, 12-20.

Pohl, P.C., Klafke, G.M., Júnior, J.R., Martins, J.R., da Silva Vaz, I., Masuda, A., 2012. ABC transporters as a multidrug detoxification mechanism in *Rhipicephalus (Boophilus) microplus*. Parasitol. Res. 111(6), 2345-2351.

Roberts, V.A., Nachman, R.J., Coast, G.M., Hariharan, M., Chung, J.S., Holman, G.M., Williams, H., Tainer, J.A., 1997. Consensus chemistry and R-turn conformation of the active core of the insect kinin neuropeptide family. Chem. Biol. 4(2), 105-117.

Schepel, S.A., Fox, A.J., Miyauchi, J.T., Sou, T., Yang, J.D., Lau, K., Blum, A.W., Nicholson, L.K., Tiburcy, F., Nachman, R.J., 2010. The single kinin receptor signals to separate and independent physiological pathways in Malpighian tubules of the yellow fever mosquito. Am. J. Physiol-Reg I 299(2), R612-R622.

Seinsche, A., Dyker, H., Lösel, P., Backhaus, D., Scherkenbeck, J., 2000. Effect of helicokinins and ACE inhibitors on water balance and development of *Heliothis virescens* larvae. J. Insect. Physiol. 46(11), 1423-1431.

Smagghe, G., Mahdian, K., Zubrzak, P., Nachman, R.J., 2010. Antifeedant activity and high mortality in the pea aphid *Acyrthosiphon pisum* (Hemiptera: Aphidae) induced by biostable insect kinin analogs. Peptides 31(3), 498-505.

Taneja-Bageshwar, S., Strey, A., Isaac, R.E., Coast, G.M., Zubrzak, P., Pietrantonio, P.V., Nachman, R.J., 2009. Biostable agonists that match or exceed activity of native insect kinins on recombinant arthropod GPCRs. Gen. Comp. Endocrinol. 162(1), 122-128.

Taneja- Bageshwar, S., Strey, A., Zubrzak, P., Pietrantonio, P.V., Nachman, R.J., 2006. Comparative structure- activity analysis of insect kinin core analogs on recombinant kinin receptors from Southern cattle tick *Boophilus microplus* (Acari: Ixodidae) and mosquito *Aedes aegypti* (Diptera: Culicidae). Arch. Insect Biochem. 62(3), 128-140.

Torfs, P., Nieto, J., Veelaert, D., Boon, D., Water, G., Waelkens, E., Derua, R., Calderon, J., Loof, A., Schoofs, L., 1999. The kinin peptide family in invertebrates. Ann. NY. Acad. Sci. 897(1), 361-373.

Wu, F., Song, G., de Graaf, C., Stevens, R.C., 2017. Structure and Function of Peptide-Binding G Protein-Coupled Receptors. J. Mol. Biol. 429(17), 2726-2745.

Xiong, C., Baker, D., Pietrantonio, P.V., 2019a. The cattle fever tick, *Rhipicephalus microplus*, as a model for forward pharmacology to elucidate kinin GPCR function in the Acari. Front. Physiol. 10, 1008.

Xiong, C., Kaczmarek, K., Zabrocki, J., Pietrantonio, P.V., Nachman, R.J., 2019b. Evaluation of Aib and PEG-polymer insect kinin analogs on mosquito and tick GPCRs identifies potent new pest management tools with potentially enhanced biostability and bioavailability. Gen. Comp. Endocrinol. 278(1 July 2019), 58-67.

Yeoh, J.G.C., Pandit, A.A., Zandawala, M., Nässel, D.R., Davies, S.-A., Dow, J.A.T., 2017. DINeR: Database for Insect Neuropeptide Research. Insect Biochem. Molec. 86, 9-19.

Zhang, C., Qu, Y., Wu, X., Song, D., Ling, Y., Yang, X., 2015. Design, synthesis and aphicidal activity of N-terminal modified insect kinin analogs. Peptides 68, 233-238.

5. A RANDOM SMALL MOLECULE LIBRARY SCREEN IDENTIFIES NOVEL ANTAGONISTS OF THE KININ RECEPTOR FROM THE CATTLE FEVER TICK, RHIPICEPHALUS MICROPLUS (ACARI: IXODIDAE)

5.1. Overview

BACKGROUND: The southern cattle tick, *Rhipicephalus microplus*, is a primary vector transmitting the deadly bovine babesiosis in tropical and subtropical regions worldwide. Arthropod-specific G protein-coupled receptors (GPCRs) are considered to be promising targets for novel pesticide development. The *R. microplus* kinin receptor is one of such targets, previously validated by silencing, which resulted in female reproductive fitness cost, including a reduced percentage of eggs hatching. RESULTS: To identify potent small molecules that bind and activate or inhibit the kinin receptor, a high-throughput screening (HTS) assay was developed using a CHO-K1 cell line expressing the recombinant tick kinin receptor ($BMLK_3$). A total of ~20,000 molecules from a random in-house small molecule library were screened in a 'dual-addition' calcium fluorescence assay. This was followed by dose-response validation of the hit molecules identified both from HTS and an *in silico* screen of ~390,000 molecules. We validated 29 antagonists, 11 of them were full antagonists with IC_{50} values lower than 10 μM. To explore the structure-activity relationships (SAR) of the small molecules, we tested the activities of 7 analogs of the most potent identified antagonists, additionally discovering three full antagonists and four partial antagonists. These three potent antagonists (IC_{50} < 3.2 μM) were validated on the recombinant mosquito kinin receptor *in vitro* showed similar antagonistic activities. *In vivo*, these three compounds also inhibited the mosquito hindgut contraction rate induced by a myotropic kinin peptidomimetic 1728. CONCLUSION: Antagonists identified in this study could become pesticide leads and are reagents for probing the kinin signaling system.

5.2. Introduction

The cattle fever tick (CFT), *Rhipicephalus microplus*, is one of the most important livestock pests Jongejan and Uilenberg (2004). It is the primary vector of the deadly disease agents *Babesia spp. and Anaplasma spp.*(Bock, 2008). Despite being eradicated from the U.S. since 1943, this tick species is well established in other tropical and subtropical countries and causes enormous economic losses to the local cattle industry (Angus, 1996; Madder et al., 2011; Rodríguez-Vivas et al., 2017). Recent observations of this tick in Texas since 2017, miles beyond the maintained quarantine zone, are now a threat to the US cattle industry (Thomas et al., 2020). Further, disease prevention relies heavily on tick control and due to the increasing acaricide resistance detected worldwide (Rodriguez-Vivas et al., 2018), there is an urgent need for novel targets for acaricide development. The G protein-coupled receptors (GPCRs) are the largest family of transmembrane protein in metazoans. They transduce diverse extracellular signals including light, protons, hormones, neuropeptide, glutamate, and lipoglycoproteins (Hilger et al., 2018). GPCRs are druggable targets as more than 30% of human drugs bind to these receptor superfamily (Hauser et al., 2017). The success of amitraz as an acaricide acting on the arthropod octopamine receptor provides the proof of principle for GPCRs as suitable targets for tick control (Kita et al., 2017). Similarly, GPCRs for small neuropeptides could be utilized for pest control by finding small molecules with agonist or antagonist activity (Audsley and Down, 2015; Pietrantonio, P.V. et al., 2018).

Insect kinins are such candidate small molecules that were initially identified for their myotropic activity in the cockroach hindgut (Holman et al., 1986), and then proved to be pleiotropic. Kinins regulate diuresis (Kersch and Pietrantonio, 2011), gut enzyme release (Harshini et al., 2003), modulate sugar taste perception in contact chemosensory neurons in

Aedes aegypti (Kwon et al., 2016), and tracheal clearance and air filling prior to ecdysis in *Drosophila* (Kim, D.-H. et al., 2018b), The exact physiological functions of the kinin system in ticks remain unknown. In a recent study, silencing of the tick kinin receptor in *R. microplus* females significantly decreased reproductive fitness, lowered the percentage of egg hatching, and, interestingly, discolored the midguts, which is presumedly linked to interference with heme uptake (Brock et al., 2019a). Our previous study predicted 17 tick kinins from the *R. microplus* kinin precursor peptide (Xiong et al., 2019a); 14 of the shorter kinins were synthesized and tested on the recombinant tick kinin receptor, and all were agonists (Xiong et al., 2019b). However, peptides are expensive for mass-production and susceptible to enzymatic degradation (Taneja-Bageshwar, Suparna et al., 2009). Therefore, the overall goal of this study was to identify small molecules as surrogates of peptide agonists and antagonists (blockers) of the tick kinin receptor to interfere with the function of the kinin signaling system. Antagonists of the tick kinin receptor are hypothesized as useful tools to mimic the detrimental reproductive effects obtained by its silencing (Brock et al., 2019a).

To identify ligands of a GPCR, monitoring the titer of the second messenger upon activation is among the most widely used methodology (Thomsen et al., 2005). The tick kinin receptor couples to $G\alpha_{q/11}$ protein (Holmes, S.P. et al., 2003), therefore, a fluorescence intracellular calcium mobilization assay was developed with the tick kinin receptor stably expressed in a CHO-K1 cell line (Xiong et al., 2019b). Here the fluorescence assay in 384-well plate format was utilized to screen a small molecule library in high-throughput mode, and consisted of a "dual-addition" for antagonist identification (Xiong et al., 2019a). High-throughput screening (HTS) of a target GPCR is a common method to discover new drugs (Thomsen et al., 2005). Chemical library selection for HTS on a tick neuropeptide GPCR is

problematic due to the great evolutionary differences between invertebrates and humans. Screening of drugs that are active on the most similar human receptors often yields low activity in the arthropod receptor counterpart, as we found previously by screening an antagonist library of the human neurokinin receptors on the tick kinin receptor, as they are not orthologues (Xiong et al., 2019a).

Here, we utilized a random screening approach to discover novel ligands of the kinin receptor in HTS mode, yielding excellent Z'-values, and applying a stringent threshold for hit selection. The screening of a random small molecule library yielded the identification of novel tick kinin receptor antagonists. We complemented this approach with successful structural-based *in silico* searches of larger libraries of small molecules. A hindgut assay further confirmed the antagonistic effect of three small molecules, SACC-0412060, SACC-04122062 and SACC-0412066, as they inhibited the increased rate of muscle contraction elicited by the potent kinin mimetic 1728.

5.3. Materials and Methods

5.3.1. Preparation of the small molecule library in "drug plates"

Small molecules utilized for this study were part of a Texas AgriLife Research compound library in the laboratory of Professor James Sacchettini, designated the SAC-2 library. This library is composed of randomly selected small molecules with diverse chemical structures. The molecules in stock plates were prepared in 100% dimethyl sulfoxide (DMSO) at approximately 1 mM in 384-well plates and stored at -20°C. Compound plates for screens (hereafter drug plates) were prepared from the stock plates at 1:10 dilution in 384-well plates (Corning® 3680, Corning, NY) by transferring 3 µl of the stock plate solution into each well containing 27 µl DPBS

(Corning®; 21-031-CV) for a 100 µM final compound concentration in 10% DMSO in DPBS. These plates were stored at 4°C before use and are referred to as "drug plates".

5.3.2. Cell culture

The target receptor, *R. microplus* kinin receptor, is stably expressed in the recombinant CHO-K1 cell line referring as $BMLK_3$, which was constructed and selected as described in Holmes et al., 2003.(Holmes, S.P. et al., 2003) Cells only transfected with empty plasmid as control are referred to as "vector only". $BMLK_3$ or "vector-only" cells were cultured in T-75 flasks with selective medium (F-12K medium containing 10% FBS and 800 µg/ml of G418 sulfate) for one to two passages before the experiment. All cells were incubated overnight at 37°C, and 5% CO_2 in a humidified incubator.

5.3.3. Kinin receptor functional calcium fluorescence assay

An intracellular calcium fluorescence assay was conducted as before (Xiong et al., 2019b). Briefly, when the cells reached about 90% confluency (Lu et al., 2011d) they were trypsinized and suspended in F-12K medium containing 1% FBS and 400 µg/ml of G418 sulfate at 4×10^5 cells/ml to be seeded in 384-well plates with black walls and clear bottom (Greiner®, 781091), coated with Poly-D-lysine (Sigma-Aldrich, St. Louis, MO). The cell suspension (25 µl; ~10,000 cells/well) was dispensed into each of the 384 wells of the plate. Unless specified, the pipetting steps for the 384-well plate fluorescence assay were performed by an Integra Viaflo® system equipped with 384-pipetting head (384/12.5 µl) (Integra Bioscience, Hudson, NH) or a CyBio® Well Vario System (384/60) (Analytik Jena AG); both allowed simultaneous addition of liquid into the 384-well plate. The plates were incubated overnight at 37°C and 5% CO_2 in an incubator. On the second day, the loading dye (1X) was prepared by diluting FLUOFORTE® (Enzo Life Sciences, E Farmingdale, NY) dye into the assay buffer (1:1,000), according to the

manufacturer's instructions. The assay buffer consists of 1X HHBS (Hank's buffer saline with 20mM HEPES) and dye efflux inhibitor (9:1). The old media in the 384-well plate was disposed of by inverting the plate on tissue paper, and it was replaced by 25 µl of loading dye (1X). The plate was then incubated at 37°C for 30 min, and equilibrated at RT for another 30 min before the cells were ready for high-throughput screening (HTS).

5.3.4. High-throughput Screening (HTS)

The "dual-addition" assay we developed here allows identification of agonist or antagonist in the same assay in a high-throughput mode (Xiong et al., 2019a). The theory of the "dual-addition" assay is reviewed elsewhere (Ma et al., 2017). In brief, the first addition of the test compound into the cell plate allowed identification of potential agonists when a higher fluorescence signal was detected compared to the solvent control. The 2nd addition of agonist kinin peptide was applied after the cells were incubated with the test molecule for 5 min. This allowed the identification of potential antagonists when a lower fluorescence signal was detected compared to the control (solvent + agonist kinin peptide).

Before beginning the HTS, each plate containing cells and 25 µl of the assay buffer per well was read to obtain an endpoint fluorescence value (Relative Fluorescence Units; RFU) as background signal. For HTS, 0.5 µl of the compounds in drug plates were dispensed into cell assay plates to reach a final concentration of 2 µM in 0.2% DMSO. Secondly, the addition of 500nM of agonist FFFSWGa (JPT Peptide Technology, Acton, MA, USA) was performed after a 5 min incubation with the compound. The fluorescent signal was read at excitation/emission wavelength of 495/525 nm in plate end-point mode with a Clariostar® plate reader (BMG Labtech, Germany). The cell responses were read immediately after the first addition, and 5 min after the second addition. For both readings, the plate was read from both forward and reverse

orientations to compensate for the decrease in signal strength in the kinetic assay during plate reading, because there was a 1 min lag time between the readings of the first and the last well. The fluorescent cellular responses to both compound addition and agonist addition were represented as the average of two values that were obtained by the forward and reverse plate readings, subtracting the background signal. Therefore, only one value represents each compound. In this study, 63 drug plates containing 19,760 unique small molecules were screened on the $BMLK_3$ cell line.

5.3.5. Quality control for HTS

The quality of each HTS assay plate was evaluated through the calculation of the *Z'* value, which involves the responses in RFU of only both negative and positive controls as indicators of the assay condition independently of the test compounds (Zhang et al., 1999). In this study, Z' values were reported in Suppl. Table 5.1. Assays with Z' value less than 0 were discarded.

$$Z' = 1 - \frac{(3\sigma_{c+} + 3\sigma_{c-})}{|\mu_{c+} - \mu_{c-}|}$$

Here the and μ_{c-} and μ_{c+} represent the average RFUs of the negative control (blank solvent, n = 64) and the positive control (blank solvent + agonist, n = 64) wells, respectively. And σ_{c-} and σ_{c+} represent their corresponding standard deviations (SDs). Therefore, 320 wells remained available for compound testing.

The assay quality for the screening of compounds (*s, n=320*) was evaluated with the Z-factor (a screening window coefficient) calculated with the equation below (Zhang et al., 1999), The positive and negative control populations (c) are the same as described above.

For an agonist screen, the samples are the average RFU from wells that received the library compounds (n=320) in the first addition. And they are compared to the positive control agonist, FFFSWGa as follows:

$$Z(agonist) = 1 - \frac{(3\sigma_s + 3\sigma_{c+})}{|\mu_s - \mu_{c+}|}$$

Whereas for an antagonist screen, the samples (n=320) are the average RFU measured from wells that received the 2nd addition of agonist peptide, and compared to the negative control.

$$Z(antagonist) = 1 - \frac{(3\sigma_s + 3\sigma_{c-})}{|\mu_s - \mu_{c-}|}$$

The Z-factor is meaningful within the range of $0 < Z \leq 1$ (Zhang et al., 1999). Assays who failed to meet the standard of Z-factor > 0 indicating the windows between samples population and control population were too narrow (Zhang et al., 1999), were considered invalid and their data, therefore eliminated.

5.3.6. Hit molecule selection

The cutoff for selecting agonist hits was set to a Normalized Percent Activation (NPA) Max Ratio > 46 %. The NPA is calculated as the percentage of the normalized response of the particular agonist relative to the normalized response of the control kinin receptor agonist (FFFSWGa at 500 nM), which was regarded as the maximal response (NPA=100 %) from $BMLK_3$ cell line (Xiong et al., 2019d). The raw fluorescence signal of each well (RFU_s) was subtracted by the respective background signal (RFU_{bg}), as follows:

$$\text{NPA} = \frac{RFU_{ago} - RFU_{bg}}{RFU_{c+} - RFU_{bg}}$$

The cutoff for selecting antagonist compounds was set to an inhibitory activity (I_0) > 42 %.

The inhibitory activity was estimated as the percentage of the normalized response to the agonist peptide of the cells preincubated with the antagonist ($RFU_{ant} - RFU_{bg}$), relative to the

normalized response to the agonist peptide of the cells preincubated with blank solvent (positive control).

$$I_0 = 1 - \frac{RFU_{ant} - RFU_{bg}}{RFU_{c+} - RFU_{bg}}$$

5.3.7. Hits validation in dose-response assay

Agonist and antagonist hit molecules obtained from the HTS with the criteria described above were subsequently validated in a dose-response assay on the $BMLK_3$ cells and vector-only cells using the same calcium fluorescence assay as described above. The analysis of the dose-response of each compound was performed using 20 dosages, starting from 25 µM (as final concentration in the assay plate) to 28 nM, resulting from a serial dilution factor of 1:1.4. Hit molecules were obtained from 96-well master plates where the concentration of each molecule is approximately 10 mM in 100% DMSO. Two µl of these solutions were added into wells of the third column in the 384-well-plate, containing 78 µl DPBS, 6.67% DMSO, as the starting concentration (250 µM) for serial dilutions. The rest of the 19 serial dilutions were in 10% DMSO in DPBS in these drug plates, and the final DMSO concentration in the assay plate was 1%.

The dose-response assays were performed with the same dual-addition assay described above, except that 1 µM of Rhimi-K-1 (QFSPWGamide, Genescript® Biotech, Piscataway, NJ, USA), an *R. microplus* endogenous kinin, was added in the second addition to achieve unbiased validation of antagonistic activity. The EC_{50} and IC_{50} were determined. Screening of the same compounds on the vector only cells allowed identifying false agonist hits, which by inducing fluorescence responses in vector only cells were activating endogenous CHO-K1 cell receptors and therefore discarded.

5.3.8. Virtual hits and analogs

Utilizing a chemical search tool available in the Collaborative Drug Discovery (CDD) vault,(Hohman et al., 2009) each of the HTS identified and validated molecules in dose-response assays were used as query for *in silico* searches of the Texas AgriLife library containing 389,957 molecules to identify virtual hits with at least 70% structural similarity. Additionally, 7 analogs of the most potent antagonist hit (SACC-0064443) were purchased from ChemBridge™ for studying the structure-activity relationships. These chemicals were validated in the 20-dosage serial dilution assay, as described above.

5.3.9. Cytotoxicity assay*

Human dermal fibroblasts (HDF) cells were used to evaluate the potential cytotoxicity of the hit molecules, following the assay protocol as described in Aggarwal et al., 2017 (2017). In brief, the cells were cultured in DMEM (Lonza) media supplemented with 10% fetal bovine serum (Lonza) and penicillin/streptomycin (10 U/ml) (Lonza). For setting the cytotoxicity assay. On the day of assay, HDF cells were trypsinized, counted and resuspended at a density of 64,000 cells/ml in the media, and test compound stocks were prepared at 800 µM in 10% DMSO in PBS. Cells (39 µl) were plated in a 384-well plate (Corning, 3680), 1 µl of compound was added into each well (three pseudo-replicate wells for each assay) at a final concentration of 20 µM in 0.25% DMSO and incubated at 37°C. After 48 h, 4 µl of resazurin dye (0.2 mg/ml) were added and the assay plates were incubated for an additional 24 h. The next day the fluorescence of the resazurin was measured on a microplate reader (BMG Labtech) to assess cell death by comparing to the percentage of fluorescence signal decreased compared to the cell incubated with buffer control. The fluorescence intensity is proportional to number of live cells. The HDF

* The Cytotoxicity assay was performed by Dr. Wen Dong from Dr. James C. Sacchettini laboratory in Biochemistry and Biophysics, TAMU.

cytotoxicity was expressed as the average percentage of cell growth inhibition in the compound treated wells compared to the control wells. The cutoff threshold for cytotoxicity was 10%.

5.3.10. Validation of antagonistic activity on the recombinant mosquito kinin receptor

Three identified potent small molecule antagonists, and as control a small molecule of very low antagonistic activity, were tested in the calcium fluorescence assay, as above, for their activity on the recombinant kinin receptor of *Aedes aegypti*, herein referred to as IGKN G12 cell line. Receptor cloning, expression and clonal cell selection were as previously described (Pietrantonio, P.V. et al., 2005). The compounds were prepared as a 10X stock in 10% DMSO in HHBS buffer. The recombinant tick kinin receptor ($BMLK_3$) was tested simultaneously as positive control for the assay. $BMLK_3$ and IGKN G12 cells were seeded in 96-well-plates (Greiner Bio-One®, B/C 655097) at a density of 4 x 10^4 cells in 100 µl of maintenance medium. Cells were prepared as described above for the calcium fluorescence assay; each well was added with 90 µl of assay buffer (section 2.3; 20 mM Hepes in Hank's buffer saline, plus dye efflux inhibitor).

Each compound 10X stock solution (10 µl) was manually added into one well of each cell line for a final concentration of 10-, 30-, and 100-µM. After 5 min incubation at room temperature, a kinin receptor agonist peptide 1728 (Xiong et al., 2019d) ([Aib]FF[Aib]WGamide, RoyoBiotech, Shanghai, China) was added manually (50 µl; 3X stock in HHBS) into each well for a final concentration of 1 µM. The cellular calcium response in RFU was immediately recorded continuously for 60 s with 3 s interval between reads using a Clariostar plate reader. The average RFU of 20 reads represented the raw response to each treatment. Three independent replicates were run for each concentration and compound. The percentage of signal reduction with respect to the control that contained solvent and analog 1728

was calculated using the average RFU registered for the treatment with each small molecule divided by the average RFU recorded for the control (100%). Data analyses were performed with the percentage reduction of the three independent replicates. Graphpad Prism was utilized for analysis and graphics.

5.3.11. Validation of antagonistic activity in the hindgut contraction inhibition assay

A mosquito colony of *Ae. aegypti* (Diptera: Culicidae), Liverpool strain, was maintained at 26.5 °C in 16L:18D light cycle, as described.(Jagge and Pietrantonio, 2008) For the experiment, 3-5 d-old females were used, and the assay was modified based on our previous protocol, as described (Kwon and Pietrantonio, 2013). A group of six female mosquitoes were cold-anesthetized on a Petri dish placed on ice, where both wings were removed. Mosquitoes became active when the plate was removed from the ice. The dissection dish was filled with Ringer solution (150 mmol l^{-1}, NaCl, 25 mmol l^{-1} Hepes, 3.4 mmol l^{-1} KCl, 7.5 mmol l^{-1} NaOH, 1.8 mmol l^{-1} $NaHCO_3$, 1 mmol l^{-1} $MgSO_4$, 1.7 mmol l^{-1} $CaCl_2$ and 5 mmol l^{-1} glucose, pH 7.1) (Clark et al., 1998) at room temperature. To extract the hindgut of each mosquito, their head and thorax were removed with forceps, and the abdomen was submerged in the Ringer solution. The hindgut, ovaries and Malpighian tubules (MTs), and midgut were taken out by pulling the last segment of the abdomen under the Ringer solution. Then, the ovaries and the majority of the midgut were removed using scissors leaving the intact hindgut and MTs. The isolated tissue was transferred with forceps, grabbing on the cuticle of the last segment, into a drop of 30 µl Ringer solution in a 12-well-plate (Greiner Bio-One®, 665102). After six mosquitoes were dissected as a group, paraffin oil (1-2 ml) was added to each well to cover the saline. The cuticle of the last abdominal segment was drawn out of the Ringer solution into the oil for better observation of the

hindgut contraction. The tissues were filmed using an Olympus SZ60 camera (Olympus America Inc, Center Valley, PA, USA) through a dissecting microscope.

First, the hindgut basal contraction rate was recorded by filming each tissue for 60 s. Secondly, 15 µl of 3X small molecule (300 µM) solution or corresponding solvent-buffer (3 or 10% DMSO in Ringer solution) was added to the drop of Ringer solution containing each tissue for a final concentration of 100 µM. After 5 min of incubation at room temperature, 15 µl of the kinin receptor agonist 1728 solution (4X in Ringer solution) was added to the Ringer solution to reach a final concentration of 10 µM. After 1h of incubation, the tissue was filmed again for 60 s.

The contractible hindgut of mosquito consists of a funnel-shaped pylorus located immediately after the posterior midgut, followed by a long, coiled ileum, and a bulbous colon which contains the rectal pads, and a tapering rectal tube at the posterior end (Odland and Jones, 1975). To analyze each video, the hindgut contraction number was counted by observing the contraction occurring at the junction between the pyloric sphincter and the most anterior ileum. The hindgut contraction rate was expressed as the number of contractions observed over 60 s. The fold change in contraction rate was calculated as the contraction rate estimated at 1h post treatment divided by the basal rate estimated before the treatment with the chemicals. Each treatment was repeated with 30 female mosquitoes independently. All statistical analyses were done by Graphpad Prism Software (v8, San Diego, CA). The differences in fold-change of the contraction rates among treatments were analyzed using the non-parametric Kruskal-Wallis test, followed by the Dunn's multiple comparison test. Only for one small molecule, SAC-0412062, that had to be dissolved using a higher DMSO concentration (10%), the difference in fold-change of the contraction rate between the control Ringer-solvent treatment and each compound treatment was analyzed by the Mann-Whitney test, a non-parametric t-test.

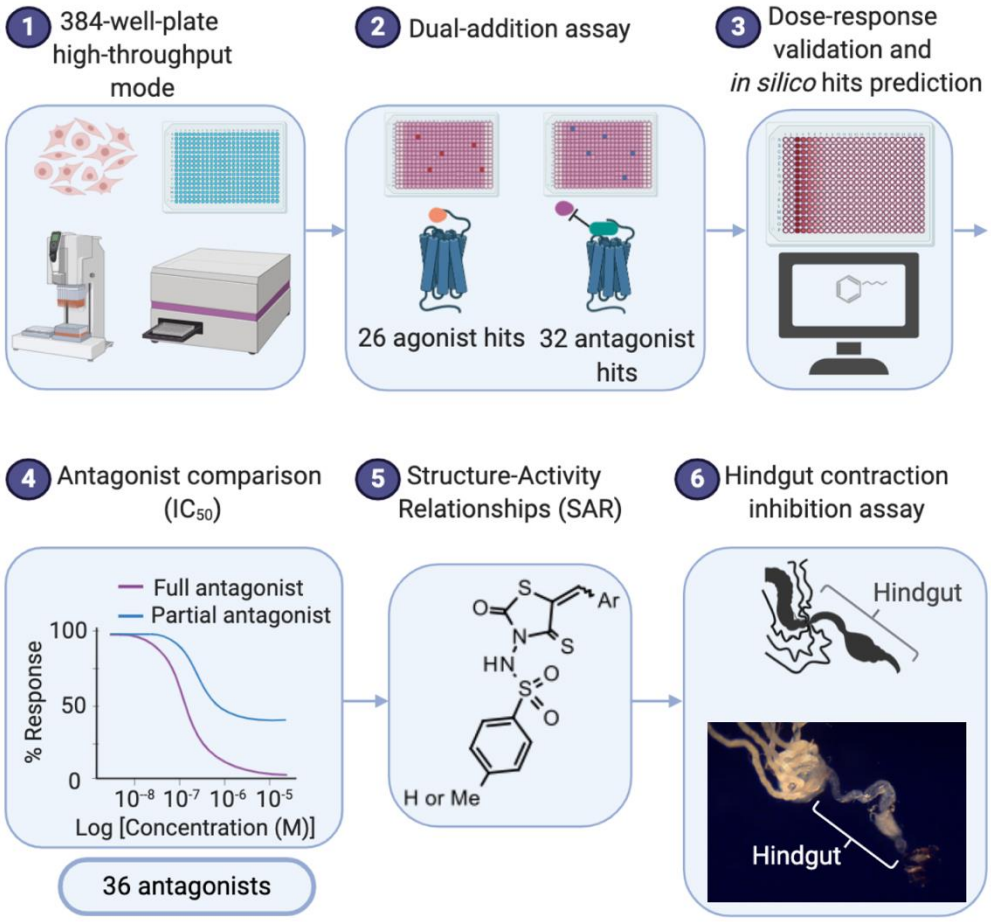

Figure 5.1 Workflow for the discovery of novel small molecules ligands of the kinin receptor from the southern cattle tick, *Rhipicephalus microplus*.
1) A high-throughput calcium fluorescence assay was developed with the recombinant tick kinin receptor-expressing cells ($BMLK_3$) in 384-well plates; 2) A "dual-addition" cell assay was developed to allow identification of agonist and antagonist molecules in the same assay; 3) Both, experimentally obtained and virtually predicted hit molecules were validated using 20 concentrations in the fluorescence response assay; 4) Validation of hit molecules was by obtaining their response curves and analyzed by comparison of their IC_{50}s; 5) Structural Activity Relationships (SAR) analyses were performed for hit molecules with high structural similarity; 6) Potent hit molecules were tested *in vivo* using a canonical hindgut contraction inhibition assay. Figure was created with BioRender.com.

5.4. Results

The pipeline for this novel ligand identification through HTS is outlined in Fig. 5.1. We developed a dual-addition calcium fluorescence assay in 384-well mode on the CHO-K1 cells permeant expressing kinin receptor from the southern cattle tick *R. microplus*. In the process, relevant variables were validated (data not shown), such as cell density (10,000 cells per well), concentration of the screened compounds (2 μM), final DMSO concentration (0.2%) in the assay plate, agonist peptide (a generic kinin analog, FFFSWGa) concentration (500 nM), pipetting speed and depth (CyBio® and Viaflo® programs in Appendix1, and reading time post-addition of the agonist peptide (5 min). The results of HTS and dose-validation were summarized in Fig. 5.2. Total of 19,760 small molecules were screened with this assay and the hit ratio was 0.29% with 58 hit molecules selected (Suppl. Table 5.2) according to the criteria described in the Materials and Methods. Among them, 26 small molecules were identified as potential agonists with (NPA $\geq$ 46 %) and 32 small molecules were potential antagonists with ($I_o \geq 42\%$). These 58 molecules were validated for their dose-dependent response on both $BMLK_3$ cells, and vector-only cells (lacking the tick kinin receptor). A summary of hit molecule characterization through concentration-response curves is shown in Fig. 5.3. The screening of compounds on the vector-only cells assisted with the exclusion of the off-target agonists when the vector-only cells respond to a compound similarly as the $BMLK_3$ cells (Fig. 5.3C as an example). Our results suggested all of the 26 putative agonists we identified were either off-target or not active (curves in Suppl. Table 5.3). The dose-response assay confirmed 18 off-target agonists as the vector-only cells produced similar dose-responses as with the $BMLK_3$ cells. The remaining 22 hit molecules (putative agonists and antagonists) did not show dose-response activities (Fig. 5.3D). In contrast, 18 molecules showed dose-dependent antagonistic activities, among them, ten molecules acted

as full antagonists which fully inhibited the cellular response to the tick kinin, Rhimi-K-1 (Fig. 5.3A as an example) and eight molecules acted as partial antagonists where the response to kinin peptide was not completely suppressed even at high concentration (Suppl. Table 5.3 and Fig. 5.3B as an example). In order to expand the hits list, we performed a structure-based *in silico* screen on the remaining existing chemical library at hand (389,957 small molecules) and found 27 small molecules with at least 70% structural similarity to the experimentally identified antagonists representing a variety of molecules (Fig. 5.2 and Suppl. Table 5.4). These molecules were subsequently validated in the same dose-response assay on the $BMLK_3$ and vector-only cells. As a result, 16 additional antagonists (5 full antagonists and 6 partial antagonists) were identified (Fig. 5.2 and Suppl. Table 5.4). In sum, 15 full antagonists and 14 partial antagonists were validated from hits identified in HTS and *in silico* prediction. Among the 15 full antagonists, 11 small molecules showed IC_{50} less than 10 μM which are presented in Fig. 5.4.

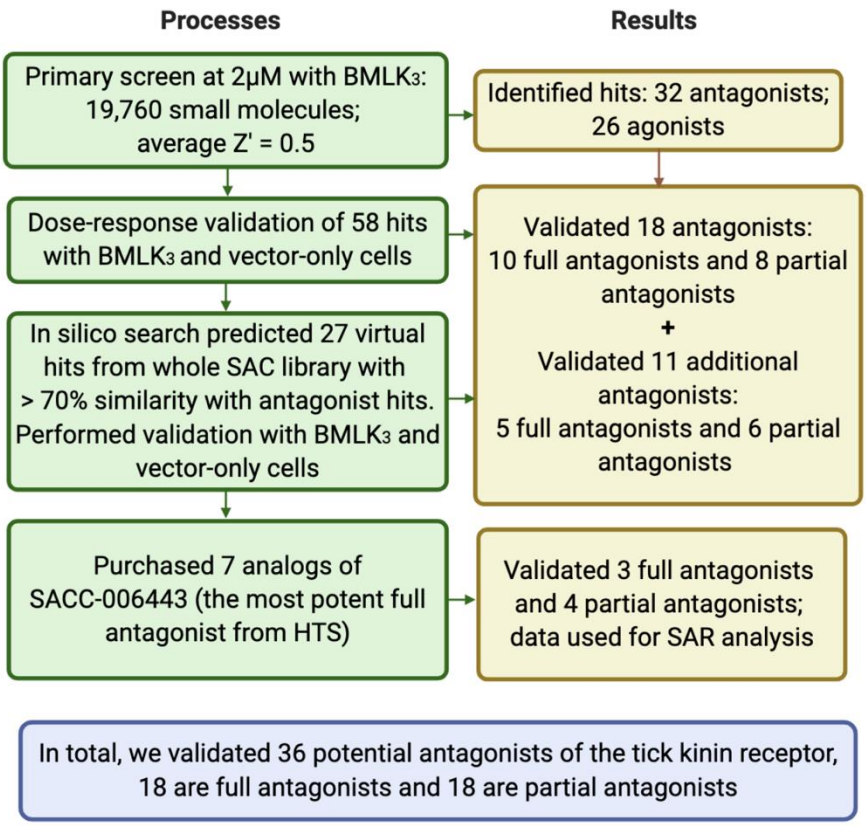

Figure 5.2 Stepwise summary of the high-throughput screening results using BMLK$_3$ cells and Vector-Only (VO, control) CHO-K1 cells.
Green boxes describe processes; yellow boxes indicate results; the blue box on the bottom is the summary of all the antagonist hit molecules discovered. Figure was created with BioRender.com.

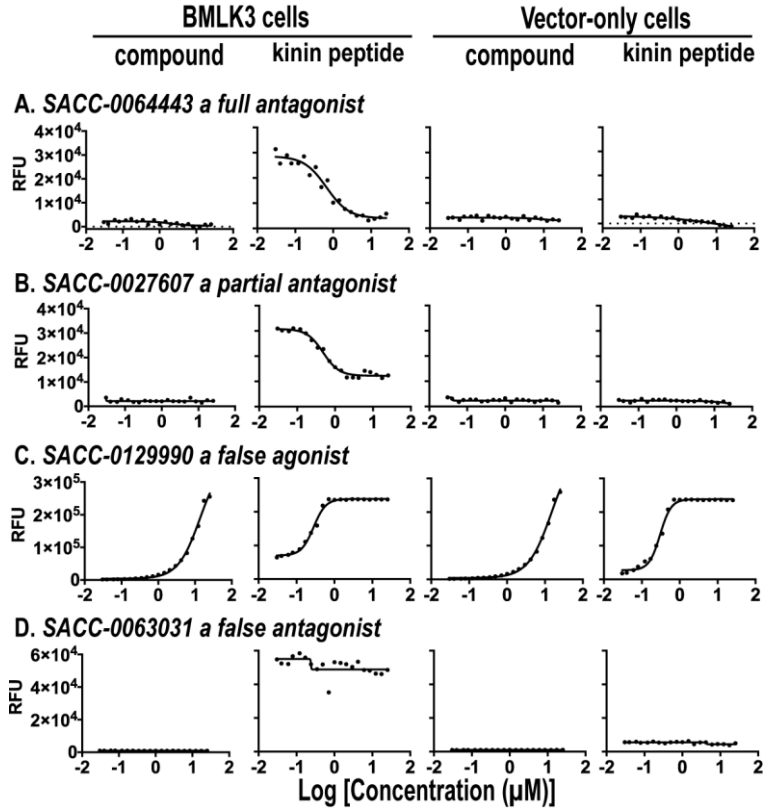

Figure 5.3 Characterization of hit molecules through concentration-response curves. The curves of four representative hit molecules identified through high-throughput screening are shown (A-D). Hit molecules were tested in a concentration-response assay on both recombinant tick kinin receptor cells (BMLK3, left two columns) and the cells transformed only with the vector plasmid (VO, right two columns). The first and third column show the calcium fluorescence responses after the assay 1st addition of test compounds. Each compound was tested through a dilution series of 20 dosages (dilution factor 1: 1.4), ranging from 28 nM to 25 μM as final concentrations**.** The second and fourth columns show the respective calcium responses 5 min after the assay 2nd addition of the tick kinin receptor agonist peptide, Rhimi-K-1 (QFSPWGamide, 1μM). Cell calcium responses in Relative Fluorescence Units (RFU) were recorded using a Clariostar Plate Reader (BMG technology®, Germany). The dose-response curves were calculated by Graphpad Prism Software using non-linear regression [log(inhibitor/agonist) vs. response - Variable slope (four parameters)]. The panels A-D each show an example of different types of hit molecule: A) a partial antagonist, which partially inhibited the calcium response to the kinin peptide but did not reach full inhibition even at highest concentration of 25 μM; B) a full antagonist, which completely inhibited the response to the kinin peptide; C) a false (non-specific) antagonist, which elicited the same agonistic dose-response in both $BMLK_3$ and VO cells; D) a false antagonist which did not inhibit the agonist peptide in a dose-response fashion.

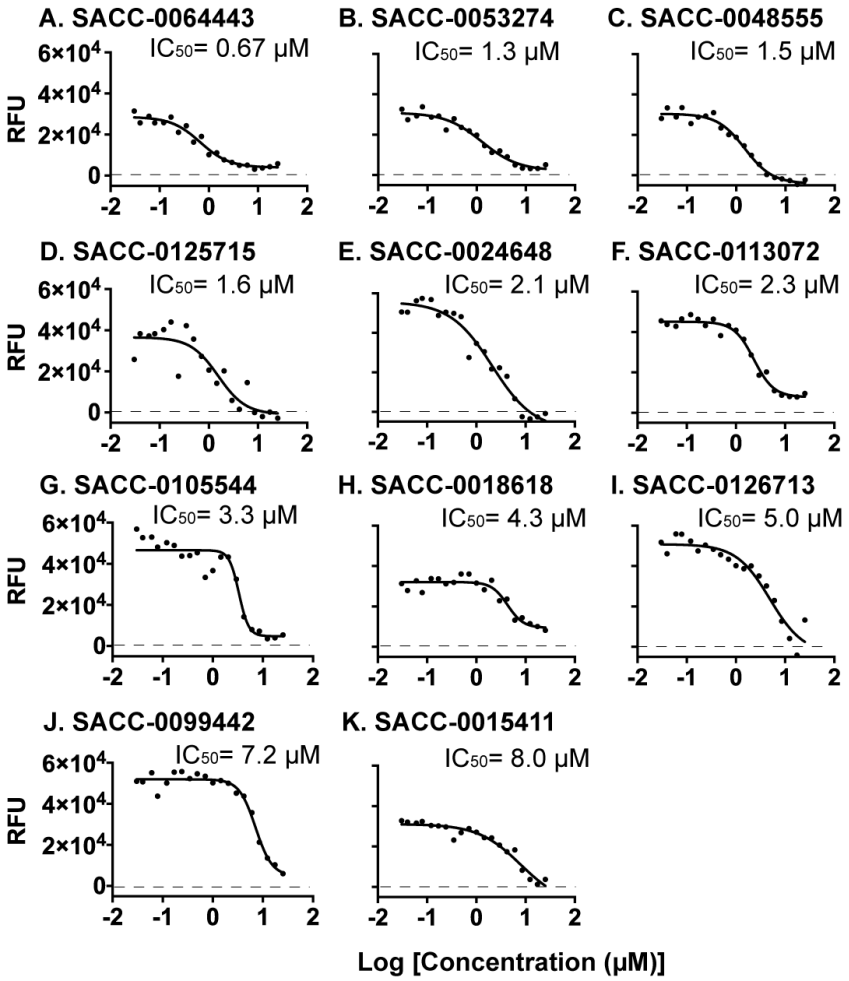

Figure 5.4 Concentration-response curves of the eleven most potent full antagonists from an in-house SAC library screening.

Hit molecules identified by the experimental high-throughput screening (A-C and E-I) and by virtual predictions (D, J and K) were validated through a concentration-response assay. Each compound was tested at 20 concentrations from 25 µM to 28 nM, obtained through serial dilutions (1: 1.4 dilution factor) as final concentrations in the cell media**.** Compounds were added into cell media and incubated with the cells for 5 min, followed by the assay 2nd addition of the tick kinin receptor agonist peptide, Rhimi-K-1 (QFSPWGamide, 1µM). The calcium responses in Relative Fluorescence Units (RFU) at 5 min after the 2nd addition was measured by the Clariostar Plate Reader (BMG technology®, Germany). The dose-response curves were generated by Graphpad Prism Software using non-linear regression [log(inhibitor) vs. response - Variable slope (four parameters)]. While twenty-nine of the hit molecules showed dose-dependent antagonistic activity on the recombinant tick kinin receptor (Suppl. Tables 3 and 4), herein only the curves for the 11 most potent hit molecules full antagonists (IC_{50} < 10µM) are shown.

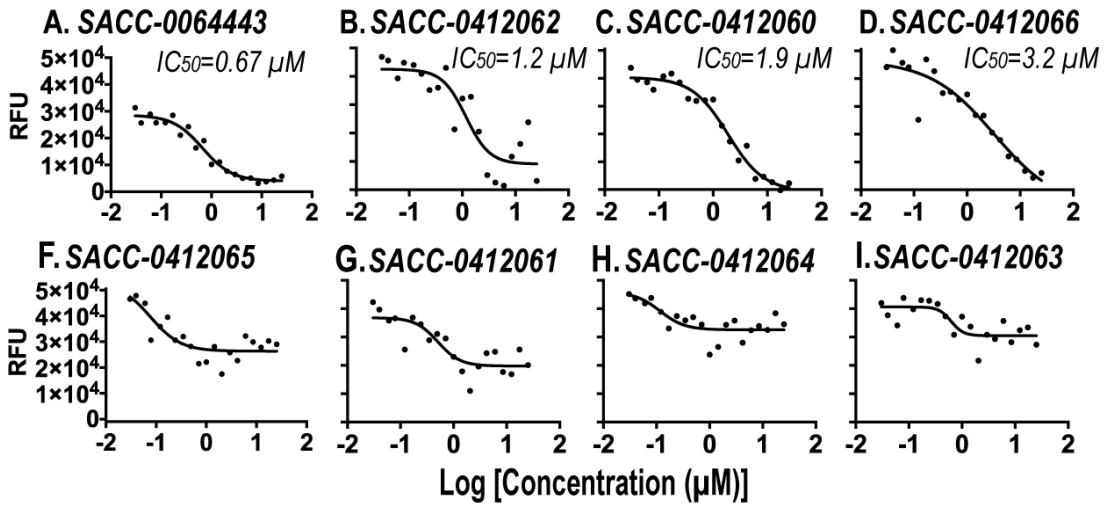

Figure 5.5 Concentration-response curves for the most potent antagonist (SACC-0064443) and for its structural analogs identified from *in silico* searches.
The eight molecules tested have 95% structural similarity. For each compound, receptor-expressing cells ($BMLK_3$) were preincubated 5 min with each of 20 concentrations from 25 µM to 28 nM, obtained through serial dilutions (1: 1.4 dilution rate). Post-incubation, a tick kinin receptor agonist peptide, Rhimi-K-1 (QFSPWGamide, 1µM), was added to the cell media, and after 5 min the cell calcium responses in Relative Fluorescence Units (RFU) were recorded by a Clariostar Plate Reader (BMG technology®, Germany). The curves were generated by Graphpad Prism Software using non-linear regression [log(inhibitor) vs. response - Variable slope (four parameters)]**.** The top four panels (A-D) show molecules that were full antagonists; panels F and G show partial antagonists; panels H and I show compounds with low antagonist activity.

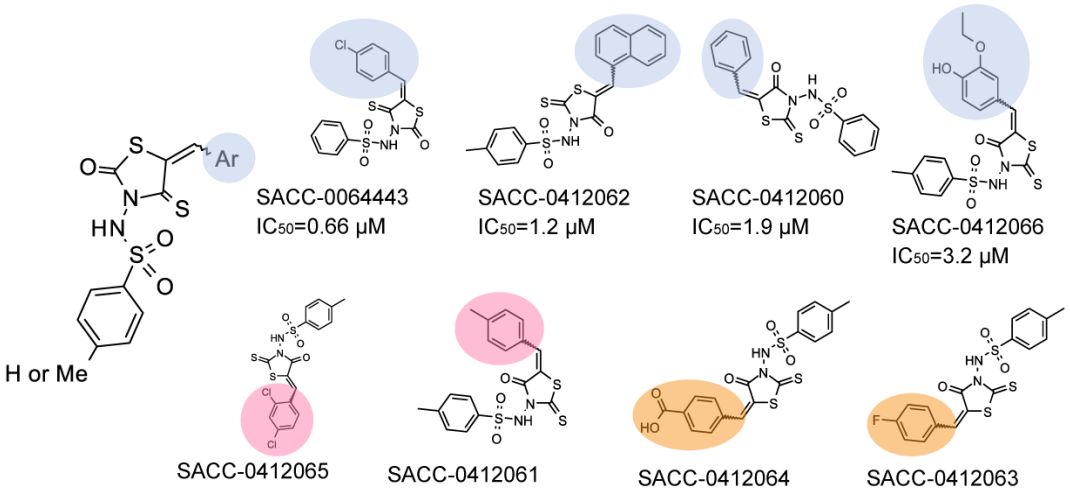

Figure 5.6 Structure-activity relationships (SAR) analyses of a validated antagonist (SACC-0064443) derived from the HTS, and of seven analogs of the same molecule identified by in silico searches of the available libraries. *

The structure on the left depicts the backbone of these eight structurally similar molecules. The change of Ar group caused different antagonistic activity. The top four molecules (aromatic group(s) in blue) acted as full antagonists of the tick kinin receptor, and the bottom molecules acted as either partial antagonists (SACC-0412065, SACC-0412061, in pink) or very weak partial antagonists (SACC-0412063 and SACC-0412064, in orange) (Dose-response curves of these eight molecules are in Fig. 5.5).

* SAR analysis was performed by Dr. Nian Zhou from Dr. James C. Sacchettini laboratory in the Department Biochemistry and Biophysics, TAMU.

One of the most potent antagonists identified from HTS, SACC-0064443 (IC_{50} = 0.67 µM, Fig. 5.4A), was selected to study structure-activity relationships (SAR). One small molecule (SACC-0412066) with 95% structural similarity with SACC-0064443 and six 2D and 3D analogs of this molecule which were obtained from ChemBridge™ Chemical. They were tested in the dose-response assay in the same fashion as mentioned above (Suppl. Table 5.5). Three compounds showed full antagonistic activity with IC_{50}s ranged from 1.2 to 3.2 µM (Fig. 5.5B-D), which were equivalent to the activity to SACC-0064443 (Fig. 5.5A). Two compounds were partial antagonists (Fig. 5.5F and G) and other two showed very weak antagonistic activity (Fig.5H and I). Based on these series of results, we predicted a backbone of tick kinin receptor antagonist with variable side chain (Ar-group) (Fig. 5.6, structure on the far left). The results suggested that the Ar-group is selected from Phenyl, naphthyl, 4-Me-phenyl, 4-Cl-phenyl, 4-F-phenyl, 4-carboxy-phenyl or 4-OH-groups. Among them, phenyl and naphthyl were best for activity, whereas substitution on phenyl decreased activity (Fig. 5.5 and 6). In addition, to determine the mammalian cellular toxicity of the 36 antagonists we validated from dose-response assay, a cell toxicity assay was performed with human epidermal fibroblast cells. Only 32 out of 36 compounds showed cytotoxicity with HDF inhibition lower than 10% when tested at 20 µM (Suppl. Table 5.5. Column K). Two of the potent antagonists, SACC-0053274 and SACC-0015411 (curves in Fig. 5.4B and K), showed low toxicity with 10-11% HDF inhibition.

To validate the bioactivity of these small molecule antagonists, the compounds were tested for inhibition of the canonical myotropic activity of the kinin peptide in the hindgut contraction inhibition assay. The most potent commercially available antagonists, SACC-0412060, SACC-0412062, and SACC-0412066 (Fig. 5.5B-D) were selected to be tested and SACC-0412064 was used as a negative control for its weak activity on the tick recombinant

receptor (Fig. 5.5H). Before the tissue bioassay, we first validated the *in vitro* antagonistic activity of these four molecules on the recombinant mosquito kinin receptor (IGKN G12). Through results of the calcium mobilization fluorescence assay, three active molecules showed antagonistic activities on IGKN G12 similar as on the BMLK3 cells. Inhibition was calculated as the percent inhibition of the maximal response that was obtained by applying solvent in the first addition and 1728 agonist peptide in the second addition of the assay (Fig. 5.7, first bar for each compound). All three tested concentrations (10, 30, and 100 µM) of SACC-0412060 and SACC-0412062 inhibited at least 50 % of this maximal response (Fig. 5.7A). SACC-0412066 at 30 µM inhibited 84% response on IGKN G12 compared to the control (Fig. 5.7A). Unexpectedly, this molecule elicited a strong calcium response at 100 µM, indicative of receptor activation. It is possible that at this high supraphysiological concentration, other endogenous receptors could have been activated. We did not explore this response further. The control molecule (SACC-0412064) did not antagonize the calcium response even at 100 µM (Fig. 5.6, lightest gray column).

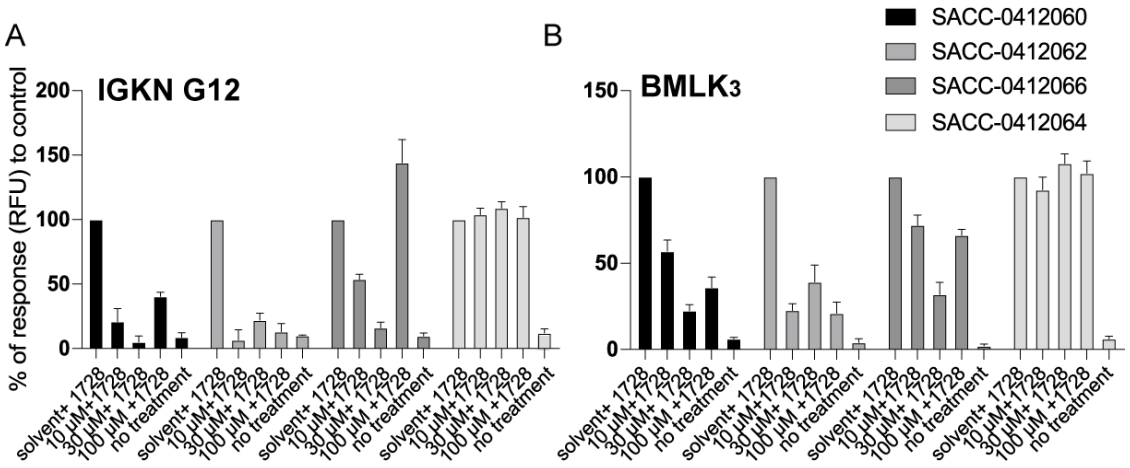

Figure 5.7 Test of potent antagonist hit molecules on the recombinant kinin receptor from mosquito *Aedes aegypti* (IGKN G12, CHO-K1 cells) in the calcium fluorescence assay. The recombinant tick kinin receptor ($BMLK_3$) was tested side-by-side for comparison. SACC-0412060, SACC-0412062, and SACC-0412066 were among the most potent antagonists. SACC-0412064 had a very weak antagonistic activity, therefore, it was used as a negative control. Each molecule was tested at three different dosages (10, 30 and 100 µM as final concentration). For testing each of these final concentrations, first, a 10X small molecule stock solution was added to the cell media. After 5 min of incubation with the compound, a 3X kinin receptor agonist 1728 ([Aib]FF[Aib]WGamide) solution was added to reach a final concentration of 1 µM. After this second addition, calcium fluorescence responses (in Relative Fluorescence Units, RFU) of the cells were immediately recorded for 60s with 3s intervals between reads using a Clariostar Plate Reader (BMG technology®, Germany). The Y-axis value was calculated as the percentage of average RFU of each treatment to the RFU of the control (solvent in first addition and 1728 in second addition = solvent + 1728), as the cell response of the control well was regarded as 100 % response in each test. Three replicates were done for each treatment (n=3, mean ± SEM).

For the hindgut contraction inhibition assay we first confirmed the contractile activity of the kinin analog 1728 on mosquito hindgut. In this assay we detected significant differences among treatments (Kruskall-Wallis test) and the Dunn's test revealed a significant (~2-fold) increase in contraction rate in hindguts incubated with 10 µM 1728 in 1% DMSO 1h post addition of the analog (Fig. 5.8A). This treatment did not differ from the joint treatment of 1728 and SACC-0412064, the latter which had low antagonistic effect in the cell assay. This low antagonistic effect can perhaps explain that the effect of 1728 plus SACC-0412064 treatment was intermediate between those of 1728 and the no treatment group, from which was also not significantly different (Fig. 5.8A). In contrast, the antagonists SACC-0412060 and -00412066 significantly reduced the mobility of the hindgut with respect to the rest of the treatments (Fig. 5.8A). Although SACC-0412066 agonized the calcium response at 100 µM, we did not observe any increase in the hindgut contraction rate in the hindgut contraction assay, supporting a potential off-target agonistic activity at high concentration on the mammalian cells only (Fig. 5.7A and B). Hindguts incubated with SACC-0412062 and 1728 showed reduced contraction rate (fold-change < 1), compared to a 2-fold increase of contraction rate in solvent plus 1728 group ($P < 0.0001$) (Fig. 5.8B).

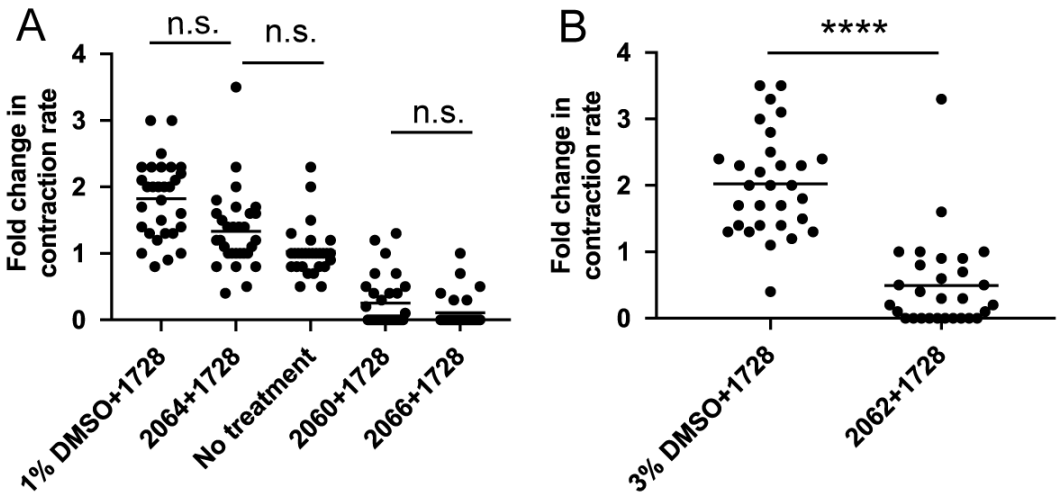

Figure 5.8 *In vivo* validation of antagonists of kinin receptors in the arthropod hindgut contraction inhibition assay.
Isolated hindguts from females of the mosquito *Aedes aegypti* were preincubated with 100µM of antagonist (SACC-0412060, SACC-0412062, or SACC-0412066), the negative control small molecule (SACC-0412064), or solvent control for 5 min. Subsequently, 10 µM of 1728 ([Aib]FF[Aib]WGamide) was added. Tissues were filmed for 60 s before treatment and for 1 h-post treatment using an Olympus ZS60 (Olympus America Inc, Center Valley, PA, USA) microscope. The fold-change in the contraction rate in 60 s was calculated by dividing the post-treatment contraction rate by the basal contraction rate; each dot represents one hindgut contraction assay (n = 30 for each treatment). A) Differences in the means of change of contraction rate were analyzed by the Kruskal–Wallis ($P < 0.05$) test followed by Dunn's multiple comparisons test ($P < 0.05$) using the Graphpad Prism Software. Black lines above results and "n.s." indicate no statistical difference between groups. B) Differences in the change of contraction rate between SACC-0412062 and solvent with analog 1728 were analyzed by the non-parametric t-test, **** $P < 0.0001$. The annotation of the small molecules on the X-axes displays only four digits of their full name due to space limitations, and the prefix 'SACC-041' should be added.

5.5. Discussion

In this study we aimed to identify novel small molecule ligands of the tick kinin receptor to expand our tool set towards elucidating the function of the tick kinin signaling system and identifying potential chemical leads for tick control. “Small molecules” for therapeutic purposes are defined by the ‘Lipinski rule of five’, and include those < 500 Da (oral administration) (Lipinski, 2016), however, this size rule is often violated for agrochemicals. In previous work we tested novel peptidomimetic ligands of the tick kinin receptor that were designed based on the sequences of endogenous tick kinins; all such mimetics were full agonists (Xiong et al., 2019b). However, peptidomimetic ligands are more costly to synthesize and may have limited penetration through the arthropod cuticle, both of which limit their potential as agrochemicals. Lack of crystal structures of arthropod neuropeptide GPCRs remains a major obstacle for predicting small molecule ligands. The alternative approach to identify novel ligands of GPCRs is through high-throughput screening (HTS) of random small molecule libraries. Currently, only two published studies have performed HTS for novel ligand discovery on arthropod vector GPCR targets. A novel small molecule agonist of the mosquito neuropeptide Y (NPY) receptor was identified through HTS.(Duvall et al., 2019) In addition, the invertebrate dopamine receptor, a biogenic amine GPCR, was subjected to HTS with target-specific libraries, and antagonists exhibiting considerable toxicity to mosquito larvae were discovered (Ejendal et al., 2012).

Our targeted screening of the random small molecule library yielded 18 antagonists after dose-response analyses of the initial 32 antagonist hits. The 18 validated antagonists comprised 0.09% of the total screened compounds. It is worth mentioning that the primary HTS and the secondary validation in the dose-response assays utilized different agonist peptides. The primary screen was done with an hexapeptide generic kinin, FFFSWGa, that although potent on the tick

receptor (Taneja- Bageshwar et al., 2006), differed in structure from the tick endogenous kinins.(Xiong et al., 2019a) This kinin analog was used because at the time the primary screen was performed, we had not yet identified and tested the *R. microplus* kinins. The implication is that the antagonist hits derived from the primary screen may have been biased towards this kinin agonist.

During validation of hits in the dose-response assays, we used one of the kinins from *R. microplus*, Rhimi-K-1, the sequence of which was deduced from cloning the peptide precursor, and its activity was verified on the tick kinin receptor (Xiong et al., 2019a; Xiong et al., 2019b). Unfortunately, no agonist molecules were validated from the 26 putative agonist hits identified from HTS. The lack of validated hits may be attributed to our rigorous standard for selecting agonists, requiring that a hit had to elicit a cellular response higher than 46% of the responses to 500 nM of the kinin peptide FFFSWGa; this concentration can elicit almost the maximal response (80 to 100%) from the recombinant tick kinin receptor cells (Xiong et al., 2019d).

The kinin agonist peptides have a conserved C-terminal motif, $FX^1X^2WGamide$ (X^1 and X^2 are variable residues) (Nachman and Holman, 1991a; Nachman et al., 2002a). In contrast, the structure of the 18 potential antagonist small molecules had very low structural similarities among themselves (Suppl. Table 5.7). A structure-based *in silico* screen search allowed identification of 27 putative antagonist hits. Concentration-response validation experiments identified 11 additional antagonists among these 27 predicted hits, 40.7 % of the hit ratio. Therefore, prediction of the ligand structure based on known antagonists improved the hit ratio of antagonists. Before the structure-activity relationships can be evaluated, it is necessary to identify a group of lead analogs. In total we validated 36 antagonists of the tick kinin receptor that, based on their structural similarities, could be clustered into 27 groups (Suppl. Table 5.7).

The larger cluster of molecules with high structural similarity included the eight analog molecules shown in Fig. 5.6. The structure-activity relationships analysis suggested that compounds with phenyl, naphthyl, or 4-Cl-phenyl at the Ar-position exhibited full antagonistic characteristics whereas substitution with four alternative groups resulted in decreased activities and loss of full antagonistic activity. Further receptor-ligand structure analyses followed by *in silico* design of hit molecules will be meaningful to improve the resolution of the SAR.

While the dose-response assay validation in vector-only cells allowed us to discard false agonist hits, the same cannot be concluded from the potential antagonist hits, therefore, a functional assay was developed to verify the inhibitory effect of the most potent antagonists. Kinin peptides were known as myokinins for their myotropic activity on the hindgut of various insect species (Bhatt et al., 2014; Holman et al., 1986). The hindgut bioassay has been the gold standard for evaluating the activity of myotropic or myoinhibitory ligands of GPCRs in insects and ticks (Kwon and Pietrantonio, 2013; Šimo and Park, 2014). To determine the antagonistic activity of the validated compounds in a bioassay, we adapted the mosquito hindgut contraction assay we previously developed (Kwon and Pietrantonio, 2013), as a hindgut contraction inhibition assay. For this we reasoned the hindgut contractions had to be first chemically stimulated to verify the inhibitory activity of the small molecules. Our lab has developed parallel pipelines for studying kinins and kinin receptors from mosquitoes and ticks (Pietrantonio, P.V. et al., 2018); both receptors were de-orphanized in our lab (Pietrantonio, P.V. et al., 2005; Xiong et al., 2019b), and many kinin peptidomimetics tested side-by-side on both recombinant receptors showed comparable stimulatory activities on both receptors (Taneja-Bageshwar, Suparna et al., 2009; Taneja- Bageshwar et al., 2006; Xiong et al., 2019d). Only one gene encoding the *Aedes*

aegypti kinin receptor[5] (annotated as substance-K receptor, Gene ID: 5574266) can be found in the most recent genome of *Ae. aegypti* (Matthews et al., 2018), two predicted transcript variants (Matthews et al., 2016) have identical protein coding region (AAEL006636-RA and RB on VectorBase[6]), therefore, there is only one form of the protein. While the *R. microplus* genome is less well-annotated, there is also only one functional kinin receptor identified so far. Although the three aedeskinins stimulate hindgut contractions in the mosquito *Ae. aegypti* at concentrations of 10^{-8} M (Veenstra et al., 1997b), and kinin peptides increase hindgut contractile activity in other insects such as cockroaches and kissing bug (Bhatt et al., 2014; Holman et al., 1986), we chose the kinin analog 1728 to stimulate the mosquito hindgut contraction previous to applying the antagonists in the hindgut contraction inhibition assay. The analog 1728 ([Aib]FF[Aib]WGa) was chosen because it is a positive control peptide with enhanced peptidase resistance, and is a very potent agonist on both mosquito and tick kinin recombinant receptors (Taneja-Bageshwar, Suparna et al., 2009). This analog is potent and induces *Rhodnius prolixus* hindgut contraction at 10^{-16} M (Bhatt et al., 2014). This analog was also active in the diuretic assays with renal organs of another dipteran, the fruit fly *Drosophila melanogaster,* at 2.5 x 10^{-5} M but not active in the 10^{-7} M range to increase fluid secretion from the renal organs (Alford et al., 2019a). Similarly, in this study the analog 1728 was active in the mosquito hindgut when tested at 10 µM (10^{-5} M). It is worth noting that the increase of hindgut contraction in response to the kinin analog 1728 had not been previously reported for the mosquito. The increase of hindgut contraction rate was best observed 1 h after the addition of analog 1728. The same time delay was also observed in tissues incubated with 1 µM of an endogenous mosquito kinin, aedeskinin 2

[5] GenBank: AY596453.1

[6] https://www.vectorbase.org/

(NPFHAWGamide, data not shown). In contrast, kinins almost immediately increased hindgut contractions in the cockroach and kissing bug (Bhatt et al., 2014; Holman et al., 1986). This difference in speed of activity could be due to the difference in the measurement methods. Other researchers (Bhatt et al., 2014; Holman et al., 1986) used electrodes to measure the movement of the hindgut, which are much more sensitive to small contractions, whereas we used video recording under the dissecting microscope and visual inspection by the same operator.

After validating the hindgut contractile activity of kinin analog 1728 in females of *Ae. aegypti*, we tested the most potent antagonist compounds that were commercially available in the hindgut contraction inhibition assay. All three molecules we tested inhibited the contraction of the hindgut. Indeed, the active compounds tested at 100 µM would shut down or reduced the amplitude of the peristaltic contraction of the hindgut in most of the tests after incubation with the tissue for 1 h. We had determined that these antagonists were able to inhibit the fluorescence response at 30 µM in the cellular assay with CHO-K1 cells (Fig. 5.7). We decided to use a higher concentration of 100 µM in the tissue assay to account for potential degradation by the tissues during the incubation period. However, the antagonists are likely active at lower concentrations. When we reduced the concentration of SACC-0412060 and SACC-0412066 to 10 µM in the hindgut bioassay, no increase in the hindgut contraction rate was observed 1 h after 1728 was added (data not shown), while the hindgut contraction rate in the 1728 treatment increased by a factor of 2 (Fig. 5.8A). These results suggested that the small molecules were able to block the myotropic activity induced by kinin analog 1728 even at 10 µM, which was consistent with results of the *in vitro* cellular assay (Fig. 5.7).

In conclusion, this study utilized a HTS of a library of random small molecules combined with a structure-based *in silico* screen to identify novel ligands of the tick kinin receptor. We

validated 36 potential antagonists on the recombinant receptor using a dual-addition cell assay. This is the first reported HTS of a neuropeptide GPCR on any tick species. Three of the most potent small molecules with similar structure were tested on the recombinant mosquito orthologous receptor and in the mosquito hindgut contraction inhibition assay. For the first time, the hindgut contractile activity of the kinin analog 1728 was reported for mosquito. The antagonists identified in the HTS and validated in dose-response cellular assays also inhibited the myotropic effect of the potent kinin analog 1728. These antagonists are tools to study arthropod kinin signaling physiology and are potentially useful for novel approaches for pest control. This study also proved that the tick kinin receptor is a druggable target.

5.6. Acknowledgements

We thank Dr. James C. Sacchettini (TAMU) for providing small molecule libraries for high-throughput screening, Wen Dong for performing the cytotoxicity assay, and Dr. Nian Zhou for assistance in SAR analysis. We also thank Dr. M. Slotman (TAMU) for providing eggs of the *Aedes aegypti* Liverpool strain colony. The authors thank the Agriculture Women Excited to Share Opinions, Mentoring and Experiences (AWESOME) faculty group of the College of Agriculture and Life Sciences at Texas A&M University for assistance with editing the manuscript. Funding for this project was from NIFA-AFRI Animal Health and Well-Being Award 2016-67015-24918 to P.V. Pietrantonio and K. Temeyer, and from competitive funds from the Texas A&M AgriLife Research Insect Vector Diseases Grant Program (FY19-21) to PVP. NIFA also supports PVP program through Hatch project TX (TEX0-2-9206), accession 1002279 (Y 2018-2023).

5.7. References

Aggarwal, A., Parai, M.K., Shetty, N., Wallis, D., Woolhiser, L., Hastings, C., Dutta, N.K., Galaviz, S., Dhakal, R.C., Shrestha, R., 2017. Development of a novel lead that targets *M. tuberculosis* polyketide synthase 13. Cell 170(2), 249-259. e225.

Alford, L., Marley, R., Dornan, A., Dow, J.A., Nachman, R.J., Davies, S.A., 2019. Desiccation, thermal stress and associated mortality in *Drosophila* fruit flies induced by neuropeptide analogue treatment. Journal of Pest Science 92(3), 1123-1137.

Angus, B.M., 1996. The history of the cattle tick *Boophilus microplus* in Australia and achievements in its control. Int. J. Parasitol. 26(12), 1341-1355.

Audsley, N., Down, R.E., 2015. G protein coupled receptors as targets for next generation pesticides. Insect Biochem. Molec. 67(Supplement C), 27-37.

Bhatt, G., da Silva, R., Nachman, R.J., Orchard, I., 2014. The molecular characterization of the kinin transcript and the physiological effects of kinins in the blood-gorging insect, *Rhodnius prolixus*. Peptides 53, 148-158.

Bock, R.E., Jackson, L.A., de Vos, A.J., and Jorgensen, W.K., 2008. Babesiosis of cattle. Cambridge University Press.

Brock, C.M., Temeyer, K.B., Tidwell, J., Yang, Y., Blandon, M.A., Carreón-Camacho, D., Longnecker, M.T., Almazán, C., de León, A.A.P., Pietrantonio, P.V., 2019. The leucokinin-like peptide receptor from the cattle fever tick, *Rhipicephalus microplus*, is localized in the midgut periphery and receptor silencing with validated double-stranded RNAs causes a reproductive fitness cost. Int. J. Parasitol. 49(3-4), 287-299.

Clark, T.M., Hayes, T.K., Holman, G., Beyenbach, K.W., 1998. The concentration-dependence of CRF-like diuretic peptide: mechanisms of action. J. Exp. Biol. 201(11), 1753-1762.

Duvall, L.B., Ramos-Espiritu, L., Barsoum, K.E., Glickman, J.F., Vosshall, L.B., 2019. Small-molecule agonists of *Ae. aegypti* neuropeptide Y receptor block mosquito biting. Cell 176(4), 687-701. e685.

Ejendal, K.F.K., Meyer, J.M., Brust, T.F., Avramova, L.V., Hill, C.A., Watts, V.J., 2012. Discovery of antagonists of tick dopamine receptors via chemical library screening and comparative pharmacological analyses. Insect Biochem. Molec. 42(11), 846-853.

Harshini, S., Manchu, V., Sunitha, V., Sreekumar, S., Nachman, R., 2003. In vitro release of amylase by culekinins in two insects: *Opsinia arenosella* (Lepidoptera) and *Rhynchophorus ferrugineus* (Coleoptera). Trends in Life Sciences 17, 61-64.

Hauser, A.S., Attwood, M.M., Rask-Andersen, M., Schiöth, H.B., Gloriam, D.E., 2017. Trends in GPCR drug discovery: new agents, targets and indications. Nat. Rev. Drug Discov. 16, 829.

Hilger, D., Masureel, M., Kobilka, B.K., 2018. Structure and dynamics of GPCR signaling complexes. Nat. Struct. Mol. Biol. 25(1), 4-12.

Hohman, M., Gregory, K., Chibale, K., Smith, P.J., Ekins, S., Bunin, B., 2009. Novel web-based tools combining chemistry informatics, biology and social networks for drug discovery. Drug discovery today 14(5-6), 261-270.

Holman, G., Cook, B., Nachman, R., 1986. Isolation, primary structure and synthesis of two neuropeptides from *Leucophaea maderae*: members of a new family of cephalomyotropins. Comp. Biochem. Phys. C. 84(2), 205-211.

Holmes, S.P., Barhoumi, R., Nachman, R.J., Pietrantonio, P.V., 2003. Functional analysis of a G protein- coupled receptor from the Southern cattle tick *Boophilus microplus* (Acari:

Ixodidae) identifies it as the first arthropod myokinin receptor. Insect Mol. Biol. 12(1), 27-38.

Jagge, C.L., Pietrantonio, P.V., 2008. Diuretic hormone 44 receptor in Malpighian tubules of the mosquito *Aedes aegypti*: evidence for transcriptional regulation paralleling urination. Insect Mol. Biol 17(4), 413-426.

Jongejan, F., Uilenberg, G., 2004. The global importance of ticks. Parasitology 129(S1), S3-S14.

Kersch, C.N., Pietrantonio, P.V., 2011. Mosquito *Aedes aegypti* (L.) leucokinin receptor is critical for in vivo fluid excretion post blood feeding. FEBS Lett. 585(22), 3507-3512.

Kim, D.-H., Kim, Y.-J., Adams, M.E., 2018. Endocrine regulation of airway clearance in *Drosophila*. Proc. Natl. Acad. Sci., 201717257.

Kita, T., Hayashi, T., Ohtani, T., Takao, H., Takasu, H., Liu, G., Ohta, H., Ozoe, F., Ozoe, Y., 2017. Amitraz and its metabolite differentially activate α- and β- adrenergic- like octopamine receptors. Pest Manag. Sci. 73(5), 984-990.

Kwon, H., Agha, M.A., Smith, R.C., Nachman, R.J., Marion-Poll, F., Pietrantonio, P.V., 2016. Leucokinin mimetic elicits aversive behavior in mosquito *Aedes aegypti* (L.) and inhibits the sugar taste neuron. Proc. Natl. Acad. Sci. 113(25), 6880-6885.

Kwon, H., Pietrantonio, P.V., 2013. Calcitonin receptor 1 (AedaeGPCRCAL1) hindgut expression and direct role in myotropic action in females of the mosquito *Aedes aegypti* (L.). Insect Biochem. Molec. 43(7), 588-593.

Lipinski, C.A., 2016. Rule of five in 2015 and beyond: Target and ligand structural limitations, ligand chemistry structure and drug discovery project decisions. Adv. Drug. Deliver. Rev 101, 34-41.

Lu, H.L., Kersch, C.N., Taneja-Bageshwar, S., Pietrantonio, P.V., 2011. A calcium bioluminescence assay for functional analysis of mosquito (*Aedes aegypti*) and tick (*Rhipicephalus microplus*) G protein-coupled receptors. Jove-J Vis Exp(50).

Ma, Q., Ye, L., Liu, H., Shi, Y., Zhou, N., 2017. An overview of Ca2+ mobilization assays in GPCR drug discovery. Expert Opin. Drug Dis. 12(5), 511-523.

Madder, M., Thys, E., Achi, L., Touré, A., De Deken, R., 2011. *Rhipicephalus* (*Boophilus*) *microplus*: a most successful invasive tick species in West-Africa. Exp. Appl. Acarol. 53(2), 139-145.

Matthews, B.J., Dudchenko, O., Kingan, S.B., Koren, S., Antoshechkin, I., Crawford, J.E., Glassford, W.J., Herre, M., Redmond, S.N., Rose, N.H., 2018. Improved reference genome of *Aedes aegypti* informs arbovirus vector control. Nature 563(7732), 501-507.

Matthews, B.J., McBride, C.S., DeGennaro, M., Despo, O., Vosshall, L.B., 2016. The neurotranscriptome of the *Aedes aegypti* mosquito. BMC genomics 17(1), 1-20.

Nachman, R.J., Holman, G.M., 1991. Myotropic Insect Neuropeptide Families from the Cockroach *Leucophaea maderae*: Structure-Activity Relationships, in: Menn, J.J., Masler, Edward P. (Ed.) Insect neuropeptides: chemistry, biology, and action. American Chemical Society, Washington, D.C., pp. 194-214.

Nachman, R.J., Strey, A., Isaac, E., Pryor, N., Lopez, J.D., Deng, J.-G., Coast, G.M., 2002. Enhanced in vivo activity of peptidase-resistant analogs of the insect kinin neuropeptide family. Peptides 23(4), 735-745.

Odland, G.C., Jones, J.C., 1975. Contractions of the hindgut of adult *Aedes aegypti* with special reference to the development of a physiological saline. Ann. Entomol. Soc. Am. 68(4), 613-616.

Pietrantonio, P.V., Jagge, C., Taneja-Bageshwar, S., Nachman, R.J., Barhoumi, R., 2005. The mosquito *Aedes aegypti* (L.) leucokinin receptor is a multiligand receptor for the three Aedes kinins. Insect Mol. Biol. 14(1), 55-67.

Pietrantonio, P.V., Xiong, C., Nachman, R.J., Shen, Y., 2018. G protein-coupled receptors in arthropod vectors: Omics and pharmacological approaches to elucidate ligand-receptor interactions and novel organismal functions. Curr. Opin. Insect Sci. 29, 12-20.

Rodríguez-Vivas, R.I., Grisi, L., de León, A.A.P., Villela, H.S., de Jesús Torres-Acosta, J.F., Sánchez, H.F., Salas, D.R., Cruz, R.R., Saldierna, F., Carrasco, D.G., 2017. Potential economic impact assessment for cattle parasites in Mexico. Revista Mexicana de Ciencias Pecuarias 8(1), 61-74.

Rodriguez-Vivas, R.I., Jonsson, N.N., Bhushan, C., 2018. Strategies for the control of *Rhipicephalus microplus* ticks in a world of conventional acaricide and macrocyclic lactone resistance. Parasitol. Res. 117(1), 3-29.

Šimo, L., Park, Y., 2014. Neuropeptidergic control of the hindgut in the black-legged tick *Ixodes scapularis*. Int. J. Parasitol. 44(11), 819-826.

Taneja-Bageshwar, S., Strey, A., Isaac, R.E., Coast, G.M., Zubrzak, P., Pietrantonio, P.V., Nachman, R.J., 2009. Biostable agonists that match or exceed activity of native insect kinins on recombinant arthropod GPCRs. Gen. Comp. Endocrinol. 162(1), 122-128.

Taneja- Bageshwar, S., Strey, A., Zubrzak, P., Pietrantonio, P.V., Nachman, R.J., 2006. Comparative structure- activity analysis of insect kinin core analogs on recombinant kinin receptors from Southern cattle tick *Boophilus microplus* (Acari: Ixodidae) and mosquito *Aedes aegypti* (Diptera: Culicidae). Arch. Insect Biochem. 62(3), 128-140.

Thomas, D.B., Klafke, G., Busch, J.D., Olafson, P.U., Miller, R.A., Mosqueda, J., Stone, N.E., Scoles, G., Wagner, D.M., Perez-De-Leon, A., 2020. Tracking the increase of acaricide resistance in an invasive population of Cattle Fever Ticks (Acari: Ixodidae) and implementation of real-time PCR assays to rapidly genotype resistance mutations. Ann. Entomol. Soc. Am.

Thomsen, W., Frazer, J., Unett, D., 2005. Functional assays for screening GPCR targets. Current opinion in biotechnology 16(6), 655-665.

Veenstra, J.A., Pattillo, J.M., Petzel, D.H., 1997. A single cDNA encodes all three aedesleucokinins, which stimulate both fluid secretion by the malpighian tubules and hindgut contractions. J. Biol. Chem. 272(16), 10402-10407.

Xiong, C., Baker, D., Pietrantonio, P.V., 2019a. The cattle fever tick, *Rhipicephalus microplus*, as a model for forward pharmacology to elucidate kinin GPCR function in the Acari. Front. Physiol. 10, 1008.

Xiong, C., Kaczmarek, K., Zabrocki, J., Nachman, R.J., Pietrantonio, P.V., 2019b. Activity of native tick kinins and peptidomimetics on the cognate target G protein- coupled receptor from the cattle fever tick, *Rhipicephalus microplus* (Acari: Ixodidae). Pest Manag. Sci.

Xiong, C., Kaczmarek, K., Zabrocki, J., Pietrantonio, P.V., Nachman, R.J., 2019c. Evaluation of Aib and PEG-polymer insect kinin analogs on mosquito and tick GPCRs identifies potent new pest management tools with potentially enhanced biostability and bioavailability. Gen. Comp. Endocrinol. 278(1 July 2019), 58-67.

Zhang, J.-H., Chung, T.D., Oldenburg, K.R., 1999. A simple statistical parameter for use in evaluation and validation of high throughput screening assays. J. Biomol. Screen 4(2), 67-73.

6. CONCLUSIONS

This study improves the understanding of the tick kinin system. We identified novel ligands of the kinin receptor as tools for kinin physiological and endocrinological studies and promising lead molecules for pest control. Moreover, the methodologies we developed though this study including functional cellular assays, automation protocols for HTS and the hindgut contraction-inhibition bioassay are useful toward validating other arthropod neuropeptide GPCRs as targets for alternative pest management.

We cloned the first complete cDNA of the kinin neuropeptide precursor in tick species, and predicted and tested tick endogenous kinins on the cognate receptor. By predicting the endogenous kinins from eight tick species that are disease vectors, we found ticks have an expanded number of kinin paracopies in the kinin gene. Further analysis of the conserved sequence of the pentapeptide kinin active core (FX_1X_2WGa) revealed a predominant proline at the 2nd variable position of the tick kinin core (X_2), revealing an evolutionary difference between tick and insect kinins. Further comparative functional analysis of peptides with restricted conformational structures can provide insights into this selection. Site-directed mutagenesis analyses of the kinin receptors can be employed to reveal the amino acid sites that are important for the ligand-receptor interaction; however this methodology is not fully error proof as mutations may affect protein folding or receptor function unrelated to the ligand binding site.

Towards identifying and validating novel ligands on the kinin receptor we first chose the approach of designing novel kinin peptidomimetics based on the sequence of mosquito kinins, or that incorporated aminoisobutyric acid for protease resistance or polyethyleneglycol for enhanced cuticular penetration, or other modifications. Dr. Ronald Nachman designed and synthesized these molecules. This approach yielded several potent peptidomimetics with

enhanced biostability and bioavailability, and some showed equal or higher potency on the receptor than a previous potent kinin analog, 1728. Analog 1728 was known to elicit aversive sugar feeding behavior in the mosquito bioassay, as well as antifeedant or disruptive activity in aphids and kissing bug. Through the analyses of both potency and efficacy of these novel peptidomimetics, we identified three peptidomimetics with equal activity as 1728 on the mosquito receptor and three peptidomimetics that showed higher activity than 1728 on tick kinin receptor. These newly validated active peptidomimetics are useful tools for studying the kinin signaling system in vitro or in vivo, and potential lead compounds for pest control.

In searching for more stable and inexpensive ligands of the kinin receptor, we screened both a targeted commercial small molecule library and a random small molecule library. These efforts led to the identification of the first antagonist of the tick kinin receptor. Meanwhile, ligands for the human neurokinin receptor elicited low antagonistic response, which demonstrated the high selectivity of the invertebrate-specific kinin receptor. Furthermore, through HTS effort and the *in silico* screen of 390,000 molecules on the tick kinin receptor, we identified some potent antagonists with IC_{50}s between 0.67-10 μM. Their bioactivities were validated through a modified canonical hindgut contraction assay, in which the contractile activity induced by a kinin analog was inhibited by the small molecule antagonists. The *in tissue* antagonistic activity is significant as the antagonists were identified using recombinant mammalian cells. The mosquito hindgut contraction assay validated the antagonistic activity in arthropod cells.

This is the first HTS performed on the neuropeptide GPCRs of any tick species. It proves that the tick/arthropod kinin receptor is a druggable target. This is a proof-of-principle for ligand discovery of invertebrate neuropeptide GPCRs. The functional cellular assays and quality control

methodologies developed in this study provide valuable protocols for HTS for ligand discovery of arthropod neuropeptide GPCRs, especially for GPCRs using PLC-IP_3-Ca^{2+} signaling pathway. We validated many variances involving in each step of the HTS assay such as cell number in each well, FBS concentration in the cell medium and wash times, automation pipetting depth and speed, the concentration and final DMSO concentration of the screen compound, incubation time, and agonist peptide concentration and incubation time, as shown in Fig. 6.1.

Due to our lack of access to the *R. microplus* ticks in College Station because of the quarantine regulations, a limited number of tick bioassays with the identified antagonists could to be performed as they had to be performed at USDA-Cattle Fever Tick Research Laboratory in Edinburg, TX. The planned tick bioassays with peptidomimetics were interrupted first by the Government shut-down in 2019 and those with small molecules by the unexpected COVID-19 situation after March 2020. The small molecule antagonists identified were therefore, alternatively, tested in the mosquito hindgut bioassay. Further tick bioassays with larvae and adults and testing different solvents will be necessary to fully validate the activity of these molecules.

The exact physiological function of kinin in ticks remains unknown. Biological assays with the novel ligands we identified in this study will help address this question. Furthermore, the releasing sites of kinin peptide in ticks are not completely clear. In insect, kinins are produced by cells in the CNS as well as in the periphery organs. Immunolocalization of kinins on different tick tissues can provide a comprehensive picture of kinin producing and releasing sites. It will also be worth investigating the physiological relevance of the expanded kinin paracopies in the kinin gene we found through this study, such as by measuring the fluctuations of kinin concentration at different physiological status. Towards converting our findings into pest control

applications, more works will need to be done to test the pesticidal effect of the novel ligands. Modeling of ligand-receptor interactions using structure of identified ligand as inputs will contribute to designing of more potent ligands.

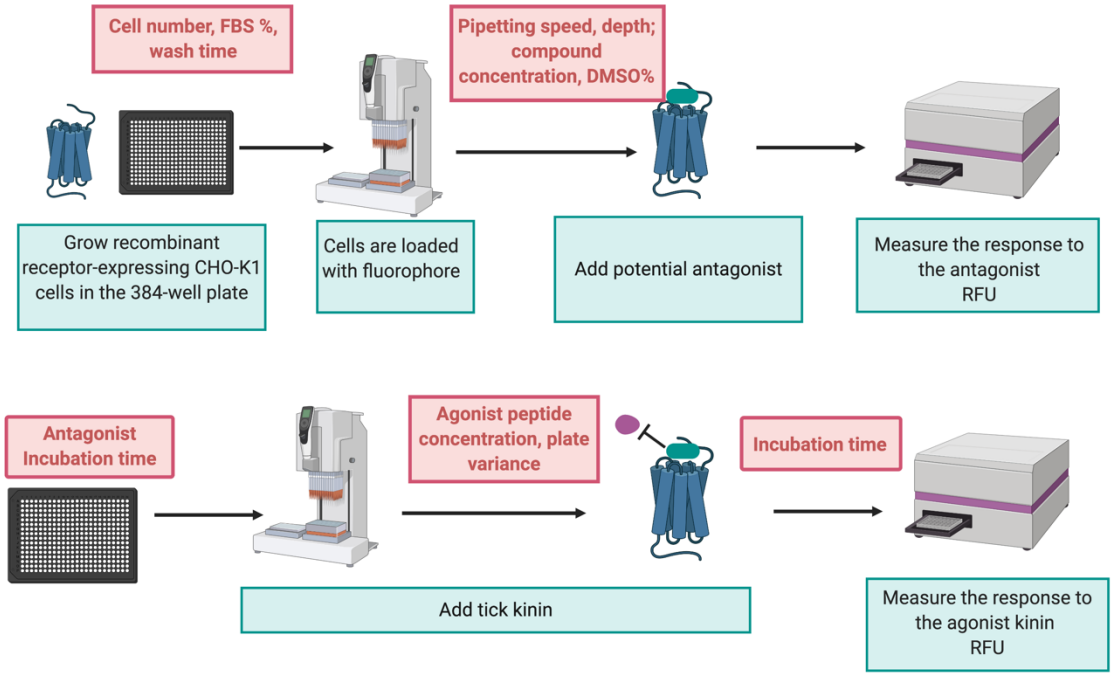

Figure 6.1 Summary of the high-throughput screening (HTS) assay valiation parameters. The green boxes indicate the process of HTS assay, and red boxes indicate the variances that were validated or optimized for HTS. Created with BioRender.com.

APPENDIX A

FOR CHAPTER 2

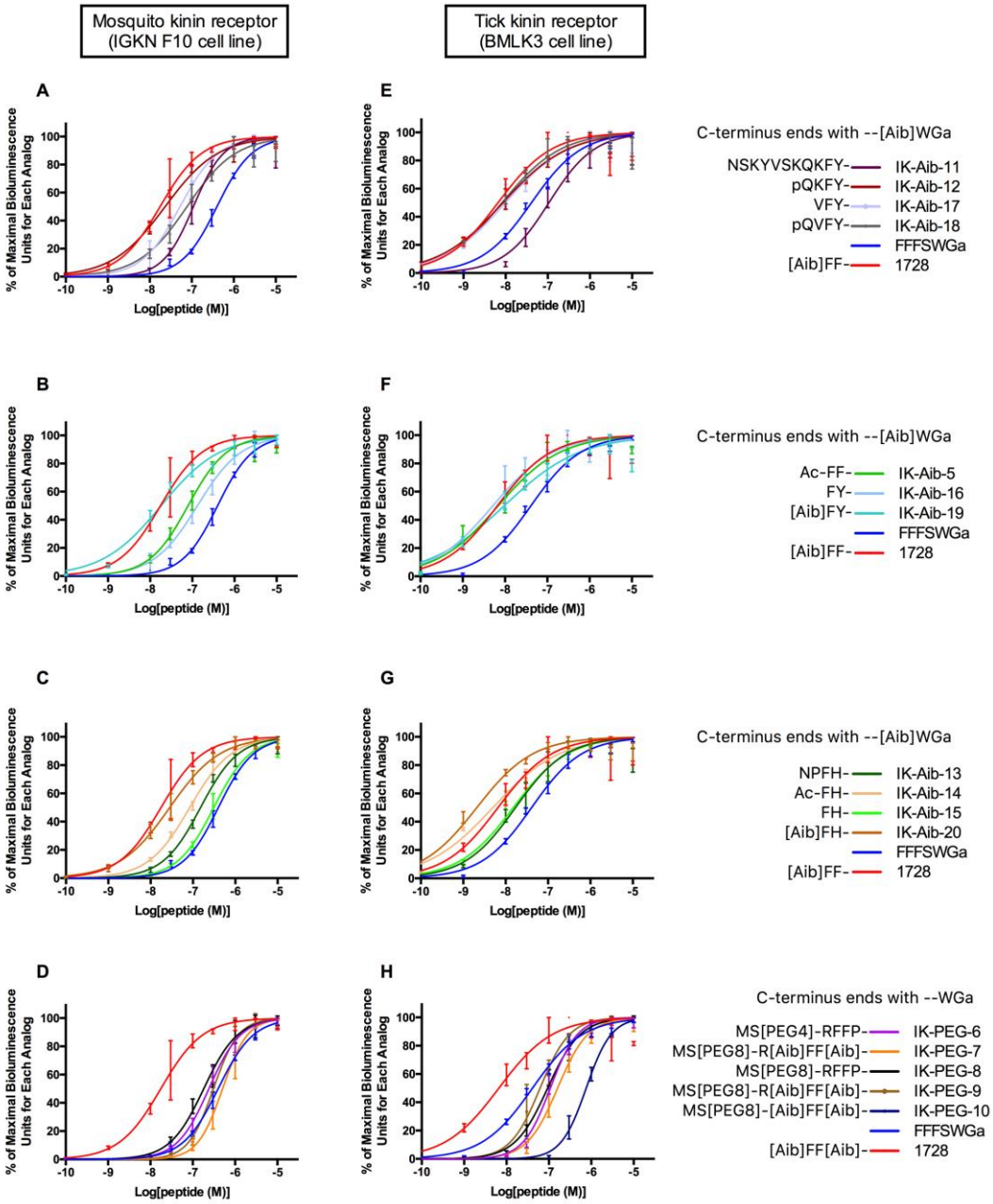

Supplementary Figure 2.1 Dose-dependent responses and relative potency (EC_{50} determination): mosquito (**A-D**) and tick (**E-H**) recombinant kinin receptors expressed in CHO-K1 cells were tested against 17- and 18- insect kinin analogs, respectively. Each analog was tested at nine concentrations from 10^{-10}-10^{-5} M (Log.[M] on X-axis) using a calcium bioluminescence assay (the IK-PEG-10 analog was not active on mosquito receptor). The Y-axis represents the percentage of bioluminescence response (average bioluminescence units of three replicates elicited during 30s after analog application) observed at each concentration as a percentage of the maximal response (100%) observed among all concentrations tested for each analog (Mean ± SEM). Three replicates were performed for all analogs except for analog 1728

(n=2). Blank buffer was injected as control for cells bioluminescence background, each bioluminescence response was subtracted by the response to this blank buffer application. Dose-response curves were generated with "non-linear regression log[agonist M] vs. normalized response - variable slope function with GraphPad GraphPad Prism 6.0 (GraphPad Software, La Jolla, CA) and used to calculate the EC_{50} as the concentration (Log EC_{50}, X axis) that elicited 50% (Y axis) of the maximal response (see Table 1). Each of the eight panels shows receptor responses to a group of analogs of similar design; their complete sequence is shown in Table 1. Each panel figure legend highlights analogs' features. **A)** and **E)**: endogenous sequence of either aedeskinin-1 or -3. **B)** and **F)**: endogenous sequence of both aedeskinin-1 and -3. **C)** and **G)**: endogenous sequence of aedeskinin-2. **D)** and **H)**: polyethylene glycol (PEG) modified-analogs. The dose-response curves for FFFSWGa (positive control) and 1728 ([Aib]FF[Aib]WGa, a potent [Aib] agonist) were included in each figure for comparison.

Supplementary Table 2.1.1 Statistical analysis of analogs' potency on recombinant mosquito *Aedes aegypti* kinin receptor.
One-way ANOVA was performed to compare the potency (Log.EC_{50}) on the mosquito kinin receptor of 17 insect kinin (IK) analogs (F = 91.09; P<0.0001). Three replicates were performed for all analogs except for analog 1728 (n=2). ANOVA was followed by Tukey multiple comparison test of means (****P<0.0001). PC = Positive control kinin peptide. FFFSWGa. 1728 = a potent kinin Aib-containing analog.

Mosquito Kinin Receptor (IGKN F10 cell line)		Log.EC_{50}	1728	IK-AIB-19	IK-AIB-12	IK-AIB-20	IK-AIB-17	IK-AIB-18	IK-AIB-5	IK-AIB-14	IK-AIB-11	IK-AIB-16	IK-AIB-13	IK-PEG-8	IK-PEG-6	IK-PEG-9	IK-AIB-15	PC	IK-PEG-7
IK analogs ranked by log.EC_{50}[1]																			
[Aib]FF[Aib]WGa	**1728**	-7.75	-																
[Aib]FY[Aib]WGa	IK-AIB-19	-7.74	ns	-															
pQKFY[Aib]WGa	IK-AIB-12	-7.63	ns	ns	-														
[Aib]FH[Aib]WGa	IK-AIB-20	-7.55	ns	ns	ns	-													
VFY[Aib]WGa	IK-AIB-17	-7.28	****	****	***	*	-												
pQVFY[Aib]WGa	IK-AIB-18	-7.11	****	****	****	****	ns	-											
Ac-FF[Aib]WGa	IK-AIB-5	-7.1	****	****	****	****	ns	ns	-										
Ac-FH[Aib]WGa	IK-AIB-14	-7.08	****	****	****	****	ns	ns	ns	-									
NSKYVSKQKFY[Aib]WGa	IK-AIB-11	-6.96	****	****	****	****	**	ns	ns	ns	-								
FY[Aib]WGa	IK-AIB-16	-6.88	****	****	****	****	***	ns	ns	ns	ns	-							
NPFH[Aib]WGa	IK-AIB-13	-6.82	****	****	****	****	****	*	*	*	ns	ns	-						
MS[PEG8]-RFFPWGa	IK-PEG-8	-6.74	****	****	****	****	****	***	***	**	ns	ns	ns	-					
MS[PEG4]-RFFPWGa	IK-PEG-6	-6.62	****	****	****	****	****	****	****	****	**	*	ns	ns	-				
MS[PEG8]-R[Aib]FF[Aib]WGa	IK-PEG-9	-6.51	****	****	****	****	****	****	****	****	****	***	**	ns	ns	-			
FH[Aib]WGa	IK-AIB-15	-6.51	****	****	****	****	****	****	****	****	****	***	**	ns	ns	ns	-		
FFFSWGa	**PC**	-6.4	****	****	****	****	****	****	****	****	****	****	****	**	ns	ns	ns	-	
MS[PEG4]-R[Aib]FF[Aib]WGa	IK-PEG-7	-6.3	****	****	****	****	****	****	****	****	****	****	****	****	**	ns	ns	ns	-

[1]EC_{50} values were calculated for each analog individually as the concentration that elicited 50% of the highest number of bioluminescence units for that analog (100%) (Table 1.). This maximum bioluminescence may or not correspond to the highest concentration tested; for a few analogs the highest concentration elicited a lower number of bioluminescence units possibly due to receptor internalization.

Supplementary Table 2.1.2 Statistical analysis of efficacy on recombinant mosquito *Aedes aegypti* kinin receptor.
One-way ANOVA was performed to compare the efficacy[1] on the tick kinin receptor of 18 insect kinin analogs (IK) (F= 15.32; P<0.0001). Three replicates were performed for all analogs except for analog 1728 (n=2). ANOVA was followed by Tukey multiple comparison test of means (****P<0.0001). PC= Positive control kinin peptide FFFSWGa. 1728= a potent kinin Aib-containing analog.

Mosquito Kinin Receptor (IGKN F10 cell line)		IK-AIB-19		IK-AIB-5	IK-AIB-18	IK-AIB-12	IK-AIB-17	IK-AIB-20	IK-AIB-11	IK-AIB-13	IK-AIB-16		IK-PEG-8	IK-PEG-6	IK-AIB-14	IK-PEG-7	IK-PEG-9	IK-AIB-15
(Ranked by binding efficay[1])			**1728**									**PC**						
[Aib]FF[Aib]WGa	IK-AIB-19	-																
[Aib]FY[Aib]WGa	**1728**	ns	-															
Ac-FF[Aib]WGa	IK-AIB-5	ns	ns	-														
pQVFY[Aib]WGa	IK-AIB-18	ns	ns	ns	-													
pQKFY[Aib]WGa	IK-AIB-12	ns	ns	ns	ns	-												
VFY[Aib]WGa	IK-AIB-17	ns	ns	ns	ns	ns	-											
[Aib]FH[Aib]WGa	IK-AIB-20	ns	ns	ns	ns	ns	ns	-										
NSKYVSKQKFY[Aib]WGa	IK-AIB-11	ns	ns	ns	ns	ns	ns	ns	-									
NPFH[Aib]WGa	IK-AIB-13	ns	ns	ns	ns	ns	ns	ns	ns	-								
FY[Aib]WGa	IK-AIB-16	ns	ns	ns	ns	ns	ns	ns	ns	ns	-							
FFFSWGa	**PC**	*	ns	ns	ns	ns	ns	ns	ns	ns	ns	-						
MS[PEG8]-RFFPWGa	IK-PEG-8	*	*	ns	ns	ns	ns	ns	ns	ns	ns	ns	-					
MS[PEG4]-RFFPWGa	IK-PEG-6	*	*	ns	ns	ns	ns	ns	ns	ns	ns	ns	ns	-				
Ac-FH[Aib]WGa	IK-AIB-14	**	*	*	ns	ns	ns	ns	ns	ns	ns	ns	ns	ns	-			
MS[PEG4]-R[Aib]FF[Aib]WGa	IK-PEG-7	***	***	***	**	**	**	**	*	ns	ns	ns	ns	ns	ns	-		
MS[PEG8]-R[Aib]FF[Aib]WGa	IK-PEG-9	****	***	***	***	**	**	**	**	ns	ns	ns	ns	ns	ns	ns	-	
FH[Aib]WGa	IK-AIB-15	****	***	***	***	**	**	**	**	ns	ns	ns	ns	ns	ns	ns	ns	-

[1]Efficacy was calculated as percentage of the bioluminescence response (average bioluminescence units elicited during 30s; this is the area under the "bioluminescence vs. time" response curve) of each analog tested at 1µM concentration, with reference to the bioluminescence response elicited by 1µM of analog FFFSWGa (PC).

Supplementary Table 2.2.1 Statistical analysis of analogs' potency on recombinant tick *Rhipicephalus microplus* kinin receptor.
One-way ANOVA was performed to compare the potency (Log.EC_{50}) on the tick kinin receptor of 18 insec kinin (IK) analogs (F = 78.08; P<0.0001). Three replicates were performed for all analogs except for analog 1728 (n=2). ANOVA was followed by Tukey multiple comparison test of means (****P<0.0001). PC= Positive control kinin peptide FFFSWGa. 1728= a potent kinin Aib-containing analog.

Tick Kinin Receptor (BMLK3 cell line) Kinin analogs ranked by log.EC_{50}[1]		Log.EC_{50}	IK-AIB-20	IK-AIB-14	IK-AIB-16	1728	IK-AIB-5	IK-AIB-18	IK-AIB-12	IK-AIB-19	IK-AIB-17	IK-AIB-15	IK-AIB-13	PC	IK-PEG-9	IK-PEG-8	IK-AIB-11	IK-PEG-6	IK-PEG-7	IK-PEG-10
[Aib]FH[Aib]WGa	IK-AIB-20	-8.68	-																	
Ac-FH[Aib]WGa	IK-AIB-14	-8.3	ns	-																
FY[Aib]Wga	IK-AIB-16	-8.29	ns	ns	-															
[Aib]FF[Aib]WGa	**1728**	-8.18	****	ns	ns	-														
Ac-FF[Aib]WGa	IK-AIB-5	-8.16	****	ns	ns	ns	-													
pQVFY[Aib]WGa	IK-AIB-18	-8.08	****	ns	ns	ns	ns	-												
pQKFY[Aib]WGa	IK-AIB-12	-8.06	****	ns	ns	ns	ns	ns	-											
[Aib]FY[Aib]WGa	IK-AIB-19	-8.02	****	ns	ns	ns	ns	ns	ns	-										
VFY[Aib]WGa	IK-AIB-17	-8	****	ns	ns	ns	ns	ns	ns	ns	-									
FH[Aib]WGa	IK-AIB-15	-7.82	****	**	*	ns	ns	ns	ns	ns	ns	-								
NPFH[Aib]WGa	IK-AIB-13	-7.77	****	**	**	ns	ns	ns	ns	ns	ns	ns	-							
FFFSWGa	**PC**	-7.39	****	****	****	****	****	****	****	***	***	*	ns	-						
MS[PEG8]-R[Aib]FF[Aib]WGa	IK-PEG-9	-7.21	****	****	****	****	****	****	****	****	****	***	***	ns	-					
MS[PEG8]-RFFPWGa	IK-PEG-8	-7.03	****	****	****	****	****	****	****	****	****	****	****	ns	ns	-				
NSKYVSKQKFY[Aib]WGa	IK-AIB-11	-6.97	****	****	****	****	****	****	****	****	****	****	****	*	ns	ns	-			
MS[PEG4]-RFFPWGa	IK-PEG-6	-6.97	****	****	****	****	****	****	****	****	****	****	****	*	ns	ns	ns	-		
MS[PEG4]-R[Aib]FF[Aib]WGa	IK-PEG-7	-6.8	****	****	****	****	****	****	****	****	****	****	****	***	*	ns	ns	ns	-	
MS[PEG8]-[Aib]FF[Aib]WGa	IK-PEG-10	-6.12	****	****	****	****	****	****	****	****	****	****	****	****	****	****	****	****	****	-

[1]EC_{50} values were calculated for each analog individually as the concentration that elicited 50% of the highest number of bioluminescence units for that analog (100%). This maximum bioluminescence may or not correspond to the highest concentration tested; for a few analogs the highest concentration elicited a lower number of bioluminescence units possibly due to receptor internalization.

Supplementary Table 2.2.2 Statistical analysis of efficacy on recombinant tick *Rhipicephalus microplus* kinin receptor.
One-way ANOVA was performed to compare the efficacy[1] on the tick kinin receptor of 18 insect kinin (IK) analogs (F= 5.747; P<0.0001). Three replicates were performed for all analogs except for analog 1728 (n=2). ANOVA was followed by Tukey multiple comparison test of means (****P<0.0001). PC= Positive control kinin peptide FFFSWGa. 1728= a potent kinin Aib analog.

Tick Kinin Receptor (BMLK3 cell line)		IK-AIB-5	IK-AIB-19	IK-AIB-18	IK-AIB-14	IK-AIB-16	IK-AIB-20	IK-AIB-13	IK-AIB-17	IK-AIB-12	**1728**	IK-AIB-15	**PC**	IK-PEG-8	IK-PEG-7	IK-PEG-6	IK-PEG-9	IK-AIB-11	IK-PEG-10
Kinin analogs ranked by binding efficay[1]																			
Ac-FF[Aib]WGa	IK-AIB-5	-																	
[Aib]FY[Aib]WGa	IK-AIB-19	ns	-																
pQVFY[Aib]WGa	IK-AIB-18	ns	ns	-															
Ac-FH[Aib]WGa	IK-AIB-14	ns	ns	ns	-														
FY[Aib]WGa	IK-AIB-16	ns	ns	ns	ns	-													
[Aib]FH[Aib]WGa	IK-AIB-20	ns	ns	ns	ns	ns	-												
NPFH[Aib]WGa	IK-AIB-13	ns	ns	ns	ns	ns	ns	-											
VFY[Aib]WGa	IK-AIB-17	ns	ns	ns	ns	ns	ns	ns	-										
pQKFY[Aib]WGa	IK-AIB-12	ns	ns	ns	ns	ns	ns	ns	ns	-									
[Aib]FF[Aib]WGa	**1728**	ns	ns	ns	ns	ns	ns	ns	ns	ns	-								
FH[Aib]WGa	IK-AIB-15	ns	ns	ns	ns	ns	ns	ns	ns	ns	ns	-							
FFFSWGa	**PC**	ns	ns	ns	ns	ns	ns	ns	ns	ns	ns	ns	-						
MS[PEG8]-RFFPWGa	IK-PEG-8	ns	ns	ns	ns	ns	ns	ns	ns	ns	ns	ns	ns	-					
MS[PEG4]-R[Aib]FF[Aib]WGa	IK-PEG-7	*	ns	ns	ns	ns	ns	ns	ns	ns	ns	ns	ns	ns	-				
MS[PEG4]-RFFPWGa	IK-PEG-6	*	ns	ns	ns	ns	ns	ns	ns	ns	ns	ns	ns	ns	ns	-			
MS[PEG8]-R[Aib]FF[Aib]WGa	IK-PEG-9	**	*	ns	ns	ns	ns	ns	ns	ns	ns	ns	ns	ns	ns	ns	-		
NSKYVSKQKFY[Aib]WGa	IK-AIB-11	**	*	*	ns	ns	ns	ns	ns	ns	ns	ns	ns	ns	ns	ns	ns	-	
MS[PEG8]-[Aib]FF[Aib]WGa	IK-PEG-10	****	****	***	**	**	**	**	**	**	*	*	*	ns	ns	ns	ns	ns	-

[1]Efficacy was calculated as percentage of the bioluminescence response (average bioluminescence units elicited during 30s; this is the area under the "bioluminescence vs. time" response curve) of each analog tested at 1µM concentration, with reference to the bioluminescence response elicited by 1µM of analog FFFSWGa (PC).

APPENDIX B

FOR CHAPTER 3

A. The putative full-length kinin precursor cDNA

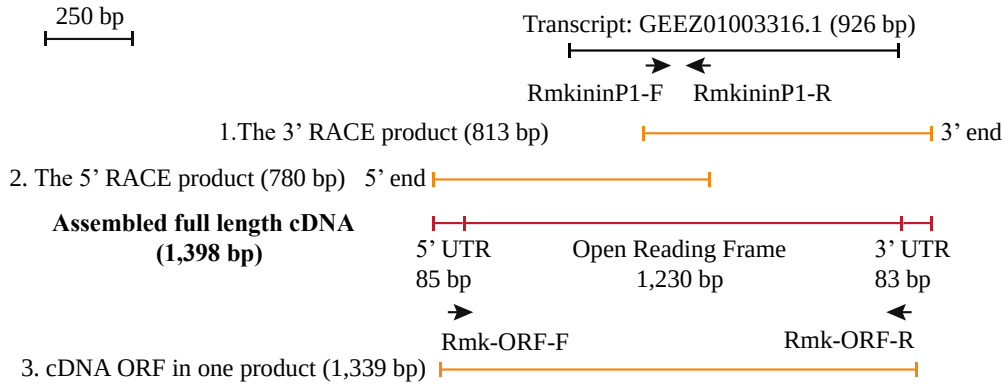

B. Amplification of the kinin gene from gDNA

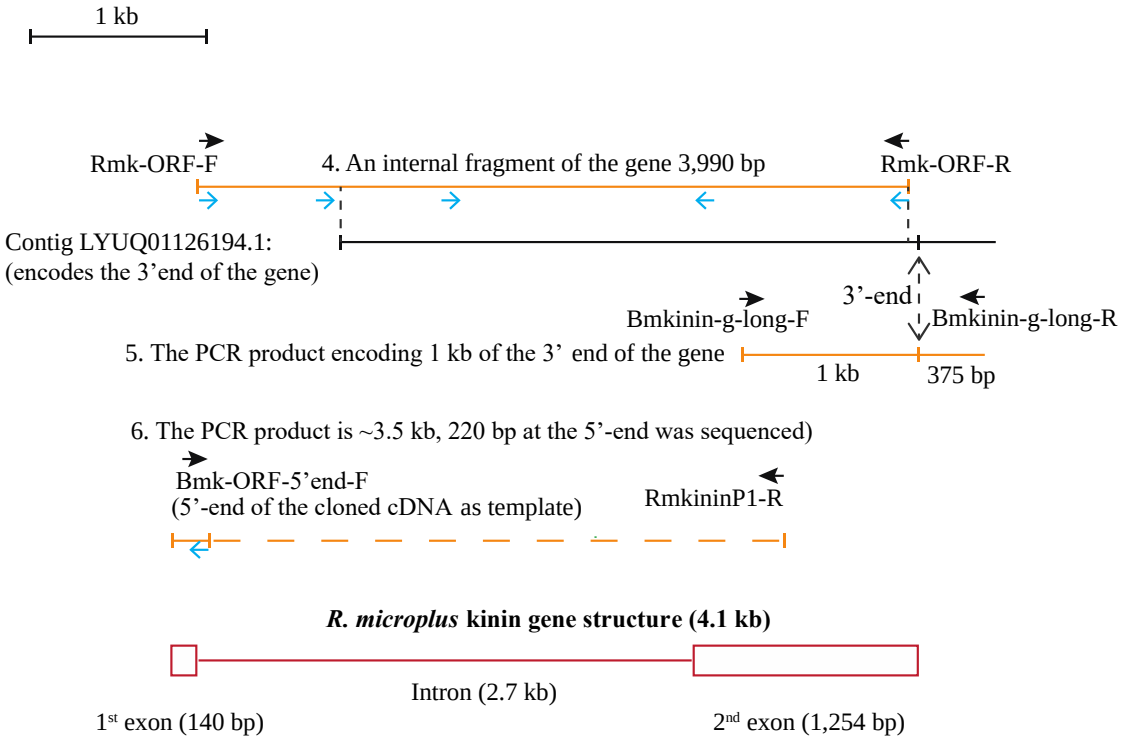

Supplementary Figure 3.1 The workflow for cloning the putative kinin precursor cDNA from *Rhipicephalus microplus* and verification of the gene structure by sequencing genomic PCR products.

In this figure, within the panels A and B, all lines representing sequences are aligned vertically to the corresponding sequence location. Notice a different scale in bp on the left of each panel. The solid black lines represent either transcriptome (A) or genomic (B) sequences identified through local NCBI BLAST using the putative kinin precursor (amino acid sequence) from *Ixodes scapularis* as query. The black arrows denote the direction and relative location of the primers on the template above the primers. The solid orange lines depict the sequenced PCR products obtained in this study. Red lines and boxes represent the deduced full-length cDNA (A) or the kinin gene (B) obtained by assembling the sequenced PCR products.
The blue arrows denote the position of primers used for sequencing. The dashed orange line depicts the region of a PCR product which was not sequenced (sequencing was not necessary because the overlapping sequence of ~200 bp at the 5' end was enough to align this product with the PCR product in reaction 4 above). **(A) The putative full-length kinin precursor cDNA from *R. microplus***: Cloning of 5'- and 3'- RACE PCR products. 1-2). A transcript predicted to encode a partial sequence of the putative kinin precursor was used to design a pair of gene-specific primers for the 3'- and 5'- RACE PCRs. The sequences of these 3'- and 5'- RACE PCR products (1-2) were aligned with DNASTAR (Lasergene, Madision, WI) to assemble the full-length cDNA. (3). A pair of primers was designed outside of the open reading frame (ORF) and were used to amplify the cDNA ORF in one product. **(B) Amplification of the kinin gene from genomic DNA.** (4). First, we amplified an internal fragment of the gene with a pair of gene-specific primers. (5). Secondly, the 3'-end of the kinin gene was amplified with a gene-specific forward primer and a reverse primer located outside of the ORF 3'-end. The sequence of this latter reverse primer was obtained from a genomic contig encoding the 3'-end fragment of the kinin gene (black line). (6). The 5'-end of the kinin gene was amplified using a forward primer which binds to the 5'-end of the cDNA, and with a reverse primer within the ORF. The DNA sequences from the PCR products above (4-6) were aligned with DNASTAR to obtain the sequence of the kinin gene shown in red: boxes represent exons, and the solid line represents the intronic region. The exons were identified by aligning the cDNA sequence with the gene sequence.

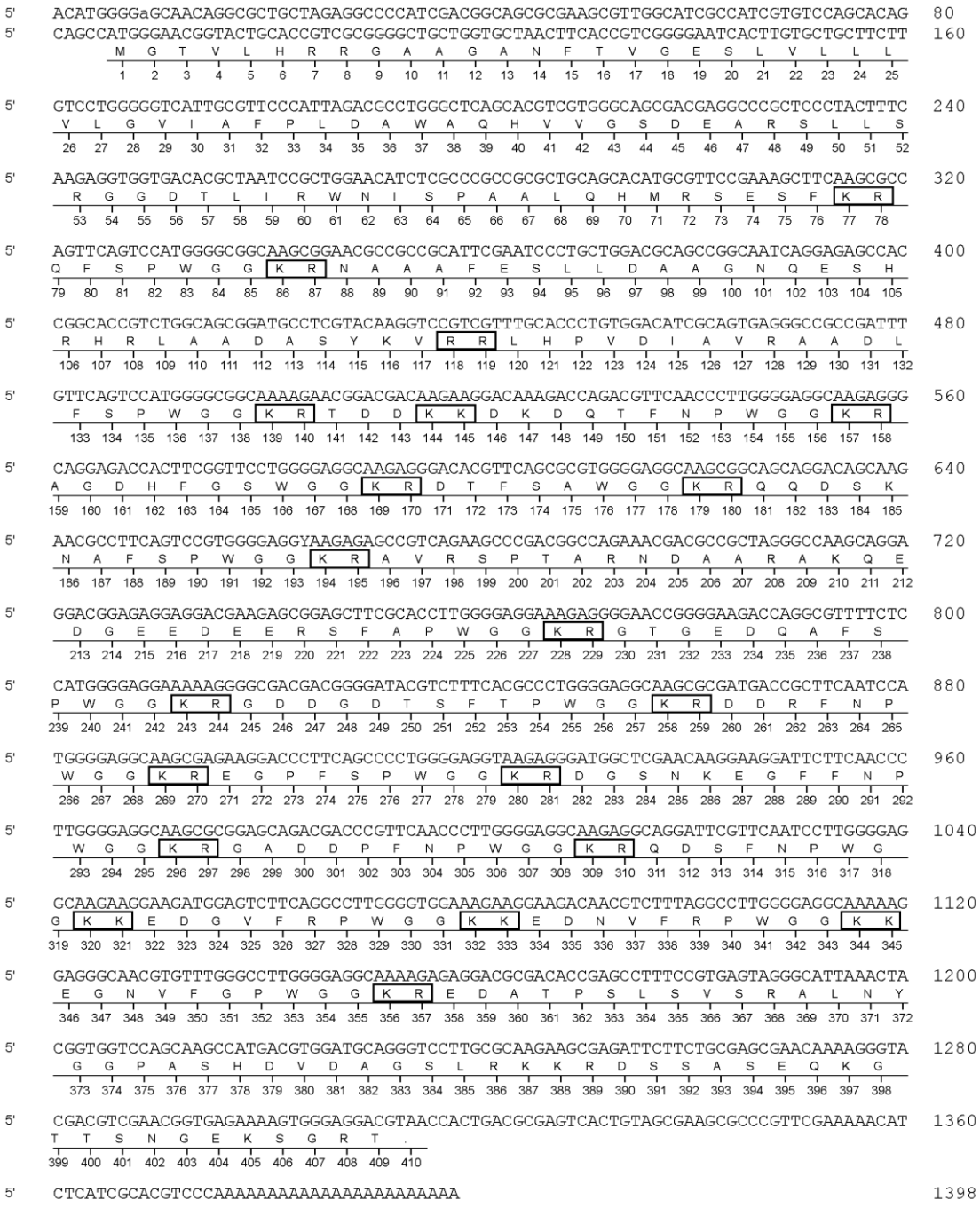

Supplementary Figure 3.2 Cloned cDNA sequence and predicted amino acid sequence of putative kinin precursor from *Rhipicephalus (Boophilus) microplus.*

The full-length cDNA sequence is 1,398 bp, with 1,227 bp ORF that encodes a 409 amino acid residue protein. The predicted enzyme cleavage sites are boxed. Seventeen kinin sequences were predicted. See Fig. 3.

```
Majority            ----LRXR-AXX---------XXXLXX----MSXXXLXQXVXXSDGDXXXXSRXGDXXIRWNISPATLQHMRS--ESFKR
                                10        20        30        40        50        60        70        80
O.turicata          --MAPAARSSQT---------FCTLRYLILSISLLASYASVEESDGDSRDDDSFEDMVIRWNISPDTLQRLRARREAIAR 69
H.dromedarii        ------------------------------------------------------------------MRS--ESFKR 8
D.variabilis        ------------------------------------------------------------------MRS--ESFKR 8
A.sculptum          MG--LRRRAAAG------ETLLLRVFLVASVLSLDVSAQHMVGSDEARSLLSRGGDTLIRWNISPATLQHMRS--ESFKR 70
R.sanguineus        MGTVLRRRGAAGANFAVGETLMLQLLLVVIAFSSDAWAQHVVGSDEARSLLSRGGDTLIRWNISPAALQHMRS--ENFKR 78
R.microplus         MGTVLHRRGAAGANFTVGESLVLLLVLGVIAFPLDAWAQHVVGSDEARSLLSRGGDTLIRWNISPAALQHMRS--ESFKR 78
Ix.ricinus          --MELRGHDAQELR------FLWTLLATTFLMSMGGLCQDVDSGSGDLGRSSRVGESFIRWNISPATLQHMRS--ESFKR 70
Ix.scapularis-mRNA  --MELRGHDAQELR------FLWTLLATTFLMSMGGLCQDVDSGSGDLGRSSRVGESFIRWNISPATLQHMRS--ESFKR 70
Ix.scapularis-gDNA  ----------------------------MSMGGLCQDVDSGSGDLGRSSRVGESFIRWNISPATLQHMRS--ESFKR 47

Majority            QFSP-WGGKRN-AAXDSLLDXAGXQXSXRHLLAADASYKVRRLHXGD-QPRD-DSFNPWGGKRXXDK-------------
                            90        100       110       120       130       140       150       160
O.turicata          PFVPRWGNQIQG---DAAVGKPYGN-----------YRDVWIYGK----KD--------------------------- 102
H.dromedarii        QFSP-WGGKRNAALLESLLDSPGNQESRRHHLAADASYKVRRLHPA--GVRDADSFNPWGGKRTDDKKDKDQTFNPWGGK 85
D.variabilis        QFSP-WGGKRNTAAFESLLDSPGDQQSHRHQLAADASYKVRRLHHTG-SPRNADSFS-----------------P---- 64
A.sculptum          QFSP-WGGKRN-AAFDYLLDAPGGD--H-QVADAASSYKVRRVHHTP-SLRN--------------------------- 116
R.sanguineus        QFSP-WGGKRNTAAFESLLDSAGNQESRRHHLAADASYKVRRLHPASIGVRDADSFSPWGGKRTDDKKDKDQTFNPWGGK 157
R.microplus         QFSP-WGGKRNAAAFESLLDAAGNQESHRHRLAADASYKVRRLHPVDIAVRAADLFSPWGGKRTDDKKDKDQTFNPWGGK 157
Ix.ricinus          QFSP-WGGKRG--VLDQALPTAHRLSGPLYLYKALHSPGAMGERRGDKQPDD-ETFNPWGGKRENDK------------ 133
Ix.scapularis-mRNA  QFSP-WGGKRG--VLDQALPTAHRLSGPLYLYKALHSPRAMGERRGDKQPDD-EAFNPWGGKRENDK------------ 133
Ix.scapularis-gDNA  QFSP-WGGKRG--VLDQALPTAHRLSGPLYLYKALHSPRAMGERRGDKQPED-EAFNPWGGKRENDK------------ 110

Majority            ------------------------------------------------------------DXERSFAPWGGKRG----
                            170       180       190       200       210       220       230       240
O.turicata          ------------------------------------------------------------AHFNPWGGKRDGTHT 117
H.dromedarii        R-----------------------------------------------DSVRVKQEDGEEDEERSFAPWGGKRG---- 112
D.variabilis        ------------------------------------------------------------ERSFAPWGGKRG---- 76
A.sculptum          ------------------------------------------------------------VFAPWGGKR----- 125
R.sanguineus        RAAAGDRFGSWGGKRETFNAWGGKRQQD-KNSFSPWGGKRAVRSPTARNEDAARARQDDGEEDEERSFAPWGGKRG---- 232
R.microplus         R--AGDHFGSWGGKRDTFSAWGGKRQQDSKNAFSPWGGKRAVRSPTARN-DAARAKQEDGEEDEERSFAPWGGKRG---- 230
Ix.ricinus          ------------------------------------------------------------DKELSFNPWGGKRGTFSS 151
Ix.scapularis-mRNA  ------------------------------------------------------------DKELSFNPWGGKRGSFSS 151
Ix.scapularis-gDNA  ------------------------------------------------------------DKELSFNPWGGKRGSFSS 128

Majority            -XGEDXAFS-----------------------------PWGGKRXDDGD-----TXFXPWGGKREDR---FNPWGGKRE
                            250       260       270       280       290       300       310       320
O.turicata          RSGLDDSSG-----------------------------SWSEKK----D------NFNPWGGKKEAS---FNPWGGKRD 154
H.dromedarii        -AGEDQAFS-----------------------------PWGGKKRDDGD-----TSFAPWGGKREDR---FNPWGGKRE 153
D.variabilis        -AAEDQAFS-----------------------------PWGGKRDSEED-----TSFAPLGGKREDR---FNPWGGKRE 117
A.sculptum          -AAEDRAFS-----------------------------PWGGKRGGDGDGG---ETFAPWGGKREDR---FNPWGGKRE 168
R.sanguineus        -TGEDQAFS-----------------------------PWGGKRGDDGD-----TSFTPWGGKREDR---FNPWGGKRE 273
R.microplus         -TGEDQAFS-----------------------------PWGGKRGDDGD-----TSFTPWGGKRDDR---FNPWGGKRE 271
Ix.ricinus          WGGKRDTFG-----------------------------PWGGKRDTFGAWGGKRDTFGPWGGKRQDKESGFNPWGGKRE 201
Ix.scapularis-mRNA  WGGKRDTFG-----------------------------PWGG----------KRDTFGPWGGKRQDKESGFNPWGGKRE 191
Ix.scapularis-gDNA  WGGKRDTFGSWGGKRDTFGPWGGKRDTFGPWGGKRDTFGPWGGKRDTFGPWGGKRDTFGPWGGKRQDKESGFNPWGGKRE 208

Majority            GPFNPWGGKRE--------GSNKEGFFNPWGGKRGADDS-FNPWGGKR-------EDSFNPWGGKXX--XDTAFXPWGGK
                            330       340       350       360       370       380       390       400
O.turicata          N-FNPWGGKKD-------------NFNPWGGKK--DSSIFNPWGGKRSDGSKDKELSFNPWGGKRQDGVGTIFGPWGGK 217
H.dromedarii        GPFNPWGGKRD--------GSNKEGFFNPWGGKRGADDS-FNPWGGKRG-----ADDSFNPWGGKR---QD-SFNPWGGK 215
D.variabilis        GPFNPWGGKRE--------GSNKEGFFNPWGGKRGADDS-FNPWGGKR-------QDSFNPWGGKR---ESGVFRPWGGK 178
A.sculptum          GPFNPWGGKRE--------GSNKEGFFNPWGGKRGADDS-FNPWGGKRG-----ADDAFNPWGGKGG--ADAAFNPWGGK 232
R.sanguineus        GPFNPWGGKRD--------GSNKEGFFNPWGGKRGADDS-FNPWGGKR-------QDSFNPWGGKR---EDGVFRPWGGK 334
R.microplus         GPFSPWGGKRD--------GSNKEGFFNPWGGKRGADDP-FNPWGGKR-------QDSFNPWGGKK---EDGVFRPWGGK 332
Ix.ricinus          DPFNPWGGKKEDKNAFSPWGGKREQNFNPWGGKKTSKDSTFSPWGGKR-------EGPFNPWGGKKGD-SDTAFAPWGGK 273
Ix.scapularis-mRNA  DPFNPWGGKKEDKNAFSPWGGKREQNFNPWGGKKTTKDSTFSPWGGKR-------EGPFNPWGGKKGD-SDTAFAPWGGK 263
Ix.scapularis-gDNA  DPFNPWGGKKEDKNAFSPWGGKRDQNFNPWGGKKTTKDSTFSPWGGKR-------EGPFNPWGGKKGD-SDTAFAPWGGK 280
```

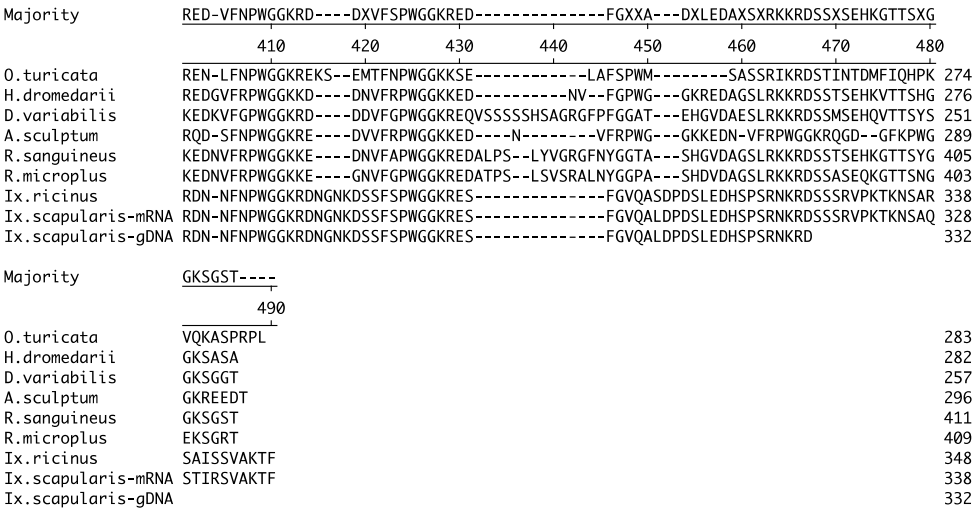

Supplementary Figure 3.3 Multiple amino acid sequence alignment of the deduced kinin precursors from eight tick species using Clustal W method by MegAlign (Lasergene, Madision, WI).

There are two sequences from *Ixodes scapularis*, the first one was deduced from three transcriptome sequences (GBBN01023680.1, GGIX01408871.1, GBBN01027580.1), and the second was deduced from a genome scaffold (DS680282) (Gulia-Nuss and Caffrey, 2016). The amino acid sequence from the latter lacks 23 residues at the N- terminus and also 23 residues at the C-terminus. The sequence deduced from the transcriptome (*Ix. scapularis*-mRNA) misses some internal amino acids within positions 250-293.

Gulia-Nuss, M., et al., (2016). Genomic insights into the *Ixodes scapularis* tick vector of Lyme disease. *Nat. Commun.* 7**,** 10507.

Supplementary Table 3.1 List of primers used in this study

Primers used in 5′/3′-RACE PCR

Primer name	Orientation	Template for primer design	Sequence (5'-3')	Purpose
RmkininP1-F	Forward	GEEZ01003316.1	GGGAGGCAAGAGGGACACGTTCAGC	3'RACE PCR
RmkininP1-R	Reverse	GEEZ01003316.1	CTTCCCCGGTTCCCCTCTTTCCTCC	5'RACE PCR
Universal primer short		Clontech® Universal primer mix	CTAATACGACTCACTATAGGGCAAGCAGTGGTATCAACGCAGAGT	3′/5′ RACE PCR
Universal primer long			CTAATACGACTCACTATAGGGC	

Primers used for cloning cDNA ORF in one product and gene amplification

Primer name	Orientation	Template for primer design	Sequence (5'-3')	Purpose
Rmk-ORF-F	Forward	cloned cDNA of the putative kinin precursor	CGCTGCTAGAGGCCCCATCGACG	regular PCR to amplify the ORF from cDNA and gDNA
Rmk-ORF-R	Reverse	cloned cDNA of the putative kinin precursor	GTTTTTCGAACGGGCGCTTCGCTAC	regular PCR to amplify the ORF from cDNA and gDNA
Bmkinin-g-long-F	Forward	LYUQ01126194.1	ACCTCAGTCCCTCTGCTGGTTCAGG	regular PCR to amplify the 3'end of kinin gene
Bmkinin-g-long-R	Reverse	LYUQ01126194.1	CCAACAGGCAGTGCGTTACCTCAGC	regular PCR to amplify the 3'end of kinin gene
Bmk-ORF-5'end-F	Forward	cloned cDNA of the putative kinin precursor	ACATGGGGAGCAACAGGCGCTGC	regular PCR to amplify the 5'end of kinin gene
RmkininP1-R	Reverse	cloned cDNA of the putative kinin precursor	CTTCCCCGGTTCCCCTCTTTCCTCC	regular PCR to amplify the 5'end of kinin gene

Primers used for sequencing

Primer name	Orientation	Template for primer design	Sequence (5'-3')	Purpose
Bmk-g-2ndF	Forward	partial kinin gene	CTGAGACACTGCGCAAGCAC	sequencing 4kb ORF region of kinin gene
Bmk-g-thirdF	Forward	partial kinin gene	GACTTCCGTTTGGTAATCAAC	sequencing 4kb ORF region of kinin gene
Bmk-g-thirdR	Reverse	partial kinin gene	GCAGAAGCGAGTACATGATG	sequencing 4kb ORF region of kinin gene
Rmk-ORF-F	Forward	cloned cDNA of the putative kinin precursor	CGCTGCTAGAGGCCCCATCGACG	sequencing 4kb ORF region of kinin gene
Rmk-ORF-R	Reverse	cloned cDNA of the putative kinin precursor	GTTTTTCGAACGGGCGCTTCGCTAC	sequencing 4kb ORF region of kinin gene
Rmkinin-5'end-R	Reverse	partial kinin gene	CGTCTACGCTTCATCGAAACG	sequencing the 5'-end of kinin gene
Bmkinin-g-long-F	Forward	LYUQ01126194.1	ACCTCAGTCCCTCTGCTGGTTCAGG	sequencing the 3'-end of kinin gene
Bmkinin-g-long-R	Reverse	LYUQ01126194.1	CCAACAGGCAGTGCGTTACCTCAGC	sequencing the 3'-end of kinin gene
T7 Promoter Primer	Forward	vector pCR2.1®	TAATACGACTCACTATAGGG	sequencing cloned cDNA sequences
M13 reverse primer	Reverse	vector pCR2.1®	CAGGAAACAGCTATGACC	sequencing cloned cDNA sequences

Supplementary Table 3.2. List of chemicals tested.

Small molecule name in this paper	Product Name (Tocris™)	Chemical Name	Mol Wt
TKSM1	L-732,138	N-Acetyl-L-tryptophan 3,5-bis(trifluoromethyl)benzyl ester	472.39
TKSM2	L-733,060 hydrochloride	(2S,3S)-3-[[3,5-bis(Trifluoromethyl)phenyl]methoxy]-2-phenylpiperidine hydrochloride	439.83
TKSM3	GR 159897	5-Fluoro-3-[2-[4-methoxy-4-[[(R)-phenylsulphinyl]methyl]-1-piperidinyl]ethyl]-1H-indole	423.55
TKSM4	SB 218795	(R)-[[2-Phenyl-4-quinolinyl)carbonyl]amino]-methyl ester benzeneacetic acid	396.44
TKSM5	SB 222200	3-Methyl-2-phenyl-N-[(1S)-1-phenylpropyl]-4-quinolinecarboxamide	380.48
TKSM6	RP 67580	(3aR,7aR)-Octahydro-2-[1-imino-2-(2-methoxyphenyl)ethyl]-7,7-diphenyl-4H-isoindol	443.07
TKSM7	SDZ NKT 343	1-[[(2-Nitrophenyl)amino]carbonyl]-L-prolyl-N-methyl-3-(2-naphthalenyl)-N-(phenylmethyl)-L-alaninamide	584.15
TKSM8	FK 888	(4R)-4-Hydroxy-1-[(1-methyl-1H-indol-3-yl)carbonyl]-L-prolyl-N-methyl-3-(2-naphthalenyl)-N-(phenylmethyl)-L-alaninamide	597.7
TKSM9	CP 96345	(2S,3S)-N-(2-Methoxyphenyl)methyl-2-diphenylmethyl-1-azabicyclo[2.2.2]octan-3-amine	412.57
TKSM10	SSR 146977 hydrochloride	N1-[1-3-[(3R)-1-Benzoyl-3-(3-(3,4-dichlorophenyl)-3-piperidinyl]propyl]-4-phenyl-piperidinyl]-N,N-dimethylurea hydrochloride	694.14
TKSM11	CP 99994 dihydrochloride	(2S,3S)-N-[(2-Methoxyphenyl)methyl]-2-phenyl-3-piperidinamine dihydrochloride	373.83
TKSM12	SR 140333	1-[2-[(3S)-3-(3,4-Dichlorophenyl)-1-[2-[3-(1-methylethoxy)phenyl]acetyl]-3-piperidinyl]ethyl]-4-phenyl-1-azoniabicyclo[2.2.2]octane chloride	674.14
TKSM13	L 760735	5-[[(2R,3S)-2-[(1R)-1-[3,5-Bis(trifluoromethyl)phenyl]ethoxy]-3-(4-fluorophenyl)-4-morpholinyl]methyl-N,N-dimethyl-1H-1,2,3-triazole-4-methanamine hydrochloride	620.99
TKSM14	SB 223412	3-Hydroxy-2-phenyl-N-[(1S)-1-phenylpropyl]-4-quinolinecarboxamide	386.95

Peptidomimetics	CAS number	Amino acid sequence	Mol Wt
Hemokinin 1 (Human)	491851-53-7	Thr-Gly-Lys-Ala-Ser-Gln-Phe-Phe-Gly-Leu-Met-NH2 (TGKASQFFGLMa)	1185.4
Antagonist G	115150-59-9	Arg-D-Trp-N(Me)Phe-D-Trp-Leu-Met-NH2 (RWFWLMa)	951.2
Spantide I	91224-37-2	D-Arg-Pro-Lys-Pro-Gln-Gln-D-Trp-Phe-D-Trp-Leu-Leu-MH2 (RPKPQQWFWLLa)	1497.8

Supplementary Table 3.2 Continued

Small molecule name in this paper	Primary Action	Activitiy on vertebrate endogenous receptors
TKSM1	Potent, selective NK1 antagonist	IC50 = 2.3 nM
TKSM2	Potent NK1 antagonist	Ki values are 0.08, 0.2 and 93.13 nM for gerbil, human and rat receptors, respectively)
TKSM3	Non-peptide, potent NK2 antagonist	Competes for binding of [3H]GR100679 to hNK2-transfected CHO cells with a pKi of 9.5
TKSM4	Potent, selective non-peptide NK3 antagonist	(Ki = 13 nM at hNK3). Displays 90-fold and 7000-fold selectivity over hNK2 and hNK1 receptors respectively.
TKSM5	Potent, selective non-peptide NK3 antagonist. Brain penetrant	Ki values are 4.4, > 100,000 and 250 nM for human NK3, NK1 and NK2receptors respectively
TKSM6	Potent and selective NK1 antagonist	Ki values are 2.9 nM and > 10 μM for rat NK1, and rat NK2 and NK3 receptors respectively
TKSM7	Highly selective, human NK1 antagonist	IC50 values are 0.62 and 451 nM for human and rat receptors respectively
TKSM8	High affinity NK1 receptor antagonist	(Ki = 0.69 nM) that displays 320-fold selectivity for human over rat NK1receptors.
TKSM9	Potent and selective NK1 antagonist	Attenuates substance P-induced salivary response and inhibits neurogenic inflammation *in vivo*.
TKSM10	Potent and selective NK3 antagonist	Ki values are 0.26 and 19.3 nM in CHO cells expressing the human NK3 and NK2 receptor respectively
TKSM11	High affinity NK1 antagonist	Ki = 0.145 nM *in vitro*
TKSM12	Potent NK1 receptor antagonist	Ki = 0.74 nM. IC50 = 1.6 nM
TKSM13	High affinity NK1 receptor antagonist	IC50 = 0.19 nM at human NK1 receptors). Selective (>300-fold) over h-NK2 and h-NK3 receptors.
TKSM14	Potent, selective non-peptide NK3 antagonist. Brain penetrant	Ki values are 1, 144 and >100000 nM for human NK3, NK2 and NK1 receptors respectively

Peptidomimetics	Primary action	Activtiy on vertebrate endogenous receptors
Hemokinin 1 (Human)	Endogenous substance P homolog that is a selective agonist at the tachykinin NK1 receptor	IC50 values are 1.8, 370 and 480 nM for NK1, NK3 and NK2 receptors respectively
Antagonist G	Substance P analog that is a broad spectrum neuropeptide antagonist and antiproliferative agent.	
Spantide I	Selective NK1 receptor antagonist	Ki values are 230, 8150 and > 10000 nM for rat NK1, NK2 and NK3 receptors respectively

Supplementary Table 3.3 First screening of the whole library in 384-well plate format.
Panel A shows in each well the 10x concentration of each compound; final concentration in the assay is 1x; Panel B is the response (1- 4min after the 1st injection) of BMLK3 cells (tick kinin rceptor recombinant cell line), to the compound; Panel C is the response of BMLK3 cells (5-9 min after the 2nd injection) to the agonist, 1 µM FFFSWGa. Panel D is the normalized response of panel C represented as the percentage of the response of positive control (blank solvent + agonist). In each panel of readout (B-D), the wells were coded by color gradient from red (highest RFU) to blue (lowest RFU).

A. Screen plate layout. Small molecules were serially diluted 1: 1.4, 19 times, from the initial concentration (1mM for 15 small molecules or 100 µM for thapsigargin, in column 3, 80 µl) into the most diluted column 22, by transferring 56 µl solution of previous higher concentration into the next well and mixing with 24 µl of blank solvent (2 % DMSO). The magenta gradient in the arrow below represents the dilution direction from high concentration (dark), to low concentration (light color).

Compound	Unit:	1	2	3	4	5	6	7	8	9	10	11	12	13	14	15	16	17	18	19	20	21	22	23	24
2-APB	A	Blank solvent (2 % DMSO in HHBS)		1000.0	700.0	490.0	343.0	240.1	168.1	117.6	82.4	57.6	40.4	28.2	19.8	13.8	9.7	6.8	4.7	3.3	2.3	1.6	1.1	Blank solvent (2 % DMSO in HHBS)	
TKSM1	B			1000.0	700.0	490.0	343.0	240.1	168.1	117.6	82.4	57.6	40.4	28.2	19.8	13.8	9.7	6.8	4.7	3.3	2.3	1.6	1.1		
TKSM2	C			1000.0	700.0	490.0	343.0	240.1	168.1	117.6	82.4	57.6	40.4	28.2	19.8	13.8	9.7	6.8	4.7	3.3	2.3	1.6	1.1		
TKSM3	D			1000.0	700.0	490.0	343.0	240.1	168.1	117.6	82.4	57.6	40.4	28.2	19.8	13.8	9.7	6.8	4.7	3.3	2.3	1.6	1.1		
TKSM4	E			1000.0	700.0	490.0	343.0	240.1	168.1	117.6	82.4	57.6	40.4	28.2	19.8	13.8	9.7	6.8	4.7	3.3	2.3	1.6	1.1		
TKSM5	F			1000.0	700.0	490.0	343.0	240.1	168.1	117.6	82.4	57.6	40.4	28.2	19.8	13.8	9.7	6.8	4.7	3.3	2.3	1.6	1.1		
TKSM6	G			1000.0	700.0	490.0	343.0	240.1	168.1	117.6	82.4	57.6	40.4	28.2	19.8	13.8	9.7	6.8	4.7	3.3	2.3	1.6	1.1		
TKSM7	H			1000.0	700.0	490.0	343.0	240.1	168.1	117.6	82.4	57.6	40.4	28.2	19.8	13.8	9.7	6.8	4.7	3.3	2.3	1.6	1.1		
TKSM8	I			1000.0	700.0	490.0	343.0	240.1	168.1	117.6	82.4	57.6	40.4	28.2	19.8	13.8	9.7	6.8	4.7	3.3	2.3	1.6	1.1		
TKSM9	J			1000.0	700.0	490.0	343.0	240.1	168.1	117.6	82.4	57.6	40.4	28.2	19.8	13.8	9.7	6.8	4.7	3.3	2.3	1.6	1.1		
TKSM10	K			1000.0	700.0	490.0	343.0	240.1	168.1	117.6	82.4	57.6	40.4	28.2	19.8	13.8	9.7	6.8	4.7	3.3	2.3	1.6	1.1		
TKSM11	L			1000.0	700.0	490.0	343.0	240.1	168.1	117.6	82.4	57.6	40.4	28.2	19.8	13.8	9.7	6.8	4.7	3.3	2.3	1.6	1.1		
TKSM12	M			1000.0	700.0	490.0	343.0	240.1	168.1	117.6	82.4	57.6	40.4	28.2	19.8	13.8	9.7	6.8	4.7	3.3	2.3	1.6	1.1		
TKSM13	N			1000.0	700.0	490.0	343.0	240.1	168.1	117.6	82.4	57.6	40.4	28.2	19.8	13.8	9.7	6.8	4.7	3.3	2.3	1.6	1.1		
TKSM14	O			1000.0	700.0	490.0	343.0	240.1	168.1	117.6	82.4	57.6	40.4	28.2	19.8	13.8	9.7	6.8	4.7	3.3	2.3	1.6	1.1		
Thapsigargin	P			100.0	70.0	49.0	34.3	24.0	16.8	11.8	8.2	5.8	4.0	2.8	2.0	1.4	1.0	0.7	0.5	0.3	0.2	0.2	0.1		

Screen plate: 10x of the final concentration solution, prepared in 2 % DMSO in Hanks' Saline Buffer containing 20 mM Hepes (HHBS)

Supplementary Table 3.3B Cell response in RFU (relative fluorescence units) to the first injection of 10X library compound (panel A): average of two reads (0-4 min) after the injection of 5 µL 10x compound or blank solvent from compound plate (top panel) into the assay plate. Two reads are obtained by performing a first reading and then inverting the orientation of the plate in the plate reader for the second read.

Compound		1	2	3	4	5	6	7	8	9	10	11	12	13	14	15	16	17	18	19	20	21	22	23	24
2-APB	A	0.2635	0.2464	0.3559	0.3277	0.2216	0.2656	0.2116	0.1895	0.1932	0.2002	0.2272	0.1869	0.2148	0.1705	0.1941	0.1711	0.2184	0.2143	0.1648	0.2031	0.1662	0.1827	0.19	0.2531
TKSM1	B	0.1884	0.2082	0.2399	0.225	0.2235	0.256	0.2451	0.2196	0.2249	0.2063	0.2305	0.1954	0.2081	0.2078	0.2314	0.2221	0.2286	0.2173	0.2275	0.2333	0.1995	0.1764	0.18	0.2019
TKSM2	C	0.2393	0.247	0.848	0.71	0.7441	0.6354	0.3742	0.3461	0.3378	0.2928	0.2631	0.2655	0.2263	0.2141	0.2599	0.2498	0.2181	0.244	0.2239	0.2579	0.2405	0.226	0.21	0.2037
TKSM3	D	0.2229	0.2307	0.3386	0.3325	0.3281	0.3388	0.276	0.2749	0.2643	0.2696	0.2548	0.2418	0.2676	0.2716	0.2505	0.2763	0.2633	0.2362	0.2617	0.2602	0.2626	0.2492	0.22	0.2997
TKSM4	E	0.241	0.2388	0.2481	0.26	0.2825	0.2919	0.2362	0.2764	0.2617	0.2452	0.2862	0.272	0.2538	0.2146	0.2188	0.2338	0.2666	0.2769	0.2358	0.2682	0.2566	0.2314	0.21	0.3022
TKSM5	F	0.1968	0.252	0.2377	0.2817	0.2817	0.2754	0.2934	0.2861	0.2978	0.2594	0.29	0.2941	0.268	0.2712	0.2661	0.2622	0.2314	0.2562	0.2543	0.2438	0.2429	0.225	0.23	0.2863
TKSM6	G	0.2509	0.2398	0.2804	0.2706	0.2606	0.3075	0.2917	0.2596	0.2965	0.2728	0.2536	0.2572	0.2444	0.2732	0.2827	0.2613	0.2662	0.264	0.2522	0.2275	0.2183	0.2434	0.24	0.2236
TKSM7	H	0.1954	0.2369	0.2426	0.2208	0.2464	0.2678	0.2971	0.274	0.2388	0.288	0.2907	0.2719	0.2732	0.2601	0.2927	0.2615	0.2592	0.2861	0.3093	0.2265	0.2576	0.2473	0.24	0.2533
TKSM8	I	0.2475	0.2722	0.2398	0.2779	0.2877	0.2541	0.2465	0.2488	0.2474	0.2825	0.2817	0.2583	0.2566	0.2487	0.2675	0.2785	0.2352	0.237	0.2598	0.2492	0.2422	0.2381	0.25	0.2707
TKSM9	J	0.2263	0.2124	0.2779	0.3043	0.3058	0.3539	0.3247	0.3177	0.2892	0.3013	0.2997	0.2634	0.277	0.2594	0.2651	0.2844	0.2448	0.2692	0.2554	0.2158	0.2477	0.2178	0.25	0.2016
TKSM10	K	0.2146	0.2017	0.4795	0.4706	0.5303	0.3728	0.3175	0.3266	0.2939	0.299	0.281	0.2955	0.2498	0.2506	0.2755	0.2743	0.2986	0.2727	0.2433	0.2652	0.2675	0.2236	0.2	0.2749
TKSM11	L	0.273	0.2637	0.3161	0.3456	0.3225	0.3095	0.3226	0.2879	0.2948	0.288	0.2595	0.2806	0.2569	0.2877	0.2804	0.2752	0.2598	0.2699	0.2754	0.2506	0.2257	0.2033	0.21	0.242
TKSM12	M	0.2643	0.3024	0.3003	0.2856	0.3141	0.2791	0.2855	0.2797	0.2722	0.3071	0.3014	0.2755	0.2827	0.2552	0.2688	0.2579	0.246	0.271	0.2445	0.2547	0.2602	0.2274	0.24	0.2477
TKSM13	N	0.3915	0.3041	0.4036	0.381	0.3601	0.3409	0.26	0.2845	0.2982	0.2791	0.2503	0.2693	0.2531	0.2765	0.3062	0.2684	0.2593	0.2623	0.2276	0.2342	0.2666	0.23	0.17	0.2045
TKSM14	O	0.2419	0.3179	0.3873	0.3871	0.3562	0.3056	0.2844	0.2826	0.2983	0.2515	0.2641	0.2281	0.225	0.2221	0.2138	0.2375	0.2445	0.2349	0.2545	0.2304	0.2053	0.223	0.33	0.2554
Thapsigargin	P	0.2786	0.2965	0.2401	0.3109	0.3862	0.3115	0.2556	0.2816	0.2632	0.3413	0.2804	0.2359	0.2471	0.3001	0.2687	0.2548	0.2514	0.2709	0.283	0.2877	0.2509	0.2282	0.3	0.2946

Supplementary Table 3.3C Cell response in RFU (relative fluorescence units) to the 2nd injection of 1µM FFFSWGa: average of two reads (5-9 min) obtained 5 min after the 2nd injection of 5.6µL 10x FFFSWGa (10µM). Two reads are obtained by performing a first reading and then inverting the orientation of the plate in the plate reader for the second read.

Compound		1	2	3	4	5	6	7	8	9	10	11	12	13	14	15	16	17	18	19	20	21	22	23	24
2-APB	A	1.0327	0.8862	0.1775	0.2471	0.2108	0.2436	0.2312	0.2533	0.2338	0.4746	0.7305	0.8645	0.9691	0.7289	0.7415	0.8813	1.0167	0.9865	0.6347	1.0478	0.7315	0.7805	0.77	0.9271
TKSM1	B	0.6508	0.8239	0.9206	0.8843	0.9491	0.9887	0.9581	0.9474	0.8788	0.9336	0.8801	0.8326	0.8234	0.8571	1.0149	0.7342	0.8026	0.7449	0.6987	0.8018	0.9967	0.8786	0.75	0.9432
TKSM2	C	0.82	0.8995	0.3135	0.2762	0.3001	0.4312	0.9134	0.8612	1.0278	0.8367	0.8917	0.8731	0.796	0.8376	0.7613	0.8044	0.8113	0.9014	0.7764	0.8088	0.8123	0.7265	0.73	0.7742
TKSM3	D	0.7984	0.8217	0.997	1.0914	0.9826	0.97	0.9088	0.9062	0.9134	0.8973	0.9579	0.8864	0.8734	0.8626	0.8402	0.8983	0.8926	0.8552	0.8416	0.8435	0.8042	0.8105	0.65	1.0166
TKSM4	E	0.7529	0.7101	0.7803	0.8776	1.0547	1.0158	0.9766	1.0623	1.149	1.0262	0.9637	1.0068	0.9148	0.7725	0.8643	0.8529	0.8513	0.9553	0.7841	0.9768	0.8178	0.7959	0.68	1.0773
TKSM5	F	0.8017	0.8995	0.9288	1.0574	0.9779	0.9895	1.0227	1.0156	1.1065	0.3189	1.0217	0.9107	1.0029	0.9303	0.9399	0.906	0.8299	0.9794	0.9687	0.9424	0.8026	0.7255	0.74	0.9554
TKSM6	G	0.8446	0.7452	0.9136	0.9827	1.0626	1.1159	1.0543	0.9691	0.9838	0.9612	0.8328	0.9409	0.9573	0.978	0.8393	0.8867	0.9885	0.282	0.9928	0.9598	0.7871	0.7801	0.74	0.7887
TKSM7	H	0.8026	0.7589	0.8384	0.9392	0.2922	0.9674	1.0387	0.9267	0.999	1.0207	1.1385	0.9501	1.0438	1.0217	0.8665	0.9477	0.9672	0.9692	0.8775	0.8897	0.7777	0.7523	0.88	0.9897
TKSM8	I	0.9602	0.7894	0.8937	1.0277	0.3339	1.0333	1.0195	1.0084	0.9741	0.9339	1.0303	0.9509	0.985	0.9614	1.0288	0.9744	0.9064	0.8385	1.0158	0.9553	0.9733	0.7251	0.98	0.8709
TKSM9	J	0.8498	0.7099	1.0117	1.0607	1.0384	1.0472	1.1244	0.3277	1.0776	1.0344	1.0459	1.0028	0.9672	0.9709	0.9585	0.9564	0.9226	0.9407	0.9399	0.83	0.8231	0.8859	0.79	0.7038
TKSM10	K	0.8012	0.7501	0.6441	0.8397	0.7416	0.9204	1.1122	1.0964	1.1177	1.0413	1.0857	1.1109	1.031	1.0078	0.9887	1.0976	0.9774	1.0156	0.8912	0.9358	0.8027	0.8859	0.86	1.011
TKSM11	L	1.0132	0.7644	1.0033	1.1037	1.1532	1.0461	1.1263	1.039	1.0558	1.0641	1.0331	0.8653	0.9582	0.9664	0.9799	0.9254	0.9927	0.9335	0.9174	0.823	1.0046	0.8477	0.81	0.9493
TKSM12	M	0.8769	0.836	0.9034	0.9364	1.0402	1.072	0.9428	0.9944	0.967	1.0167	1.0433	1.0309	0.9971	0.9547	0.9592	0.8732	0.8702	0.9654	0.9723	0.8961	0.9625	0.8342	0.82	0.7784
TKSM13	N	1.2174	0.8037	0.572	0.6593	0.8581	0.9704	1.0051	1.0363	1.0513	1.0417	0.8922	1.0193	1.0055	0.8833	0.9165	0.9246	0.9129	0.9767	0.7564	0.9422	0.9407	0.8397	0.68	0.7138
TKSM14	O	0.7777	0.8007	0.2707	0.3042	0.3105	0.6211	0.9056	0.9489	0.9617	0.8705	0.9493	0.9545	0.9272	0.8362	0.803	0.8901	0.903	0.8988	0.897	0.7983	0.7962	0.7922	1.12	0.8055
Thapsigargin	P	0.9231	0.9707	0.7776	0.9878	1.2028	0.9811	0.8872	0.9553	0.8703	1.1182	0.8832	0.8365	0.792	0.9442	0.8622	0.7843	0.809	0.8964	0.9633	0.9326	0.7965	0.8323	0.94	0.9229

Supplementary Table 3.3D % of the RFU of the Positive Control on the four edge columns (blank buffer + FFFSWGa).

% of the RFU of PC		1	2	3	4	5	6	7	8	9	10	11	12	13	14	15	16	17	18	19	20	21	22	23	24
2-APB	A	122%	105%	21%	29%	25%	29%	27%	30%	28%	56%	86%	102%	115%	86%	88%	104%	120%	117%	75%	124%	87%	92%	91%	110%
TKSM1	B	77%	98%	109%	105%	112%	117%	113%	112%	104%	111%	104%	99%	97%	101%	120%	87%	95%	88%	83%	95%	118%	104%	89%	112%
TKSM2	C	97%	106%	37%	33%	36%	51%	108%	102%	122%	99%	106%	103%	94%	99%	90%	95%	96%	107%	92%	96%	96%	86%	86%	92%
TKSM3	D	95%	97%	118%	129%	116%	115%	108%	107%	108%	106%	113%	105%	103%	102%	99%	106%	106%	101%	100%	100%	95%	96%	77%	120%
TKSM4	E	89%	84%	92%	104%	125%	120%	116%	126%	136%	121%	114%	119%	108%	91%	102%	101%	101%	113%	93%	116%	97%	94%	80%	128%
TKSM5	F	95%	107%	110%	125%	116%	117%	121%	120%	131%	38%	121%	108%	119%	110%	111%	107%	98%	116%	115%	112%	95%	86%	88%	113%
TKSM6	G	100%	88%	108%	116%	126%	132%	125%	115%	116%	114%	99%	111%	113%	116%	99%	105%	117%	33%	118%	114%	93%	92%	88%	93%
TKSM7	H	95%	90%	99%	111%	35%	115%	123%	110%	118%	121%	135%	112%	124%	121%	103%	112%	115%	115%	104%	105%	92%	89%	104%	117%
TKSM8	I	114%	93%	106%	122%	40%	122%	121%	119%	115%	111%	122%	113%	117%	114%	122%	115%	107%	99%	120%	113%	115%	86%	116%	103%
TKSM9	J	101%	84%	120%	126%	123%	124%	133%	39%	128%	122%	124%	119%	115%	115%	113%	113%	109%	111%	111%	98%	97%	105%	93%	83%
TKSM10	K	95%	89%	76%	99%	88%	109%	132%	130%	132%	123%	129%	132%	122%	119%	117%	130%	116%	120%	106%	111%	95%	105%	102%	120%
TKSM11	L	120%	91%	119%	131%	137%	124%	133%	123%	125%	126%	122%	102%	113%	114%	116%	110%	118%	111%	109%	97%	119%	100%	96%	112%
TKSM12	M	104%	99%	107%	111%	123%	127%	112%	118%	114%	120%	124%	122%	118%	113%	114%	103%	103%	114%	115%	106%	114%	99%	97%	92%
TKSM13	N	144%	95%	68%	78%	102%	115%	119%	123%	124%	123%	106%	121%	119%	105%	109%	109%	108%	116%	90%	112%	111%	99%	80%	85%
TKSM14	O	92%	95%	32%	36%	37%	74%	107%	112%	114%	103%	112%	113%	110%	99%	95%	105%	107%	106%	106%	95%	94%	94%	132%	95%
Thapsigargin	P	109%	115%	92%	117%	142%	116%	105%	113%	103%	132%	105%	99%	94%	112%	102%	93%	96%	106%	114%	110%	94%	99%	111%	109%

Supplementary Table 3.4 Second screening of "library subset " in 384-well plate format. Panel A shows in each well the 10x concentration of each compound; final concentration in the assay is 1x; Panel B is the response (1-4 min after the 1st injection) of BMLK3 (tick kinin rceptor recombinant cell line, left half of the assay plate) and vector only cells (empty vector transfected cell line, right half of the assay plate) to the compound; Panel C is the response of BMLK3 and vector only cells (5-9 min after the 2nd injection) to the agonist, 1 µM FFFSWGa. Panel D is the normalized response of panel C, represented as the percentage of the response of the positive control (blank solvent + agonist). In each panel of readout (B-D), the wells were coded by color gradient from red (highest RFU) to blue (lowest RFU).

A. Screen plate layout. Small molecules were serially diluted 1: 1.4, 9 times, from the various initial concentrations (in column 3, 80 µl) into the most diluted column 12, by transferring 56 µl solution of previous higher concentration into the next well and mixing with 24 µl of blank solvent (10% DMSO). A duplicate dilution was made from column 22 (initial highest concentration) to column 13 (most diluted). The magenta gradient in the arrows below represents the dilution direction from high concentration (dark), to low concentration (light color).

Compound	Unit: µM	1	2	3	4	5	6	7	8	9	10	11	12	13	14	15	16	17	18	19	20	21	22	23	24
Thap	A	Blank solvent (10 % DMSO in HHBS)		100.00	70.00	49.00	34.30	24.01	16.81	11.76	8.24	5.76	4.04	4.04	5.76	8.24	11.76	16.81	24.01	34.30	49.00	70.00	100.00	Blank solvent (10 % DMSO in HHBS)	
TKSM5	B			100.00	70.00	49.00	34.30	24.01	16.81	11.76	8.24	5.76	4.04	4.04	5.76	8.24	11.76	16.81	24.01	34.30	49.00	70.00	100.00		
TKSM7	C			100.00	70.00	49.00	34.30	24.01	16.81	11.76	8.24	5.76	4.04	4.04	5.76	8.24	11.76	16.81	24.01	34.30	49.00	70.00	100.00		
TKSM8	D			500.00	350.00	245.00	171.50	120.05	84.04	58.82	41.18	28.82	20.18	20.18	28.82	41.18	58.82	84.04	120.05	171.50	245.00	350.00	500.00		
TKSM14	E			500.00	350.00	245.00	171.50	120.05	84.04	58.82	41.18	28.82	20.18	20.18	28.82	41.18	58.82	84.04	120.05	171.50	245.00	350.00	500.00		
TKSM2	F			1000.00	700.00	490.00	343.00	240.10	168.07	117.65	82.35	57.65	40.35	40.35	57.65	82.35	117.65	168.07	240.10	343.00	490.00	700.00	1000.00		
TKSM10	G			1000.00	700.00	490.00	343.00	240.10	168.07	117.65	82.35	57.65	40.35	40.35	57.65	82.35	117.65	168.07	240.10	343.00	490.00	700.00	1000.00		
TKSM13	H			1000.00	700.00	490.00	343.00	240.10	168.07	117.65	82.35	57.65	40.35	40.35	57.65	82.35	117.65	168.07	240.10	343.00	490.00	700.00	1000.00		
TKSM4	I			50.00	35.00	24.50	17.15	12.01	8.40	5.88	4.12	2.88	2.02	2.02	2.88	4.12	5.88	8.40	12.01	17.15	24.50	35.00	50.00		
TKSM6	J			10.00	7.00	4.90	3.43	2.40	1.68	1.18	0.82	0.58	0.40	0.40	0.58	0.82	1.18	1.68	2.40	3.43	4.90	7.00	10.00		
TKSM9	K			100.00	70.00	49.00	34.30	24.01	16.81	11.76	8.24	5.76	4.04	4.04	5.76	8.24	11.76	16.81	24.01	34.30	49.00	70.00	100.00		
2-APB	L			100.00	70.00	49.00	34.30	24.01	16.81	11.76	8.24	5.76	4.04	4.04	5.76	8.24	11.76	16.81	24.01	34.30	49.00	70.00	100.00		
TKSM2	M	2% DMSO in HHBS [1] (see note at the bottom)		1000.00	700.00	490.00	343.00	240.10	168.07	117.65	82.35	57.65	40.35	40.35	57.65	82.35	117.65	168.07	240.10	343.00	490.00	700.00	1000.00	2% DMSO in HHBS [1] (see note at the bottom)	
TKSM10	N			1000.00	700.00	490.00	343.00	240.10	168.07	117.65	82.35	57.65	40.35	40.35	57.65	82.35	117.65	168.07	240.10	343.00	490.00	700.00	1000.00		
TKSM13	O			1000.00	700.00	490.00	343.00	240.10	168.07	117.65	82.35	57.65	40.35	40.35	57.65	82.35	117.65	168.07	240.10	343.00	490.00	700.00	1000.00		
TKSM14	P			500.00	350.00	245.00	171.50	120.05	84.04	58.82	41.18	28.82	20.18	20.18	28.82	41.18	58.82	84.04	120.05	171.50	245.00	350.00	500.00		

Screen plate: 10x of the final concentration solution, prepared in 10 % DMSO in Hanks' Saline Buffer containing 20 mM Hepes (HHBS)

Supplementary Table 3.4B Cell response in RFU (relative fluorescence units) to the first injection of 10x library compound (panel B): average of two reads (0-4 min) after the injection of 5 µL 10x compound or blank solvent from compound plate (top panel) into the assay plate. Two reads are obtained by performing a first reading and then inverting the orientation of the plate in the plate reader for the second read.

Compound		1	2	3	4	5	6	7	8	9	10	11	12	13	14	15	16	17	18	19	20	21	22	23	24
Thap	A	0.065	0.225	1.6121	2.1302	2.1519	1.7569	2.1769	1.4702	2.374	1.2116	1.0908	0.6384	1.0694	0.5071	1.8103	1.9908	2.4275	2.458	2.1758	2.8492	2.3463	2.4557	0.0625	0.1138
TKSM5	B	-0.0392	0.0419	-0.0278	-0.0094	0.054	0.0658	0.0551	0.04	0.0424	0.0564	-0.0266	0.0106	0.1018	0.0047	0.089	0.0408	0.08	-0.0268	0.0154	0.0527	-0.0351	0.0524	0.0729	0.0263
TKSM7	C	0.0791	0.0624	0.0142	0.0043	0.109	-0.0069	0.0737	0.0106	0.0057	0.0612	0.066	0.0448	0.0724	0.0341	0.0827	0.0247	0.0499	0.087	0.0367	-0.0373	0.0607	0.0626	0.0307	0.0355
TKSM8	D	-0.0144	0.0029	-0.068	0.081	0.0131	0.0313	0.0226	0.0709	0.1582	0.0288	0.0323	0.047	0.0309	0.0413	0.055	0.0672	0.0308	0.0562	0.0877	0.0093	0.0398	0.0714	0.0341	0.0624
TKSM14	E	0.0347	0.0053	0.2728	0.112	0.1054	0.1757	-0.0175	0.1483	0.0912	0.0991	0.0863	0.0198	0.0459	0.0689	0.0777	0.0079	0.0901	0.0979	0.1665	0.1785	0.1118	0.2437	0.1585	-0.0142
TKSM2	F	0.0179	0.0296	0.7043	0.8064	0.6633	0.5832	0.4893	0.4156	0.2236	0.1943	0.1295	0.1726	0.0408	0.0723	0.2744	0.3283	0.3752	0.6272	0.7111	0.5455	0.5652	0.3954	0.045	0.0351
TKSM10	G	0.0259	0.0153	0.2522	0.3523	0.3408	0.1871	0.2543	0.1404	0.1999	0.0553	0.0595	0.0271	0.0329	0.0478	-0.0143	0.0539	0.0841	0.1991	0.3078	0.2654	0.4409	0.4897	0.0068	0.02
TKSM13	H	-0.0292	0.0057	0.2434	0.2273	0.2891	0.3242	0.3349	0.2527	0.2065	0.0757	0.0813	0.0899	0.0875	0.0928	0.1087	0.2197	0.3128	0.2629	0.3992	0.2677	0.3457	0.3006	0.045	0.0267
TKSM4	I	0.0728	0.0492	0.1125	0.1164	0.0828	0.0506	0.034	0.0382	0.0532	0.0735	0.0224	0.04	0.0623	0.0327	0.0626	0.0211	0.066	0.0825	0.0076	0.0256	0.0363	0.0097	0.0535	0.0119
TKSM6	J	0.1054	0.0533	0.0892	0.0674	0.0105	0.0192	0.0351	0.0474	0.0646	0.072	0.0745	0.0444	0.0546	0.0421	0.0699	0.0438	0.0511	0.068	0.0535	0.0123	-0.0517	0.0465	-0.0207	-0.0129
TKSM9	K	0.124	0.0685	0.1572	0.0387	0.0226	0.095	0.0066	0.0334	0.0513	0.083	0.0858	0.0445	0.0151	0.0329	0.0635	0.0693	0.0732	0.078	0.1372	0.0572	-0.0117	0.1765	0.073	0.0284
2-APB	L	0.0878	0.0594	0.1355	0.1858	0.1434	0.118	0.1489	0.0512	0.0808	0.0626	0.0612	0.0934	0.0387	0.0972	0.0113	0.1503	0.1417	0.1397	0.1146	0.1268	0.1316	0.0957	0.0262	0.0312
TKSM2	M	0.056	0.0392	0.3559	0.3201	0.3253	0.3914	0.3821	0.3105	0.0919	0.1336	0.1095	0.1109	0.0775	0.0724	0.1159	0.2231	0.3132	0.2489	0.4245	0.5752	0.4924	0.4382	0.0057	0.0217
TKSM10	N	0.003	0.0377	0.2124	0.1574	0.1739	0.076	0.1014	0.0316	0.0696	0.0148	0.0132	0.051	0.0559	0.086	0.0235	0.0233	0.0899	0.0306	0.0117	0.0471	0.0396	0.1007	0.001	0.0435
TKSM13	O	0.0211	0.0329	0.1242	0.1315	0.101	0.1283	0.086	0.1495	0.0644	0.0338	0.0276	0.0122	0.0759	0.1067	0.045	0.0918	0.2172	0.1377	0.0805	0.1253	0.1257	0.1286	0.0663	0.0694
TKSM14	P	0.0433	0.0122	0.0871	0.0891	0.1213	0.1116	0.0044	0.0399	0.0509	0.0213	0.0073	0.0347	0.0416	0.0017	-0.0352	0.0446	0.0252	0.0516	-0.0745	0.1242	0.1046	-0.009	0.0488	0.0045
		BMLK3 cells												Vector Only cells											

Supplementary Table 3.4C Cell response in RFU (relative fluorescence units) to the 2nd injection of 1µM FFFSWGa: average of two reads (5-9 min) obtained 5 min after the 2nd injection of 5.6µL 10x FFFSWGa (10µM). Two reads are obtained by performing a first reading and then inverting the orientation of the plate in the plate reader for the second read.

Compound		1*	2	3	4	5	6	7	8	9	10	11	12	13	14	15	16	17	18	19	20	21	22	23	24
Thap	A	0.5575	0.5712	1.0796	1.3972	1.4019	1.0819	1.4419	1.1342	1.33	1.2946	1.3353	1.4749	1.3309	1.131	1.3113	1.0988	1.387	1.221	1.0493	1.2637	1.1198	1.1137	-0.0104	0.014
TKSM5	B	0.6062	0.5728	0.59705	0.5434	0.652	0.7803	0.5994	0.566	0.6435	0.5961	0.5169	0.6585	0.0871	0.0302	0.0909	0.0587	0.083	0.0066	0.0437	0.0016	0.0037	0.02145	0.0008	0.04
TKSM7	C	0.7454	0.6256	0.65305	0.4385	0.6229	0.7111	0.639	0.6275	0.6451	0.6466	0.719	0.6539	0.0242	0.0174	0.0313	0.018	0.0319	0.048	0.0221	-0.0193	0.0698	-0.02705	0.0508	-0.0108
TKSM8	D	0.492	0.5807	0.53175	0.6509	0.588	0.5757	0.6655	0.5579	0.7074	0.6372	0.6781	0.5899	0.0216	0.0647	0.0475	0.0848	0.0571	0.1346	0.1866	0.1366	0.2334	0.35175	-0.0025	0.1961
TKSM14	E	0.7591	0.6848	0.2203	0.2215	0.3267	0.5848	0.4675	0.5849	0.6394	0.6884	0.5951	0.6093	0.0483	0.0896	0.0483	-0.0286	0.0459	-0.0005	0.0863	0.1059	-0.0221	0.01665	0.1375	0.0037
TKSM2	F	0.501	0.6365	0.0333	0.17	0.3688	0.5996	0.9953	0.8555	0.8369	0.8341	0.7757	0.6885	0.0488	0.0158	0.1792	0.214	0.2449	0.3231	0.314	0.3176	0.2872	0.1093	0.1032	0.0645
TKSM10	G	0.5143	0.59	0.13585	0.2936	0.7831	0.68	0.8093	0.8035	0.7811	0.7781	0.7113	0.7147	0.0083	0.0455	0.0175	0.131	0.1162	0.2078	0.2118	0.2272	0.3029	0.34055	0.0807	0.1204
TKSM13	H	0.5828	0.7478	0.40345	0.5791	0.2242	0.314	0.2766	0.5048	0.6594	0.6011	0.716	0.6346	0.1101	0.0977	0.1528	0.1773	0.2098	0.209	0.2228	0.1921	0.2745	0.206	0.097	0.1066
TKSM4	I	0.6677	0.6484	0.56545	0.6795	0.6205	0.5307	0.6849	0.6749	0.6617	0.6583	0.5345	0.5725	0.0372	0.0577	0.0601	0.0927	0.1068	0.0726	-0.016	0.0704	0.0129	0.051	0.0496	0.0528
TKSM6	J	0.5452	0.5822	0.61615	0.7005	0.7757	0.7792	0.6187	0.6728	0.6368	0.6411	0.7111	0.6037	0.0511	0.0546	0.0739	0.0655	0.0862	0.0677	0.0288	0.0368	0.0724	0.0492	0.0085	0.0987
TKSM9	K	0.0342	0.7112	0.7349	0.9113	0.8805	0.6378	0.8623	0.6717	0.6501	0.686	0.6147	0.6537	0.0414	0.1551	0.0686	0.1407	0.0845	0.0968	0.0883	0.0921	0.0286	0.08555	0.0693	0.078
2-APB	L	0.0206	0.7102	-0.03965	-0.0184	-0.0051	-0.005	0.0351	0.5551	0.1985	0.2246	0.422	0.4117	0.0089	0.0673	0.0658	0.0643	0.0716	0.0157	0.0535	0.0252	0.0015	-0.02145	0.0963	0.0699
TKSM2	M	0.0703	0.6544	0.593	0.7087	0.8868	0.7748	0.8835	0.7775	1.1778	0.9831	0.6315	0.7781	0.0677	0.0845	0.0924	0.164	0.2661	0.3165	0.4203	0.4175	0.3519	0.2478	0.0496	0.0806
TKSM10	N	0.0225	0.6749	1.0272	0.8583	1.0901	0.8799	0.8387	0.7587	0.7677	0.7225	0.6947	0.7295	0.0548	0.1089	0.0445	0.0722	0.1342	0.079	0.1262	0.1262	0.1276	0.23245	0.0408	0.1297
TKSM13	O	0.4507	0.6446	0.7065	0.7632	0.7525	0.4241	0.4661	0.4489	0.8189	0.6434	0.5924	0.5257	0.0816	0.0856	0.135	0.1122	0.1957	0.151	0.1308	0.1548	0.1545	0.1547	0.082	0.0682
TKSM14	P	0.5263	0.6067	0.09735	0.5351	0.4268	0.4669	0.5275	0.445	0.5467	0.789	0.752	0.6949	0.1066	0.1046	0.0269	0.0896	0.0775	0.0394	-0.0753	0.0151	0.0256	-0.0207	0.0053	-0.0359
		BMLK3 cells												Vector Only cells											

* the reads from column1 were not used for calculating response of BMLK3 to PC.

Supplementary Table 3.4D % of the RFU of the Positive Control (blank buffer + FFFSWGa).

D		1*	2	3	4	5	6	7	8	9	10	11	12	13	14	15	16	17	18	19	20	21	22	23	24
Thap	A	87%	89%	169%	218%	219%	169%	225%	177%	208%	202%	209%	230%	208%	177%	205%	172%	217%	191%	164%	197%	175%	174%	-2%	2%
TKSM5	B	95%	89%	93%	85%	102%	122%	94%	88%	101%	93%	81%	103%	14%	5%	14%	9%	13%	1%	7%	0%	1%	3%	0%	6%
TKSM7	C	116%	98%	102%	69%	97%	111%	100%	98%	101%	101%	112%	102%	4%	3%	5%	3%	5%	7%	3%	-3%	11%	-4%	8%	-2%
TKSM8	D	77%	91%	83%	102%	92%	90%	104%	87%	111%	100%	106%	92%	3%	10%	7%	13%	9%	21%	29%	21%	36%	55%	0%	31%
TKSM14	E	119%	107%	34%	35%	51%	91%	73%	91%	100%	108%	93%	95%	8%	14%	8%	-4%	7%	0%	13%	17%	-3%	3%	21%	1%
TKSM2	F	78%	99%	5%	27%	58%	94%	156%	134%	131%	130%	121%	108%	8%	2%	28%	33%	38%	50%	49%	50%	45%	17%	16%	10%
TKSM10	G	80%	92%	21%	46%	122%	106%	126%	126%	122%	122%	111%	112%	1%	7%	3%	20%	18%	32%	33%	36%	47%	53%	13%	19%
TKSM13	H	91%	117%	63%	90%	35%	49%	43%	79%	103%	94%	112%	99%	17%	15%	24%	28%	33%	33%	35%	30%	43%	32%	15%	17%
TKSM4	I	104%	101%	88%	106%	97%	83%	107%	105%	103%	103%	84%	89%	6%	9%	9%	14%	17%	11%	-2%	11%	2%	8%	8%	8%
TKSM6	J	85%	91%	96%	109%	121%	122%	97%	105%	100%	100%	111%	94%	8%	9%	12%	10%	13%	11%	5%	6%	11%	8%	1%	15%
TKSM9	K	5%	111%	115%	142%	138%	100%	135%	105%	102%	107%	96%	102%	6%	24%	11%	22%	13%	15%	14%	14%	4%	13%	11%	12%
2-APB	L	3%	111%	-6%	-3%	-1%	-1%	5%	87%	31%	35%	66%	64%	1%	11%	10%	10%	11%	2%	8%	4%	0%	-3%	15%	11%
TKSM2	M	11%	102%	93%	111%	139%	121%	138%	121%	184%	154%	99%	122%	11%	13%	14%	26%	42%	49%	66%	65%	55%	39%	8%	13%
TKSM10	N	4%	105%	161%	134%	170%	137%	131%	119%	120%	113%	109%	114%	9%	17%	7%	11%	21%	12%	20%	20%	20%	36%	6%	20%
TKSM13	O	70%	101%	110%	119%	118%	66%	73%	70%	128%	101%	93%	82%	13%	13%	21%	18%	31%	24%	20%	24%	24%	24%	13%	11%
TKSM14	P	82%	95%	15%	84%	67%	73%	82%	70%	85%	123%	118%	109%	17%	16%	4%	14%	12%	6%	-12%	2%	4%	-3%	1%	-6%
		BMLK3 cells												Vector Only cells											

Supplementary Information File 5. Below is the screen shoot of the alignment of fourteen kinin precursors shown in Mesquite window (Version 3.6) for phylogenetic analysis in the manuscript.

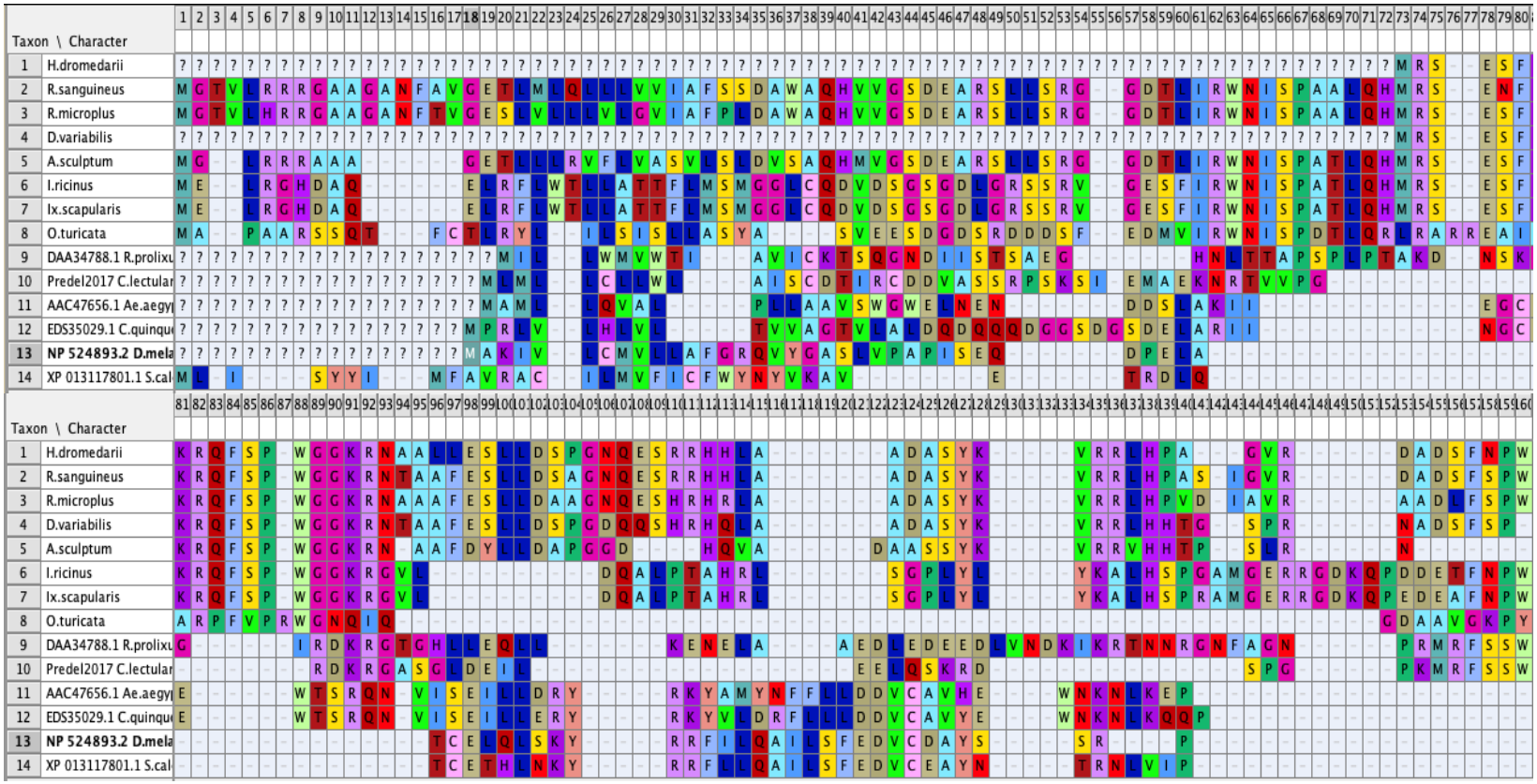

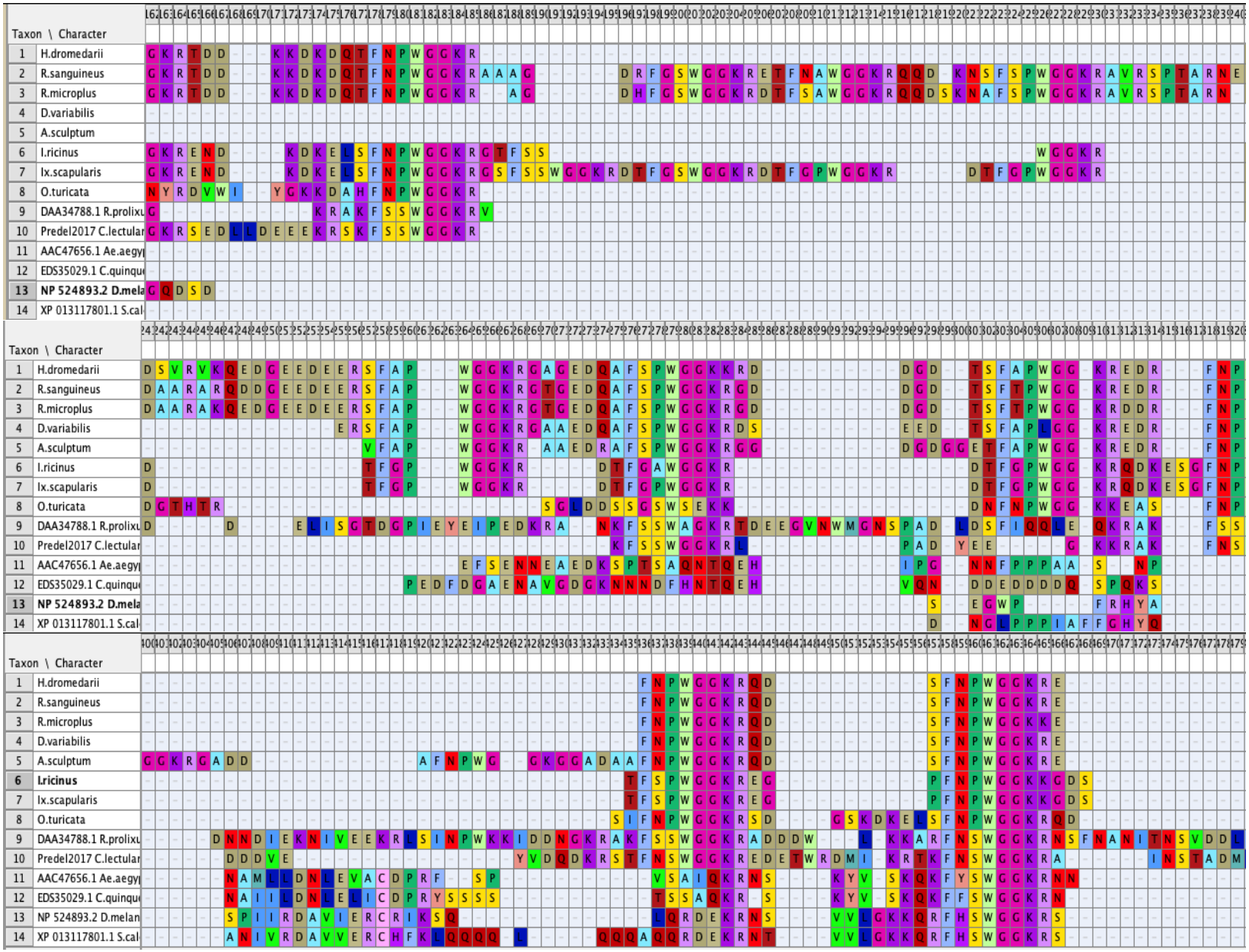
Taxon \ Character
1 H.dromedarii
2 R.sanguineus
3 R.microplus
4 D.variabilis
5 A.sculptum
6 I.ricinus
7 Ix.scapularis
8 O.turicata
9 DAA34788.1 R.prolixu
10 Predel2017 C.lectular
11 AAC47656.1 Ae.aegyp
12 EDS35029.1 C.quinque
13 NP 524893.2 D.mela
14 XP 013117801.1 S.cal

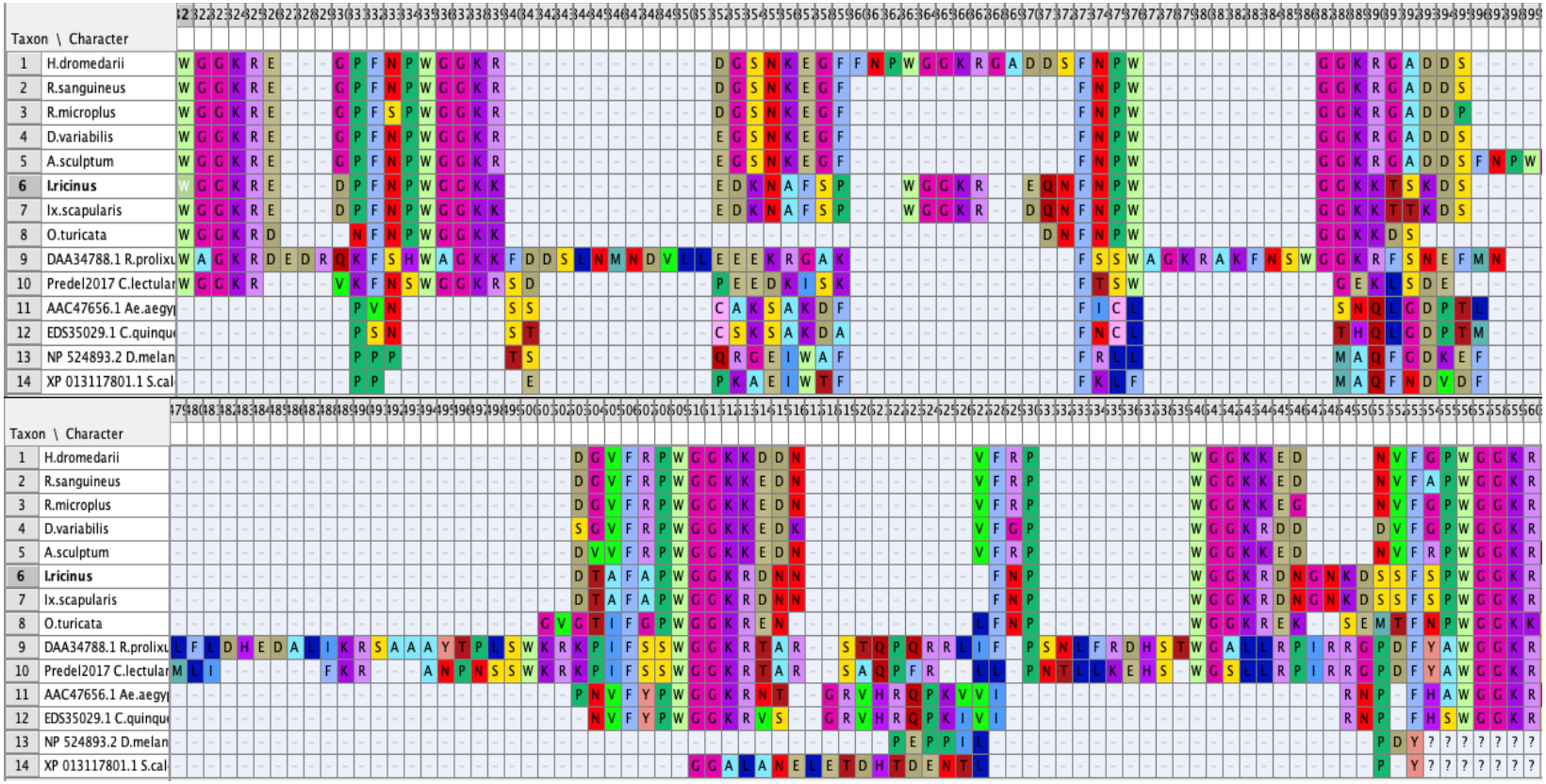
Taxon \ Character
1 H.dromedarii
2 R.sanguineus
3 R.microplus
4 D.variabilis
5 A.sculptum
6 I.ricinus
7 Ix.scapularis
8 O.turicata
9 DAA34788.1 R.prolixu
10 Predel2017 C.lectular
11 AAC47656.1 Ae.aegyp
12 EDS35029.1 C.quinqu
13 NP 524893.2 D.melan
14 XP 013117801.1 S.cal

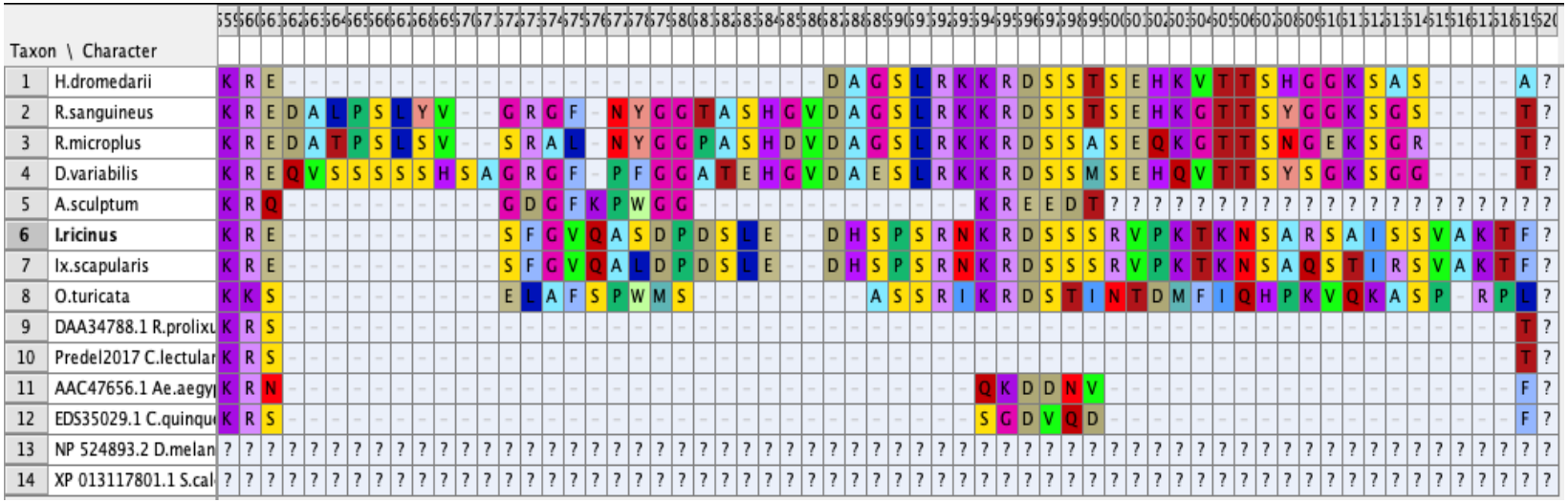
Taxon \ Character
1 H.dromedarii
2 R.sanguineus
3 R.microplus
4 D.variabilis
5 A.sculptum
6 I.ricinus
7 Ix.scapularis
8 O.turicata
9 DAA34788.1 R.prolixu
10 Predel2017 C.lectular
11 AAC47656.1 Ae.aegy
12 EDS35029.1 C.quinqu
13 NP 524893.2 D.melan
14 XP 013117801.1 S.cal

APPENDIX C

FOR CHAPTER 4

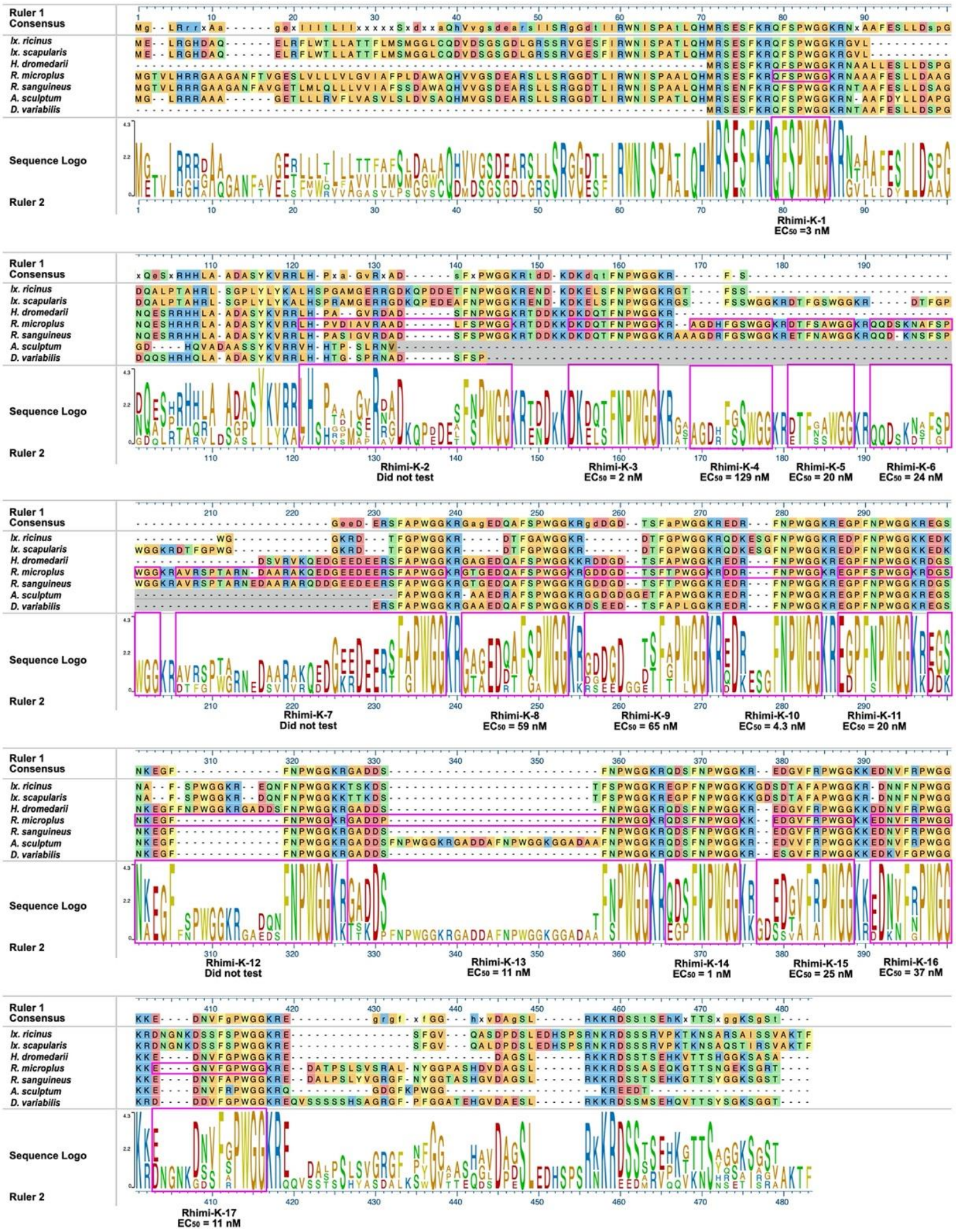

Supplementary Figure 4.1 Multiple sequence alignment of kinin precursors from seven hard tick species. The protein sequences were obtained from Xiong et al., (2019)(Xiong et al., 2019a) and were aligned using MAFFT with E-INS-i algorithm by MegaPro (DNASTAR, Lasergene v16.0). *R. microplus* kinins and corresponding sequence Logo areas were boxed. The height of each letter on the sequence logo represents the frequency (in bits) of each amino acid residue across tick species. The gray areas in the sequences of *Dermacentor variabilis* and *Amblyomma sculptum* indicate the gaps in the transcriptomes (Xiong et al., 2019a).

Supplementary Table 4.1. Tukey's multiple comparison test on the potency (EC_{50}) of endogenous tick kinins, * $p<0.05$, ** $p<0.01$, *** $p<0.001$, **** $p<0.0001$

			Rhimi-K-14	IK-Aib-20	Rhimi-K-3	1728	Rhimi-K-1	Rhimi-K-10	Rhimi-K-8	Rhimi-K-17	Rhimi-K-13	Rhimi-K-5	Rhimi-K-11	Rhimi-K-6	Rhimi-K-15	Rhimi-K-16	Rhimi-K-9	Rhimi-K-4
ID	**Sequence**	**EC_{50}**	0	0	0	2E-09	0	0	0	0	0	0	0	0	0	0	0	0
Rhimi-K-14	QDSFNPWGa	1E-09																
IK-Aib-20	[Aib]FH[Aib]WGa	2E-09	ns															
Rhimi-K-3	DKDQTFNPWGa	2E-09	ns	ns														
1728	[Aib]FF[Aib]WGa	2E-09	ns	ns	ns													
Rhimi-K-1	QFSPWGa	3E-09	ns	ns	ns	ns												
Rhimi-K-10	DDRFNPWGa	4E-09	ns	ns	ns	ns	ns											
Rhimi-K-8	ɠTGEDQAFSPWGa	6E-09	ns	ns	ns	ns	ns	ns										
Rhimi-K-17	EGNVFGPWGa	1E-08	ns	ns	ns	ns	ns	ns	ns									
Rhimi-K-13	GADDPFNPWGa	1E-08	ns	ns	ns	ns	ns	ns	ns	ns								
Rhimi-K-5	DTFSAWGa	2E-08	ns	ns	ns	ns	ns	ns	ns	ns	ns							
Rhimi-K-11	EGPFSPWGa	2E-08	ns	ns	ns	ns	ns	ns	ns	ns	ns	ns						
Rhimi-K-6	)QDSKNAFSPWGa	2E-08	ns	ns	ns	ns	ns	ns	ns	ns	ns	ns	ns					
Rhimi-K-15	EDGVFRPWGa	3E-08	ns	ns	ns	ns	ns	ns	ns	ns	ns	ns	ns	ns				
Rhimi-K-16	EDNVFRPWGa	4E-08	ns	ns	ns	ns	ns	ns	ns	ns	ns	ns	ns	ns	ns			
Rhimi-K-9	ɠDDGDTSFTPWGa	6E-08	**	**	*	*	*	*	*	*	*	ns	ns	ns	ns	ns		
Rhimi-K-4	AGDHFGSWGa	1E-07	****	****	****	****	****	****	****	****	****	****	****	****	****	**	*	

Supplementary Table 2.2 Tukey's multiple comparison test on the potency (EC_{50}) of Aib-analogs incorporating tick sequence and other modifications, * p<0.05, ** p<0.01, *** p<0.001, **** p<0.0001

			2414	2412	2411	IK-Aib-20 (2356)	2359	1728	2415	2416	2345	2413	2361	2346	2173-1
ID	Sequence	EC_{50}	0	0	0	3E-09	0	0	0	0	0	0	0	0	0
2414	[Aib]FS[Aib]WGa	9E-10													
2412	[Aib]FG[Aib]WGa	1E-09	ns												
2411	[Aib]FN[Aib]WGa	3E-09	ns	ns											
IK-Aib-20	[Aib]FH[Aib]WGa	3E-09	ns	ns	ns										
2359	AKFS[Aib]WGa	4E-09	ns	ns	ns	ns									
1728	[Aib]FF[Aib]WGa	6E-09	ns	ns	ns	ns	ns								
2415	[Aib]FR[Aib]WGa	7E-09	ns	ns	ns	ns	ns	ns							
2416	[Aib]FA[Aib]WGa	7E-09	ns	ns	ns	ns	ns	ns	ns						
2345	pQRFH[Aib]WGa	9E-09	ns	ns	ns	ns	ns	ns	ns	ns					
2413	[Aib]FT[Aib]WGa	1E-08	ns	ns	ns	ns	ns	ns	ns	ns	ns				
2361	A[Aib]FS[Aib]WGa	2E-08	ns	ns	ns	ns	ns	ns	ns	ns	ns	ns			
2346	c-[dR]FH[Aib]WGa	5E-08	****	****	****	****	****	****	***	***	***	**	**		
2173	Hca-F[Aib]WGa	8E-07	****	****	****	****	****	****	****	****	****	****	****	****	

CyBio Program #1 Cell Plating

position3 (position 3)	>15 mL of cell suspension in an Integra™ 150ml reservoir
Position4	384 well plate, CELLSTAR® flat, black wall, clear bottom, Greiner Bio-one 781091. Plates were coated with 10 µl/well of 0.05 mg/ml solution in water of poly-D-Lysine (Sigma) before use.
Purpose	Cell plating: Take 25 µl of cell suspension from position3 to position4 and mix 10µl for three times in the 384 well plate.
Protocol	
Program Steps	Piston speed 5µl/s
1	Aspirate 25 µl of cell suspension from position3 from 805 (805 is Z position in Cybio equipment; vertical axis)
2	Dispense 25 µl into position4 at 800
3	Mix 10 µl for three times at 800

Cybio Program #2 Addition Of FLUOFORTE®(ENZO) Dye

Position3	>15 mL of 1x loading dye
Position4	384 well assay plate (cell inside, medium removed)
Purpose	take 25 µl of 1x dye from position3 to position4
Protocol	
Program steps	Piston speed 4 µl/s
1	Aspirate 25 µl of 1x dye from position3 from 805
2	Dispense 25 µl into position4 at 790

CyBio Program #3 Addition of test compounds

Position3 384 well plate (Corning®, 3680) with 40 µl of 5 x compound solution of the final concentration in each well

Position4 384 well assay plate (contains cells in 25 µl of 1x dye)

Purpose take 5.2 µl of compound solution from position3 to position4

Protocol

Program

Steps Piston speed 3µl/s

1. Mix of compound at position3 by aspirating (810) and dispensing (790) 10 µl of compound solution
2. Aspirate 5.2 µl of compound solution from position3 from 810
3. Dispense 5.2 µl into position4 at 790

APPENDIX D

FOR CHAPTER 5

CyBio Program #1 Cell Plating

position3 (position 3)	>15 mL of cell suspension in an Integra™ 150ml reservoir
Position4	384 well plate, CELLSTAR® flat, black wall, clear bottom, Greiner Bio-one 781091. Plates were coated with 10 µl/well of 0.05 mg/ml solution in water of poly-D-Lysine (Sigma) before use.
Purpose	Cell plating: Take 25 µl of cell suspension from position3 to position4 and mix 10µl for three times in the 384 well plate.
Protocol	
Program Steps	Piston speed 5µl/s
1	Aspirate 25 µl of cell suspension from position3 from 805 (805 is Z position in Cybio equipment; vertical axis)
2	Dispense 25 µl into position4 at 800
3	Mix 10 µl for three times at 800

Cybio Program #2 Addition Of FLUOFORTE®(ENZO) Dye

Position3	>15 mL of 1x loading dye
Position4	384 well assay plate (cell inside, medium removed)
Purpose	take 25 µl of 1x dye from position3 to position4
Protocol	
Program steps	Piston speed 4 µl/s
1	Aspirate 25 µl of 1x dye from position3 from 805
2	Dispense 25 µl into position4 at 790

CyBio Program #3 Addition of test compounds

Position3	384 well plate (Corning®, 3680) with 30 µl of 50 x compound solution of the final concentration in each well
Position4	384 well assay plate (contains cells in 25 µl of 1x dye)
Purpose	take 0.5 µl of 1x dye from position3 to position4
Protocol	
Program	
Steps	Piston speed 3µl/s
1	Mix of compound at position3 by aspirating (810) and dispensing (790) 10 µl of compound solution
2	Aspirate 0.5 µl of 1x dye from position3 from 810
3	Dispense 0.5 µl into position4 at 790

CyBio Program #4 Addition of peptides

Position3	>15 mL of cell suspension in an Integra™ 150ml reservoir
Position4	384 well assay plate (contains cells in 25 µl of 1x dye)
Purpose	take 3 µl of peptide solution from position3 to position4
Protocol	
Program	
Steps	Piston speed 3µl/s
1	Aspirate 25 µl of 1x dye from position3 from 805
2	Dispense 3 µl into position4 at 790

Viaflo Program #1 Cell Plating

Position	
A	>15 mL of cell suspension in an Integra™ 150ml reservoir

Position B	384 well plate, CELLSTAR® flat, black wall, clear bottom, Greiner Bio-one 781091. Plates were coated with 10 µl/well of 0.05 mg/ml solution in water of poly-D-Lysine (Sigma) before use.
Purpose	Cell plating: Take 25 µl of cell suspension from positionA to positionB
Protocol	
Program	
Steps	Piston speed 3.1µl/s
1	Aspirate 12.5 µl of cell suspension from positionA from 11.8 mm (is Z position in Cybio equipment; vertical axis),
2	Dispense 25 µl into positionB at 11.8 mm
3	Repeat 1-2 once

Viaflo Program #2 Addition of FLUOFORTE®(ENZO) Dye

Positiona	>15 mL of 1x loading dye in an Integra™ 150ml reservoir
Positionb	384 well assay plate (cell inside, medium removed)
Purpose	take 25 µl of 1x dye from positionA to positionB
Protocol	
Program	
Steps	Piston speed 3.8 µl/s
1	Aspirate 12.5 µl of 1x dye from positionA from 12.2 mm
2	Dispense 12.5 µl into positionB at 12mm
3	Repeat 1-2 once

Viaflo Program #3 Addition of Test Compounds

Positiona	384 well plate (Corning®, 3680) with 30 µl of 50 x compound solution of the final concentration in each well
Positionb	384 well assay plate (contains cells in 25 µl of 1x dye)
Purpose	add 0.5 µl of 50x test compound into 25 µl 1x dye in cell plate
Protocol	

Program

Steps Piston speed 1µl/s

1 Mix of compound at positionA by aspirating (11.2 mm) and dispensing (11.2 mm) 10 µl of compound solution
2 Aspirate 1.5 µl of drug from positionA at 11.4 mm
3 Dispense 0.5 µl into positionB at 12.5 mm

Viaflo Program #3 Addition of agonist peptide

Positiona >15 mL of cell suspension in an Integra™ 150ml reservoir

Positionb 384 well assay plate (contains cells in 25 µl of 1x dye and 0.5 µl compound)

Purpose add 3 µl of 10x peptide solution into 25 µl 1x dye in cell plate

Protocol

Program

Steps Piston speed 3.1 µl/s

1 Aspirate 3 µl of drug from positionA at 12.1 mm
2 Dispense 3 µl into positionB at 12.5 mm

Please see the separate excel file for Supplementary Table 5.1-5.7.